The Role of Nitric Oxide Synthase (NOS) and the Cofactor Tetrahydrobiopterin (BH4) in Diabetic Cardiomyopathy

Thesis submitted for the degree of

Doctor of Philosophy

University of Oxford

Drew Duglan

Cardiovascular Medicine

Radcliffe Department of Medicine

&

St. Cross College

Supervisors: Professor Barbara Casadei

Professor Kim Dora

Dr. Ricardo Carnicer

February 2016

Half of what we know is wrong, the purpose of science is to determine which half

- Arthur Kornberg -

Abstract

The Role of Nitric Oxide Synthase (NOS) and the Cofactor Tetrahydrobiopterin (BH4) in Diabetic Cardiomyopathy

The work presented within this thesis investigates the mechanisms which underlie the cardiovascular phenotype observed in a mouse model of type 1 diabetic cardiomyopathy. It demonstrates the protective effects of augmenting the NOS cofactor, BH4, to said cardiomyopathy, and explores the different pathways potentially involved in conferring protection.

Chapter 1 summarises the current understanding of how hyperglycaemia triggers dysfunction in the vascular endothelium via the over-production of ROS. It describes the role of the NOS enzyme in both the vasculature and the myocardium, and the critical action of the BH4 cofactor to maintain NOS coupling and redox balance. The contribution of NOS "uncoupling" to diabetes pathophysiology is then discussed, examining the extent to which it has been implicated in the development of cardiomyopathy.

Chapter 2 includes full descriptions of the materials and experimental techniques employed within this study.

Chapter 3 investigates the role of neuronally-derived NO in the constrictor and dilator responses of rat resistance arteries. Organ bath experiments using wire myography and electrical stimulation reveal that NO released from perivascular neurons acts to oppose nerve-mediated vasoconstrictor responses in the rat mesenteric artery, in a frequency-dependent fashion. The perivascular localisation of nNOS is confirmed in rat and mouse mesenteric arteries with immunostaining, and the implications for nitrergic nerve dysfunction in diabetic neuropathy is discussed.

Chapter 4 explores the function of the aorta and mesenteric arteries in the type 1 diabetic mouse, showing early impairment of endothelium-dependent vasodilatation in the aorta after 4 weeks of hyperglycaemia, which further persists after 12 weeks. This dysfunction in diabetes is associated with oxidative stress and indicative of NOS uncoupling, as evidenced by increased vascular superoxide production and a reduction in BH4 bioavailability. In contrast to the aorta, mesenteric vessels are protected from hyperglycaemic damage and do not show functional impairment. In these experiments, specific myocardial overexpression of the GCH1 transgene (to augment myocardial BH4) does not influence vascular outcomes, as expected.

Chapter 5 examines the diabetic cardiomyopathy *in vivo* and in isolated cardiomyocytes, demonstrating significant LV diastolic dysfunction in WT diabetic mice, which precipitates only after 12 weeks and not as an early event. mGCH1 overexpression is able to improve LV performance in both control and diabetic hearts, accelerating cardiomyocyte relaxation and protecting against the development of LV dysfunction in the diabetic state. This dysfunction is associated with altered passive stiffness and changes to LV collagen content, but not with oxidative stress and NOS uncoupling as the principal driver. mGCH1 overexpression is able to improve LV mitochondrial ATP flux, increasing energy availability and potentially restoring metabolic flexibility to the heart in the setting of insulin insufficiency. The implementation of a 6-week oral BH4 supplement successfully elevates myocardial biopterin levels and NOS activity; whether this will provide protection against cardiomyopathy remains to be investigated. In contrary to mGCH1 overexpression, any potential mechanism is seemingly distinct from altered cardiomyocyte metabolism.

Chapter 6 summarises the totality of the study findings, elaborating on potential signalling pathways mediated by BH4, as well as highlighting study limitations and directions for future work.

Acknowledgements

All of the work presented here has been possible only with the funding provided by the British Heart Foundation, both through my own studentship and the programme grant awarded to Barbara Casadei. I would also like to acknowledge the travel grants and additional funds offered by St. Cross College, which has been extremely valuable throughout my DPhil.

I am thankful to Kim Dora and Chris Garland in the Department of Pharmacology, who granted me a place in their lab for first year rotation and cultivated an environment where I could begin to advance my knowledge and skills base in the area of vascular function. I would also like to specifically thank Chloe Lim from that department, who was extremely supportive and helpful during the initial difficulties of my first year. Since that time, her creative and pragmatic nature has helped direct my thinking both inside and outside of the lab.

For the remainder of my PhD at the John Radcliffe Hospital I am fortunate to have been surrounded by such a knowledgeable, generous and light-hearted group of lab colleagues. I have learned a great deal from these folks during my time and there have been countless laughs along the way. Since I started, every day (almost) at work has been fun and exciting, and I attribute this to the lab and the wider staff in Cardiovascular Medicine.

I would like to thank my primary supervisor, Barbara, who has really enabled my personal development over the last 3 years. I am thankful for the care and time she has dedicated to me as a student, and grateful for her guidance and advice to me a scientist. The experience she has passed down is invaluable and has been instrumental in the way I think about and approach scientific challenges.

Special thanks must also be made to my colleague, supervisor and friend, Ricardo. He welcomed me into the department in the early days and instilled a passion in me for the forthcoming investigation into diabetes. He has been a fantastic teacher throughout these 3 years; he has trained me in how to be precise, yet efficient, in a vast array of experimental techniques; he has additionally enhanced the way I read, write and communicate science; he has strongly pushed me at every turn, whilst also retaining a great degree of patience and understanding; most of all, he has been a great source of positive energy and motivation each and every day. I will truly miss our regular discussions on all things metabolism, diabetes and the English-Spanish language barrier.

I would then like to thank my partner Meghan, who has given me huge confidence in everything I do, and who has been extremely caring and considerate during all the highs and the lows. She has also broadened my outlook on so many different topics, and as a researcher herself, has offered valuable and practical ideas on wider scientific considerations, such as applications, networking and public engagement.

Last but not least, I am the most grateful to my family Anne, Ray and Holly, who have provided me with ongoing love and support throughout the years, not to mention endless encouragement and excellent advice along the road. Needless to say, none of this would have been possible without them.

Drew Duglan

St. Cross College, February 2016

Publication

Simon JN, **Duglan D**, Casadei B, Carnicer R. *Nitric oxide synthase regulation of cardiac excitation-contraction coupling in health and disease.* J Mol Cell Cardiol. 2014. 73; 80-91.

Scientific communication

D. Duglan, R. Carnicer, J.N. Simon, S. Chuaiphichai, A. Hale, K.M. Channon, B. Casadei. *Diabetic cardiomyopathy: Role of NOS and the cofactor BH4.*

Abstract accepted for oral presentation

British Heart Foundation National Graduate Meeting

Manchester, UK, April 2013

D. Duglan, R. Carnicer, J.N. Simon, S. Chuaiphichai, A. Hale, K.M. Channon, B. Casadei. *The role of nitric oxide synthase (NOS) and its essential cofactor tetrahydropbiopterin (BH4) in diabetic cardiomyopathy.*

Abstract accepted for moderated poster presentation

Frontiers in Cardiovascular Biology Congress

Barcelona, Spain, July 2014

D. Duglan, R. Carnicer, J.N. Simon, S. Chuaiphichai, A. Hale, K.M. Channon, B. Casadei. *The role of nitric oxide synthase (NOS) and its essential cofactor tetrahydropbiopterin (BH4) in diabetic cardiomyopathy.*

Abstract accepted for moderated poster presentation

European Society of Cardiology Congress

London, UK, August 2015

Thesis word count: approx. 42 000 words

Table of Contents

Abstract 3

Acknowledgements 4

Publication and scientific communication 5

Table of contents 6

Table of figures 11

List of abbreviations, pharmacological agents and antibodies and gene probes 15

Chapter 1 – General Introduction 21

Pathology of diabetes mellitus 22

Which detrimental pathways are triggered by hyperglycaemia? 22

Polyol pathway flux 22

Advanced glycation end products 23

Protein Kinase C activity 24

Hexosamine pathway 25

All paths stem from ROS 26

Oxidative stress initiates the pathways of diabetic damage 28

Nitric oxide synthase and NO signalling 32

NOS structure 32

Physiological role of NOS in the vasculature 33

NOS in the myocardium 35

The role of BH4 in NOS function 37

BH4 metabolism 37

Catalytic role of BH4 37

NOS uncoupling 38

Vascular NOS uncoupling in the setting of diabetes 39

NOS and the diabetic cardiomyopathy 40

NOS coupling and LV diastolic function 41

Myocardial NOS uncoupling in diabetes 42

Thesis objectives 43

Chapter 2 – General Methods 45

Introduction 46

Animals 46

Generation of transgenic mice 47

Induction of type 1 diabetes 47

Genotyping 48

Standard solutions 49

Tissue collection 51

Preparation of LV homogenates 51

Protein quantification 52

Western blot sample preparation 53

Blotting 54

Quantitative real-time RT PCR 54

RNA extraction 55

cDNA synthesis 55

Quantitative RT PCR 56

Superoxide production 58

Lucigenin-enhanced chemiluminescence 58

HPLC detection 60

LV cardiomyocyte isolation 61

Acquisition of cell shortening data 62

Cell shortening measurements 63

$[Ca^{2+}]_i$ transient measurements 64

Biopterin measurements 65

NOS activity 66

Collagen assay 67

Glutathione assay 69

Vasomotor studies 72

Vessel preparation 73

Myograph calibration and normalisation 74
Peri-arterial nerve stimulation 76
Arterial immunohistochemistry 77
Creatine kinase activity 77
Echocardiography 80
Histology 81
Lipid content 81
Myofilament mechanics 82
Plasma insulin quantification 84
Oral BH4 supplementation 86
Statistical analysis 86

Chapter 3 – The role of nNOS in resistance vessels 87
Introduction 88
The vascular origins of nNOS-derived NO 88
The putative "nitrergic" nerve 89
nNOS as a modulator of non-adrenergic, non-cholinergic (NANC)-mediated vasodilatation 89
Methods 91
Vasomotor studies 91
Immunohistochemistry of pinned out arteries 91
Results 91
NOS involvement in nerve-mediated vasoconstriction 91
Contribution of NOS to neurogenic vasodilatation 94
Isoform selectivity of available NOS inhibitors 94
Specific impact of neuronal NOS in nerve-mediated vasoconstriction 98
Immunohistochemical study of nNOS expression in mesenteric arteries 100
Conclusions 102
Discussion 102

Chapter 4 – The pathology of diabetes in the vasculature 106

Introduction 107

Glucose transport and endothelial cell vulnerability 107

Impaired NO-dependent vasodilatation 108

Effects on other mediators of endothelial-dependent vasorelaxation 110

Temporal effects 110

Methods 111

Vasomotor studies 111

Superoxide production 112

Biopterin quantification 112

Plasma insulin concentration 112

Results 113

STZ-treated mice exhibit early and sustained hyperglycaemia 113

Hyperglycaemia is accompanied by insulin insufficiency 114

Endothelial dysfunction in aorta is an early event in diabetes development 117

12 week diabetic mice exhibit endothelial dysfunction and enhanced vasoconstriction in aorta 117

Resistance vessels are protected from diabetes-induced vascular dysfunction 118

Oxidative stress underlies the endothelial dysfunction in diabetes 123

Conclusions 127

Discussion 127

Chapter 5 – The pathology of diabetes in myocardium and the effect of mGCH1 overexpression 135

Introduction 136

Clinical cardiomyopathy phenotype 136

Animal models of diabetic cardiomyopathy 138

Changes to cardiomyocyte physiology 139

The involvement of archetypal hyperglycaemia-induced mechanisms 141

Is ROS the primary driver? 144

Methods 146

Superoxide production 146

Cardiomyocyte isolation 147

Cell shortening and $[Ca^{2+}]_i$ transients 147
Echocardiography 148
Creatine kinase activity 148
Glutathione assay 148
Immunoblotting 149
Quantitative real-time RT PCR 149
Histology 149
Biopterin quantification 150
Myofilament mechanics 150
NOS activity 151
BH4 supplementation 151
Results 152
No cardiomyopathy is evident after 4 weeks of diabetes 152
mGCH1 overexpression protects against the later onset of diabetic cardiomyopathy 153
Increased ROS production does not underlie the LV dysfunction in diabetes 165
EC-coupling protein expression and myofilament mechanics 170
The role of fibrosis and markers of inflammation 178
mGCH1 overexpression prevents altered energy metabolism in the diabetic heart 185
Metabolic changes may precede the onset of diabetic cardiomyopathy 202
BH4 supplementation increases cardiac biopterins and improves LV NOS activity 205
BH4 supplementation may not alter the same metabolic pathways as mGCH1 overexpression 208
Conclusions 211
Discussion 211

Chapter 6 – Conclusions and general discussion 224
Limitations and areas for further study 231
Final summary and clinical implications 235

References 237

Table of Figures

Chapter 1 – General Introduction

Figure 1.1 Aberrant PKC signalling in response to hyperglycaemia. 25

Figure 1.2 Hexosamine pathway activation by high intracellular glucose. 26

Figure 1.3 Energy production from glucose in the mitochondrial electron transport chain. 28

Figure 1.4 NOS structure and NO synthesis. 32

Figure 1.5 Mechanism of PKG-mediated vascular smooth muscle relaxation. 34

Figure 1.6 Cellular pathways of BH4 biosynthesis 38

Chapter 2 – General Methods

Figure 2.1 Identification of mGCH1-Tg mice by PCR. 49

Figure 2.2 Protein quantification assay. 53

Figure 2.3 Principle of the TaqMan gene expression assay. 56

Figure 2.4 Superoxide detection by chemiluminescence. 59

Figure 2.5 Langendorff perfusion set-up for the isolation of murine LV cardiomyocytes. 62

Figure 2.6 Set-up for the measurement of isolated cardiomyocytes. 63

Figure 2.7 Data acquisition in isolated cardiomyocytes. 64

Figure 2.8 Generated standard curve for the Quickzyme collagen assay. 69

Figure 2.9 Enzymatic cycling of glutathione. 70

Figure 2.10 Fluorescence emission in the assay of glutathione. 70

Figure 2.11 Calibration of LabChart with myograph organ bath. 75

Figure 2.12 Normalisation protocol in organ bath experiments. 75

Figure 2.13 Imaging set-up for the performance of 2D-echocardiography. 81

Figure 2.14 Raw trace of force-Ca^{2+} sensitivity and tension development procedure in demembranated trabeculae. 83

Figure 2.15 Reference curve generated from insulin standards during the ELISA assay. 86

Chapter 3 – The role of nNOS in resistance vessels

Figure 3.1 Potential mechanisms of the regulation of vascular tone by neuronally-derived nitric oxide. 90

Figure 3.2 NOS inhibition augments electrically stimulated constrictor responses. 93

Figure 3.3 CGRP contributes more than NOS to neurogenic vasodilatation. 96

Figure 3.4 AAA-N and SMTC show greater selective nNOS inhibition. 97

Figure 3.5 nNOS-derived NO opposes nerve-mediated vasoconstriction at higher frequencies. 99

Figure 3.6 nNOS is expressed in perivascular nerve varicosities in mesenteric artery. 101

Chapter 4 – The pathology of diabetes in the vasculature

Figure 4.1 STZ-treated mice exhibit rapid and sustained hyperglycaemia, as well as reductions in body weight. 115

Figure 4.2 Insulin insufficiency accompanies hyperglycaemia in STZ-treated mice. 116

Figure 4.3 4-week diabetic mice exhibit normal vasoconstrictor responses, but endothelial dysfunction in aorta 119

Figure 4.4 Enhanced vasoconstriction accompanies persistent endothelial dysfunction in aorta from 12 week diabetic mice. 120

Figure 4.5 Mesenteric artery is protected from diabetes-induced vascular impairment. 121

Figure 4.6 NO is still a major mediator of endothelium-dependent vasodilatation in the mesenteric artery. 122

Figure 4.7 12 weeks of hyperglycaemia causes increased O_2^- production in aorta. 124

Figure 4.8 NOS inhibition abolishes the diabetes-induced increased in O_2^- production. 125

Figure 4.9 Hyperglycaemia is associated with decreased BH4 bioavailability in the aorta. 126

Chapter 5 – The pathology of diabetes in myocardium and the effect of mGCH1 overexpression

Figure 5.1 Systolic function remains normal after 4 weeks of diabetes. 155

Figure 5.2 No defects in diastolic function are evident after 4 weeks of diabetes. 156

Figure 5.3 Cardiomyocyte contractility is not altered in short term diabetes. 157

Figure 5.4 Cardiomyocyte relaxation remains normal after 4 weeks of diabetes. 158

Figure 5.5 Myocardial NOS expression is unchanged in the early stages of T1D. 159

Figure 5.6 mGCH1-Tg mice are equally protected against systolic impairment after 12 weeks of diabetes. 160

Figure 5.7 mGCH1 overexpression protects against the LV diastolic dysfunction in long term diabetes. 161

Figure 5.8 Heart rate is slower in mGCH1-Tg mice during the assessment of systolic function 162

Figure 5.9 12 week diabetic cardiomyopathy is also evident at the cardiomyocyte level. 163

Figure 5.10 Cardiomyocytes from 12 weeks diabetic mice do not exhibit impaired contractility. 164

Figure 5.11 Diabetic hearts do not exhibit increased production of ROS. 166

Figure 5.12 Diabetes does not result in reduced BH4 bioavailability. 167

Figure 5.13 Myocardial NOS expression still remains unaltered in the later stages of T1D. 168

Figure 5.14 NOS activity and glutathione status is enhanced in hearts overexpressing mGCH1. 169

Figure 5.15 SERCA expression remains unchanged in diabetes. 172

Figure 5.16 Diabetes does not alter the fraction of phosphorylated serine[16] on PLB. 173

Figure 5.17 Phosphorylation status of PLB threonine[17] is not reduced in diabetes. 174

Figure 5.18 Levels of NCX expression remain unchanged in LV homogenates in long term diabetes. 175

Figure 5.19 Myofilament mechanics in demembranated trabeculae. 176

Figure 5.20 Myofilament dimensions in demembranated trabeculae. 177

Figure 5.21 12 weeks of diabetes is not associated with altered LV collagen 1A1 gene expression. 180

Figure 5.22 12 week diabetic mice exhibit increased LV collagen content. 181

Figure 5.23 Inflammation is not implicated in the development of diabetic cardiomyopathy. 182

Figure 5.24 PKCβII expression is not upregulated in the LV of diabetic mice. 183

Figure 5.25 Diabetes is not associated with excessive acetylation of histone protein 3 in the myocardium. 184

Figure 5.26 mGCH1 overexpression prevents the impairment in mitochondrial ATP flux in diabetes. 188

Figure 5.27 Non-mitochondrial isoforms of creatine kinase do not exhibit reduced activity in diabetic hearts. 189

Figure 5.28 Diabetic hearts demonstrate increased expression of uncoupling protein 3. 190

Figure 5.29 Long term diabetes is not associated with altered LV mitochondrial density. 191

Figure 5.30 Long term diabetes is not associated with altered GLUT4 gene expression in the myocardium. 192

Figure 5.31 T1D does not alter LV expression of GLUT4 protein. 193

Figure 5.32 mGCH1-Tg hearts demonstrate upregulated GLUT1 gene expression. 194

Figure 5.33 mGCH1 overexpression increases GLUT1 protein levels in the myocardium. 195

Figure 5.34 Neither diabetes nor mGCH1 overexpression is associated with AMPK activation. 196

Figure 5.35 Myocardial expression of MCAD is not upregulated in diabetic mice. 197

Figure 5.36 Long term diabetes does not upregulate myocardial PPARα expression. 198

Figure 5.37 LV expression of PDK4 is not increased after 12 weeks of diabetes. 199

Figure 5.38 Diabetes does not change the myocardial expression of αKGD. 200

Figure 5.39 Lipid deposition is reduced in the liver of diabetic mice. 201

Figure 5.40 Mitochondrial UCP3 upregulation is an early event in the development of diabetic cardiomyopathy. 203

Figure 5.41 mGCH1 overexpression increases GLUT1 levels prior to the onset of diabetic LV dysfunction. 204

Figure 5.42 BH4 supplementation elevates plasma biopterins. 206

Figure 5.43 BH4 supplementation increases cardiac BH4 and improves NOS activity. 207

Figure 5.44 BH4 supplementation does not prevent the diabetes-induced increase in UCP3 expression. 209

Figure 5.45 BH4 supplementation does not upregulate LV GLUT1 expression. 210

Chapter 6 – Conclusions and general discussion

Figure 6.1 Hearts from diabetic patients show no evidence of increased oxidative stress or NOS uncoupling. 227

Figure 6.2 Proposed mechanisms by which mGCH1 overexpression and BH4 supplementation could prevent LV dysfunction in diabetes. 231

List of abbreviations

ΔG	Gibbs free energy
AAH	amino acid hydroxylase
ACC	acetyl-CoA carboxylase
AcH3	acetylated histone 3
AGE	advanced glycation end product
AMDCC	Animal Models of Diabetic Complications Consortium
AMPK	5' adenosine monophosphate-activated protein kinase
AR	aldose reductase
Arg	arginine
ATP	adenosine triphosphate
BCA	bicinchoninic acid
BH2	dihydrobiopterin
BH3	trihydrobiopterin
BH4	tetrahydrobiopterin
BKca	large conductance calcium-activated potassium channel
BSA	bovine serum albumin
CaM	calmodulin
CaMKII	calcium-calmodulin dependent kinase II
cAMP	cyclic adenosine monophosphate
cGMP	cyclic guanosine monophosphate
CGRP	calcitonin gene-related peptide
CICR	calcium-induced calcium release
CK	creatine kinase
CoQ	coenzyme Q
CuZnSOD	copper-zinc superoxide dismutase
Cyt C	cytochrome C
DAG	diacylglycerol
DM	diabetes mellitus
DHE	dihydroethidium
DHFR	dihydrofolate reductase
DHPR	dihydropteridine reductase
DOCA	deoxycorticosterone acetate
E/A	ratio of early to late ventricular filling
ECM	extracellular matrix
EDHF	endothelium-derived hyperpolarising factor
EF	ejection fraction
EJP	excitatory junctional potential
Emax	maximal drug response (efficacy)
eNOS	endothelial nitric oxide synthase
ET-1	endothelin-1
ETC	electron transport chain
F-6-P	fructose 6-phosphate
FA	fatty acid

FAD	flavin adenine dinucleotide
Fe	ferritin
FMD	flow-mediated dilatation
FMN	flavin mononucleotide
GAPDH	glyceraldehyde 3-phosphate dehydrogenase
GCH1	gtp cyclohydrolase 1
GFAT	glutamine fructose-6-phosphate amidotransferase
GlcN-6-P	glucosamine-6-phosphate
GLUT	glucose transporter
GSH	glutathione (reduced)
GSSG	glutathione (oxidised)
GTP	guanosine-5'-triphosphate
H_2O_2	hydrogen peroxide
HbA1c	glycated haemoglobin
hph-1	hyperphenylalaninemic mutant
HPLC	high-performance liquid chromatography
HRP	horseradish peroxidase
I/R	ischemia/reperfusion
IcaL	L-type calcium current
IFN-γ	interferon-γ
IKCa	intermediate conductance calcium-activated potassium channel
IL	interleukin
iNOS	inducible nitric oxide synthase
IPC	ischemic preconditioning
IVRT	isovolumic relaxation time
KDG	ketoglutarate dehydrogenase
KO	knock-out
LV	left ventricle
MCAD	medium chain acyl CoA dehydrogenase
MCP	monocyte chemotactic protein
mGCH1	myocardial-specific GCH1
MHC	myosin heavy chain
min	minute(s)
MLC	Myosin light chain
MMP	matrix metallopeptidase
MyBP-C	myosin-binding protein C
NAD	nicotinamide adenine dinucleotide
NADPH	nicotinamide adenine dinucleotide phosphate
NCX	sodium-calcium exchanger
NF-κB	nuclear factor kappa-light-chain-enhancer of activated B cells
nNOS	neuronal nitric oxide
NO	nitric oxide
NOS	nitric oxide synthase
O_2^-	superoxide
OCR	oxygen consumption
OGA	O-GlcNAcase

O-GlcNAc	O-linked N-acetylglucosamine
OGT	O-GlcNAc transferase
2-OHE	2-hydroxyethidium
ONOO-	peroxynitrite
ORO	oil red O
Ox-Phos	oxidative phosphorylation
PAI-1	plasminogen activator inhibitor-1
PARP	poly(ADP-ribose) polymerase
PCD	pterin-4a-carbinolamine dehydratase
PCr	phosphocreatine
PDK	pyruvate dehydrogenase kinase
PGH2	prostaglandin H2
PKA	protein kinase A
PKC	protein kinase C
PKG	protein kinase G
PLB	phospholamban
PPAR	peroxisome proliferator-activated receptor
PTPS	6-pyruvoyl-tetrahydropterin synthase
RAGE	receptor for advanced glycation end products
RLU	relative light unit
ROS	reactive oxygen species
RV	right ventricle
RyR	ryanodine receptor
s	seconds
SERCA	sarcoendoplasmic reticulum calcium ATPase
sGC	soluble guanylyl cyclase
SKca	small conductance calcium-activated potassium channel
SNS	sympathetic nervous system
SOD	superoxide dismutase
SR	sepiapterin reductase
SR	sarcoplasmic reticulum
T1D	type 1 diabetes
T2D	type 2 diabetes
TAG	triglyceride
TCA	tricarboxylic acid cycle
TDI	tissue Doppler imaging
Tg	transgenic
TGF	transforming growth factor
TNFα	tumour necrosis factor α
TXA2	thromboxane A2
UCP	uncoupling protein
UDP-GlcNAc	uridine diphosphate N-acetylglucosamine
VDAC	voltage-dependent anion channel
VEGF	vascular endothelial growth factor
VOCC	voltage-operated calcium channel
WT	wild-type

List of pharmacological agents

Acetylcholine	2-acetyloxyethyl(trimethyl)azanium
Antimycin A	[(2R,3S,6S,7R,8R)-3-[(3-formamido-2-hydroxybenzoyl)amino]-8-hexyl-2,6-dimethyl-4,9-dioxo-1,5-dioxonan-7-yl] 3-methylbutanoate
Apamin	CNCKAPETALCARRCQQH (peptide sequence)
BH4	(6R)-5,6,7,8-Tetrahydrobiopterin
D-NAME	NG-nitro-D-arginine methyl ester
FCCP	Carbonyl cyanide 4-(trifluoromethoxy)phenylhydrazone
L-NAME	NG-nitro-L-arginine methyl ester
Lucigenin	bis-N-methylacridinium nitrate
L-VNIO	Vinyl-l-N-5-(1-imino-3-butenyl)-l-ornithine
nor-NOHA	N-hydroxy-nor-L-arginine
Oligomycin A	(1S,4R,5E,5'S,6'S,7E,10R,11S,12R,14S,15R,16R,18S,19R,20S,21E,25R,26S,27R,29R) -4-ethyl-11,12,15,19-tetrahydroxy-6'-[(2R)-2-hydroxypropyl]-5',10,12,14,16,18,20,26,29-nonamethylspiro[24,28-dioxabicyclo[23.3.1]nonacosa-5,7,21-triene-27,2'-oxane]-13,17,23-trione
Phenylephrine	3-[(1R)-1-hydroxy-2-(methylamino)ethyl]phenol
SMTC	S-methyl-L-thiocitrulline
Tiron	4,5-Dihydroxy-1,3-benzenedisulphonic acid
Tram-34	1-[(2-Chlorophenyl)diphenylmethyl]-1H-pyrazole
U46619	(Z)-7-[(1S,4R,5R,6S)-5-[(E,3S)-3-hydroxyoct-1-enyl]-3-oxabicyclo[2.2.1]heptan-6-yl]hept-5-enoic acid

List of antibodies and gene probes

Protein of interest	Dilution	Host Species	Source
ACC	1:1000	Rabbit	Cell Signalling, USA
ACC-Phospho Ser79	1:1000	Rabbit	Cell Signalling, USA
eNOS	1:2000	Mouse	BD Biosciences, USA
GAPDH	1:25 000	Rabbit	Millipore, USA
GLUT-1	1:1000	Rabbit	Millipore, USA
GLUT-4	1:5000	Rabbit	Millipore, USA
Histone H3	1:1000	Rabbit	Abcam, UK
Histone H3-Ac	1:1000	Rabbit	Millipore, USA
iNOS	1:1000	Rabbit	Abcam, UK
MCAD	1:1000	Mouse	Abcam, UK
NCX	1:2000	Rabbit	Santa Cruz, USA
nNOS	1:1000	Mouse	Santa Cruz, USA
PDK4	1:1000	Rabbit	Abgent, USA
PKCβII	1:1000	Rabbit	Santa Cruz, USA
PKCβII/δ-Phospho Ser660	1:1000	Goat	Santa Cruz, USA
PLB	1:5000	Mouse	Badrilla, UK
PLB-Phospho Ser16	1:2000	Rabbit	Badrilla, UK
PLB-Phospho Thr17	1:2000	Rabbit	Santa Cruz, USA
PPARα	1:1000	Rabbit	Sigma-Aldrich, USA
RAGE (C-)	1:5000	Rabbit	ThermoScientific, USA
RAGE (N-)	1:1000	Mouse	Santa Cruz, USA
SERCA	1:5000	Goat	Santa Cruz, USA
TnI	1:2000	Rabbit	Santa Cruz, USA
UCP3	1:1000	Rabbit	ThermoScientific, USA
UCP3 blocking peptide	1:1000	Rabbit	ThermoScientific, USA
VDAC	1:2000	Mouse	Abcam, UK
α-KGD	1:1000	Goat	Santa Cruz, USA
Goat anti-mouse IgG	1:5000		Promega, USA
Goat anti-rabbit IgG	1:5000		Promega, USA
Donkey anti-goat IgG	1:5000		Santa Cruz, USA

Gene of interest	Reference sequence no.
IL-1β	NM_008610.2
MCP-1	NM_011333.3
MMP-2	NM_008610.2
MMP-9	NM_013599.3
Collagen 1A1	NM_007729.2
GLUT-1	NM_148938.3
GLUT-4	NM_009204.2
α-actinin	NM_033268.4

Declaration

I, Drew Duglan, confirm that I am the author of this work. This work has been carried out by myself, unless otherwise stated in the methodology. The contributions of additional persons is duly noted and all cited references within this thesis have been consulted. None of the work contained in this thesis has previously been accepted for a higher degree.

Drew Duglan, October 2015

Chapter 1

General Introduction

Pathology of diabetes mellitus

Diabetes is a condition characterised by long-term hyperglycaemia that arises as a result of metabolic dysregulation. Depending on the type, this dysregulation originates either from auto-immune destruction of pancreatic β-cells and ensuing insulin deficiency (type I), or tissue insulin resistance (type II). Estimates for the next decade project that in the UK alone, greater than 4 million people will have a diagnosis of diabetes, with at least 10% of these being type I in aetiology (1). While dietary and lifestyle interventions have been shown to effectively put type II diabetes into remission (2-4), type I still remains a chronic and incurable condition.

A significant proportion of the mortality and morbidity associated with diabetes comes from the development of cardiovascular complications; notably ischaemic heart disease and stroke, as well as conditions of the periphery such as neuropathy, nephropathy, retinopathy and peripheral vascular disease (5). These conditions often result from significant alterations to circulating factors and cellular cascades in the diabetic state. For example, insulin resistance or lack of insulin signalling is in itself detrimental, while increases in circulating lipids and inflammatory cell recruitment (driving atherosclerosis) have been implicated in the development of diabetic complications. The other significantly damaging effects on the vascular endothelium and neurones can be brought about directly by the presence of hyperglycaemia.

Which detrimental cellular pathways are triggered by hyperglycaemia?

Polyol pathway flux

High intracellular glucose concentrations activates a number of detrimental cascades, one of which being increased polyol pathway flux. The enzyme aldose reductase, which normally acts to convert toxic aldehydes to inert alcohols, can also reduce high levels of glucose to sorbitol (6). However, this process overconsumes the cofactor NADPH, which is also normally critical to the generation of the abundant intracellular antioxidant reduced glutathione (GSH) (7). Indeed, in diabetic patients and

animal models an increase in sorbitol accumulation has been reported in the lens and peripheral nerves (8-10); furthermore, pharmacological inhibition or genetic deletion of aldose reductase was shown to prevent the depletion of GSH and halt diabetic neuropathy (11, 12).

Advanced glycation end products

The hyperglycaemic environment in diabetes also induces the formation of advanced glycation end products (AGEs), formed from the non-enzymatic glycation reaction (Maillard reaction) between glucose (and other saccharide intermediates) and reactive protein residues (13, 14). Brownlee and colleagues have shown that cultured endothelial cells exposed to hyperglycaemia rapidly accumulate intracellular AGEs, which can modify proteins critical to vascular injury, such as fibroblast growth factor (15, 16). In addition, it has been suggested that AGE adducts may contribute to impaired cellular proteolytic activity associated with diabetes, potentially exposing proteins to damaging oxidative modifications (17). Aside from intracellular targets, AGEs can also induce cross-links on extracellular matrix proteins such as laminin, fibronectin and collagen, which has been shown to alter cellular morphology, as well as negatively impact matrix self-assembly and cellular outgrowth and adhesion (18-21).

After diffusion from the cell, AGEs can have more remote effects through the modification of plasma proteins and their subsequent interaction with cell surface receptors, predominantly scavenger receptors, galectin-3 and the receptor for AGEs (RAGE). It is hypothesised that scavenger receptors and galectin-3 expressed on macrophages play an important role in the endocytic clearance of glycated proteins (22, 23), with any barrier to this process potentially exacerbating peripheral diabetic pathologies (24, 25). The major receptor for AGEs, RAGE, can be expressed directly on vascular endothelial cells, which has been shown to be upregulated in patients with diabetes, as well as associated with markers of chronic inflammation (26, 27). Furthermore, animal models with either RAGE overexpression or inhibition have been shown to result in either the exacerbation or prevention of diabetic vasculopathies, respectively (28-30). The pro-inflammatory response is likely attributed to

the activation of RAGE on macrophages, where its expression is tied closely to NF-κB, IFN-γ and IL-6 at the transcriptional level (31). It has been suggested that the reciprocal regulation of RAGE and these inflammatory cytokines can establish a positive feedback loop, in which the release of RAGE ligands during tissue damage can drive further production of both pro-inflammatory molecules and RAGE, leading to sustained activation of the innate (32), and potentially the adaptive immune response (33).

Protein Kinase C activity

The unregulated entry of glucose into endothelial and neuronal cells in the diabetic state stimulates the *de novo* synthesis of the lipid derivative diacylglycerol (DAG) via the glycolytic intermediate dihydroxyacetone phosphate (DHAP) (34, 35); moreover, this DAG increases the activation of its downstream target PKC, particularly the β and δ isoforms (36-38). PKC acts as an effector of numerous downstream cellular pathways; it promotes pro-inflammatory gene expression, stimulates smooth muscle cell proliferation, activates intracellular sources of ROS and impairs endogenous mediators of vasodilatation; all of which coalesce to facilitate vascular dysfunction (Figure 1.1; for review see (39)). Furthermore, the aberrant activation of additional PKC isoforms by upstream AGE accumulation has also been reported in experimental diabetes (40-42), which highlights the reinforcing interaction between these cellular mechanisms in the promotion of diabetic complications.

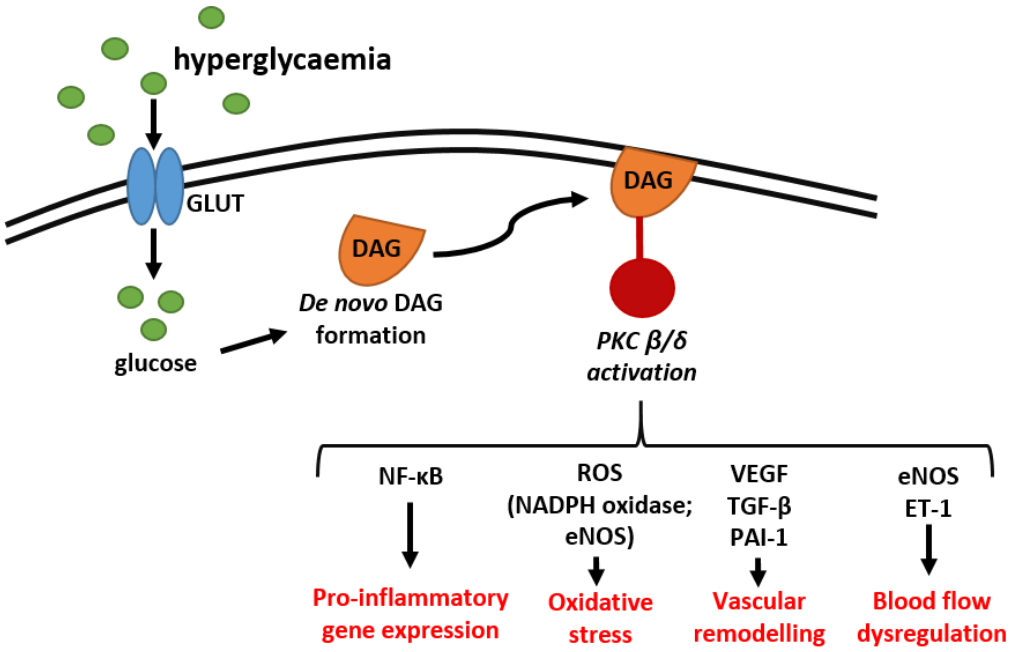


Figure 1.1. Aberrant PKC signalling in response to hyperglycaemia.

Increased intracellular glucose leads to greater formation of the lipid derivative diacylglycerol (DAG). DAG is recruited to the cell membrane where it increases the activation of PKC β/δ isoforms. PKC activates a number of detrimental cascades downstream: it alters the transcriptional profile towards a pro-inflammatory state; it promotes ROS production through NADPH oxidase and reduced NO availability; it stimulates vascular growth factor signalling to induce proliferation and remodelling; and it can lead to blood flow abnormalities by altering the balance of mediators that regulate vasodilatation and vasoconstriction.

Hexosamine Pathway

A principal feature in the development of vascular disease in diabetes (as well as other cardiovascular conditions) is excessive growth factor signalling and an increase in vascular cell proliferation (43-45). A prime mediator of this vascular remodelling is an increase in the transcription of the transforming growth factors (TGF), as well as plasminogen activator inhibitor-1 (PAI-1), which inhibits the process of fibrinolysis and promotes thrombosis (46-48). The pathological pattern of gene expression appears to be initiated by the accumulation of excess intermediates of glycolysis, specifically fructose-6-phosphate (F-6-P; (49)). In the hexosamine pathway, F-6-P amidotransferase (GFAT) converts F-6-P with glutamine into the products glucosamine-6-phosphate (GlcN-6-P) and glutamate. Further metabolism leads to the production of UDP-N-acetylglucosamine (UDP-GlcNAc), which is a modifier of serine/threonine residues on cytosolic and nuclear proteins (Figure 1.2). This GlcNAc signalling has been directly linked to the altered transcriptional programming of vascular cells during

hyperglycaemia (50-52). This, combined with the markedly higher expression of GFAT in vascular smooth muscle cells as compared to other tissues (53), may contribute to the characteristic vascular complications in the progression of diabetes.

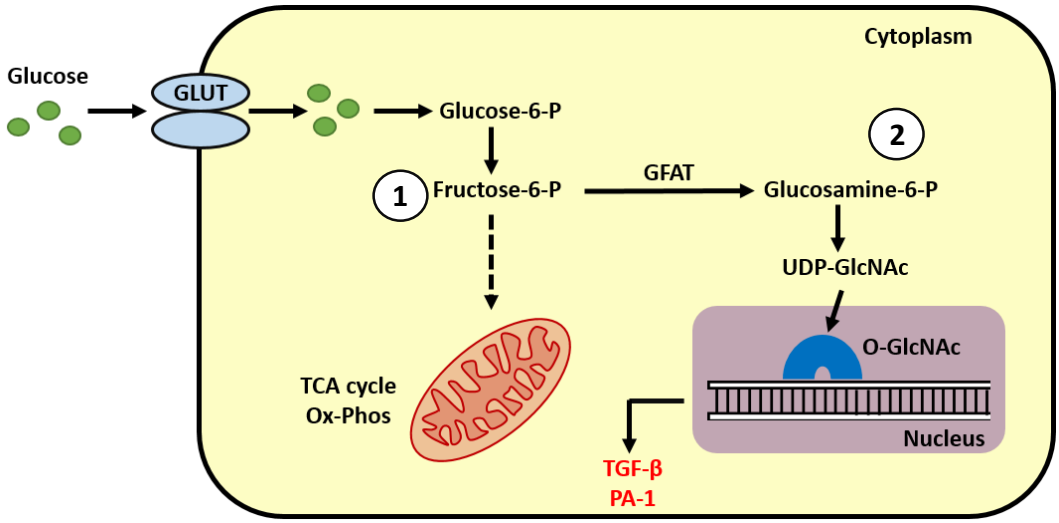


Figure 1.2. Hexosamine pathway activation by high intracellular glucose.

Under normal conditions, glycolysis continues from fructose-6 phosphate through a number of intermediates to produce pyruvate for the TCA cycle in the mitochondria, subsequently generating electrons for oxidative phosphorylation **(1)**. However, under conditions of high glucose, some of this fructose-6-phosphate is diverted to produce glucosamine-6-phosphate by GFAT, with the final product being UDP-N-acetylglucosamine **(2)**. The action of transferases can add the N-acetylglucosamine substrate as O-glycosidic linkages to cytosolic and nuclear proteins; the end result is modified protein function and the increased transcription of genes involved in vascular remodelling.

All paths stem from ROS

It is hypothesised that the common denominator in all of these cellular mechanisms is the generation of cellular oxidative stress. Oxidative stress is driven by the increased production of free radicals, which are highly reactive in the cell due to the availability of unpaired electrons within their molecular structure. Although reactive oxygen species (ROS) appear to play an important role in cellular signalling pathways and likely contribute to adaptive hormetic stress responses (see (54) for review), chronically elevated ROS production and oxidative stress have been implicated in the pathology of several disease states (55-58).

Hyperglycaemia drives mitochondrial ROS production

Normal glucose metabolism through the tricarboxylic acid (TCA) cycle generates NADH, and to a lesser extent $FADH_2$, which then act as electron donors to the mitochondrial electron transport chain (ETC). As electrons are transferred along the ETC from Complexes I to IV, their energy is used to pump H^+ ions across the mitochondrial membrane to generate a voltage gradient. This voltage gradient can be used at the site of the ATP synthase enzyme to produce energy in the form of ATP, which is likely regulated by uncoupling proteins (UCPs) as a way of maintaining stable rates of ATP production (Figure 1.3).

However, in the diabetic state, elevated intracellular glucose disrupts the normal anaerobic and aerobic stages of metabolism, whereby the voltage gradient generated across the membrane can be dispersed through aberrant electron leakage in the ETC. (59). It is hypothesised that electrons accumulate at coenzyme Q and are donated to molecular oxygen to produce superoxide (O_2^-), although the exact site of superoxide generation within the chain is still a matter of debate (60, 61). There is also the suggestion that the distinct complexes produce differing levels of ROS, which can actually be modulated by different substrate utilisation, which may underpin some of the mechanisms associated with ageing and intermittent fasting (62). Nevertheless, endothelial cells exposed to high glucose concentrations have been shown to generate increased ROS, which can be abolished by inhibition of complex II, as well as by dissipating the proton gradient through increased uncoupling (63).

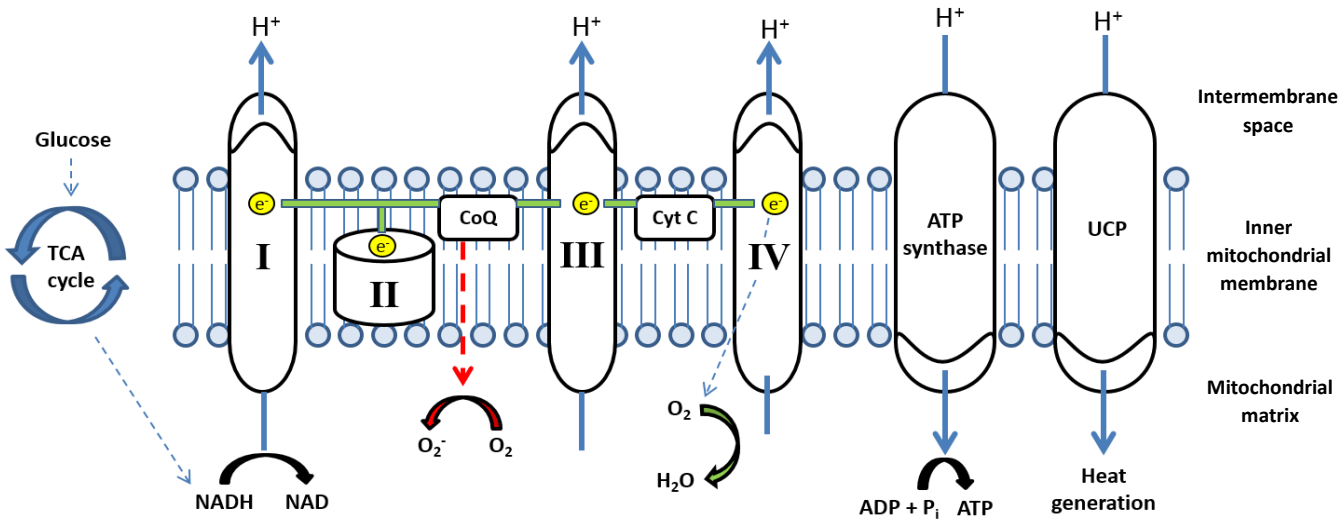


Figure 1.3. Energy production from glucose in the mitochondrial electron transport chain.

As glucose is metabolised through glycolysis and the TCA cycle, the generated NADH and $FADH_2$ donate electrons to complex I (and complex II) of the electron transport chain. The energy from electron transfer along the chain is used to extrude protons into the intermembrane space, generating a voltage gradient across the inner mitochondrial membrane. The proton gradient is used to drive the ATP synthase enzyme to produce ATP in the mitochondrial matrix. Uncoupling proteins in the membrane function to dissipate some of the proton gradient as heat, thereby regulating ATP production. Under normal conditions, electrons are donated at complex IV to molecular oxygen to produce H_2O. Under conditions of high intracellular glucose, electron donor flux is increased and the mitochondrial voltage increases towards a critical threshold. At this point, flux is blocked and excessive electrons are donated to molecular oxygen, instead producing the damaging free radical superoxide (O_2^-).

Oxidative stress initiates the pathways of diabetic damage

In many of these studies, a strong interplay has been revealed between oxidative stress and the onset of pathways associated with hyperglycaemic damage. The excessive consumption of NADPH through polyol pathway flux and the depletion of GSH reduces a cell's antioxidant capacity and leaves it vulnerable to redox stress (64-66). The production of glucosamine via hexosamine pathway flux similarly reduces NADPH generation and availability by inhibiting normal glucose metabolism through the pentose phosphate pathway (67). Glucosamine is also a potential trigger of further oxidative stress, where it has been shown to increase hydrogen peroxide production in pancreatic β-cells, which may underlie the impaired function of these cells from GFAT overexpression (68).

Nishikawa et al. have shown that preventing mitochondrial O_2^- production prevents the increases in PKC activation induced by high intracellular glucose (63), moreover, PKC activation in the diabetic state can be normalised experimentally with antioxidant treatment (69). It has also been suggested that

PKC contributes to the notion of “hyperglycaemic memory,” where persisting ROS-mediated vascular dysfunction even after glucose normalisation has been linked to an epigenetic cascade activated by PKCβII (70).

AGE formation is dependent on the initial rearrangement of Schiff bases and subsequently Amadori products, which require oxidation to generate the advanced glycation species (71). This demonstrates how an environment of oxidative stress can contribute first to the generation of AGEs, as well as provide conditions that promote their detrimental modifying actions. At the level of the cell it has also been demonstrated that AGEs induce further oxidative stress, where they are able to activate pro-inflammatory cascades, for example PKCβ and NF-κB (72, 73).

Linking mitochondrial ROS production to these detrimental cellular cascades is the cellular depletion of glyceraldehyde-3 phosphate dehydrogenase (GAPDH). Du et al. demonstrated that the O_2^- generated by mitochondria under high glucose conditions can induce DNA strand breaks, at the same time increasing the poly(ADP-ribosylation) of GAPDH (74). Poly(ADP-ribose) polymerase (PARP) is a critical enzyme required for DNA repair and may produce these polymers of ADP-ribose after the translocation of GAPDH to the nucleus (74, 75). This modification is thought to reduce the activity and availability of cytosolic GAPDH, thereby causing an accumulation of glycolytic intermediates further upstream (74). This decrease in GAPDH activity has indeed been associated with the diversion of intermediates into the aforementioned damaging metabolic pathways (74, 76); moreover, Garcia et al. showed that PARP inhibition could prevent the impaired endothelial function observed in diabetic animals (77).

In addition to mitochondrial O_2^- production, cellular redox balance is also dependent on other ROS sources and antioxidant pathways, many of which have been implicated in the pathology of diabetes. Another major producer of O_2^- and H_2O_2 is NADPH oxidase, which can be activated in endothelial cells (and indeed cardiomyocytes) incubated under high glucose conditions (78-81), as well as by oxidised LDL (82). Moreover, NADPH oxidase inhibition has been shown to be successful in preventing vascular

dysfunction in diabetes (83) and in the amelioration of diabetic nephropathy (84). As well as the circulating factors of hyperglycemia and dyslipidemia, NADPH oxidase activity can be induced via other intracellular pathways and modifications that are upregulated in the diabetic state. The generation of AGEs has been linked to NADPH oxidase activity, where a number of studies have demonstrated the activation of NADPH oxidase by glycated proteins, which is likely mediated via PKC (41, 85, 86).

Xanthine oxidase is also a source of O_2^- production, which is normally derived from purine metabolism in the generation of uric acid. Xanthine oxidase can in fact bind to the vascular endothelium to produce O_2^- (87), moreover, the elevation in vascular ROS production in diabetic animals can be normalised by inhibiting the enzyme with allopurinol (88, 89). Desco et al. have also shown that the same treatment in human type 1 diabetic subjects is able to attenuate glutathione depletion and the formation of lipid peroxides (88).

The neutralisation of O_2^- involves the activity of superoxide dismutase (SOD), which is expressed in cytoplasmic, mitochondrial and extracellular forms, and converts the superoxide to H_2O_2. In various cell types from different diabetic models studies have reported decreases in SOD activity (90, 91), moreover, in the vasculature, exogenous SOD treatment has been shown to rescue the impairment in endothelial-dependent vasodilatation, likely due to maintained NO bioavailability (92, 93). Closely associated with SOD is the enzyme catalase, which further dismutates H_2O_2 to water and oxygen. Similar to SOD, diabetes is linked with depressed catalase activity in the vascular endothelium in association with increased oxidative stress (94, 95). Conversely, Ye et al. have demonstrated that in type 1 diabetic mice, catalase overexpression was able to attenuate the oxidative damage in isolated cardiomyocytes, as well as the functional deficit (Ye Diabetes 2004). Similar protective effects of catalase have also been observed in insulin-producing cell lines, suggesting the possible damaging effects of H_2O_2 on pancreatic ß-cells during the onset of diabetes (96).

Other antioxidant enzymes with H_2O_2 as a major substrate include glutathione peroxidase, which, depending on the genetic variant, has been associated with vascular morphology in type 2 diabetic

patients, potentially being predictive of vascular disease (97). Similarly, lower serum levels of the peroxidase enzyme in general have been observed in diabetic patients and implicated in the development of nephropathy (98). In animal studies, Lewis et al. have shown that genetic deficiency in glutathione peroxidase leads to accelerated atherosclerosis in diabetes, ascribed to increases in oxidative stress and pro-inflammatory signalling (99).

More recently recognised is the role of peroxiredoxin in H_2O_2 neutralisation, a deficiency of which can increase susceptibility to oxidative damage and apoptosis (100-102). Interestingly, genetic ablation of peroxiredoxin has been shown to simulate diabetic pathophysiology, leading to insulin resistance and reduced insulin secretion (103). Underlying this was an alteration in pancreatic islet morphology and increased inflammatory signalling, suggesting that peroxiredoxin may be essential for antioxidant defence against pancreatic damage during diabetes. Also critical for peroxiredoxin function is thioredoxin, which is utilised (oxidised) in the process of dismutating H_2O_2. Tochetti et al. have shown that mitochondrial function in cardiomyocytes from db/db mice is impaired, and that this is associated with greater H_2O_2 emission and reduced status of the thioredoxin system (104). While a number of redox systems have evolved to neutralise H_2O_2, enabling substitution when necessary (e.g. thioredoxin for GSH), a common requirement between them is a continuous supply of NADPH-dependent reducing equivalents. Thus, in the event of increased polyol pathway flux described in diabetes, the depletion of NADPH would compromise several antioxidant defences in addition to glutathione.

Up until this point, the discussion of oxidative stress in diabetic pathology has mostly centred on direct intracellular ROS production, as well as the positive feedback loop between ROS and the cellular pathways activated during hyperglycaemia. However, a major bridge between all of these elements and the observed vascular endothelial dysfunction in diabetes is the impairment in nitric oxide (NO) signalling.

Nitric oxide synthase and NO signalling

NOS structure

Since the 1980s the significance of NO has been recognised, in that this free radical molecule is the endothelium-derived relaxing factor responsible for the dilatation of the vasculature (105, 106). NO is generated by nitric oxide synthase (NOS), a dimeric 300kDa enzyme composed of two identical monomers, each of which contains a C-terminal reductase domain and an N-terminal oxygenase domain (107). Critical to NOS function is a series of cofactors: NADPH, flavin adenine dinucleotide (FAD) and flavin adenine mononucleotide (FMN) bind to the reductase domain, while the oxygenase domain binds haem ion (to enable electron flux between domains) and tetrahydrobiopterin (BH4, see below). Between these domains lies the calcium calmodulin complex (CaM), which acts as a molecular switch to facilitate electron flow during catalysis (108). Under physiological conditions, NOS catalyses amino acid conversion, utilising L-arginine and molecular oxygen to produce both L-citrulline and NO. (Figure 1.4).

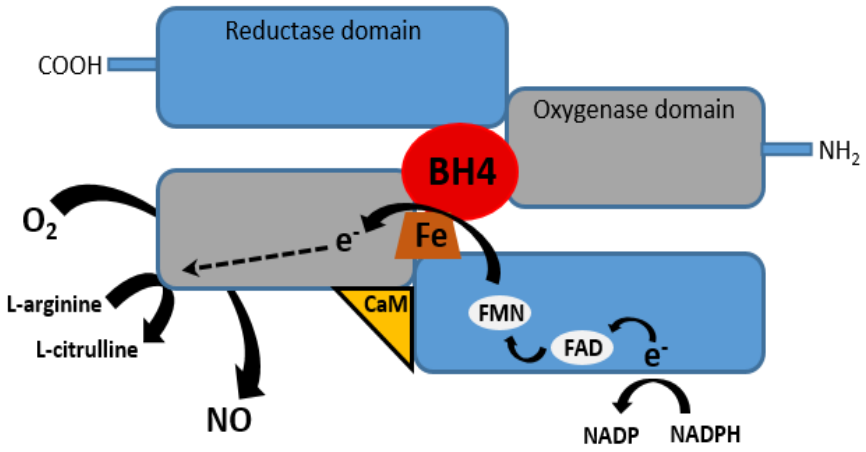


Figure 1.4. NOS structure and NO synthesis.

NADPH donates electrons to FAD in the C-terminal reductase domain, which flows to FMN and subsequently to the oxygenase domain, where it is used to drive NO production and L-citrulline from O_2 and L-arginine. The BH4-ferritin complex functions to promote and stabilise dimerization, as well as facilitate electron transfer.

Physiological role of NOS in the vasculature

Constitutive NO production is carried out by the endothelial (eNOS) and neuronal (nNOS) isoforms, while the inducible form (iNOS) is normally expressed and active in response to acute injury and inflammation (109). In the circulation eNOS is a regulator of vascular tone, where it is highly expressed and activated in response to mechanical laminar shear stress and endogenous mediators e.g. bradykinin. The NO produced by eNOS then diffuses to the neighbouring vascular smooth muscle cells where it acts on the enzyme soluble guanylyl cyclase (sGC). sGC catalyses the formation of cyclic nucleotide monophosphate (cGMP), which acts as a second messenger that can trigger several cellular components, largely acting through its immediate downstream target – protein kinase G (PKG). Carrier et al. have shown that a PKG-dependent increase in potassium conductance through BK_{Ca} channels promotes vasorelaxation through K^+ efflux and vascular smooth muscle cell hyperpolarisation (110). PKG is also associated with intracellular events that reduce the level of cytosolic calcium, thereby favouring vasodilatation. Rapoport has suggested a PKG-mediated inhibition of IP_3 formation, which consequently impairs Ca^{2+} liberation from the sarcoplasmic reticulum (111). This may then be complemented by phosphorylation of phospholamban for activation of the SR Ca^{2+}-ATPase pump and sequestration of calcium back into intracellular stores (112). The other main effect of PKG is a direct inhibition of the cellular contractile machinery, stimulating the action of kinases to dephosphorylate the myosin light chain (113) (Figure 1.5). Along with actively stimulated NO production, eNOS has also been implicated in a mechanism of continuous release, potentially contributing to setting basal vascular tone through tonic vasodilatation (114).

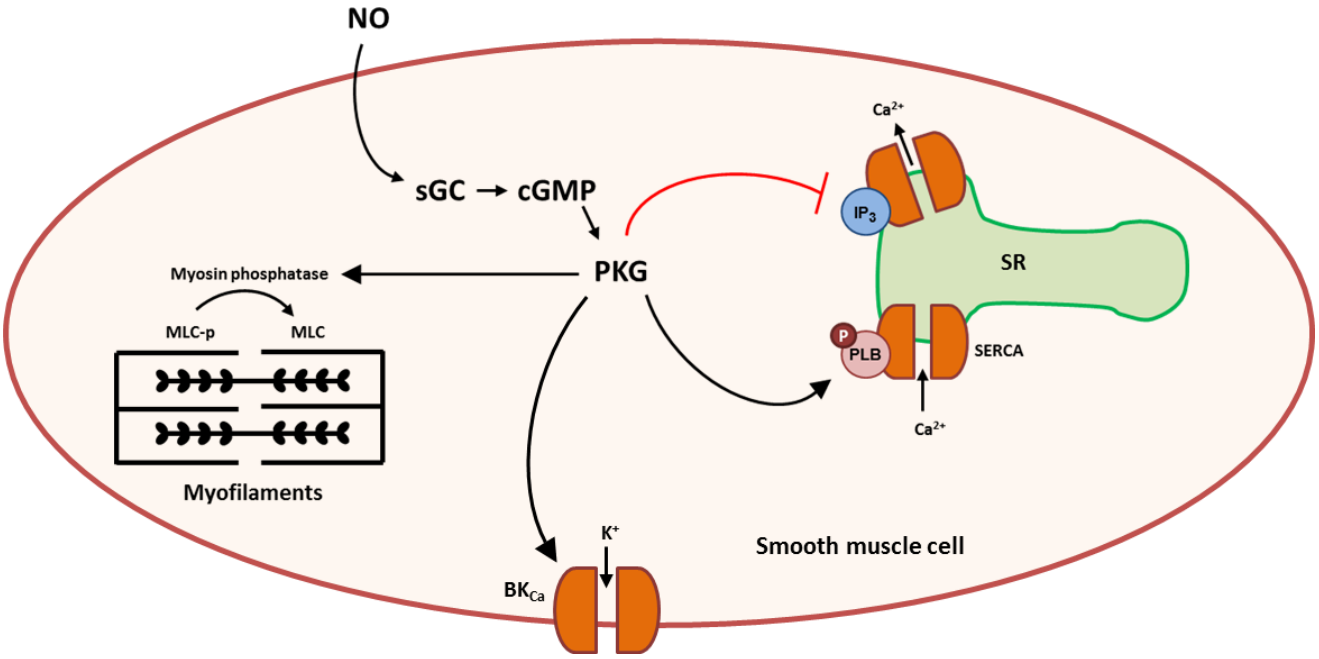


Figure 1.5. Mechanisms of PKG-mediated vascular smooth muscle relaxation.

The diffusion of nitric oxide from adjacent vascular endothelial cells facilitates vasorelaxation largely through the actions of PKG downstream. PKG simultaneously regulates different calcium channels on the sarcoplasmic reticulum (SR), promoting Ca^{2+} sequestration through SERCA, as well as inhibiting IP_3-triggered Ca^{2+} liberation. PKG additionally activates large-conductance, Ca^{2+}-activated K^+ channels (BK_{Ca}) on the cell membrane, leading to increased K^+ efflux and relaxation via cell hyperpolarization. The myofilaments of the smooth muscle cell can also be influenced by PKG more directly. The activation of myosin phosphatase enables the dephosphorylation of the regulatory myosin light chain (MLC), subsequently preventing the development of actin-myosin cross-bridges and ultimately leading to muscle relaxation.

The focus shifted more recently to explore the influence of the neuronal isoform on vascular control, enabled largely through the advent of the nNOS-specific inhibitor SMTC. Indeed, original studies of the renal vasculature in rodents determined that nNOS inhibition led to increased vasoconstriction and thus a significant reduction in the observed arteriolar diameters (115). Additionally, Seddon et al. have now established a major regulatory role for nNOS in the human circulation, via blood flow measurements in both brachial and coronary arteries (116, 117). These experiments also pointed to a system of regulation in which the nNOS isoform helps to modulate the basal level of arterial tone, whereas its endothelial counterpart may be more responsible for changes to the local distribution of blood flow. However, this conclusion has been challenged by studies in other experimental settings, which, taken together, suggest that the control of vascular tone may be further dependent on the specific vascular bed and the nature of the local stimulus (117-119). Despite an established role for

nNOS-derived NO on blood flow regulation, there is still no consensus on the cellular origin of this species, which will be discussed in more detail in Chapter 3.

NOS in the myocardium

Aside from the vasculature, constitutive NOS is also expressed in cardiomyocytes, where it helps to modulate cardiac EC-coupling. eNOS is largely localised to caveolae within the sarcolemmal membrane (120), although it can additionally bind to the nuclear membrane (121). Functionally, eNOS-derived NO in the heart has been associated by some with the negative regulation of β-adrenergic signalling. At the level of the myocyte, Martin et al. have shown that older (but not younger) $eNOS^{-/-}$ mice have a reduced inotropic response to β-stimulation (122), while Wang and colleagues reported a reduction in response and attributed this to a decrease in the L-type Ca^{2+} current (ICa_L) (123). However, Godecke et al. showed no change in the β-responsiveness of isolated cells from $eNOS^{-/-}$ mice, despite seeing the effect *in vivo* and in the perfused heart (124). Aside from the potential confounders of experimental protocol and mouse strain and age differences, it has been proposed that conflicting findings may be dependent on the varying degrees of both autocrine and paracrine influences of eNOS-derived NO in the abovementioned studies (124, 125).

In the cardiomyocyte nNOS is predominantly localised to the sarcoplasmic reticulum, where it associates with the ryanodine receptor (RyR) (126) and the enzyme xanthine oxidase (XO) (127), although a proportion of nNOS also exists at the sarcolemmal membrane as part of the dystrophin-glycoprotein complex, in association with the plasma-membrane Ca^{2+}-ATPase (PMCA) (128, 129). nNOS has been shown to regulate several components of EC-coupling under normal physiological circumstances; acute inhibition or genetic deletion of nNOS has been shown to increase Ca^{2+} influx across the sarcolemmal membrane and is associated with enhanced LV ejection fraction (130). Equally, Carnicer et al. have demonstrated in a model with increased myocardial nNOS activity (via increased BH4 levels) that ICa_L density is reduced (131).

Along with regulation of calcium entry into the cardiomyocyte, nNOS may also be involved in the control of calcium-induced calcium release (CICR) through the RyR. Gonzalez et al. have shown that a loss of nNOS-derived NO causes a reduction in S-nitrosylation of the RyR, accompanied by an increase in open probability and diastolic Ca^{2+} leak (132). However, this is in direct contrast to other reports of reduced RyR leak after nNOS gene deletion (133), as well as increased diastolic Ca^{2+} leak during enhanced myocardial nNOS activity (131). Some of this discrepancy may be explained by different intracellular conditions and a biphasic action of NO dependent on concentration, as has been suggested for RyR activity in skeletal muscle (134). Given the sensitivity of the RyR to different redox modifications (135, 136) and the reactive nature of NO with other modifiable species, the role of nNOS in RyR function is likely dependent on the overall nitroso-redox balance (137, 138).

Along with the potential role for nNOS in the Ca^{2+} release portion of EC-coupling, strong evidence exists for the role of nNOS in the regulation of Ca^{2+} reuptake to facilitate myocardial relaxation. Zhang et al. have shown that LV myocytes subjected to acute nNOS inhibition or from $nNOS^{-/-}$ mice both display prolonged relaxation time, which was accompanied by decreased phosphorylation (Ser^{16}) of phospholamban (PLB) mediated through PKA (139). This has since been reinforced by Carnicer et al., who showed that enhanced myocardial nNOS activity increased the phosphorylated PLB fraction, thereby increasing Ca^{2+} sequestration by SERCA and accelerating cardiomyocyte relaxation time (131). In addition to the widespread reports in the vasculature, this latter study has also highlighted the importance of the coupled status of NOS in the myocardium with respect to function, and the reliance on its biopterin cofactor BH4.

The role of BH4 in NOS function

BH4 metabolism

The linear *de novo* pathway in biopterin biosynthesis ultimately terminates with the generation of BH4, for which the rate-limiting step is catalysed by the enzyme GTP cyclohydrolase I (GCH1) (140). Following this primary reaction, enzymes 6-pyruvoyl tetrahydrobiopterin synthase (PTPS) and sepiapterin reductase (SR) catalyse subsequent reactions via the intermediates 7,8-dihydroneopterin triphosphate and 6-pyruvoyl-tetrahydrobiopterin (Figure 1.6). Aside from *de novo* formation, BH4 can also be produced through a salvage pathway from 7,8-dihydrobiopterin (BH2) by dihydrofolate reductase (DHFR). BH2 can be generated either directly from sepiapterin (since SR participates in both the *de novo* and salvage pathways) or from the oxidation of BH4 in an environment of redox imbalance. In addition, BH4 can also be regenerated after it has been utilised as a cofactor by the aromatic acid hydroxylases (AAH), where the oxidised product tetrahydrobiopterin 4a-carbinolamine is reconverted back to BH4 through sequential dehydration and reduction reactions (141).

Catalytic role of BH4

As a cofactor for NOS, BH4 binds with heme and the substrate L-arginine in the oxygenase domain, which forms the active site for NO biosynthesis (142). Klatt et al. showed that BH4 largely acts as an allosteric modulator of NOS to increase the binding affinity of L-arginine, as well as a stabiliser for NOS subunit dimerization (143, 144). However, it has also been recognised that BH4 has a redox contribution to NOS catalysis through electron donation to the heme-oxygen complex, resulting in the formation of a trihydrobiopterin (·BH3) radical (145, 146). This contribution has further been evidenced by studies utilising redox "silent" analogues of BH4 that appear unable to support enzymatic turnover (147, 148).

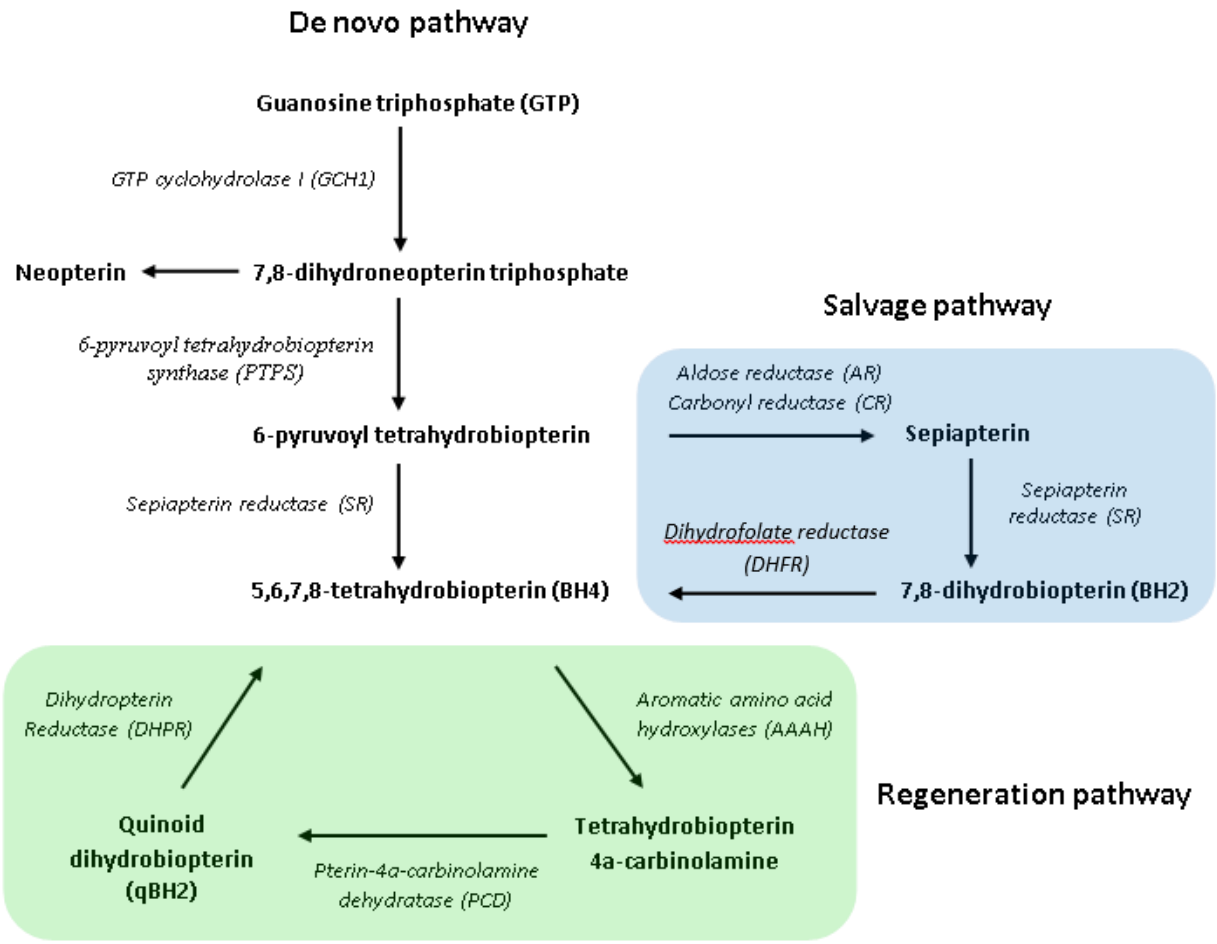


Figure 1.6. Cellular pathways of BH4 biosynthesis.

BH4 is synthesised *de novo* from the nucleoside substrate GTP, with GCH1 catalysing the rate-limiting step. Biopterin intermediates sepiapterin and BH2 can also be recycled back to BH4 via the salvage pathway (blue). In addition, BH4 can be regenerated from by-products of AAH reactions after its initial utilisation as a cofactor (green).

NOS uncoupling

The significance of BH4 bioavailability to proper NOS function is apparent from the concept of "uncoupling," whereby BH4 insufficiency causes electron flow to be uncoupled from L-arginine oxidation; a reduction of molecular oxygen results in the formation of the reactive oxygen species superoxide (O_2^-) instead of NO (149, 150). Furthermore, the reaction of NO with O_2^- generates peroxynitrite ($ONOO^-$), which has been shown to rapidly oxidise BH4 to ·BH3 and subsequently BH2 (151, 152). The consequences for NO production are two-fold: BH4 oxidation further reduces its bioavailability for NOS catalysis, moreover, BH2 can actively diminish NO synthesis by competing with

BH4 for the NOS binding site, despite its own lack of cofactor activity (153, 154). This demonstrates an environment where NO production is dependent not solely upon the levels of BH4, but perhaps more on the ratio of BH4 to its other oxidised pterin intermediates (155). With this in mind, studies have shown the importance of the salvage pathway in the maintenance of NOS coupling, specifically the role of DHFR. Crabtree et al. have established that DHFR inhibition *in vivo* significantly increases BH4 oxidation to BH2 in the lung and aorta, which is most pronounced in a setting of pre-existing BH4 deficiency (156). This impairment in BH4 recycling may also be crucial in the myocardium, as has been suggested by Ren et al., who reported depressed levels of DHFR following severe streptozotocin (STZ)-induced diabetes (157). A further recently recognised mechanism of eNOS uncoupling is through S-glutathionylation of specific cysteine residues by oxidised glutathione (GSSG), as shown by Chen et al. *in vitro*. In addition, these authors also observed impaired endothelial-dependent vasodilation *ex vivo* after prior incubation of aortic rings with BCNU, an inhibitor of the recycling enzyme glutathione reductase (158).

Vascular NOS uncoupling in the setting of diabetes

The association between BH4 status and diabetic pathophysiology has been made through observations of endothelial dysfunction and upstream oxidative stress. Reports from both animal models and human patients have shown that NO bioavailability is compromised as a result of eNOS uncoupling, which can give rise to impaired endothelial-dependent vasodilatation (155, 159, 160). Indeed this has been observed under pathological conditions, where Alp et al. have shown that experimental diabetes leads to increased vascular oxidative stress and uncoupling of endothelial NOS (eNOS), with a reduction in vascular BH4 despite no change in total biopterin levels (155). Moreover, in animal models and human studies of pathologies affecting the circulation, it has been shown that BH4 augmentation, through either exogenous supplementation or targeted overexpression of endothelial GCH1 (eGCH1), can re-couple eNOS and restore endothelial function (155, 159, 161). The same benefits to vascular function have also been observed in atherosclerosis and diabetes with

sepiapterin treatment (162, 163), thereby recruiting the salvage pathway to reconstitute BH4 through the activity of SR and DHFR (Figure 1.6).

However, the positive effects of treatment have been disputed by some findings that demonstrated either no effect of sepiapterin exposure on endothelium-dependent vasodilatation (164), or even an exacerbation of established endothelial dysfunction (165). The disparity in these reports is likely due to the enzymatic process of salvaging BH4 from sepiapterin, which requires the BH2 intermediate. Given that NOS coupling relies on a favourable BH4:BH2 ratio, the preservation or decline in NO-mediated vasorelaxation may also depend on the expression or catalytic activity of DHFR in the final step, which could have been variable in the abovementioned studies. The relative importance of the salvage and *de novo* BH4 pathways have been recently explored in cultured endothelial cells by Crabtree et al., who showed that both pharmacological inhibition and genetic knockdown of DHFR led to the oxidation of BH4 to BH2 and subsequent eNOS uncoupling (166). This change in BH4:BH2 ratio was not observed in cells with knockdown of GCH1, despite the reduction in total biopterins, suggesting that the *de novo* pathway dictates overall BH4 biosynthesis, while DHFR is more important in maintaining the relative levels of reduced and oxidised BH4 (166).

NOS and the diabetic cardiomyopathy

As described, most of the complications that present early in the progression of diabetes can be grouped under the umbrella of vascular disease. As a result, basic cardiovascular research in the context of diabetes has explored in detail the cellular mechanisms underlying the endothelial dysfunction (described above). However, far less understood is the development of a condition known as diabetic cardiomyopathy, a distinct type of cardiac dysfunction that is seemingly independent of conventional risk factors e.g. coronary artery disease and hypertension (167, 168). The characteristic phenotype of diabetic cardiomyopathy is one of impaired left ventricular (LV) diastolic function, which has been reported in both type 1 and type 2 diabetes (169-171). In addition, these human studies, as well as several animal models, have revealed that LV diastolic dysfunction is the predominant feature

in the initial stages of the cardiomyopathy, even though systolic function may be preserved (172-176). Another reported feature, and indeed potential mechanism, underlying the cardiomyopathy in diabetes is a dysfunction in myocardial energetics, resulting in reduced energy availability (177-179). Reduced energy production has been linked to changes in substrate utilisation (180, 181) possibly from decreased glucose uptake, a process which is normally heavily insulin-dependent in the cardiomyocyte (182).

NOS coupling and LV diastolic function

With respect to NOS coupling in diabetes, much of the work on the impact of BH4 has focused on eNOS and the downstream function of the vascular endothelium. As described, both the endothelial and neuronal isoforms of the enzyme are also expressed in cardiomyocytes, where the constitutively produced NO has been shown to influence excitation-contraction (EC) coupling in health and disease (see above and for review see (183)). It is logical to assume therefore that BH4 levels are also critical for maintaining NOS coupling in the cardiomyocyte and thus overall cardiac performance. The study by Carnicer et al. investigated this with a transgenic mouse model of cardiomyocyte-specific GCH1 overexpression (mGCH1-Tg). Left ventricular (LV) myocytes from these mice showed increased levels of BH4, but no increase in the BH4:BH2 ratio, in accordance with the belief that the *de novo* pathway may be limited in its capacity to maintain BH4 bioavailability. In spite of this, mGCH1-Tg cardiomyocytes still had reduced O_2^- production and increased nNOS activity, consistent with improvements in calcium handling and speed of relaxation through increased PLB phosphorylation (131). Under pathological circumstances, Silberman et al. also investigated NOS and BH4 bioavailability in LV diastolic function using the DOCA-salt model of heart failure (184). They showed that the diastolic impairment in these mice was associated with oxidation of cardiac BH4 and the uncoupling of nNOS, consistent with a reduction in the relative ratio of phosphorylated to total PLB (184). Although this ratio was somewhat normalised with BH4 supplementation, suggesting consequential improvements in calcium handling, a lack of data on the calcium transient in isolated

cardiomyocytes makes this difficult to confirm. Nevertheless, this report largely dovetailed with the findings of Carnicer and colleagues in the non-pathological state, who showed that augmented BH4 through mGCH1 overexpression both increased this PLB ratio, as well as improving calcium handling relative to control (131).

An alternative or perhaps additional putative mechanism of cardioprotection by BH4 has developed from a very recent study using the same DOCA-salt heart failure model. Jeong et al. reported that the diastolic dysfunction was not only accompanied by reduced BH4 availability and NOS uncoupling, but also depressed myofilament cross-bridge kinetics, correlated with S-glutathionylation of myosin binding protein C (MyBP-C) (185). Along with amelioration of the diastolic impairment, BH4 treatment was shown to reduce this oxidative modification of MyBP-C and improve myofilament dynamics (185, 186).

Myocardial NOS uncoupling in diabetes

Although there is an association of reduced NO bioavailability and increased ROS production with various cardiac diseases, insight into the potential role of BH4 and NOS uncoupling in disease progression still remains limited. Some of the best evidence has come from a model of pressure-overload cardiac hypertrophy, where Takimoto and colleagues have observed chronic remodelling and declining myocardial function in association with LV eNOS uncoupling and increased production of NOS-dependent superoxide. In addition, they further demonstrated that oral BH4 supplementation in these mice was able to recouple eNOS and prevent oxidative stress, together with attenuation of the cardiac remodelling and LV dysfunction (187, 188). There is also some data to suggest that BH4 could be beneficial in recoupling NOS and restoring LV function after ischemia-reperfusion (I/R) injury (189, 190), although Dumitrescu et al. observed a diminished benefit after longer periods of ischemia, suggesting degradation of BH4 to its other biopterin intermediates under conditions of increasing oxidative stress (189). Ge et al. have shown that specific mGCH1 overexpression could increase myocardial BH4 and preserve the positive effects of ischemic preconditioning (IPC) during

hyperglycaemia, however, NOS uncoupling and ROS production was not directly measured, while the model was not truly representative of the diabetic state (191).

In a rat model of type 1 diabetic cardiomyopathy, Lei et al. demonstrated that the LV diastolic dysfunction was associated with an increase in myocardial O_2^- production and nitrative stress, as well as a reduction in NO levels. This has potentially been attributed to eNOS uncoupling, although the authors also demonstrated an increase in cardiac iNOS expression, thus the existence of an inflammatory processes in some models may also be a factor (192). iNOS uncoupling specifically in the diabetic heart was also reported by Jo et al., however, only secondary markers of oxidative stress were measured in this study, without a direct assessment of myocardial O_2^- generation by NOS (193). Furthermore, the reported findings come from a mouse model with very low survival rates (5–25%), implying a diabetic phenotype that may not be easily extrapolated to the human disease. Most of these available studies are based on models with broad cardiac dysfunction instead of specifically LV diastolic dysfunction, moreover, none of the studies comprehensively measure whole heart and isolated myocyte function with reliable assays of BH4, NOS activity and ROS production. With a lack of robust evidence linking myocardial NOS uncoupling to the development of diabetic cardiomyopathy, it has consequently been difficult to substantiate a role for biopterins in NOS function under these circumstances.

Thesis objectives

In the context of the subject background and the existing literature described in this chapter, this thesis aims to answer the following:

How does neuronally-derived NO impact nerve-mediated vasoconstriction in resistance arteries?

Along with eNOS, the neuronal isoform of NO has been identified as an important regulator of vascular tone (115-119). *Ex vivo* studies will investigate the role of nNOS in opposing the vasoconstriction

mediated by perivascular nerves. This foundational year study will incorporate wire myography, a technique which will then be utilised subsequently in the diabetic mouse model.

What is the cardiovascular phenotype in the STZ mouse model of type 1 diabetes?

The consequences of hyperglycaemia on both vascular and cardiac function will be explored, assessing the existence of a specific cardiomyopathy and investigating potential temporal effects.

Which cellular mechanisms underlie the LV dysfunction observed in the diabetic state?

The presence of oxidative stress will be determined in the vasculature of the diabetic mouse, as it is often described as a key instigator of hyperglycaemia-induced damage. In light of this, a similar assessment will be made in the myocardium to establish whether redox imbalance and NOS uncoupling also contribute to functional deficits at the cardiomyocyte level. In the potential absence of such findings, other distinct cellular pathways underlying the cardiomyopathy will be considered.

Can augmentation of myocardial BH4 protect against the development of diabetic cardiomyopathy?

Enhancement of myocardial BH4 biosynthesis and NOS activity has been shown previously to improve LV cardiomyocyte function (131). The use of myocardial-specific GCH1 overexpression in the type 1 diabetic mouse will assess the potential beneficial effects of the transgene in the diseased state. Experiments will then aim to dissect the cellular basis of any functional improvement.

Finally, the translational potential of these findings will be explored in a subset of mice supplemented with oral BH4. This will assess whether BH4 feeding augments BH4 bioavailability in the myocardium, and whether any future findings of cardioprotection with the supplement implicates the same underlying mechanism of action as the mCGH1 transgene.

Chapter 2

General Methods

Introduction

This chapter comprises a catalogue of the experimental techniques used to produce the data contained in this thesis, with detailed descriptions wherever appropriate on the theory of certain assays and the process of measurement. A variety of techniques have been performed, using both isolated vessels and LV cardiomyocytes ex vivo, LV homogenates, as well as in vivo studies of global cardiac function. As will become apparent in the respective chapters, some of these techniques have been applied to the study of control and type 1 diabetic mice (after 4 weeks and 12 weeks of treatment), and in the presence or absence of myocardial-specific GCH1 overexpression.

Wherever possible (and wherever described) experiments *in vivo, ex vivo* and using stored tissue were conducted blind to the mouse genotype and treatment. Samples were identified purely on the basis of cage number and ear notch number (allocated by an independent experimenter), which were only related back to genotype and treatment group following the experiment and subsequent analysis.

Animals

All animal treatment and protocols were conducted in accordance with the UK Home Office under the guidance of the operation of the Animals (Scientific Procedures) Act 1986, and as detailed in the project licence under Barbara Casadei (No. 30/2804; January 2011). Unless otherwise stated, regulated procedures were performed under the Personal Licence (PIL) 30/10075.

Mice were bred and housed both at the Biomedical Services Unit (BMSU) on the site of the John Radcliffe Hospital, or at the Functional Genetics Facility (FGF) at the Wellcome Trust Center for Human Genetics, Oxford. Breeding colonies were established on the background of C57Bl/6J; for experiments on mGCH1-Transgenic mice, animals heterozygous for the transgene were used, as well as their WT littermates as controls. Only male mice in all experimental groups were studied.

Generation of transgenic mice

Targeted overexpression of the GCH1 gene specifically in cardiomyocytes was achieved by integration of the murine alpha myosin heavy chain (α-MHC) promoter within the GCH1 transgene. The plasmid construct containing the transgene was generated at the FGF and confirmed by DNA sequencing, after which the GCH1 transgene fragment was excised and incorporated by pro-nuclear microinjection into fertilised eggs from super-ovulated mice. Generation of the GCH1 transgene and all breeding of mGCH1-Tg mice was carried out by staff at the FGF. For use in experimental studies, the genotypes of transgenic founders were screened by polymerase chain reaction (PCR) of mouse DNA samples.

Induction of type 1 diabetes

To observe the effects of persistent hyperglycaemia, diabetes was induced via a 5 consecutive day intra-peritoneal injection protocol of streptozotocin (STZ), in the low dose range of 42-45mg/kg/day, as validated previously (176, 194). STZ is an alkylating compound that causes destruction of pancreatic β-cells, thereby impairing insulin production. STZ (10mg/ml, Sigma-Aldrich, USA) was dissolved in 25mM sodium citrate buffer (pH 4.5) immediately prior to carrying out injections; control mice were injected in parallel with the equivalent volume of citrate buffer. Mice were injected between at the age of 14-16 weeks and regularly monitored for body weight and plasma glucose for up to 12 weeks after the point of the last injection. Plasma glucose was measured with an Aviva Accu-Chek (Roche, USA) glucose monitor and hyperglycaemia was classified as a glucose concentration above 16mM. 12 weeks was the terminal end point for the study, at which point mice were euthanized (Schedule 1) and tissues collected. If body weight fell below 80% of the initial recorded weight at any point prior to week 12 of the protocol, the established humane end-point was reached and the mouse sacrificed.

Genotyping

To determine if mice were WT or transgenic, genomic DNA was isolated from mouse ear notch samples using a previously validated DNA HotSHOT protocol (195), extracting DNA by alkaline lysis.

After DNA extraction, sample supernatants were added to water, a PCR mix containing deoxynucleoside triphosphates and Taq polymerase (BioMix Red, Bioline, UK), $MgCl_2$ and primers specific for the human GCH1 sequence.

GCH1 primers:

Forward 5'- CCTTCCTCACCCCCTGGCTTGTCC – 3'

Reverse: 5'-AGTCGGGCACGTCGTAGGGGTAGG-3'

Samples were run using the following PCR protocol:

Step	Action
1	Incubate at 94°C for 5 min
	Denaturation
2	Incubate at 95°C for 1 min
	Annealing
3	Incubate at 64.5°C for 1 min
	Extension
4	Incubate at 72°C for 40 s
5	Cycle to step 2 for 32 more times
6	Incubate at 72°C for 10 min
7	Incubate at 10°C for 30 min

Following PCR, 14µl of each sample was loaded into lanes of 1.5% agarose gel (4g agarose, 200ml TAE buffer, 10µl ethidium bromide) alongside 2µl of DNA ladder (New England BioLabs, USA) used as a reference marker. Electrophoresis of these samples was performed at 120V for 40 min, after which sample bands were visualised on a ChemiDoc MP system (BioRad, UK). The transgenic genotype was confirmed by the presence of a 500bp band corresponding to the mGCH1 gene (Figure 2.1).

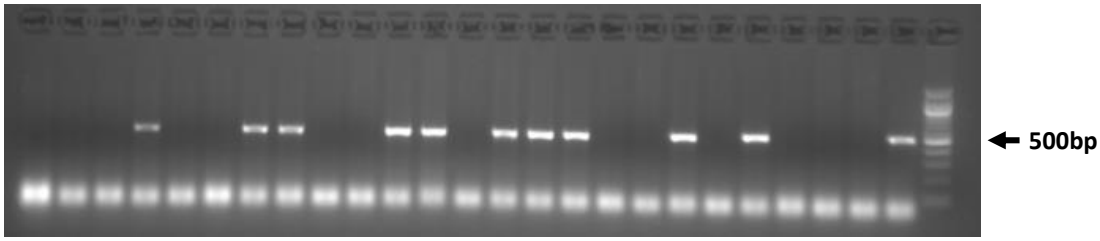


Figure 2.1. Identification of mGCH1-Tg mice by PCR.

Typical genomic DNA screen displaying the presence of the mGCH1 transgene at 500bp, as compared to a DNA reference ladder (final lane, far right).

General solutions

Krebs Henseleit Buffer (KHB, in mM): NaCl 120, KCl 4.7, $MgSO_4$ 1.2, KH_2PO_4 1.2, $NaHCO_3$ 25, Glucose 5.5, $CaCl_2$ 2.5; bubbled with 95% O_2/5% CO_2 on ice and pH adjusted to 7.4 with NaOH or HCl.

Isolation solutions

Isolation Solution (in mM): NaCl 130, KCl 5.6, $MgCl_2$ 3.5, Glucose 10, Hepes 5, Na_2HPO_4 0.4, Taurine 20; filtered and pH adjusted to 7.4 with NaOH or HCl.

Storage Solution (in mM): NaCl 120, KCl 5.6, $MgSO_4$ 5, $CaCl_2$ 0.2, Na pyruvate 5, Glucose 20, Taurine 20, Hepes 10; pH adjusted to 7.4 with NaOH or HCl.

Collagenase Solution I: collagenase II 1mg/ml (Worthington Biochemical Corp), protease 0.133 mg/ml, bovine serum albumin (BSA) 1.65mg/ml, $CaCl_2$ 50 µM; oxygenated at 37°C.

Collagenase Solution II: collagenase II 1mg/ml, BSA 1.65 mg/ml, $CaCl_2$ 50 µM; oxygenated at 37°C.

Perfusion solution (in mM): NaCl 140, KCl 4, $MgCl_2$ 1, Glucose 10, Hepes 5, $CaCl_2$ 1.4; pH adjusted to 7.4 with NaOH or HCl.

Western Blot solutions

Western Blot Electrophoresis Running Buffer (in mM): Tris-Base 25, Glycine 192, 1% SDS

Western Blot Transfer Buffer (in mM): Tris-Base 25, Glycine 192, 20% methanol

CK activity solutions

Ice buffer (in mM): KH_2PO_4 buffer 0.1, EGTA 1, β-mercaptoethanol 1, 0.1% Triton

HPLC solutions

Re-suspension buffer (in mM): phosphate-buffered saline (PBS) 50, ethylenediaminetetraacetic acid (EDTA) 1, dithioerythritol (DTE) 1; pH adjusted to 7.4 with NaOH or HCl.

Acid precipitation buffer (10x in mM): trichloroacetic acid (TCA) 2000, phosphoric acid 1000, DTE 1; solution made up in PBS.

HPLC mobile phase (in mM): sodium acetate 50, EDTA 0.048, DTE 0.16, citric acid 5; pH adjusted to 5.22 with NaOH or HCl.

Myofilament solutions

Tyrode solution (in mM): NaCl 130, KCl 5.6, HEPES 5, Na_2HPO_4 0.4, $MgCl_2$ 3.5

Glycerinated relaxing solution (in mM): EGTA 10, $MgCl_2$ 5.6, KCl 100, imidazole 20, ATP 5, PCr 10, glycerol (50%), protease inhibitors

Skinning solution: 99% glycerinated relaxing solution, 1% triton X-100

Dissecting solution (in mM): EGTA 10, $MgCl_2$ 5.6, KCl 100, imidazole 20, ATP 5, PCr 10, BDM 20, protease inhibitors

Pre-activating solution (in mM): EGTA 0.1, $MgCl_2$ 1, MOPS 80, HDTA 14.9, ATP 5, KCl 170 (ionic strength)

Force fibre solution: Ionic strength 170 mM, pMg 3, total EGTA 15 mM, total MOPS 80 mM, MgATP 5 mM, total CP 15 mM, free K^+ 83 mM, free Na^+ 52 mM, pCa between 4-9

Tissue collection

Mice were euthanized by cervical dislocation (Schedule 1), pinned down on a Sylguard (Dow Corning, USA) coated plate and the thorax immediately opened. Blood was collected with heparin and 1µl of 1M DTE (to prevent BH4 oxidation), and then centrifuged at 10 000 rpm for 5 min (4°C). Plasma supernatant was removed and separated into several aliquots for storage at -80°C. The right ventricle (RV) and left ventricle (LV) were perfused respectively with ice cold PBS to flush out the remaining blood, before the heart was dissected out and placed in PBS. Both atria the RV were dissected away, before the LV was momentarily placed on tissue paper to remove excess fluid and quickly weighed. Atria and LV were placed in separate cryotube and frozen on dry ice, at which point samples of remaining organs were similarly collected by a second person e.g. liver, lung, kidney, spleen, pancreas and skeletal muscle. These samples were then labelled and stored in a -80°C freezer until required for experimental assays.

Preparation of LV homogenates

LV samples were first removed from -80°C storage and maintained on dry ice. Prior to homogenisation, LV samples were transferred from their cryotube to a small layer of aluminium foil atop dry ice to prevent thawing. The foil was tightly covered over and the LV swiftly mechanically fragmented with a blunt, glass bottle. A segment of approximately ¼ of the entire LV was selected for homogenisation, with the remaining ¾ being placed back into the cryotube for storage. The chosen LV segment was added into a specific buffer solution (depending on the experiment and protocol) and rapidly homogenised on ice using a pre-sterilised electronic Polytron homogeniser (PT2100 Kinematika, Switzerland). LV tissue was homogenised for 8-10 s initially, then repeated for a further 8-10 s to ensure full breakdown of the tissue and consistency across all samples. Homogenates were centrifuged for 10 min at 10 000 rpm (4°C) and the supernatants maintained on ice. A sample of each supernatant was used to make a 1:10 dilution for protein quantification.

Protein quantification

Prior to experimental assays, equal protein loading between samples was ensured by the quantification of protein using a BCA assay kit (Thermo Fisher Scientific, USA). This method is based on a colorimetric reaction in which bicinchoninic acid (BCA) is chelated by a cuprous ion (with a reduction from Cu^{2+} to Cu^{1+}), yielding a purple colour that increases in intensity with greater protein concentrations, as represented by its absorbance at a wavelength of 562nm. A reference standard range was prepared by serial dilutions from a 2mg/ml solution of bovine serum albumin (BSA) as follows:

Final BSA conc (mg/ml)	**0**	**0.2**	**0.4**	**0.6**	**0.8**	**1**	**1.2**	**1.6**	**2**
BSA stock (µl)	**0**	**5**	**10**	**15**	**20**	**25**	**30**	**40**	**50**
MQ H_2O (µl)	**50**	**45**	**40**	**35**	**30**	**25**	**20**	**10**	**0**

Reference standards and the diluted samples were incubated at 37°C for 30 min with a BCA mixture at the ratio of 50:1 for reagent A and reagent B, respectively. After incubation, standards and diluted samples were loaded into a 96-well microplate in duplicate to ensure greater accuracy for construction of the reference standard curve. Colour changes were detected using an Omega Fluostar plate reader (BMG Labtech, UK), which measured the absorbance of light at 562nm. The recorded values were logged in MARS data analysis software and used for the calculation of the standard curve, for which the protein sample values could be compared and the protein concentration determined (Figure 2.2).

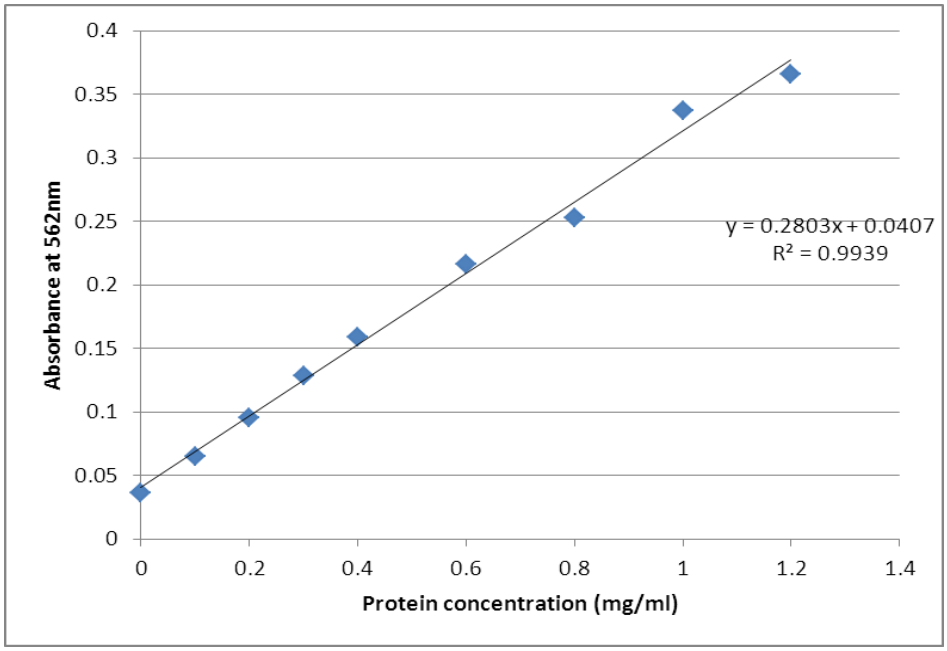


Figure 2.2. Protein quantification assay.

Representative example of the standard reference curve generated from the BCA assay. The absorbance (at 562nm) increases in proportion to the concentration of each known standard, producing a linear relationship that can be used for the quantification of unknown protein samples.

Western Blot sample preparation

Frozen LV samples were first homogenised as described above in 400µl of 1x RIPA buffer containing protease inhibitors (Complete protease inhibitor cocktail, Roche). Sample homogenates were centrifuged and diluted as described. Protein was quantified using the BCA assay as described above and samples calculated for the provision of 20µg of protein per lane for gel electrophoresis. Protein loading samples were loaded alongside a rainbow protein marker into 18 well criterion gels (4-15%) and then run in Tris-Glycine running buffer for 45 min at 185V. Gels were isolated, cut and loaded into cassettes with PVDF membrane in Tris-Glycine transfer buffer. Proteins were then transferred at 35V for 90 min at 4°C; successful transfer was then confirmed with Ponceu staining.

Blotting

All membrane incubations were performed using TBST containing 5% milk, set upon a shaker plate for the allotted time. Membranes were first incubated for 1 hour to block non-specific protein binding, after which time they were washed 3 times in TBST at 5min intervals between washes. Primary antibodies (see table, page 19) were added at the respective dilutions and the membranes incubated for 2 hours (unless manufacturer instructions specified overnight incubation at 4°C). After 3 washes, membranes were incubated in secondary antibodies conjugated to horseradish peroxidase (HRP) for 1.5-2 hours, after which time membranes were washed a further 5 times. For exposure, membranes were first incubated (30s-5min) in West Pico chemiluminescent substrate (Thermo Fisher Scientific), or in the case of weak signal, West Dura extended duration substrate (Thermo Fisher Scientific). Membranes were then immediately exposed with either an X-ograph developer using hyperfilm (Amersham), or with the ChemiDoc MP system (BioRad). Protein expression was determined by densitometry quantification of each band using either Scion Image software for film or Image Lab software (BioRad) for ChemiDoc analysis. Quantification was expressed relative to a suitable house-keeping protein: GAPDH or TnI. GAPDH is regularly used as a standard loading control for its ubiquity in tissues and its often unchanged status even in treated or diseased states. However, in the event that the metabolic status of the myocardium might change in the diabetic state, potentially affecting GAPDH expression, TnI was additionally used as a loading control.

Quantitative real-time RT PCR

Real-time RT-PCR was conducted with *Alice Recalde*, and was used as a highly sensitive method for quantifying gene expression in LV homogenates. Through this process, sample RNA is reverse transcribed into its complementary DNA sequence and amplified by PCR, which can then be used for the quantification of the gene transcript.

RNA extraction

For the protection and stabilisation of RNA, during tissue collection ¼ of the LV was placed into a microtube containing RNAlater solution (Thermo Fisher Scientific), after which it was stored at -80°C. For the extraction of RNA, samples were removed from storage and maintained on dry ice prior to processing. LVs were first homogenised in 1ml in ice-cold Trizol (Sigma-Aldrich) and incubated in 200µl chloroform for 5 minutes, after which they were briefly vortexed and then centrifuged for 15 min at 13 000 rpm, 4°C. The aqueous top phase was transferred to a new microtube containing an equal volume of 70% ethanol dissolved in RNAase-free water, which is added to promote the selective binding of RNA to membranes during purification. RNA was purified using RNeasy Mini Kits (Qiagen, Netherlands), following the protocol as supplied by the manufacturer. Sample mixtures were added to spin columns and centrifuged for 15 s at 8 000 rpm to elute unwanted contaminants. An RNA clean-up procedure was then performed with the sequential addition of RW1 buffer, DNAase, RPE buffer and 80% ethanol dissolved in RNAase-free water. In sequence, these components were added, briefly mixed and quickly centrifuged before discarding. RNA collection was finally achieved with the addition of RNAase-free water to the spin column and a last centrifugation for 1 min at 13 000 rpm in closed-lid tubes. A nano-drop 1000 spectrophotometer (Thermo Fisher Scientific) was used to quantify the final RNA yield. A 260/280nm ratio of greater than 1.8 (applying the Beer-Lambert Law) was required to indicate the purity of extracted RNA for subsequent RT-PCR.

cDNA synthesis

cDNA was synthesised in a 2-step procedure using a QuantiTect Reverse Transcription Kit (Qiagen). According to manufacturer's instructions, in step 1 the purified RNA samples were combined with a DNA wipeout reagent (2 min at 42°C) to eliminate any genomic DNA that could contaminate the sample and be amplified during PCR. Reverse transcription then occurs in step 2; samples were mixed with the Quantiscript reverse transcriptase, the RT buffer and RT primer mix. Reverse transcription proceeded over 15 min at 42°C, after which time the reverse transcriptase was inactivated and the

reaction terminated by incubation for 3 min at 95°C. The synthesised cDNA product was then stored at -80°C until needed for the PCR.

Quantitative RT-PCR

During amplification in the PCR, the exponential increase in cDNA with each cycle corresponds to a similar increase in the fluorescence of the reporter dye. The reporter probe is part of a TaqMan gene expression assay (designed and optimised by Applied Biosystems, USA), which consists of forward and reverse primers with 2 complementary fluorophores: a 5' reporter (FAM) and a 3' quencher (TAMRA). Fluorescence of the reporter is prevented by the proximity of the quencher prior to hybridization. However, as Taq polymerase extends the primer sequences during PCR, the annealed dual-labelled probe is cleaved and the separation of the reporter from the quencher relieves the suppression, thereby permitting an increase in fluorescence (Figure 2.3).

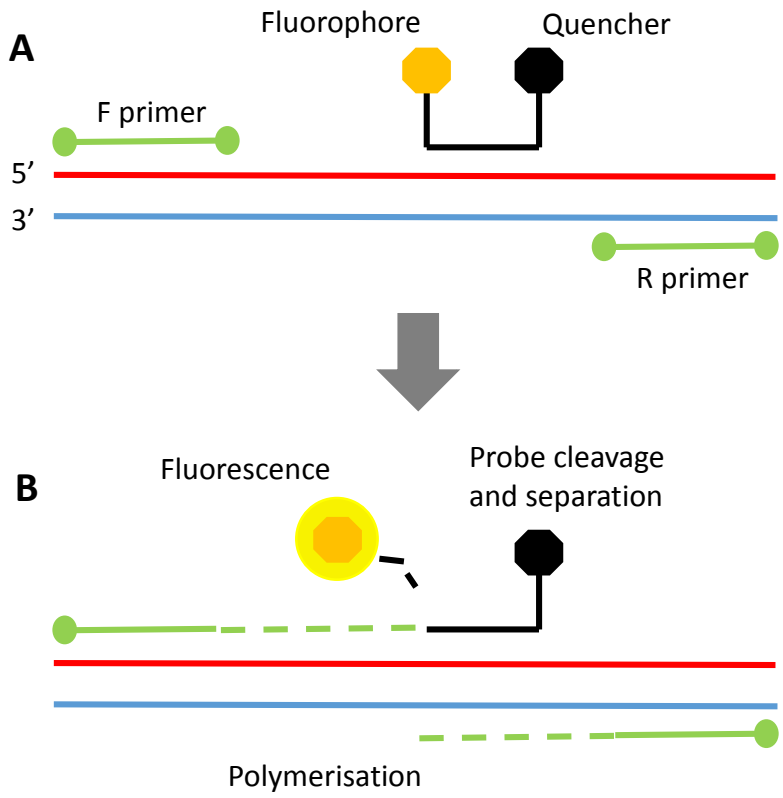


Figure 2.3. Principle of the TaqMan gene expression assay.

(A) Both forward and reverse primers, as well as the TaqMan reporter probe, anneal to specific DNA regions on the template strand. The proximity of the probe's fluorophore and quencher is such that any emitted fluorescence is inhibited by the quencher molecule. **(B)** As the Taq polymerase extends the primers and synthesises a new strand in the 5' to 3' direction, the probe is cleaved, releasing the fluorophore from the quencher and permitting an increase in fluorescence.

As the reaction proceeds, the amplification rate of the target eventually decreases (as dNTPs become limiting) to produce a plateau. The linear, exponential phase of the PCR plot is used to set the cycle threshold (Ct), which can be normalised back to the Ct of the house-keeping gene α-actinin. The gene of interest was therefore expressed as the ΔCt, i.e. the fold difference between the Ct value of the target and the Ct value of the house-keeping control gene. Primers for the gene of interest are displayed in Table 1; both probes and primers overlapped with intron sequences to prevent the amplification of genomic DNA.

Samples were loaded into 96-well optical plates (Applied Biosystems) and RT-PCR performed with an iCycler IQ real-time system (BioRad), coupled to a fluorescence detector (TaqMan ABI PRISM 7700 Sequence Detection System, Applied Biosystems). For preparation, 13.5µl of cDNA (100ng/µl), 15µl TaqMan master mix, and 1.5µl TaqMan gene expression assays were mixed together per reaction. RT-PCR reactions proceeded under the following conditions: 10 min at 50°C, 10 min at 95°C, 50x cycles of 15 s at 95°C and 1 min at 60°C. cDNA amplification was quantified via the Livak method and results were displayed as the fold change (ΔCt) as compared to the expression of the housekeeping gene, selected for normalisation.

Gene of interest	**Reference sequence no.**
IL-1β	NM_008610.2
MCP-1	NM_011333.3
MMP-2	NM_008610.2
MMP-9	NM_013599.3
Collagen 1 A1	NM_007729.2
GLUT-1	NM_148938.3
GLUT-4	NM_009204.2
α-actinin	NM_033268.4

Table 1. Genes of interest detected in quantitative real time RT-PCR experiments, listed alongside corresponding accession numbers. Respective TaqMan probes were all purchased from Applied Biosystems.

Superoxide (O_2^-) production

Lucigenin-enhanced chemiluminescence

O_2^- production was measured by lucigenin-enhanced chemiluminescence with a single-tube luminometer (FB12, Berthold, Bad Wildbad, Germany) maintained at 37˚C, as previously validated in the laboratory (196). Lucigenin (*bis*-N-methylacridinium nitrate) is commonly used for the sensitive and reliable detection of superoxide in tissue homogenates and cells; an unstable dioxetane is produced from its reaction with O_2^-, which subsequently breaks down to form methylacridone. The excitation state of methylacridone emits a photon of light which can then be detected by luminometry. Some previous reports suggested that through redox cycling, lucigenin could be reduced to act as a generator itself of O_2^- production (197). However, this is reported to be the case for high concentrations of lucigenin (>20µM); for this reason chemiluminescence experiments were performed using a low concentration of lucigenin (5µM).

For measurements in LV homogenates, frozen LV samples were first homogenised as described, in KHB containing protease inhibitors. Protein was quantified using the BCA assay as described. 300-400µg of sample protein was incubated in a scintillation vial of KHB (1ml minus required sample volume) containing 5µM lucigenin for 2 min to ensure a stable background signal. This was followed by the addition of sample supernatant, with the recording of basal chemiluminescence for 10 min. The effect of inhibiting NOS activity on O_2^- production was determined by the addition of 1mM L-NAME and recording for a further 5-8 min. For control runs, the inactive isomer D-NAME (1mM) was used. Finally, to confirm the origin of the ROS signal was O_2^-, 10mM of the specific O_2^- scavenger tiron was added and recording resumed for 5 min (Figure 2.4). For the addition of all substances, recording was resumed only after 60 s to allow for acclimatisation and avoid artefactual signals from the entry of external light. Chemiluminescence levels were assessed over the final 2 min of each period of recording and the values expressed as the tiron-inhibitable fraction, measured as relative light units, per mg protein, per second (RLUs/mg/s).

For vascular O_2^- production, the thoracic aorta was freshly dissected, cleaned of connective tissue (during the protocol described in *Tissue collection*), before incubation in 1mM D-NAME or L-NAME for 30 min prior to luminometry measurements. Chemiluminescence was similarly recorded for 10 min before the addition of 10mM tiron. To normalise O_2^- production between samples, aortas were incubated overnight at 37˚C and weighed; results were then expressed as RLUs per mg dry weight.

Experiments in both LV homogenates and aorta were conducted blind to the mouse genotype and treatment. Samples were identified purely on the basis of cage number and ear notch number (allocated by an independent experimenter), which were only related back to genotype and treatment group following the experiment and subsequent analysis.

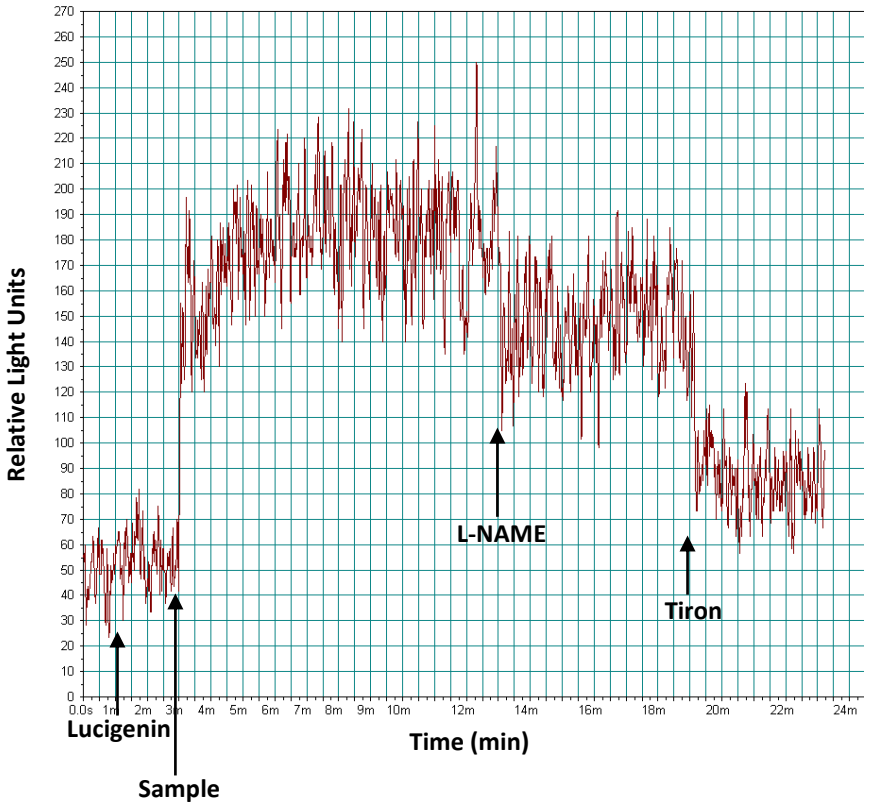


Figure 2.4. Superoxide detection by chemiluminescence.

Representative trace for the measurement of superoxide by chemiluminescence in LV homogenates. The NOS contribution was determined by the addition of L-NAME (1mM), while superoxide detection was confirmed by the signal change upon the addition of tiron (10mM).

HPLC detection

To support the data with lucigenin-enhanced chemiluminescence, superoxide production was also measured with HPLC, via the detection of 2-hydroxyethidium (2-OHE). This was selected as an alternative, highly specific assay, since the superoxide anion reacts selectively with dihydroethidium (DHE) to produce a 2-OHE peak, while other oxidant species in the experimental preparation (e.g. hydrogen peroxide, peroxynitrite) do not react with DHE in this way.

For sample preparation, LV tissue was homogenised in KHB buffer on ice as previously described, and protein quantified using the BCA assay. Samples were diluted in KHB to achieve a concentration of 100µg/ml, and 100µL was aliquotted into new Eppendorf tubes for each sample condition. Samples were incubated for 15 min at 37˚C, after which experimental reagents were added. Subsets of supernatants were pre-incubated with L-NAME (1mM) or the inactive isomer D-NAME (1mM), as well as the O_2^- scavenger tiron (10mM). All samples were then placed back into the incubator for 30 min at 37˚C.

During this incubation, the DHE solution was prepared. A 5mM stock solution of DHE (Invitrogen, USA) was made previously by dissolving the vial contents in DMSO in a dark room, before aliquotting into dark, opaque Eppendorf tubes and storing at -20˚C. The working DHE solution could then be prepared on each experimental day by performing a 1:10 dilution of the DHE aliquot with 0.1M HCl, again conducted in the dark and on ice. Samples were removed from incubation and taken to the dark room, where 5µL of the working DHE solution was added to each tube. Samples were covered in foil to prevent degradation of DHE in light, and then incubated for 15 min at 37˚C. To cease the reaction with DHE and allow for deproteinization, 100µL of 100% methanol and 0.1M HCl were added sequentially to each sample, with vortex and centrifugation (13 000 rpm, 5 min) carried out after each addition.

Final supernatants (150µL) were transferred to amber glass vials for HPLC analysis. Separation of DHE, 2-OHE and ethidium was performed using the gradient HPLC system (Jasco Ltd, UK) with reverse-phase column (Hichrom, UK), as described previously (156, 198). Gradient elution was achieved from mobile

phase A (0.1% trifluoroacetate in water) to mobile phase B (0.085% trifluoroacetate in acetonitrile). Values of detected 2-OHE were adjusted for using a 1µM 2-OHE standard. Results were expressed as the tiron-inhibitable fraction.

LV cardiomyocyte isolation

Langendorff perfusion followed by enzymatic dispersion was used to isolate LV cardiomyocytes. Initially, mice were euthanized by cervical dislocation (Schedule 1), pinned out and the chest cavity opened to expose the heart. After removal of adherent connective tissue, the aorta was exposed and a thread of surgical suture loosely looped around the vessel. A cannula (fashioned from a 23G needle and pre-filled with isolation solution) was inserted into the cut aorta and briefly laid to rest while the suture loop was pulled tight and tied off to secure the vessel around the cannula. The heart and connected cannula was then completely excised from the thorax and attached to a Langendorff perfusion system, surrounded by a water jacket heated to 37˚C**.** The heart was then perfused with Ca^{2+}-free isolation solution (oxygenated at 37˚C) for 3 min, followed by 9 min of perfusion with collagenase solution I (Figure 2.5). The heart was removed from the perfusion rig and the atria and right ventricle excised. The LV was cut into several smaller, even-sized pieces and placed into a conical flask containing collagenase solution II (5ml). This was fixed into a water bath heated to 37˚C and shaken for 2 min at 300 rpm. The flask was removed and the supernatant from this first digestion was filtered into a centrifuge tube. The LV tissue remaining in the flask was re-suspended in a fresh 5ml of collagenase solution II and placed back into the water bath to be shaken for a further 10 min. This process was repeated once more, which would eventually yield three separate tubes containing LV myocytes. 5ml of 1% BSA in isolation solution was added to the supernatant in the centrifuge tube, which was then spun for 3 min at 600 rpm. After the removal and discarding of the supernatant, the pellet of LV myocytes was re-suspended in another 5ml of the 1% BSA in isolation solution and centrifuged again for 3 min at 600 rpm. After removal of the supernatant, the pellet was again re-

suspended, this time in 5ml of storage solution. LV myocytes were stable in this storage solution for 6 hours after isolation and maintained in the suspension for use in single cell shortening experiments.

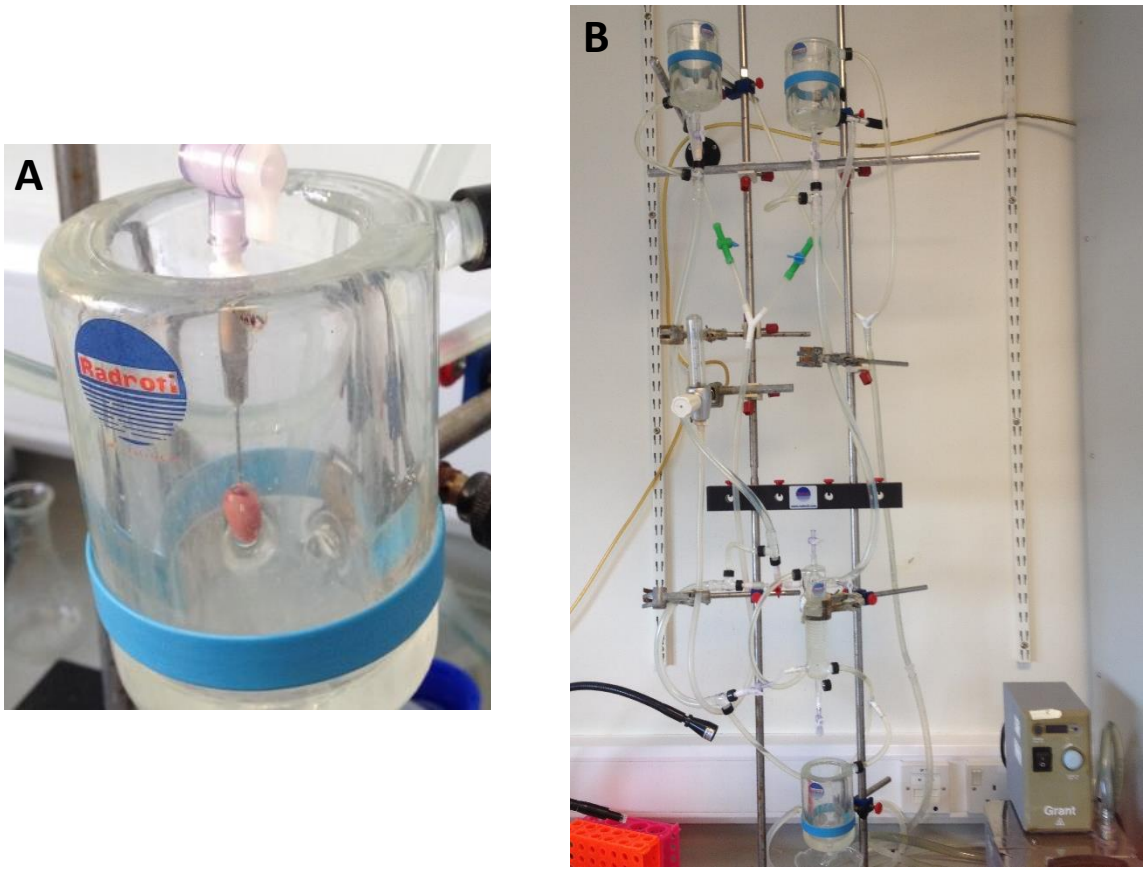


Figure 2.5. Langendorff perfusion set-up for the isolation of murine LV cardiomyocytes.

(A) The mouse heart was excised and cannulated for perfusion, maintained at 37˚C with a surrounding water jacket. **(B)** The cannulated heart was connected to the Langendorff perfusion system, perfused in sequence with isolation solution and collagenase to commence the digestion of LV myocytes.

Acquisition of cell shortening data

Prior to data acquisition, the recording bath, perfusion system and microscope was set-up as shown in Figure 2.6. The recording bath was constructed from a Perspex chamber attached to a glass coverslip, which was then mounted on a mobile stage which could be controlled with micro-manipulators. The stage rested upon a high-resolution inverted microscope (Leica, Germany), which was all based upon a pneumatic anti-vibration table (Newport, USA). Perfusion solution heated to 35 ± 1.5 ˚C was perfused through the recording bath at one end and removed by suction at the other,

ensuring a uniform flow (5ml/min) across the bath. Once this was achieved, the solution was momentarily drained and the perfusion halted to add a suspension of the isolated LV myocytes in storage solution. This suspension was added to the recording bath and the LV myocytes allowed to adhere to the coverslip for 30 s before the perfusion system was restarted, providing a constant flow of perfusion solution across all cells in the bath.

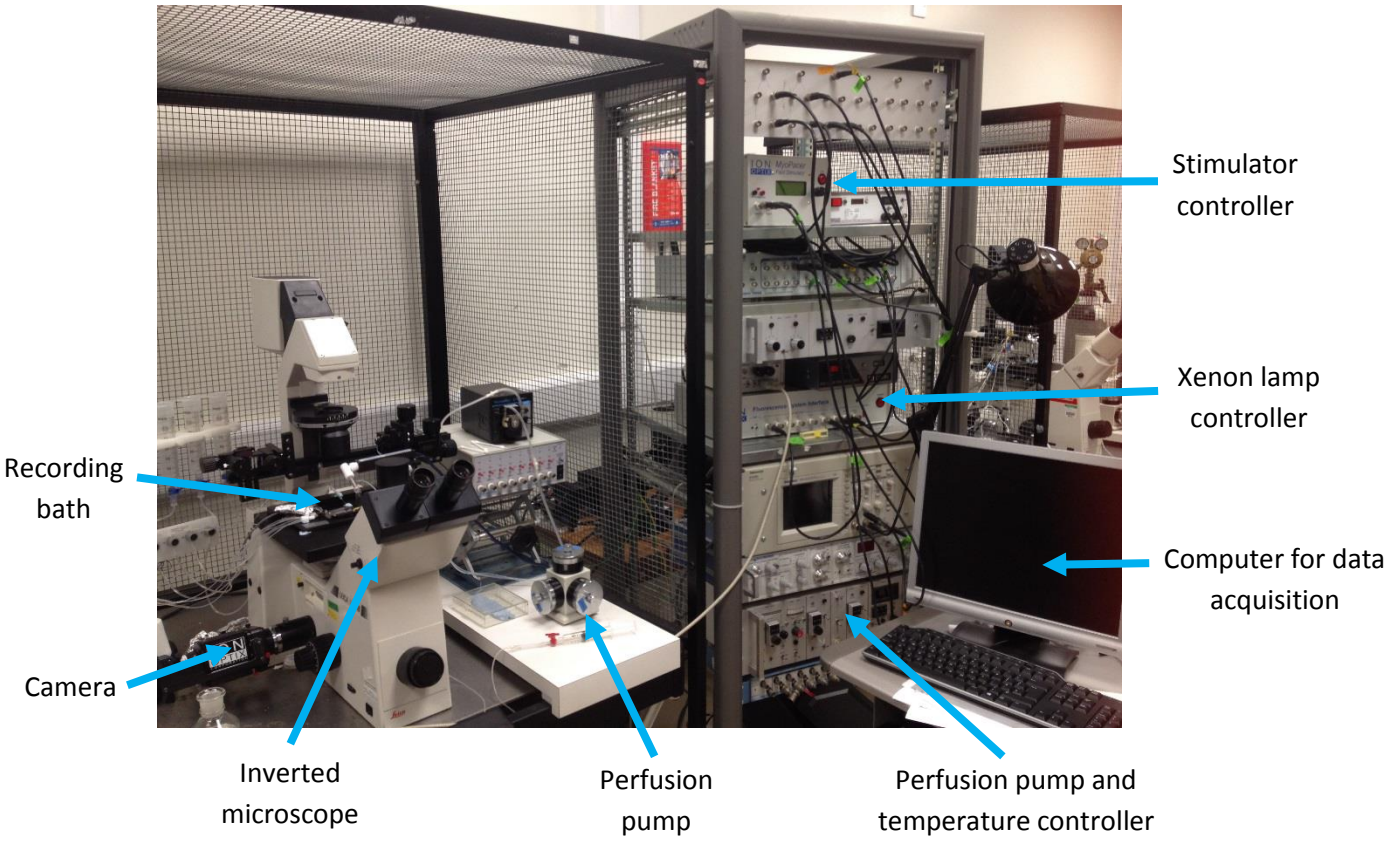


Figure 2.6. Set-up for the measurement of isolated cardiomyocytes.

Microscope and perfusion arrangement for the assessment of contractile function, $[Ca^{2+}]_i$ transient and cell dimensions in isolated cardiomyocytes.

Cell shortening measurements

To electrically stimulate LV myocytes, two electrodes were positioned at each side of the recording bath and connected to a digital stimulator box (IonOptix, USA). Electrical-field stimulation was performed at 40V depolarising pulses of 5 ms duration, at a frequency of 3 Hz. For myocyte selection, the microscope lens was first set to the 10x magnification. Cells were carefully observed and selected for measurement on the criteria that they were rod-shaped, striated and contracted regularly and

uniformly. The magnification was then increased to the 40x lens and immersed in oil; cells were monitored and recorded using a video-edge detection system (IonOptix) with the data acquired and displayed using IonWizard software on the neighbouring computer. Both the cell dimensions and shortening cycles were recorded; shortening measurements were determined from the average of at least 10 steady-state contractions per cell that all yielded consistent traces (Figure 2.7).

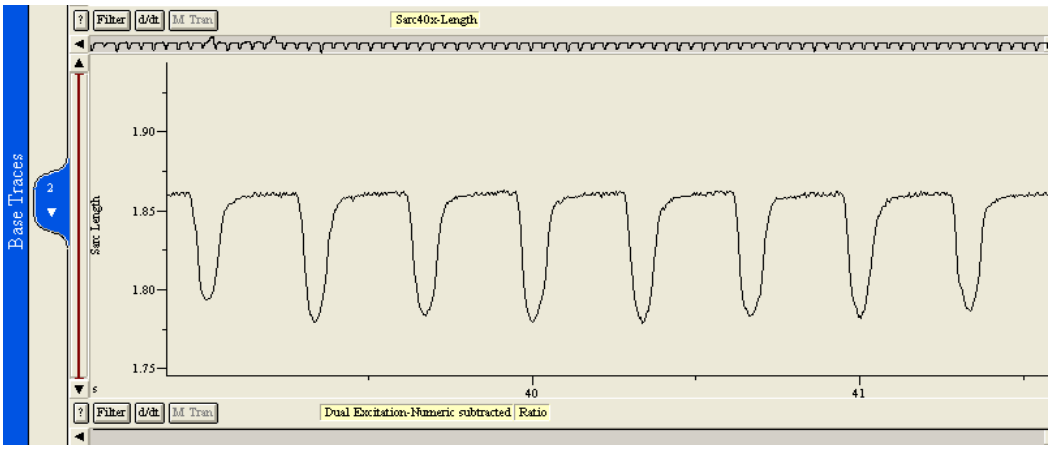


Figure 2.7. Data acquisition in isolated cardiomyocytes.

Example screenshot of IonOptix software depicting changes in sarcomere length during contraction.

$[Ca^{2+}]_i$ transient measurements

Fluorescence measurements were performed with *Ricardo Carnicer*. To enable the measurement of $[Ca^{2+}]_i$, LV myocytes were pre-loaded with Fura-2 (Invitrogen), a fluorescent and ratiometric probe that is Ca^{2+}-sensitive. A suspension of LV myocytes was placed in an opaque Eppendorf tube in 1ml of perfusion solution with 5µM acetoxymethyl ester of Fura-2 (from a stock solution prepared in DMSO). 250µM $CaCl_2$ and 2µl pluronic acid (for cell permeability). This solution containing LV myocytes was left to incubate at room temperature for 15 min. The supernatant was then removed and replaced with a fresh 1ml perfusion solution containing 500µM $CaCl_2$ to be incubated at room temperature for 10 min. The supernatant was removed for a final time and the myocytes suspended in a fresh 1ml perfusion solution of 500 µM $CaCl_2$ concentration. This myocyte preparation, as well as the fluorescence experiments, were all performed in the laboratory in darkness.

For fluorescence measurements LV myocytes were perfused and stimulated in the same way as for cell shortening experiments. A xenon arc lamp was used to generate Fura-2 fluorescence; the light was passed through an interference filter (first at 340nm and then at 380nm) and the microscope lens aperture adjusted to ensure light collection from only the individual cell of interest. Areas in the field of view that were absent of myocytes were used for background fluorescence, which was then subtracted from fluorescence values obtained from myocytes at both wavelengths for excitation. The $[Ca^{2+}]_i$ transient was determined from the Fura-2 fluorescence ratio (excitation at 340nm compared with 380nm); this ratiometric measurement diminishes any effects from uneven dye loading and changes in proportion to intracellular $[Ca^{2+}]$. Baseline values were representative of diastolic $[Ca^{2+}]_i$, while peak values represented systolic $[Ca^{2+}]_i$; the amplitude of the $[Ca^{2+}]_i$ transient was then calculated by: peak $[Ca^{2+}]_i$ – baseline $[Ca^{2+}]_i$. The time constant for the decay of the $[Ca^{2+}]_i$ transient (tau) was calculated by fitting a curve with a bi-exponential function using Axon Clampfit 8.2 software. As with cell shortening experiments, values were determined from the average of at least 10 steady state $[Ca^{2+}]_i$ transients per cell.

Biopterin measurements

The detection of the different biopterins BH4, BH2 and B (biopterin) was performed with *Ricardo Carnicer and Ashley Hale*, and achieved by separation and quantification by reverse phase HPLC (166). Biopterins were quantified by sequential electrochemical and fluorescence detection. The concentration of BH4 is determined from the current generated by the oxidation of BH4 to quinonoid BH2 (qBH2), followed by its reduction to regenerate BH4. The concentration of BH2 and B were measured simultaneously by fluorescence detection. Tissues and plasma were prepared from frozen (in -80°C storage); 20-30mg of LV tissue or whole aorta samples were homogenised as previously described in 500µl ice cold re-suspension buffer, followed by 2 centrifugations (15 min at 13 000 rpm and 4°C). For mGCH1-Tg mice, LV samples were prepared for use at 1:10 dilution. For plasma, 18µl of

plasma was added to 162µl re-suspension buffer. The BCA assay was performed as described previously to ensure equal protein content between samples.

Prior to processing, a volume of 180µl of the supernatant was taken from samples and standards and added to Eppendorf tubes containing 20µl of ice-cold 10x acid precipitation buffer. These were mixed well by vortexing and centrifuged for 5 min at 13 000 rpm (4°C). Supernatants were injected into the isocratic HPLC system; biopterins were separated using a Carbon-18 column (Hichrom) with a flow of mobile phase at the rate of 1.3 ml/min. Biopterins were quantified by sequential electrochemical (Coulochem III, ESA Inc, USA) and fluorescence (Jasco Ltd) detection. A background current of +500 nA at electrode 1 and -50 nA at electrode 2 was used for oxidation and reduction reactions for the detection of BH4. Loading samples were randomised into different batches with no more than 8 samples in each batch to minimise any oxidation during the assay run.

Biopterin concentrations were quantified by comparison with the following BH4 and BH2 reference standards (in nM): 100, 10, 7.5, 5, 2.5 and 1. These final concentrations were made up from stock solutions diluted with re-suspension buffer. BH4 and BH2 stocks (Schirks Laboratories, Switzerland) were made up in 20mM HCl to a final concentration of 10mM, which was subsequently verified with a UV spectrometer.

NOS activity

NOS activity was assayed jointly with *Ricardo Carnicer*, via radiochemical detection of the conversion of L-arginine substrate to L-citrulline, as detailed previously (199). The metabolic products of L-arginine were separated by ion exchange HPLC (Jasco Ltd) and online radiochemical scintillation detection (Lablogic systems, UK). The analysis of recorded data was performed using Azur software (Datalys, France). Frozen LV tissue was removed from -80°C storage and maintained on dry ice. Half of the LV was homogenised as described previously in 420µl of ice-cold KHB, also containing 5µM of N-hydroxy-nor-L-arginine (nor-NOHA, Millipore, USA). nor-NOHA acts an analogue of arginine which inhibits arginase activity; this is required to more accurately determine NOS activity since the activity

of arginases intrinsic to the LV tissue could potentially confound the readout. The concentration of 5µM was used as it allows for effective arginase blockade without compromising selectivity; nor-NOHA has been reported to inhibit the activity of nNOS and iNOS only at concentrations >1.5mM.

Sample homogenates were centrifuged for 10 min at 13 000 rpm (4°C). Supernatants were transferred to fresh Eppendorf tubes and maintained on ice, while a small volume was removed for protein quantification using the BCA assay as previously described. Samples were adjusted accordingly to contain 0.8mg protein in a volume of 200µl per sample. Supernatants were incubated on ice for 30 min with the addition of exogenous NOS cofactors: FMN 1mM, FAD 1µM, NADPH 1mM). This was performed in the absence or presence of the non-specific NOS inhibitor L-NAME (1mM), followed by 4 hour incubation at 37°C with 0.75µl of labelled ^{14}C L-arginine (1.85MBq/ml, Amersham Biosciences Ltd).

For de-proteination, 60µl of 10% TCA was added to each sample and samples were then centrifuged for 20 min at 13 000 rpm (4°C). 220µl of the supernatant was transferred to vials for HPLC also containing 100µl of 10% TCA and 450µl of MilliQ H_2O. To undergo chromatographic analysis, sample mixtures were loaded into the autosampler and cooled down to 4°C. Elution time was determined using standards of ^{14}C L-arginine (1µM), L-citrulline (0.1 µM) and L-orthinine (0.2 µM; all from Amersham Biosciences Ltd), with ^{14}C detected using scintillation counting. Chromatographic peaks were integrated and expressed in proportion to the total ^{14}C counts for each sample. The results were expressed as the L-NAME-inhibitable fraction of L-citrulline to represent the NOS-attributable component.

Collagen Assay

Total collagen in LV tissue was measured using a commercial assay kit (QuickZyme Biosciences, Netherlands); the assay is based on the detection of hydroxyproline, an amino acid which is abundant in collagen to increase stability of the triple helix. The assay relies on the production of a chromogen that can be absorbed at a wavelength of 540-580nm.

Frozen LV tissue was removed from -80°C storage and maintained on dry ice. Sections of LV were mechanically removed and quickly placed back on dry ice to prevent thawing. LV samples were weighed (approximately 10-20mg) and immediately transferred to screw-capped microtubes containing 100µl 6M HCl. Samples were incubated for 20 hours overnight at 95°C, after which they were removed and allowed to cool to room temperature. Samples were centrifuged at 13 000 rpm for 10 min at room temperature and the supernatants transferred to new microtubes and diluted with 4M HCl.

Collagen reference standards were prepared by dilution of the supplied stock solution (1200µg/ml in 0.02M acetic acid). 125µl of the stock solution was mixed with an equal volume of 12M HCl in a screw-capped microtube to give a final solution of 600µg/ml (in 6M HCl). This was incubated for 20 hours in exactly the same conditions as the samples, similarly followed by cooling to room temperature and centrifugation. The hydrolysed supernatant was then removed and used to make a standard line dilution (S1 to S8), with dilutions made up using 4M HCl in the following preparation design:

Standard no.	Sample source	4M HCl required	Final conc (µg/ml)
S1	**125µl of stock**	**125µl**	**300**
S2	**120µl of S1**	**60µl**	**200**
S3	**90µl of S2**	**90µl**	**100**
S4	**90µl of S3**	**90µl**	**50**
S5	**90µl of S4**	**90µl**	**25**
S6	**90µl of S5**	**90µl**	**12.5**
S7	**90µl of S6**	**90µl**	**6.25**
S8	**0µl**	**90µl**	**0**

35µl of reference standards and unknown samples were pipetted in duplicate into a 96-well microplate, followed by 75µl of assay buffer to each well. A supplied adhesive plate seal was pressed on to cover the plate, thereby preventing any loss of solution during the 20 min incubation on a vibrating plate shaker. Detection reagents A and B were prepared in a ratio of 2:3, with a total volume that allowed for 75µl per well. Following plate incubation, 75µl of the detection mixture was added to each well and a new adhesive seal applied to the plate. Plates were briefly placed back on to the shaker to mix the wells thoroughly before incubating for 1 hour at 60°C. The plate was then removed and

cooled on ice down to room temperature. The bottom of the plate was wiped clean ready for detection; colour changes were detected using an Omega Fluostar plate reader (BMG Labtech), measuring absorbance at 562nm. The recorded values were logged in MARS data analysis software and used for the calculation of the collagen standard curve, for which the unknown sample values could be compared and the collagen concentration determined (Figure 2.8) These concentrations were then normalised to the initial weight of the tissue sample used to give the total collagen content in µg/mg of tissue.

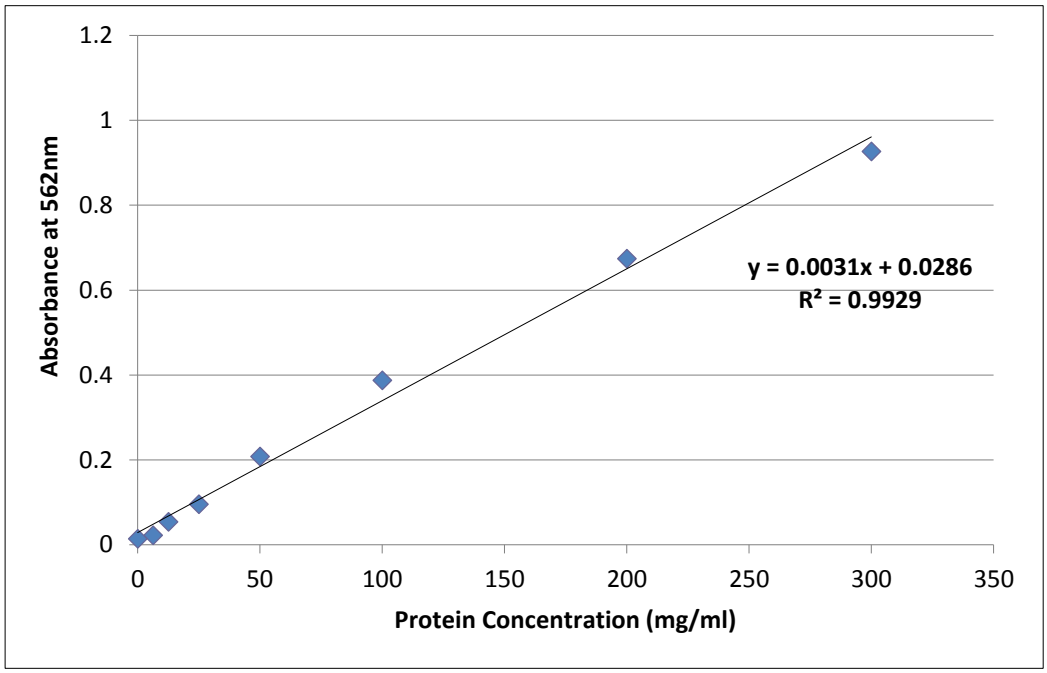


Figure 2.8. Generated standard curve for the Quickzyme collagen assay.

The absorbance (at 562nm) increases in proportion to the concentration of each known standard, producing a linear relationship that can be used for the determination of total collagen content in unknown hydrolysed tissue samples.

Glutathione assay

Glutathione was measured with *Esther Rosello-Lleti*, using a commercially available assay kit (Trevigen), based on the method of enzymatic recycling. The interconversion of glutathione between its reduced and oxidised form is an intracellular mechanism activated during oxidative stress (Figure 2.9).

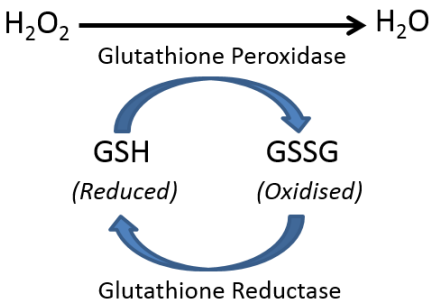


Figure 2.9. Enzymatic cycling of glutathione.

During oxidative stress, the reduced form of glutathione (GSH) is oxidised to GSSG by glutathione peroxidase, in the process reducing free radical hydroperoxides into H_2O. Through enzymatic recycling, GSSG can then be restored back to GSH by glutathione reductase.

During the assay, GSH reacts with the compound 5,5'-dithio-bis-(2-nitrobenzoic acid) (DTNB) to produce 5-thio-2-nitrobenzoic acid (TNB), which emits yellow fluorescence that can be detected at 405-414nm. The reaction of GSH and TNB also produces the mixed disulphide GSTNB; the recycling of GSTNB by glutathione reductase back to GSH then produces more TNB (Figure 2.10). The extent of TNB production is directly proportional to the recycling reaction, which is then directly proportional to the glutathione concentration. Since the assay relies on the enzymatic activity of glutathione reductase, the assay endpoint is reflective of overall total glutathione. The kit can also be used to isolate GSSG exclusively via glutathione reductase inhibition with 4-vinylpyridine.

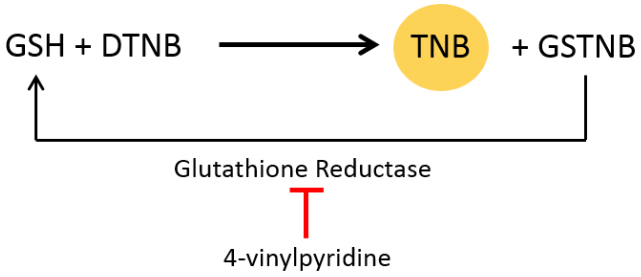


Figure 2.10. Fluorescence emission in the assay of glutathione.

The sulfhydryl group of GSH reacts with DTNB, producing both GSTNB and the fluorescent compound TNB. Recycling through glutathione reductase facilitates further TNB production, which is proportional to the sample glutathione concentration.

LV tissue was removed from -80°C storage and maintained on dry ice prior to preparation. LV segments were homogenised according to assay instructions using a manual glass dounce tissue grinder (Kimble-Chase, USA). Segments were placed into the grinding chamber containing ice-cold 5% metaphosphoric acid and homogenised sequentially with glass pestles A and B; pestle A for coarse grinding and pestle

B for finer tissue particulate. Homogenates were centrifuged at 13 000 rpm for 10 min at 4°C and the supernatants transferred to fresh Eppendorf tubes and maintained on ice prior to the assay.

Prior to plate loading, the supplied 25x assay buffer was diluted with MQ H_2O to obtain 1x assay buffer. The supplied reaction mix was prepared by reconstitution with 8ml MQ H_2O and gently mixed over 10-15 min to ensure the contents were fully dissolved. Immediately prior to the addition of the reaction mix to the standards and samples, the supplied vial of glutathione reductase was vortexed and 10µl added to complete the reaction mixture.

To determine total glutathione concentration, samples were first diluted 1:10 with 1x assay buffer. GSSG reference standards were prepared to establish a glutathione standard curve. 50µl of 1x assay buffer was first added in triplicates to rows A-E of a 96-well microplate. 50µl of the 4 µM GSSG stock was added to the 3 wells of row A and carefully mixed by trituration. A standard line dilution was then prepared from this as follows:

Row	Sample source	Final GSSG conc (pM per well)
A	**50µl GSSG stock**	**100**
B	**50µl of A**	**50**
C	**50µl of B**	**25**
D	**50µl of C**	**12.5**
E	**Blanks**	**0**

50µl of diluted experimental samples were then added in triplicate to separate rows and columns of the plate. For determining oxidised glutathione concentration, additional triplicate wells were allocated for standards and samples containing 4-vinylpyridine. For standards, 1µl of 2M 4-vinylpyridine was added to the 50µl of 4 µM GSSG stock. Serial dilutions of the 4-vinylpyridine-treated GSSG standards were then performed as displayed above. Similarly, 1µl of 4-vinylpyridine was added per 50µl of each experimental sample. Finally, 150µl of the completed reaction mixture was added to each wall and the absorbance detected at 405nm using an Omega Fluostar plate reader (BMG

Labtech). Absorbance was recorded over a 10 min period at 1 min intervals and the values logged in MARS data analysis software for the calculation of the GSSG standard curve.

Triplicate readings were averaged at each time point for each standard, each sample and blanks. These average values were plotted against incubation time to generate curves for each; the slope of the linear portion of each curve was then determined. The background slope was subtracted from slopes of the standards and the samples, and the net slopes of the standards were plotted against concentrations (pM) of GSSG. The net slopes of the samples were then compared with those of the standard curve to ultimately determine the concentrations of GSSG (total glutathione) in experimental samples. To establish the concentration of oxidised glutathione in each sample, the same procedure was carried out as described above, this time using the 4-vinylpyridine-treated standards and samples to obtain the net slopes. Lastly, the concentration of oxidised glutathione in each sample was subtracted from the concentration of total glutathione, thereby revealing the pM of reduced glutathione in each sample.

Vasomotor studies

Vascular reactivity was assessed *ex vivo* by isometric tension studies using wire myography. Vasomotor function was studied in aorta and mesenteric arteries in parallel; vascular beds were isolated from the same animals, at the same time, on the same day. Mesenteric arteries were studied by myself, while *Surawee Chuaiphichai* conducted experiments on aorta. Both experimenters used identical Mulvany-Halpern wire myograph systems (Multi-Myograph 610M, Danish Myo Technology, Denmark) and LabChart software (ADInstruments, New Zealand). Moreover, both experimenters were completely blinded to the mouse genotype and treatment group, as previously described. Prior to vascular experiments, each organ bath was calibrated and vessels normalised (see *myograph calibration and normalisation*).

Vessel preparation

For vessel preparation, 2 arterial segments of 2mm length were dissected from either the thoracic aorta or mesenteric artery, were dissected, cleaned of adherent connective tissue and mounted in the myograph organ baths using 25µm or 15µm diameter (for aorta and mesenteric arteries, respectively) gold-plated tungsten wire (Goodfellow, UK). All experiments were performed in KHB, 5ml per organ bath. After 30 min equilibration, optimal baseline tension was established by a stepwise-distension procedure and the construction of a passive tension-diameter curve, as previously described (200, 201). Following further equilibration for 30 min at the normalised basal tension (1-2 milliNewtons; mN), tissue viability was determined by constriction to a high-potassium salt solution (60mM KCl). This response is receptor independent and relies on the depolarisation of the smooth muscle cell membrane by high [K^+], which subsequently opens voltage-operated Ca^{2+} channels (VOCC) and facilitates calcium influx. All subsequent constrictor responses for each arterial ring were normalised to the respective KCl-induced constriction.

Vasoconstriction dose-response curves in aorta were achieved by the cumulative addition of half-log concentrations of phenylephrine (PE; 10^{-9} to 10^{-5} M). Given the rapidly waning responses to PE in mouse mesenteric arteries, vasoconstriction dose-response curves in mesenteric arteries were achieved using the thromboxane A_2 receptor agonist U46619 (10^{-9} to 10^{-5} M). Between all dose-response curves, vessels were washed 3 times with KHB and left to equilibrate for 30 min. Arterial rings were then preconstricted with the PE or U46619 dose necessary to achieve 90% maximal contraction, before assessing relaxation dose-responses.

Endothelial-dependent vasodilatation was determined by cumulative half-log additions of acetylcholine (ACh; 10^{-9} to 10^{-5} M). Identical relaxation dose-response curves were also carried out in the presence of the global NOS inhibitor L-NAME (10^{-4} M). Finally, to assess endothelium-independent vasorelaxation, dose-response curves were established with the NO donor sodium nitroprusside (SNP; 10^{-10} to 10^{-6} M). All relaxation responses were expressed as a percentage of the preconstricted tension.

Myograph calibration and normalisation

To ensure the accuracy of the tension readout on LabChart, the force transducer in each organ bath was calibrated using the supplied calibration kit (bridge and balance). The bridge was placed either side of the organ bath and the balance rested on top so that the pin lay between mounted wires on opposing jaws. A known 2g weight was applied on one of the pan arms, displacing the pin position to produce a force on the mounted wires. This unit weight was calibrated to a force of 9.81mN based on the following equation:

$$F_T = \frac{2\ cm \cdot (2\ g \cdot 9.81\ ms^{-2}) \cdot \sin 90}{4\ cm \cdot \sin 90}$$

$$F_T = 9.81\ gram \cdot m \cdot s^{-2}$$

Where:

- *2cm and 4cm correspond to the length of both pan arms*
- *2g represents the applied weight*
- *sin90 is the sine function for the 90° angle of the arms*
- *$9.81ms^{-2}$ is the constant acceleration of gravity*

For complete calibration with LabChart, a 2-point unit conversion procedure was performed by using the change in trace amplitude obtained after the addition of the weight to the balance arm (Figure 2.11). Each signal was subsequently set to corresponding tension values of 0mN and 9.81mN.

Prior to experimental protocols, a normalisation protocol was performed on each vessel segment to determine the appropriate baseline tension. A step-wise distension procedure was performed, recording force values at several incremental micropositioner settings (Figure 2.12), which could then be translated into measures of tension and vessel internal circumference. The internal circumference

was calculated for the optimum passive tension at a typical transmural pressure (for the specific artery and species), which was then used to determine the normalised lumen diameter and the correct micropositioner setting for the organ bath.

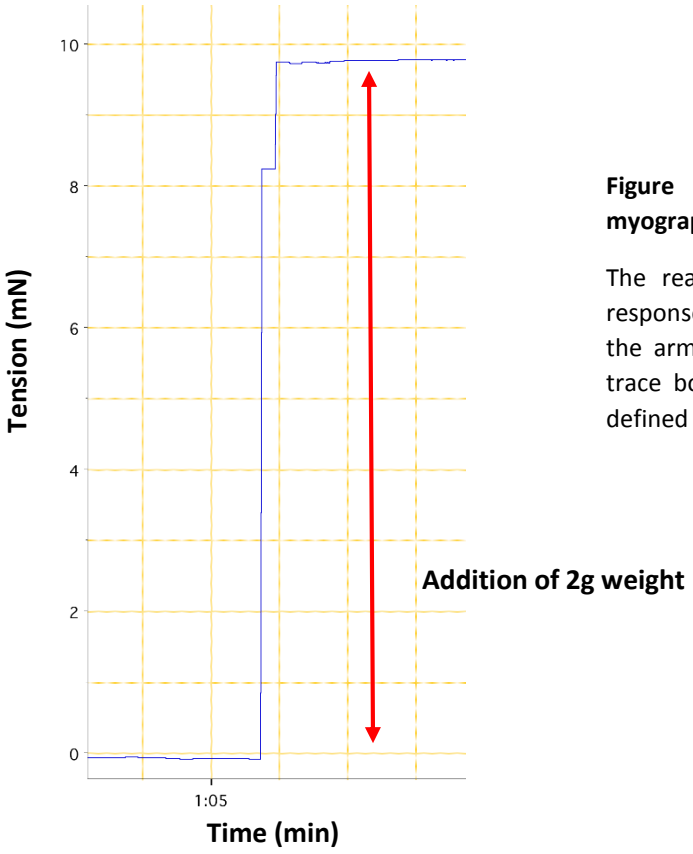


Figure 2.11. Calibration of LabChart with myograph organ bath.

The real-time readout of tension changes in response to the addition of the 2g unit weight to the arm of the calibration balance. The stable trace both pre- and post-addition were set to defined values of 0mN and 9.81mN respectively.

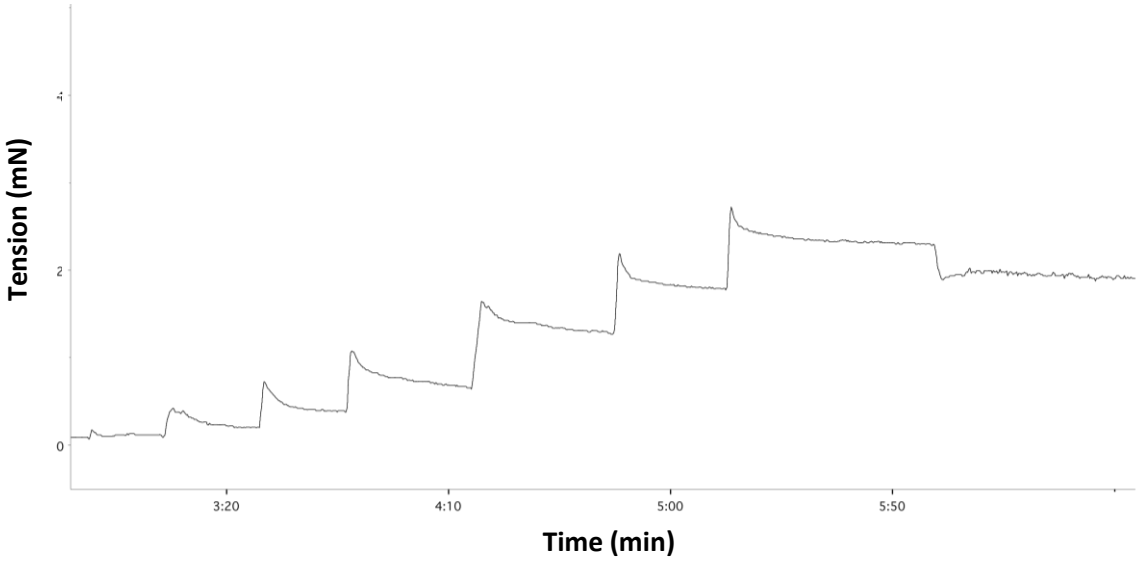


Figure 2.12. Normalisation protocol in organ bath experiments.

Representative LabChart trace for the step-wise distension procedure to normalise a vessel's baseline tension, as determined from its lumen diameter.

Peri-arterial nerve stimulation

For assessing perivascular nerve-mediated responses, platinum electrodes fixed to fine micromanipulators were lowered into the myograph chamber and carefully positioned either side of the vessel segment in parallel. Following normalisation and tests of tissue viability, a "wake-up" protocol was performed to stimulate quiescent nerves and re-initiate the synthesis and release of neurotransmitters *ex vivo*. This consisted of short (2 s duration) trains of electrical pulses delivered in increasing number (5, 10, 20, 30 40, 50), with a 30 s recovery between trains, all at electrical parameters that yielded functional responses, but which did not over-stimulate the nerves and cause irreversible neurotransmitter depletion (typically 25V, 10Hz and 0.8 ms pulse width). Similarly, following this, a "voltage-test" was carried out to determine the optimal voltage for that preparation, i.e. the voltage at which consistent, sub-maximal vasoconstrictor responses were observed (typically 25-30V). Frequency-response curves were performed at that established voltage, with a 10 s duration and a 5 min recovery period between stimulations at each frequency. Where appropriate, pharmacological agents were again pre-incubated for at least 30 min prior to stimulation; vessels were washed 3 times with fresh KHB between experimental runs and equilibrated for 30 min. Isolated nerve-mediated responses were confirmed by the abolition of response in the presence of 1µM tetrodotoxin (TTX). Maximal contractions were observed at the end of the experimental day following the addition of 40mM KCl + 10µM PE; where appropriate, electrically-stimulated vasoconstrictor responses (tension change from baseline) were expressed as a percentage of this maximal tension. For denudation of the vascular endothelium, a human hair was passed gently through the lumen of the vessel (as described in (202)) after it had be stably mounted in the organ chamber. Successful removal was confirmed by abolished responses to ACh, yet a maintained smooth muscle constrictor response to PE.

Arterial immunohistochemistry

2nd order mesenteric arteries from rat or mouse were dissected as above and pinned down at either end onto a Sylgard well-plate. Vessels were fixed in 2% paraformaldehyde (PFA) for 10 min at 37˚C and washed thoroughly with phosphate-buffered saline (PBS; 0.01M). Vessels were incubated in blocking buffer (1% bovine serum albumin (BSA), 0.1% Tween20 in PBS) for 1 hour at 37˚C, prior to overnight incubation at 4˚C in primary antibody dissolved in blocking buffer. The subsequent day, vessels were again washed with PBS and incubated for 2 hours in secondary antibody dissolved in blocking buffer (1% BSA, 0.01% Tween20 in PBS). Propidium iodide (45µM) and Lucifer Yellow (15µM) were added to stain for nuclei and the internal elastic lamina (IEL), respectively. Vessels were transferred to glass slides and imaged by confocal microscopy using FluoView Software (Olympus, Japan). Images were acquired through a water immersion objective at 1024 x 1024 pixels; *z*-stacks through the arterial wall were taken at 0.5-1µm increments.

Creatine kinase activity

Creatine kinase (CK) is an enzyme that acts as an energy shuttle between the mitochondria and the cytosol, catalysing the reversible conversion of ATP + creatine to ADP + phosphocreatine (PCr). Activity of the enzyme can be assayed by detecting the change in absorbance due to reaction products downstream. The generated ATP in the reverse reaction is used by hexokinase to phosphorylate available glucose to glucose-6-phosphate. In the presence of NAD, glucose-6-phosphate is oxidised to 6-phosphoglucanate; NAD is reduced to NADH in this process which alters the absorbance that can be detected at 340nm.

CK activity was measured by *Hannah Whittington*. LV samples were removed from -80°C storage and maintained on dry ice. Approximately 5mg of tissue was used per sample; the tissue segment was quickly weighed and placed directly into a homogenising vessel containing 1ml of ice buffer. Samples were homogenised using a pre-cooled glass homogenising rod at a speed of 1300 revs/min for approximately 5 s, until the solution no longer contained any visible tissue fragments. Further volumes

of ice buffer were added to each homogenate to achieve 5mg/ml, this volume dependent on the initial weight of the LV segment.

150µl of the homogenate solution was removed and split into triplicates of 50µl in fresh microtubes for use in the protein assay. The remaining homogenate volume was calculated in order to determine the Triton-X 100 (10% stock) volume required to give a final concentration of 0.1% in solution. After the addition of Triton-X 100, the sample mixtures were vortexed and allowed to precipitate on ice for 30 min.

For analysis of the different CK isoenzymes, separation and quantification was achieved using a rapid gel electrophoresis (REP) unit (Helena Laboratories, UK). This technique enables the separation of creatine kinase isoforms due to their distinct differences in isoelectric points (203, 204). Following precipitation, 80µl of sample supernatants were added to 80µl of 0.9% NaCl solution and the mixture vortexed prior to loading in duplicate into wells (75µl per well) of the sample tray. The REP CK isoenzyme control was also added to one of the wells to verify the proper location of the sample bands. The vial of supplied CK reagent was then resuspended in 700µl of the CK diluent. This CK reagent consists of the metabolites and enzymes necessary for the CK assay reaction: ADP, AMP, creatine phosphate, NAD, glucose, hexokinase, glucose-6-phosphate dehydrogenase; in addition it contains N-acetylcysteine (NAC), an activator of CK, along with magnesium acetate to maintain CK stability. 14µl of 1mM Ap5A (giving 20µM final conc.) was also added to the CK reagent to inhibit adenylate kinase, which has previously been shown to mimic some of the CK isoenzyme fractions during electrophoresis (205). The CK reagent was thoroughly mixed and loaded into the REP machine, after which 750µl of REP Prep solution was placed into the gel area and the gel inserted into the REP chamber. Carbon electrodes were then cleaned and placed at either end of the gel to commence electrophoresis (3 min, 1200V, 13°C). The REP unit densitometer automatically calculated the relative percentage and absolute readings for each detected band, displaying different peaks that represent each of the following CK isoenzymes:

Isoenzyme	Expression
CK-Mito	Mitochondria
CK-MM	Skeletal muscle, heart
CK-MB	Heart
CK-BB	Brain

For CK activity by spectrophotometry, 10ml of MQ H_2O was added to the CK-NAC reagent and the mixture incubated in a water bath at 30°C. Samples were assayed in triplicate; in separate microtubes, 20µl of sample was mixed with 80µl of ice buffer and then maintained on ice. 20µl of this mixture was loaded into cuvettes with 1ml CK reagent and the absorbance detected at 340nm in the spectrophotometer. Results were expressed as mIU/mgww.

CK-Mito activity was normalised to citrate synthase activity; citrate synthase is localised to the mitochondrial matrix and is a reliable marker of a tissue's oxidative capacity due to its involvement in the primary stages of the citric acid (TCA) cycle. Specifically the enzyme catalyses the reaction of oxaloacetic acid and acetyl CoA to produce citric acid and CoA. The reaction mixture for assaying citrate synthase activity was therefore made up of acetyl CoA (10mM), DTNB (1mM) and oxaloacetic acid (10mM; to be added immediately prior to detection), As previously described (see Glutathione assay), DTNB reacts with free thiol groups, in this case from CoA, to produce the fluorescent compound TNB. The intensity of this fluorescence is then proportional to the level of citrate synthase activity in the sample. Samples were measured individually in duplicate; 50µl of sample was added to a cuvette containing 850µl of the reaction mixture (acetyl CoA + DTNB). The reaction was allowed to take place for 3 min, after which 100µl of oxaloacetic acid was added and mixed, followed by detection of absorbance at 412nm. Absorbance readings were taken at 2 s intervals over a 40 s duration and automatically plotted.

Echocardiography

Global cardiac function was studied *in vivo* using a high-resolution 2D-echocardiography system (Vevo 2100, Visual Sonics, Canada) with an ultra-high frequency MS400 transducer probe (18-38 MHz). Echocardiography procedures were conducted jointly with *Ricardo Carnicer and Klemen Ziberna*, following which analysis was conducted by all 3 parties and evaluated for consistency between individuals. Before procedures were conducted, experimenters were blinded to genotype and treatment group, being assigned the mice independently purely on the basis of numerical ID. The echocardiography system was set-up as shown in Figure 2.13. The mouse was placed in an induction chamber and anaesthesia was induced by 4% isoflurane 21% oxygen, before transfer of the mouse to an imaging table with integrated heating pad. Anaesthesia was subsequently reduced to 2% and maintained via inhalation, while the heating pad was maintained at constant temperature of 38˚C (maintaining internal body temperature at 41˚C). Protection of the eyes during the procedure was ensured with viscotear gel (Novartis, UK). 2D images (standard B-mode) of the heart were obtained, as well as mitral blood inflow and tissue velocities by pulse-wave Doppler. LV wall dimensions were determined in the parasternal short-axis view (M-mode), from which measures of ejection fraction and fractional shortening were derived. Systolic function could be assessed at physiological heart rates of ~500 beats/min.

Diastolic properties were determined by observed peaks from tissue Doppler velocities denoting early (E') and late (A') filling. To ensure adequate separation and measurement of early and late filling phases, anaesthesia was adjusted accordingly to achieve a necessary heart rate in the region of ~350 beats/min. Early filling represents the natural movement of blood from the atrium to the ventricle by virtue of the natural pressure gradient, as generated by LV isovolumic relaxation. Late filling represents the remainder of blood pumped into the ventricle from active atrial contraction. The E'/A' ratio is used as a standard indicator of diastolic function and is also complemented by the E/E' ratio, where E signifies the early transmitral flow velocity, as opposed to E', which represents the early

diastolic tissue velocity. Following each procedure, mice were placed in a recovery chamber maintained at 37˚C. Traces were analysed using the Vevo software and summary data comprised of at least 3 cardiac cycles for each parameter.

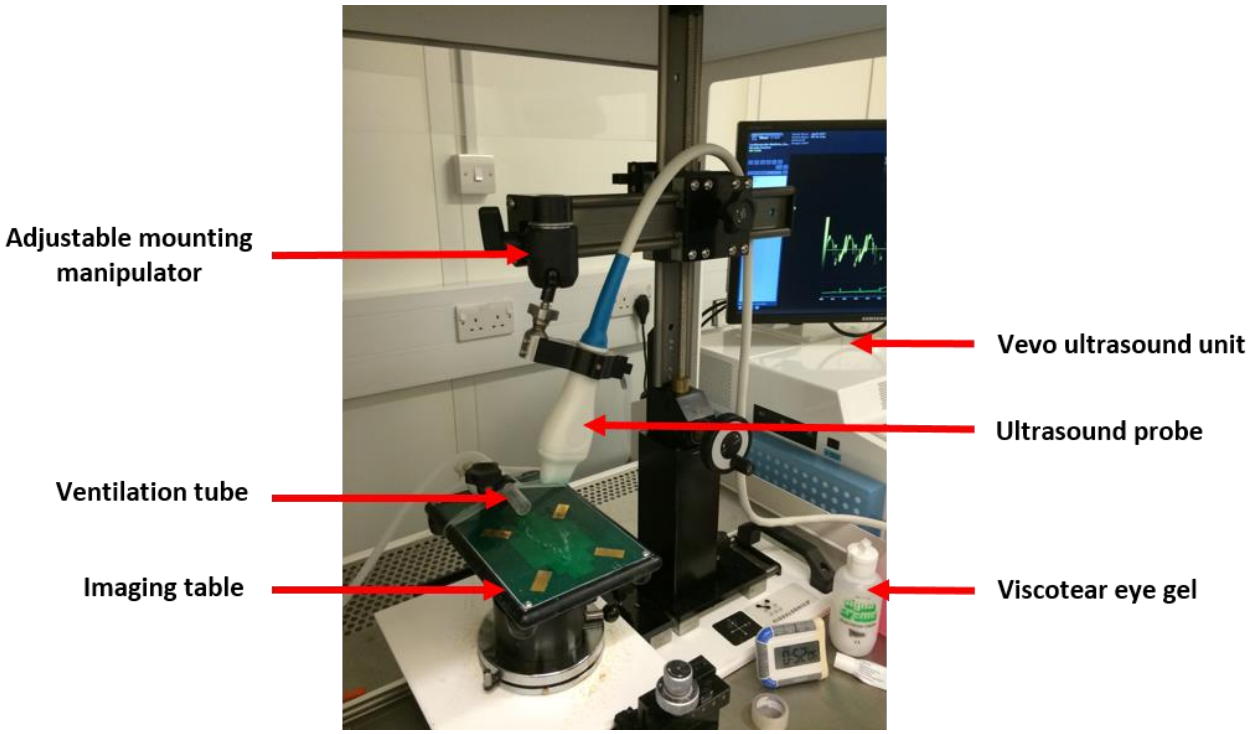


Figure 2.13. Imaging set-up for the performance of 2D-echocardiography.

Imaging was performed inside a ventilated hood in the animal facility, with the ultrasound probe connected to the adjacent, high-resolution echocardiography mobile unit.

Histology

Lipid content

Lipid accumulation in the myocardium was assessed by *Esther Rosello-Lleti* using the oil red O (ORO) stain. ORO is a diazol fat-soluble dye which can be used to stain for neutral lipids (triglycerides, diacylglycerols and cholesterol esters). The hydrophobic nature of the dye causes its migration from the solvent to associate with lipids present in the tissue section. To enable lipid quantification, LV tissue was collected in optimal cutting temperature (OCT) compound (VWR, USA) and placed in a bath of isopentane bathed in liquid nitrogen to flash-freeze and maintain tissue integrity. OCT compound

was selected over standard paraffin for embedding because the process of deparaffinisation and alcohol fixation would cause the extraction of present lipids.

For tissue preparation, ORO stock was prepared according to manufacturer's instructions (Sigma-Aldrich). 2.5g of ORO was added to 400ml of 99% isopropyl alcohol and mixed by stirring for 2 hours at room temperature. For the ORO working solution, 1.5 parts stock solution was added to 1 part MQ H_2O and the solution allowed to thicken over 10 min at 4°C. Before use, the solution was filtered to remove any precipitates. Embedded LV tissue was removed from -80°C storage and maintained on dry ice prior to sectioning. LVs were quickly sectioned on a cryostat into 12µm-thick sections; 3 cross-sections were taken for each LV at different depths and collected onto the same slide.

For staining, ORO working solution was added to sections so that they were completely covered and the sections incubated for 5 min. Slides were placed into a holder and the ORO was washed away by rinsing with water intermittently for approximately 30 min. Slides were air-dried and mounted with coverslips using aqueous mounting medium and sealed using nail polish. Stained sections were imaged the same day using a bright-field light microscope (Nikon Eclipse TE2000U Inverted Microscope) with 20x magnification. Staining intensity was quantified using ImageJ software (v. 1.46r; National Institutes of Health, USA).

Myofilament mechanics

Myofilament function was determined in experiments by *Cameron Turtle*, using demembranated trabeculae, which enables the assessment of Ca^{2+}-sensitivity and force development (over $-\log_{10}$ calcium concentrations; pCa), as well as passive stiffness. For skinning trabeculae, mice were sacrificed and the hearts quickly excised and placed in ice-cold Tyrode solution. Trabeculae (80-250µm in width; 1-3mm in length) were dissected from the LV wall while submerged in dissecting solution. Trabeculae were placed in a microtube of skinning solution and placed on a rotator at 4°C overnight, after which they were transferred to glycerinated relaxing solution and secured between aluminium T-clips (Kem-Mil, USA).

Measurements were performed using a permeabilised fibre test system (Aurora Scientific, Canada), with skinned trabeculae attached either end by T-clips to the pin hooks of a force transducer. Sarcomere length was then detected via laser diffraction. Initially, the muscle fibres were stretched to a sarcomere length of 2.3µm and equilibrated in force fibre solution of pCa 9.0. Trabeculae were briefly bathed in a pre-activating solution (pCa 9.0) which lacked EGTA, thereby limiting potential Ca^{2+} chelation once fibres were transferred to activating solution. Initial activation was performed at pCa 4.0, after which trabeculae were correctly repositioned and sarcomere length re-established at 2.3 µm. An eyepiece graticule was then used to measure fibre width to allow normalisation of measurements to the cross-sectional area of the fibre.

To determine force-Ca^{2+} sensitivity and tension development, fibres were placed in incremental pCa solutions corresponding to the sequence displayed in Figure 2.14. The force production of the fibre was monitored in each pCa solution until it reached equilibrium. Fibres were shortened to 85% of their original length (0.85*L_0), held for 50ms, re-stretched to 1.05*L_0 and then returned back to the original length. For assessing passive stiffness and stress relaxation, fibres were stretched and held at different lengths; the induced stress then decreases with time, which is a known property of viscoelastic materials (206). Fibres were initially placed in pCa 9.0 force fibre solution and stretched to a sarcomere length of 2.0µm. A stretch and hold procedure was then performed, with fibres stretched over a period

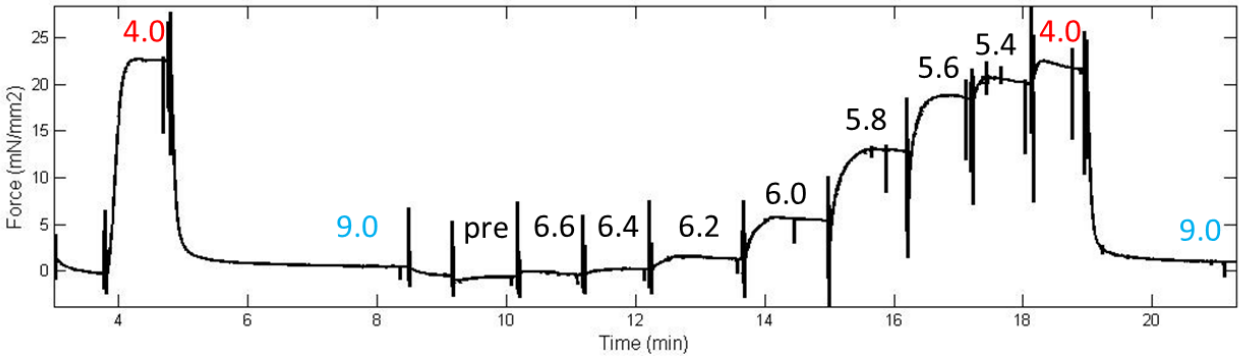


Figure 2.14. Raw trace of force-Ca^{2+} sensitivity and tension development procedure in demembranated trabeculae.

Fibres were subjected to solutions of incremental pCa solutions and the force production measured at each level of calcium. The maximum isometric force was generated at a pCa of 4.0 and was measured both at the beginning and end of the incremental protocol. This permitted a calculation of the "rundown" in force throughout the experiment. Fibres that had a rundown of greater than 15% were excluded from analysis.

of 15 s, followed by a hold for 180 s. This was performed to generate the following lengths: 1.05*L_0, 1.10*L_0, 1.15*L_0, 1.20*L_0, 1.25*L_0, and 1.30*L_0, with sarcomere length recorded after each stretch.

A custom-built application was developed using Matlab software (Mathworks, USA) for the analysis of force-Ca^{2+} sensitivity and tension redevelopment. The force generated at each pCa was determined by taking the baseline force and subtracting the force recorded after the shortening of the fibres to 0.85*L_0. The rate of tension redevelopment was ascertained by fitting an exponential curve according to the following equation:

$$Force = F_{Max} * \left(1 - e^{k_{tr} * t}\right) + F_{Res}$$

Where:

- F_{Max} *represents maximum tension*
- K_{tr} *is the rate of tension redevelopment*
- *t denotes the time after re-stretch*
- F_{Res} is residual tension following restretch

To determine Ca^{2+}-dependent force specifically, the measure of passive stiffness was subtracted from the force generated at each pCa. This value for passive stiffness was derived from the force measured in pCa 9.0 solution at the start and end of each experimental run. The Ca^{2+}-dependent force was plotted against each pCa and so the force-Ca^{2+} sensitivity relationship could be resolved.

Plasma insulin quantification

The concentration of insulin present within the plasma was determined using a rat/mouse insulin ELISA kit (Millipore), which detects insulin on the basis of a sandwich ELISA assay. Plasma samples were removed from -80°C storage and thawed on ice prior to loading. 18µL of plasma samples were aliquotted along with supplied insulin standards (0.2, 0.5, 1, 2, 5 and 10ng/mL) into wells of the 96-well microtiter plate coated with mouse monoclonal anti-rat insulin antibody. To ensure quality

control of the ELISA, two independent control samples, which were supplied by the manufacturer and covered the analytical range of the assay, were also loaded into the plate. All samples, standards and controls (including blanks) were loaded in duplicate. The following steps were carried out using a multi-channel pipette to ensure consistent loading and reaction times across wells.

Biotinylated anti-insulin detection antibody was added to all wells, after which the plate was sealed and incubated for 2 hours at room temperature on an orbital plate shaker at 300 rpm. Solutions were carefully decanted from the wells and washed 3 times with the supplied wash buffer (5mM TBS containing Tween20) to remove any unbound antibody-insulin complexes. Enzyme solution containing horseradish peroxidase was added to all wells; the plate was then resealed and placed back onto the shaker for 30 min. Solutions were again decanted and wells washed 6 times with wash buffer to remove any unbound antibody-enzyme conjugates. Substrate solution containing 3,3',5,5'-tetramethylbenzidine was added to all wells, after which the plate was sealed and placed back onto the shaker for a final 20 min. The reaction was terminated by the addition of stop solution (0.3M HCl), transforming the solution from blue to yellow due to acidification. The plate was carefully shaken by hand to ensure mixing of all wells, checked for bubbles and then immediately loaded into the plate reader for detection. Absorbance was read at 450nm and 590nm and the difference between the two sets of values used for analysis.

The mean of all duplicates was calculated and a reference curve produced from the insulin standards. A dose-response curve was fitted to the standards using a sigmoidal 4-parameter logistic equation (Figure 2.15), which was subsequently used to determine the concentrations of insulin within plasma samples (displayed as ng/ml).

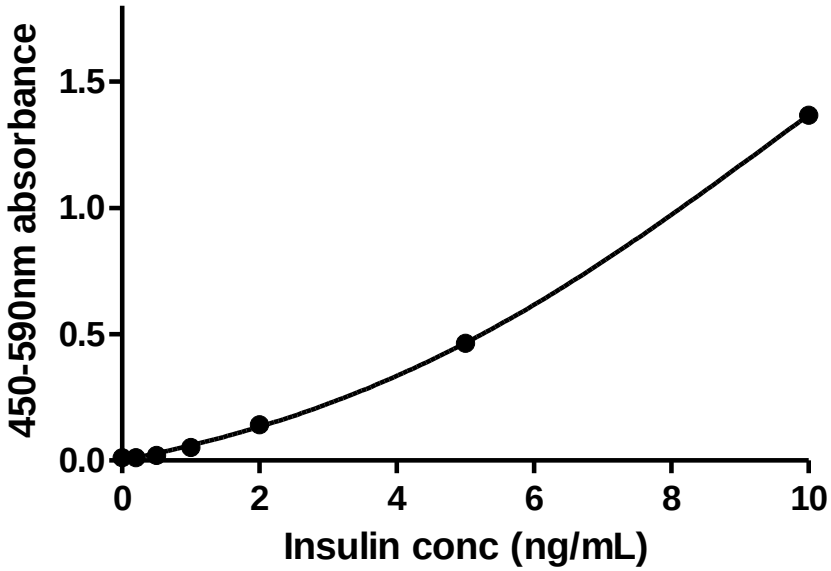


Figure 2.15. Reference curve generated from insulin standards during the ELISA assay.

The absorbance (at 450nm, corrected for at 590nm) increases in proportion to the insulin concentration of each known standard, producing a dose-response relationship that can be used for the determination of insulin levels in unknown plasma samples.

Oral BH4 supplementation

BH4 supplementation was performed by *Klemen Ziberna*, and was implemented on a subset of mice after 6 weeks of the diabetes protocol. Oral BH4 (Schirks Laboratories) was incorporated into mouse chow, the volume of which was calculated to achieve 200mg/kg/day dose. Supplementation continued for the remaining 6 weeks until the 12 week terminal end point.

Statistical analysis

All data are expressed as the mean ± SEM; *n* represents the number of samples, myocytes or mice and will be stated as appropriate. Data were assessed for normality of distribution and for comparisons between two independent groups, an un-paired (two-tailed) Student's t-test was performed. For comparisons between more than two means, a two-way analysis of variance (ANOVA) was performed with a Bonferroni correction. Statistical analysis was performed using GraphPad Prism 5 software. At a value of $P < 0.05$ the null hypothesis was rejected. Throughout my results, levels of statistical significance are denoted by the following:

* = P < 0.05 ** = P < 0.01 *** = P < 0.001

Chapter 3

The role of nNOS in resistance vessels

Introduction

In addition to the long-appreciated effects of eNOS, the neuronal isoform of NOS (nNOS) has received more recent recognition for its own influence on the control of vascular tone. Seddon and colleagues were able to show in clinical studies that nNOS was involved in the modulation of both peripheral and coronary blood flow, potentially acting as a tonic regulator, independent of the dynamic eNOS-mediated changes to blood flow (116, 117). However, to label nNOS-derived NO as purely a modulator of basal arterial tone is likely a simplification. For instance, nNOS has been linked with modulating myogenic tone, as suggested by data revealing the interaction between nNOS and the plasma membrane Ca^{2+}-ATPase (PMCA) in arterial smooth muscle (118). Furthermore, specifically blocking the action of nNOS in other experimental protocols has highlighted its likely role in the vasodilator responses evoked during mental-stress (117) and whole-body heat stress (119). Assembling this data together suggests that the control of vascular tone and consequent blood pressure changes may be regulated not just by the type of NOS isoform, but also at the level of the specific vascular bed and the nature of the local stimulus.

The vascular origins of nNOS-derived NO

Despite the recognised significance of nNOS-derived NO on local vascular responses, the exact origins of this species still remain unclear. Some have advocated vascular smooth muscle cells themselves as the source, as identified pharmacologically and from physiological tests of reduced KCl-induced contraction following specific nNOS inhibition (207). Along with typical eNOS expression, a case has also been made for endothelial cell expression of the neuronal isoform. In the eNOS-KO mouse, Huang et al. observed preserved flow-induced vasodilatation; the effect was then significantly attenuated by putative nNOS inhibition using 7-NI. Moreover, this inhibition was ineffective in wild-type animals, suggesting a compensatory upregulation of endothelial nNOS expression and activity in an environment of eNOS deficiency (208). In terms of the redistribution of cardiac output, exercise requires a complex vascular response, which could be facilitated partly via the activity of nNOS located

within skeletal muscle. The site of this nNOS appears to be the sarcolemma, where it is anchored to the membrane through a dystrophin-glycoprotein complex. The significance of this is highlighted in Duchenne muscular dystrophy (DMD), where the nNOS deficiency is manifested as functional muscle ischemia (209).

The putative "nitrergic" nerve

Being the neuronal isoform of the enzyme, nNOS is indeed expressed within nerves; the exact type and location of those nerves for neurovascular control, however, is unclear. The characteristic cGMP-mediated vasorelaxation has led to the concept of a "nitrergic nerve" within the perivascular bundles innervating blood vessels. Double immunostaining in resistance arteries have also indicated that nitrergic nerves and noradrenergic nerves coalesce extensively, whereby it is suggested the nNOS-derived NO inhibits vasoconstriction by modulating release of noradrenaline (210), as opposed to a direct post-junctional inhibitory effect (211). The potential mechanism is not known, though studies on neurotransmission in different tissue types might suggest that activation of the NO-cGMP pathway could result in phosphorylation and closure of voltage-operated calcium channels (VOCCs), thereby diminishing vesicular release (212). However, conflicting evidence has argued against pre-junctional modulation, with the observations that inhibition of this pathway did not increase vasoconstrictor responses to endogenous noradrenaline. Instead the NO may reduce the biological activity of noradrenaline already secreted across the junction, as demonstrated in studies of direct chemical interactions between NO and catecholamines (213).

nNOS as a modulator of non-adrenergic, non-cholinergic (NANC)-mediated vasodilatation

Alternatively, or perhaps in addition to these distinct nitrergic nerves, Hatanaka and colleagues have suggested that nNOS is expressed in primary sensory afferents (capsaicin-sensitive), whereby NO is released as a co-transmitter with calcitonin gene-related peptide (CGRP) (211). As well as regulating adrenergic-mediated vasoconstriction, other studies report that NO can also inhibit the release of CGRP from sensory nerves to modulate non-adrenergic, non-cholinergic (NANC)-mediated

vasodilatation (214). Taking such findings together suggests that NO originating in either nitrergic or sensory neurons may not only produce its own vasodilator activity, but could also provide dual negative feedback over opposing responses, which may account for the very tight regulation of vascular tone (Figure 3.1).

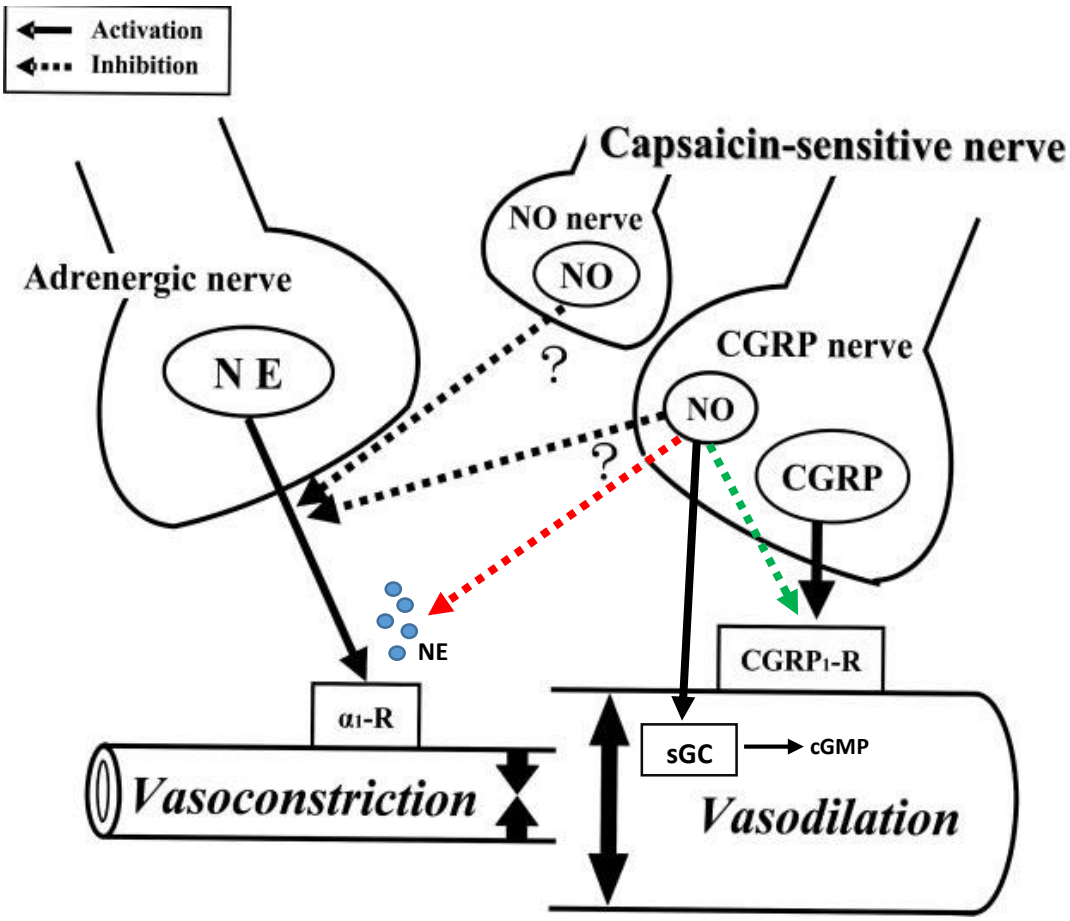


Figure 3.1. Potential mechanisms of the regulation of vascular tone by neuronally-derived nitric oxide.

NO released from sensory-motor nerves or a distinct subset of nitrergic nerves may inhibit the pre-junctional release of noradrenaline (black). Alternatively, vasoconstriction may be attenuated through an NO-mediated reduction in the bioavailability of noradrenaline (red). Despite its own vasodilator effects (via soluble guanylyl cyclase), NO may also serve to regulate the neurogenic dilator function of CGRP (green).

Modified from [173].

Methods

Vasomotor studies

2nd order branches from rat mesenteric arteries were isolated and dissected clean of adherent connective tissue. Vascular reactivity was measured as described in Chapter 2, employing a dual platinum electrode for the stimulation of peri-arterial nerves. Frequency-response curves were performed at the voltage established during the "voltage-test" protocol, with a 10 s duration and a 5 min recovery period between stimulations at each frequency. Pharmacological agents were pre-incubated for at least 30 min prior to stimulation; vessels were washed 3 times with fresh KHB between experimental runs and equilibrated for 30 min. Electrically-stimulated vasoconstrictor responses (tension change from baseline) were expressed as a percentage of maximal tension.

Immunohistochemistry of pinned out arteries

Mesenteric arteries from rat or mouse were dissected as above and pinned down at either end onto a Sylgard covered dish. For isolation of the myenteric plexus, a section of the surrounding mesentery was dissected such that the longitudinal muscle layer could be peeled away from the mucosal layers. Subsequent to fixation and antibody incubation, tissues were imaged by confocal microscopy using FluoView Software (Olympus), as explained in Chapter 2. Images were acquired through a water immersion objective at 1024 x 1024 pixels; *z*-stacks through the arterial wall were taken at 0.5-1µm increments.

Results

NOS involvement in nerve-mediated vasoconstriction

The nature of vasoconstrictor responses mediated by the surrounding perivascular nerves was investigated using electrical stimulation. To achieve primary constrictor responses that were reproducible and of sufficient magnitude, as well as to isolate the NO-mediated component of the resulting competing vasodilatation, experiments were conducted in the presence of the β_1/β_2-

adrenergic receptor antagonist propranolol (100nM) and the CGRP antagonist (8-37) (3µM) as both mechanisms play an important role in triggering vasodilator responses following the stimulation of perivascular nerves. Electrically induced vasoconstriction was frequency dependent; as initially established in the optimisation protocol, trains at 2Hz produced a contraction that was <1% of maximum, while the response at 15Hz was 10% of maximal contraction.

NOS inhibition with the putative nNOS inhibitor N5-(1-Imino-3-butenyl)-L-ornithine (L-VNIO) (100µM) caused augmented constrictor responses at all frequencies of stimulation, which were most significant at 12 and 15Hz (Figure 3.2A). Removal of the endothelium enhanced vasoconstriction at each frequency as compared to intact vessels. However, incubation of denuded arteries with L-VNIO produced only a minor increase in achieved tension (17% vs 14% of maximum; Figure 3.2B). This potentially indicated a lack of nNOS specific inhibition by L-VNIO and a greater role played by endothelium-derived NO versus neuronally-derived NO in opposing the electrically-induced vasoconstriction. To confirm that observed responses were nerve-mediated in origin and not due to direct electrical stimulation of vascular smooth muscle, vessels were incubated with TTX, which subsequently abolished all responses (Figure 3.2C).

Nerve-mediated vasoconstriction

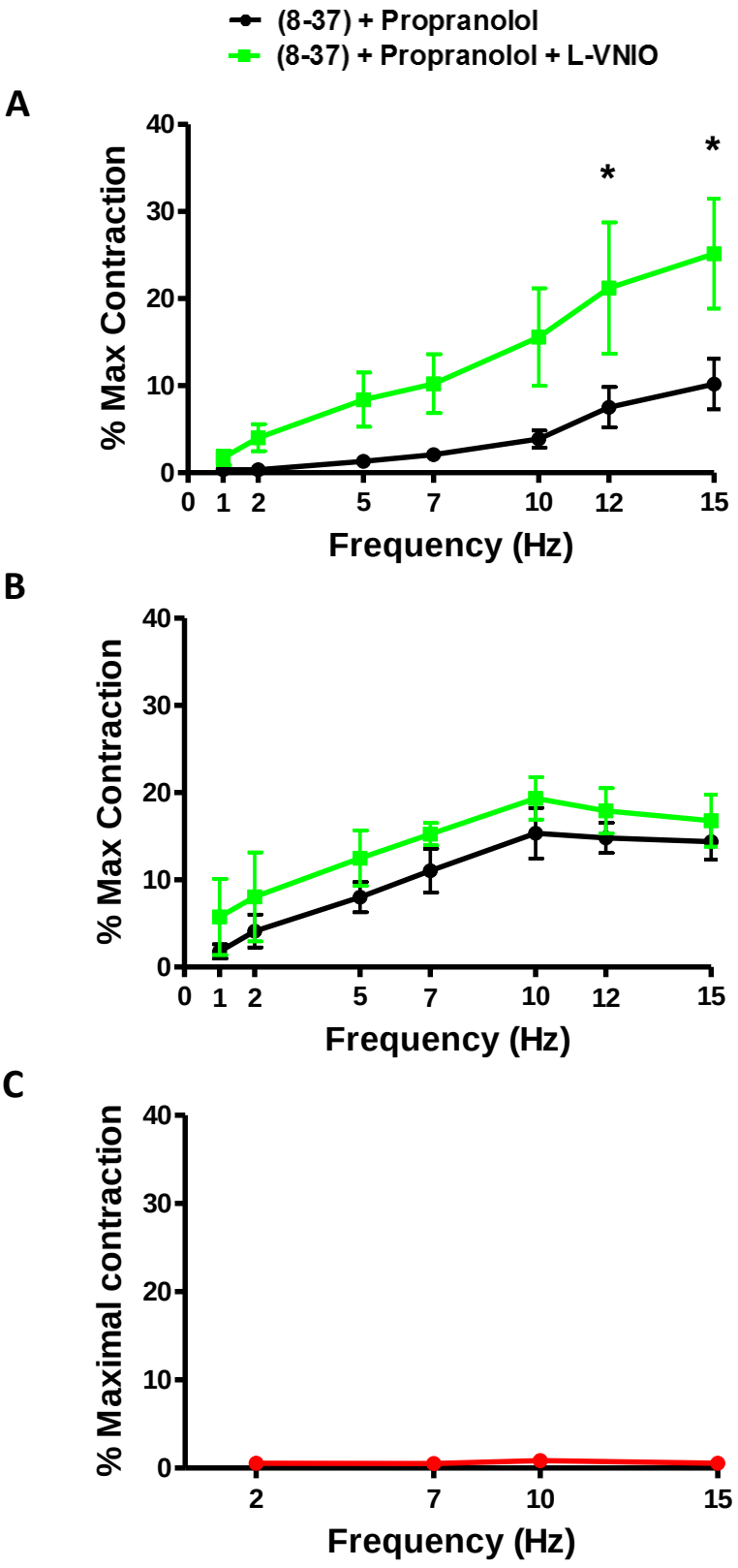


Figure 3.2. NOS inhibition augments electrically stimulated constrictor responses.

Peri-arterial nerve stimulation produced a vasoconstriction that was frequency dependent, observed in both **(A)** intact and **(B)** denuded vessels. Electrical stimulation was performed in the presence of CGRP (8-37) and propranolol, as well as following the addition of L-VNIO. **(C)** Nerve-mediated changes in tension were confirmed by the abolition of responses in the presence of 1µM tetrodotoxin (TTX). Measurements were taken from the initial peak in achieved tension. *P<0.05; n = 3-5 mice per treatment.

Contribution of NOS to neurogenic vasodilatation

To elicit a specific sensory nerve-mediated vasodilatation, without the confounding effects of other nerves activated during general electrical stimulation, rat mesenteric arteries were treated with the transient receptor potential cation channel V1 (TRPV1) agonist capsaicin (1μM) after stable preconstriction with the prostaglandin analogue U46619 (300nM). Intact control vessels exhibited a rapid relaxation (>90% relaxation within 80s; Figure 3.3B) following sensory neurotransmitter depletion induced by capsaicin. CGRP receptor inhibition with (8-37) nearly completely abolished this vasodilatation, while the maximal relaxation achieved after NOS inhibition with L-VNIO still reached 72%, albeit at a slower rate, indicating a greater vasodilator effect of CGRP than NO following sensory nerve activation. Endothelium removal significantly reduced the extent of relaxation under control conditions compared to intact vessels, reaching a maximum of only 41% at 60s after the addition of capsaicin (Figure 3.3C). Once again, CGRP blockade nearly completely abolished the vasodilator response, while incubation with L-VNIO led to a vascular relaxation that was similar to that observed under control conditions. These results suggest that the vasodilatation triggered by TRPV1-induced depletion of sensory nerves is more sensitive to CGRP than to NOS inhibition; moreover, the extent of this vasodilatation is blunted considerably by the absence of a functional endothelium.

Isoform selectivity of available NOS inhibitors

As previous data suggested that L-VNIO might be non-selective for nNOS at the concentration used, vasorelaxation dose-response curves to ACh were performed in the presence of inhibitors of the small-conductance and intermediate-conductance calcium-activated potassium channels (SKCa and IKCa), responsible for endothelium-dependent hyperpolarising factor (EDHF)-mediated dilatation in the rat mesentery. Under these conditions, ACh-induced vasodilatation could be attributed to the actions of eNOS, for which the effects of the NOS inhibitors were tested. At all three test concentrations, L-VNIO significantly right-shifted the ACh dose-response curve, demonstrating substantial blockade of eNOS-mediated dilatation; this effect was most marked with the 100μM L-VNIO concentration (as used

earlier in the study), whereby 50% relaxation was only attained at a maximum dose of 10µM ACh (Figure 3.4A). The purported nNOS/iNOS inhibitor 1400W showed a slight right-shift in eNOS-mediated relaxation at the 100µM concentration, while the curves constructed in the presence of lesser inhibitory concentrations showed no difference compared to control (Figure 3.4B). AAA-N, a putative nNOS inhibitor used previously in the lab following its earlier identification (215), showed no inhibition of eNOS-dependent vasodilatation, as dose-response curves remained identical at all AAA-N concentrations used (Figure 3.4C). Finally, S-methylthiocitrulline (SMTC), a compound widely used by the laboratory and others for selective nNOS blockade (115-117), was also investigated. The profile of vascular relaxation to ACh in the presence of SMTC was similar to that with AAA-N; there was no impairment of eNOS-mediated dilatation (Figure 3.4D). This screening demonstrated the relative nNOS-selective inhibition conferred with the experimental use of SMTC and AAA-N as compared to the other currently commercially available isoform-specific NOS inhibitors.

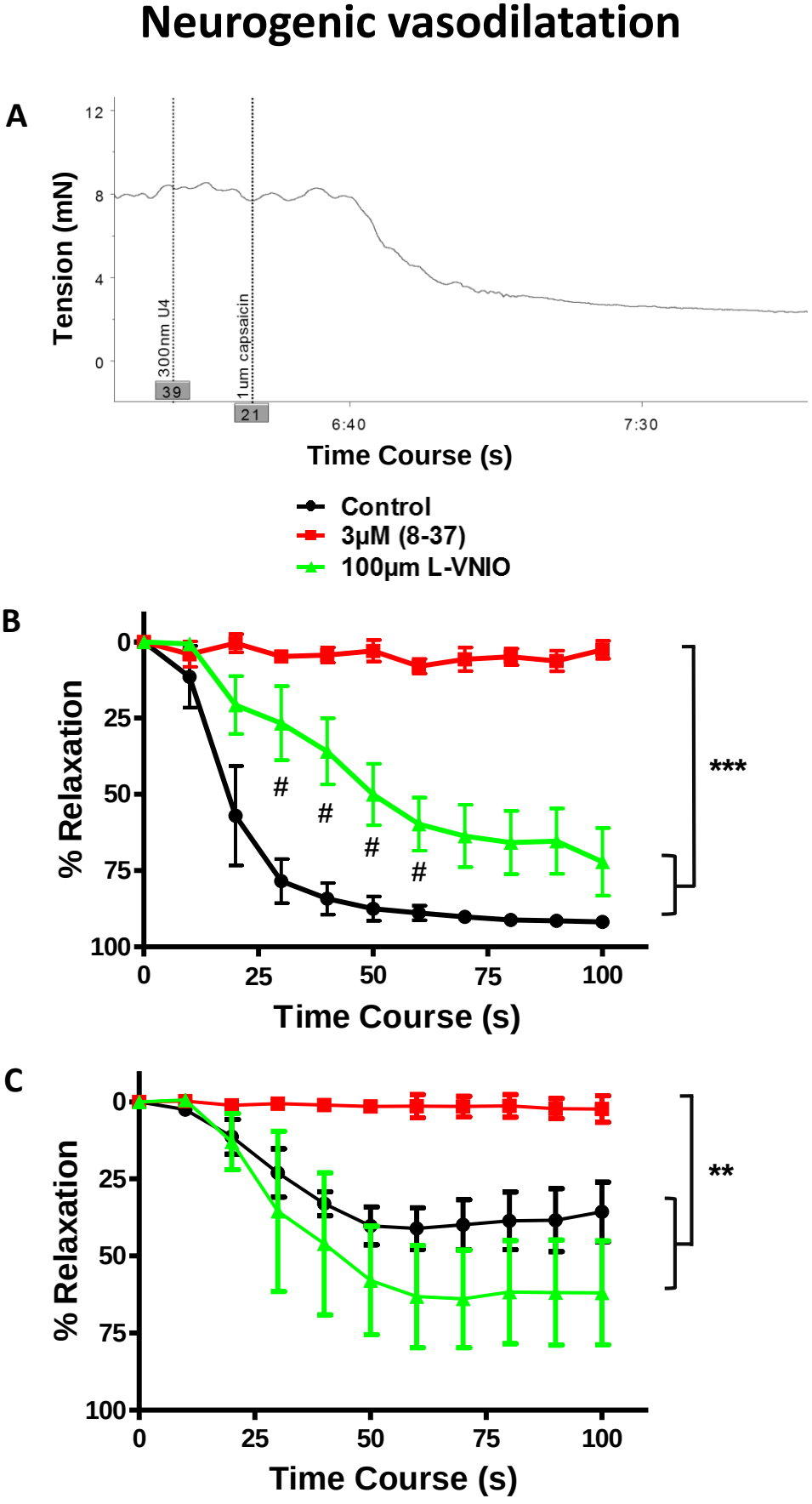


Figure 3.3. CGRP contributes more than NOS to neurogenic vasodilatation.

(A) Representative trace illustrating the time course measurement of relaxation after the immediate addition of 1µM capsaicin. In both intact **(B)** and denuded **(C)** rat mesenteric vessels, preconstruction was achieved with U46619 (300nM), also in the presence of CGRP (8-37) or L-VNIO (2-Way ANOVA; ** *P<0.01, ***P<0.001* for CGRP (8-37) vs control; # *P<0.05* for L-VNIO vs control; n = 3-5 mice per treatment.

nNOS inhibitor selectivity

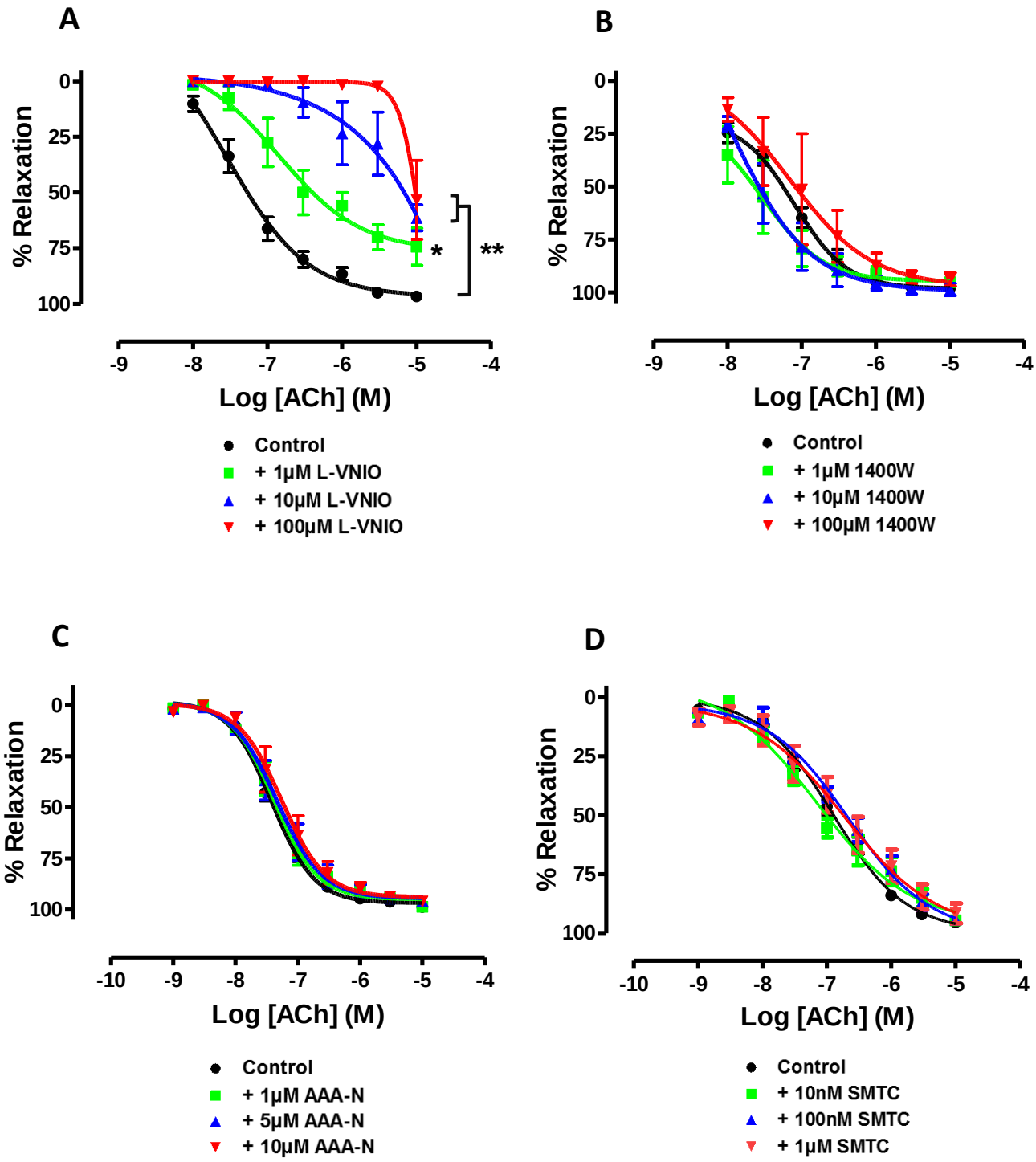


Figure 3.4. AAA-N and SMTC show greater selective nNOS inhibition.

Vasorelaxation dose-response curves to ACh following preconstriction with 5μM PE, in the presence of 1μM TRAM-34 and 50nM Apamin (control). Curves were repeated with prior incubation with either **(A)** L-VNIO, **(B)** 1400W, **(C)** AAA-N or **(D)** SMTC (2-way ANOVA; *P<0.05, **P<0.01 vs control; paired data from n = 3-7 animals).

Specific impact of neuronal NOS in nerve-mediated vasoconstriction

To study the effects of nNOS inhibition on neurotransmission and the resulting vasoconstrictor response, peri-arterial nerve stimulation was repeated in the presence of SMTC (100nM). As well as the discontinuation of AAA-N in commercial supply, SMTC was selected given its established use in both animal and clinical studies (115-117). In this series of experiments the pattern of tension changes over the 10 s stimulation period was now measured at each frequency. In vessels incubated with CGRP (8-37) and propranolol, electrical stimulation at lower frequencies produced a very minor vasoconstriction, only attaining a level of tension that was <3% of maximal (Figure 3.5A); this response was not altered following stimulation in the presence of SMTC. The magnitude of vasoconstriction increased in a frequency-dependent manner, demonstrating a response that reached 44% of maximal at 15Hz (Figure 3.5B). At this frequency, specific nNOS inhibition caused a small degree of augmented nerve-mediated vasoconstriction which was statistically non-significant; point-by-point tension changes also revealed that there was no overall alteration in the profile of tension changes (Figure 3.5C). These data demonstrate that the opposition of nerve-mediated vasoconstriction by NO is most likely dependent on endothelium-derived NO sources and not from nNOS specifically.

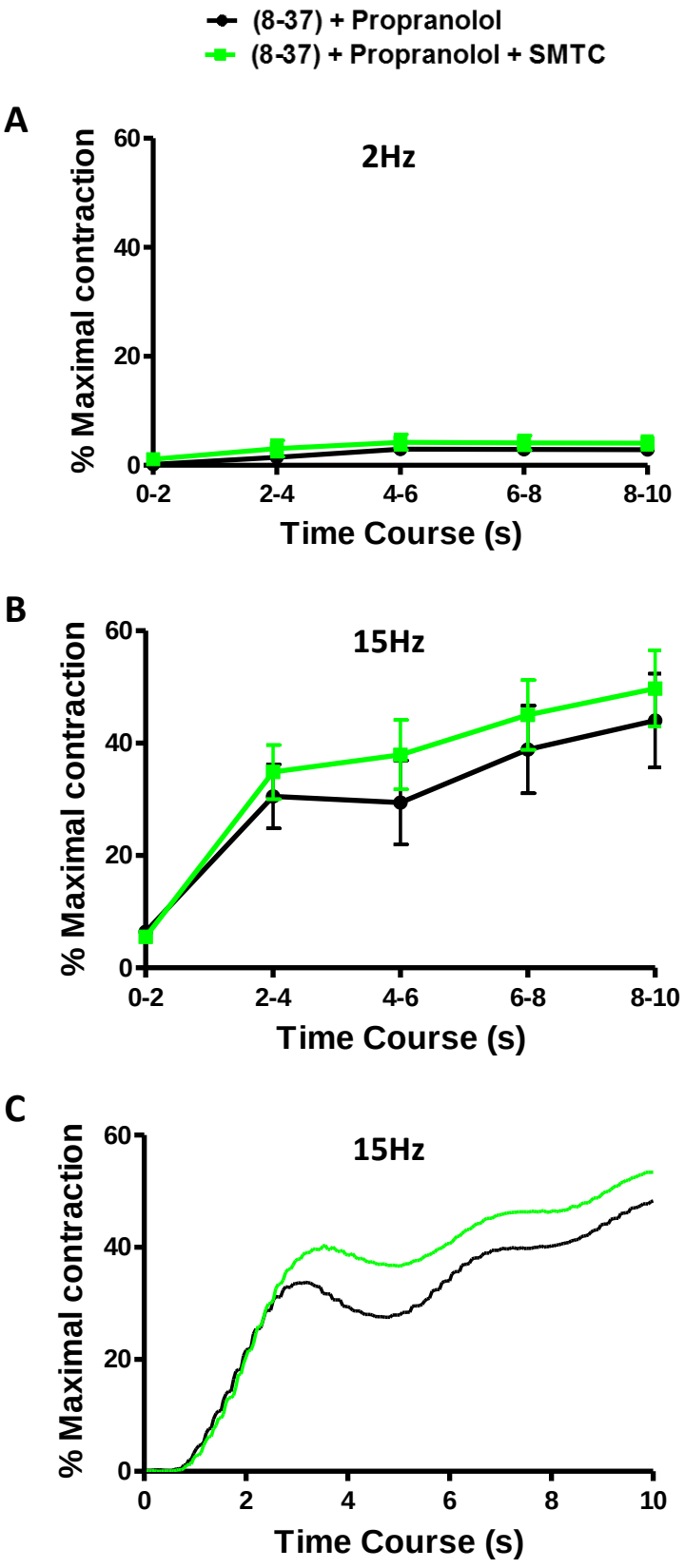


Figure 3.5. nNOS-derived NO opposes nerve-mediated vasoconstriction at higher frequencies.

(A) nNOS inhibition with SMTC did not impact the minimal vasoconstrictor responses observed at 2Hz. **(B)** SMTC blockade resulted in some augmentation of constrictor responses at 15Hz stimulation. **(C)** Point-by-point tension changes (at each 50ms) revealed the pattern of the constrictor responses over the 10s period. Error bars omitted in **(C)** (Paired data from n = 5 animals).

Immunohistochemical study of nNOS expression in mesenteric arteries

Immunohistochemistry and confocal imaging of pinned out arteries was performed to evaluate the expression and localisation of nNOS. In rat mesenteric arteries, trains of punctate staining within the neurone cell layer indicated the expression of nNOS in perivascular nerve varicosities (Figure 3.6A). Furthermore, these nNOS-containing nerves coalesced with nerves expressing tyrosine hydroxylase (TH), responsible for catecholamine biosynthesis (Figure 3.6B), which could be confirmed by superimposing the images.

With the availability of mice with deletion of the gene encoding nNOS, nNOS expression was also investigated in mesenteric arteries from WT and nNOS-KO mice. Immunohistochemical analysis demonstrated punctate staining for nNOS, delineating neurone varicosities (Figure 3.6C). These punctate neuronal networks were absent in nNOS-KO mice (Figure 3.6D). Some residual staining was apparent in the nNOS-KO, but superimposition with staining of neuronal cell nuclei suggested that this was actually due to cross-detection of propidium iodide (PI) (Figure 3.6E). As a control, in both genotypes immunohistochemistry was also performed on the myenteric plexus (known to contain a dense population of nNOS-containing neurones). nNOS deficiency in KO mice was confirmed by the absence of nNOS expression in the myenteric plexus (Figure 3.6F and G). Overall these data indicate that nNOS-expressing nerve fibres co-localise with noradrenergic afferents, where it is hypothesised that they may modulate neurotransmitter release.

nNOS expression and localisation

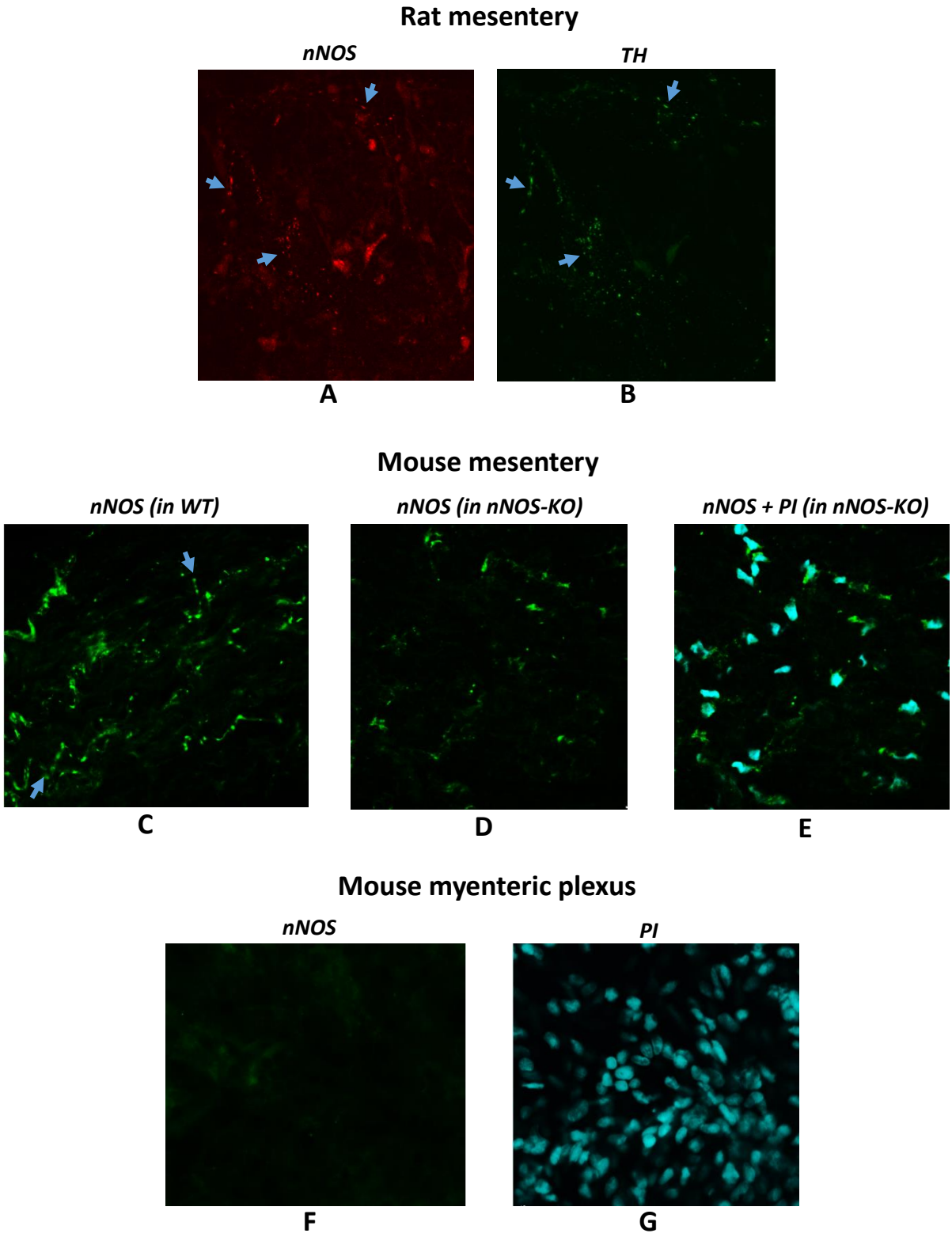


Figure 3.6. nNOS is expressed in perivascular nerve varicosities in mesenteric artery.

Representative images of immunohistochemical staining. **(A)** Trains of punctate staining (arrows) in rat mesenteric artery demonstrated nNOS expression. **(B)** Tyrosine hydroxylase expression corresponded to the same localisation as nNOS. In the mouse mesenteric artery, punctate staining of neurone networks and varicosities (arrows) was observed in **(C)** WT, but not **(D)** nNOS-KO mice. **(E)** Residual staining in nNOS-KO arteries could be attributed to cross-over with PI or non-specific staining of nuclear proteins. The myenteric plexus was used as a negative control in the nNOS-KO mouse, similarly stained for **(F)** nNOS and **(G)** nuclei (Paired data from n = 3 mice).

Conclusions

The main findings presented in this chapter demonstrate that:

1. NO acts to oppose nerve-mediated vasoconstrictor responses in the rat mesenteric artery in a frequency-dependent fashion.

2. nNOS is expressed in both rat and mouse mesenteric arteries, where it appears localised to perivascular neurone bundles.

Discussion

Despite not being a finding on physiological mechanisms *per se*, one important result is the apparent non-specificity of commercially available nNOS inhibitors. As a general point, much of the original insight on NOS function developed mainly from experimental data using non-selective inhibitors (L-NAME, L-NMMA), alongside the application of NO donors. In more recent years, methods have now advanced with the generation of e/n/i NOS gene KO mice to tease out the more intricate roles of NOS signalling. However, specific NOS isoform blockade is still a necessary experimental tool for clinical and animal studies, as well as biochemical experiments, thus confidence in the specificity of the treatment is of paramount importance.

L-VNIO was originally characterised by Babu et al. as a highly selective inhibitor of nNOS, which exhibited ~100-fold lower affinity for eNOS and iNOS compared to the neuronal isoform (216). Although this conclusion was derived from biochemical experiments using cell-free based assays, L-VNIO has been used considerably since, where its purported specificity has been substantiated (217-219). As well as the contradictory findings from my studies, this notion has been challenged by Pigott et al., who showed recently that in both hippocampal slices and aorta, L-VNIO exhibited significantly less nNOS selectivity than previously reported – in the region of only 5-fold (220). Similar results were also observed in this study with other commercially available inhibitors, including 1400W, which is in line with its characterisation by Garvey et al. as a predominant iNOS inhibitor (221). This non-

selectivity concern also applies to other compounds not tested in this study, particularly 7-Nitroindazole (7-NI). Despite its widespread use, reports suggest that 7-NI has only ~2-fold selectivity for nNOS vs eNOS (222, 223), furthermore, it may also have unintended pharmacological effects on monoamine oxidase activity (224). The profile of SMTC was the most promising, having previously been shown to have ~17 fold selectivity for nNOS over eNOS in rat brain slices and aorta. In addition, its utility was verified more recently by Seddon et al. in clinical studies, where the compound demonstrated no effect on eNOS-mediated vasodilatation, in response to either flow or ACh infusion (117). It is difficult to classify these pharmacological inhibitors with a high degree of certainty, largely because their value may depend on the experimental circumstances. For example, differences in the NOS preparation and the tissue being tested (e.g. cerebellar slices, aorta, mesenteric artery etc.) will likely account for some of the reported variance, not to mention obvious strain and species differences. Inhibitor incubation times is another important consideration that differs between studies, moreover, any variability in NOS substrate availability and drug permeability within the incubation conditions is entirely possible.

These findings from arterial electrical stimulation have shown that NOS inhibition leads to augmented contractile responses induced by perivascular nerves. The predominant vasoconstrictor response results from α-adrenergic influence, which in most species is achieved mainly via the activation of the post-junctional α_1-receptor subtype on vascular smooth muscle (225, 226). The α_2 subtype appears to play a significant pre-junctional role as an autoreceptor; α_2-AR inhibits further noradrenaline secretion at the nerve terminal, which can itself modulate constrictor tone in resistance vessels (227). Despite the major role for noradrenaline, it is now well established that other endogenous agents are co-released within sympathetic perivascular nerves, which can influence local blood flow through both their own signalling pathways and by positively or negatively regulating other neurotransmitter effects. This co-transmission has been observed with ATP; Sneddon and Burnstock demonstrated that excitatory junctional potentials (EJPs) in nerves innervating rat resistance arteries persisted during α-AR blockade, but could be abolished by P_2-purinoceptor blockade (228). More specifically, this work

highlighted the biphasic nature of the vascular contractile response; an initial fast phase of neurotransmission mediated by ATP, after which noradrenaline accounts for the slower second phase. In addition, the relative contributions of each neurotransmitter and the consequences to vascular tone are frequency-dependent i.e. low frequency nerve stimulation (2-5Hz) leads to vesicular release of ATP, whereas higher frequency impulses trigger noradrenaline-mediated responses (229). The fact that NOS inhibition in my study enhanced constrictor effects most significantly at the higher frequencies suggests that NO normally acts to dampen noradrenergic activity to regulate vasomotor tone, in agreement with earlier studies of mesenteric perivascular nerves (230). Indeed, Boric et al. showed that endogenous or exogenous α_1 and α_2-AR activation in this vascular bed could directly stimulate endothelial NO production (231). This is supported by the data presented here, which indicated that electrically-induced vasoconstriction was augmented following endothelial removal or acute non-specific NOS inhibition.

My findings have suggested very minimal regulatory actions specifically from neuronally-derived NO, since vasoconstriction was largely diminished in denuded arteries treated with L-VNIO, as well as in intact vessels treated with the nNOS-specific inhibitor SMTC. Minimal effects of nNOS-derived NO were observed only at higher frequencies of stimulation, perhaps permissive of the role of nNOS-derived NO on either the pre- or post-synaptic repression of sympathetic vasoconstriction, which has been previously reported (210, 211, 213). The expression of nNOS in TRPV1-containing nerves, as previously described (211), is reinforced by my results illustrating vasorelaxation to the agonist capsaicin, where nNOS blockade appears to reduce the extent of relaxation. It has been proposed that nNOS-derived NO may in fact be released from sensory nerves as a co-transmitter, either stimulating, or in response to, CGRP (232). The involvement of CGRP as a major regulator of neuronally-mediated vasoconstriction is well recognised (233) and has been further highlighted in my study, irrespective of any interacting effect of NOS inhibition. Surprisingly, the relaxation in untreated denuded arteries was far less marked than that in untreated intact vessels. Although unclear, a potential reason for this could be the removal of CGRP receptors expressed on the endothelium that normally mediate some

of the vascular smooth muscle relaxation, as has been reported in the rat (234). The immunohistochemical data is also in agreement with other studies, which together reveal the co-localisation of nitrergic and noradrenergic nerves (210). Although the exact origin still remains unclear, Boric et al. demonstrated that both α-AR inhibition and sympathectomy was insufficient to reduce NO release, arguing against nNOS expression in vascular smooth muscle cells or sympathetic nerve fibres (231).

Although this work was not extended to the diabetic mouse, the dysfunction and degeneration of nitrergic nerves in the setting of diabetes has been recognised within specific tissues. A loss of nNOS-expressing neurones has been demonstrated in the enteric nervous system during diabetes, which can impair normal gastric emptying (235), and may explain abnormal gastric accommodation observed in patients (236). The breakdown of normal nitrergic autonomic function has also been reported in the cerebral circulation of STZ-induced diabetes, which may occur in a two-step process. Cellek et al. observed that the first phase involves a depletion in nNOS content, possibly due to defective axonal transport. The second phase leads to apoptosis of nitrergic neurons, triggered by the prior accumulation of nNOS in the cell body and the onset of AGE formation and oxidative stress (237, 238). This neuropathy has also been reported in penile arteries, where nNOS-mediated neurogenic vasodilatation is not only impaired, but may actually shift to excessive vasoconstriction in the diabetic state (239). This dysfunction was associated with an increased production of O_2^-, while pre-treatment of the vessels with BH4 was able to restore the NO-mediated vasodilatation in response to electrical stimulation. Together, these recent findings suggest that the destruction of nitrergic nerves in the diabetic state may be due to excessive ROS, moreover, it highlights the potential virtues of BH4 treatment for arresting or reversing neuropathy.

Chapter 4

The pathology of diabetes in the vasculature

Introduction

Glucose transport and endothelial cell vulnerability

Glucose is transported into tissues by a family of carriers called the facilitative glucose transporters (GLUTs), in an energy-independent process that relies on facilitated diffusion (excluding the Na^+/glucose symporter class expressed in the small intestine and kidney) (240, 241). A significant proportion of peripheral glucose disposal is into skeletal muscle and to a lesser extent adipose tissue, which is an insulin-dependent process (242, 243). This is mediated largely through the GLUT4 receptor, with numerous studies showing that GLUT4 deficiency leads to insulin resistance and the onset of diabetic pathologies (244, 245), while GLUT4 overexpression can restore insulin sensitivity and improve glucose tolerance (246). Experiments with muscle biopsies from patients with insulin resistance have also demonstrated impaired glucose uptake in association with defective GLUT4 localisation (247, 248). These observations not only highlight the importance of GLUT4 to overall glucose homeostasis, but also that insulin resistance and reduced GLUT4 activity can be seen as an adaptive response to protect tissues against the damaging effects of high intracellular glucose described in chapter 1.

The specific vulnerability of the vasculature to hyperglycaemia is largely due to the unregulated transport of glucose across the endothelial cell membrane. GLUT1 is highly expressed in endothelial and epithelial blood-tissue barriers, especially those of the retina, brain microvessels, kidney, peripheral nerves and colon (249, 250). Moreover, GLUT1 has a high affinity for glucose, with K_m estimates ranging from 3-7mM (251-253), suggesting that even in normoglycaemia these tissues have a considerable rate of glucose uptake. Unlike the reduced transport of glucose through GLUT4 in a background of hyperglycaemia and insulin resistance, cell culture experiments have shown that the vascular endothelium is unable to appropriately downregulate glucose uptake (254). Heilig et al. have then demonstrated that glomerular cells increase their GLUT1-mediated transport in response to high extracellular glucose, moreover, the same authors have also extended this to glomerular glucose

uptake in diabetic mice (255, 256). Similarly, experimentally-induced GLUT1 overexpression leads to increased basal glucose uptake in the absence of insulin (257).

Some of these experimental models have additionally established the link between increased basal glucose uptake and some of the downstream cellular mechanisms initiated by hyperglycaemia. Overexpression of GLUT1 in cultured mesangial cells leads to increased glucose uptake in association with PKC activation and sorbitol accumulation, as well as the increased deposition of fibronectin and collagen (258, 259). This has subsequently been corroborated by Wang et al., who also demonstrated that GLUT1-Tg mice exhibit several features of diabetic nephropathy, including altered glomerular morphology in association with increased expression of PKCβ1, VEGF, TGF-β1 and NFκB (260). Although this has been most extensively studied in the renal circulation, some evidence has also implicated GLUT1 in the development of diabetic retinopathy. Despite observations of unchanged or downregulated GLUT1 expression in retinal cells from diabetic rats (261, 262), Zhang et al. did report glucose and sorbitol accumulation in the diabetic retina, as well as an increase in GLUT1-mediated glucose uptake in cultured retinal endothelial cells (261). Additionally, Lu et al. have used GLUT1 knockdown in STZ-treated diabetic mice and shown that retinal cells from these animals had reduced glucose levels. Interestingly, these authors also investigated the link between elevated basal glucose uptake and ROS, where they showed that pharmacological GLUT1 inhibition reduced superoxide production (and VEGF gene expression) in diabetic retina (263).

Impaired NO-dependent vasodilatation

While the above reports describe how uncontrolled glucose entry across endothelial-tissue barriers can contribute to the complications associated with diabetes, other investigators have looked extensively at the direct dysfunction resulting from glycaemic insult to the vascular endothelium. In the STZ-treated rat, Pieper et al. showed that in diabetes the aorta displayed impaired endothelium-dependent (but not –independent) vasodilatation in response to acetylcholine (ACh); the effect was subsequently abolished by quenching ROS using superoxide dismutase (SOD) and catalase (93). This

finding has been replicated in several other rodent models of diabetes, where authors have described a reduction in NO bioavailability, NADPH oxidase activation and increased ROS production in association with the impaired vasorelaxation (264-267). Aside from the effects of hyperglycaemia on NOS dysfunction, impaired insulin signalling itself has also been identified as a cause of diminished NO bioavailability and vascular abnormalities. Insulin normally triggers the PI3-kinase/Akt signalling cascade, activating eNOS through phosphorylation of serine1179 to increase NO production (268-270). Equally, it has been demonstrated in diabetes that the activation of eNOS by insulin is reduced, as is NO production, which are associated with impaired endothelium-dependent vasodilatation (271, 272). In addition, secretion of endothelin-1 and expression of vascular cell adhesion molecules is also regulated by insulin (273, 274), further highlighting the potential for vascular dysfunction in the setting of diabetes.

With evidence to suggest that ROS mediates the endothelial dysfunction in diabetes, other studies have focused in more detail on the coupling state of NOS and the role of the cofactor BH4. In a rat model of insulin resistance, Shinozaki et al. described reduced NO-mediated vasodilatation in association with a reduction in eNOS activity and altered biopterin balance; namely, a decreased BH4 and an increased BH2 level (275). Alp et al. have then demonstrated that specific endothelial overexpression of GCH1 significantly increased BH4 bioavailability in the aorta (despite significant loss of BH4 to oxidation), which was sufficient to maintain NOS coupling in the diabetic state and translated to improved endothelium-dependent vasodilatation (155). In addition, these authors later showed that diabetic mice not only exhibit NOS uncoupling in the aorta, but also a decrease in the level of functional eNOS dimers (267). The eGCH1 transgene was able to increase this dimer:monomer ratio in the diabetic aorta, suggesting a further mechanism by which adequate BH4 can maintain NO availability and prevent oxidative stress in the diabetic state.

Effects on other mediators of endothelial-dependent vasorelaxation

The majority of these studies have based their conclusions on biochemical and functional experiments on the aorta, understandably for practical reasons, as well as the fact that vasorelaxation in conduit vessels is strongly NO-dependent (93, 276, 277). However, the vascular complications associated with diabetes present in both peripheral and macrovascular beds, thus it is also important to consider the importance of NO and the impact of diabetes on small resistance arteries. Indeed, it has been reported that the contribution of NO to vasodilator responses decreases as the vessel diameter decreases; instead these vessels rely more heavily on the action of endothelial-dependent hyperpolarizing factor (EDHF) (278-280), which seems to have been most widely studied in the mesenteric circulation. In the diabetic state, Fitzgerald et al. showed that mesenteric arteries did not exhibit reduced overall vasodilation to ACh, although they did see impaired EDHF-mediated responses and propose possible compensatory increases in NO-signalling (281, 282). Different authors support some of these conclusions, whilst still finding classical endothelial dysfunction in the mesenteric vasculature (283), whereas others have reported no alteration in the EDHF pathway with diabetes (284, 285), and even a compensatory increase in other vasodilatory mediators such as prostanoids (286). Some of these differences are likely explained by the model of diabetes, the order of mesenteric arterial branch studied, as well as the age of the animal at the time of tissue harvest.

Temporal effects

Another consideration in the development of associated vascular disease is the duration of diabetes, where it has been suggested that endothelial dysfunction is a relatively early phenomenon. Some small clinical studies have indicated that impaired flow-mediated dilatation (FMD) can present in patients in as little as 5 years since diagnosis, and that this occurs in the absence of any other atherogenic risk factors (287, 288). Experimentally, Wein et al. have shown that porcine retinal arteries display impaired FMD after only 2 weeks of hyperglycaemia (289), which has also been supported by findings from retinal dilator responses in the diabetic rat (290). However, reports in

other vascular beds have been more varied, which may be attributable to a biphasic vascular response to diabetes under some circumstances. For example, Orie et al. showed that the aorta from 4-week diabetic rats exhibited impaired ACh-induced vasodilatation (291), while a later comparable study described no change in this relaxation response after 2-3 weeks (292). This has been further elucidated by Pieper et al., who studied endothelium-dependent vasodilatation in the aorta from rats at several different time points (293). These authors saw that relaxation was enhanced acutely at 24 hours of diabetes, which normalised to show no difference at 1 and 2 weeks, finally then becoming a significant impairment at 8 weeks of diabetes. This is also in agreement with some of the findings from rat mesenteric arteries, where vasodilation may be enhanced or unchanged up to 6 weeks of diabetes, whereas a further 6 weeks of hyperglycaemia may trigger endothelial dysfunction (294, 295).

This chapter investigates the impact of hyperglycaemia on vascular function at both early and late time points, also exploring conduit vs resistance vessel differences and the potential role of NOS uncoupling.

Methods

Vasomotor studies

To assess vascular reactivity, measurements in aorta were performed at both 4 weeks and 12 weeks, while 2nd order mesenteric arteries were measured at 12 weeks in parallel with aorta. Despite the specificity of the transgene to the myocardium, vessels from mGCH1-Tg mice were included in these studies as an added control, ensuring that the transgene did not have pleiotropic effects on vascular function. Vasomotor function was measured as described in chapter 2. Vessel segments (2mm length) were dissected and mounted into the organ baths of a Mulvany-Halpern wire myograph system containing KHB buffer. Dose-response curves were generated to determine vasoconstrictor properties, as well as endothelium-dependent and –independent vasodilatation. Pre-treatment with 100µM L-NAME was used to inhibit NOS. In mesenteric arteries, vessels were pre-treated with 1µM TRAM-34 and 50nM apamin to inhibit IK_{Ca} and SK_{Ca} conductance channels; these calcium-activated

potassium channels have been shown in numerous preparations to be key components of EDHF-mediated relaxation (296-298). Tension measurements were recorded in LabChart and stable plateau values during either contraction or dilatation were used to generate response curves.

Superoxide production

Vascular O_2^- production was determined using lucigenin-enhanced chemiluminescence, as described. Thoracic aorta was dissected and incubated in either D-NAME or L-NAME for 30 min prior to measurements. Aortas were loaded (in KHB) into a single-tube luminometer maintained at 37˚C, and chemiluminescence detected for 10 min before the addition of the O_2^- scavenger tiron. Chemiluminescence levels were assessed over the final 2 min of each period of recording and the values expressed as the tiron-inhibitable fraction (in RLUs per mg dry weight).

Biopterin quantification

The detection of the different biopterins BH4, BH2 and B was achieved by separation and quantification by reverse phase high-performance liquid chromatography (HPLC), as described. Thoracic aortas were dissected and homogenised in re-suspension buffer, with BH4 oxidation prevented by maintain on dry ice. Supernatants were thawed, loaded into a 96-well plate and placed in the pre-cooled HPLC autosampler. Biopterins were separated using a Carbon-18 column and quantified by sequential electrochemical and fluorescence detection. Biopterin concentrations were quantified by comparison with BH4 and BH2 reference standards (previously verified with a UV spectrometer).

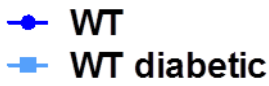
Plasma insulin quantification

Plasma insulin concentration was determined using a rat/mouse insulin ELISA kit. Plasma samples were aliquotted along with supplied insulin standards (0.2, 0.5, 1, 2, 5 and 10 ng/mL) into wells of the 96-well microtiter plate coated with mouse monoclonal anti-rat insulin antibody. Samples, standards and quality controls were loaded in duplicate. Biotinylated anti-insulin detection antibody was added

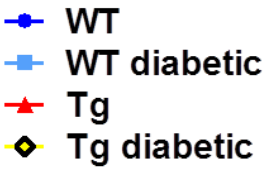
to all wells, followed by washing of unbound antibody-insulin complexes and the addition of horse-radish peroxidase enzyme solution. Unbound antibody-enzyme conjugates were removed and a substrate solution containing 3,3',5,5'-tetramethylbenzidine was added. The reaction was terminated by the addition of stop solution (0.3M HCl) and the plate immediately loaded into the plate reader for detection. Absorbance was read at 450nm and 590nm and the difference between the two sets of values used for analysis. A reference curve was produced from the insulin standards and a dose-response curve fitted to the standards using a sigmoidal 4-parameter logistic equation, which was subsequently used to determine sample insulin concentration.

Results

For only WT vs WT diabetic comparisons, the following colours are assigned for each treatment group:



For comparisons between treatment and genotype (mGCH1-Tg), the following colours are assigned for each group:



STZ-treated mice exhibit early and sustained hyperglycaemia

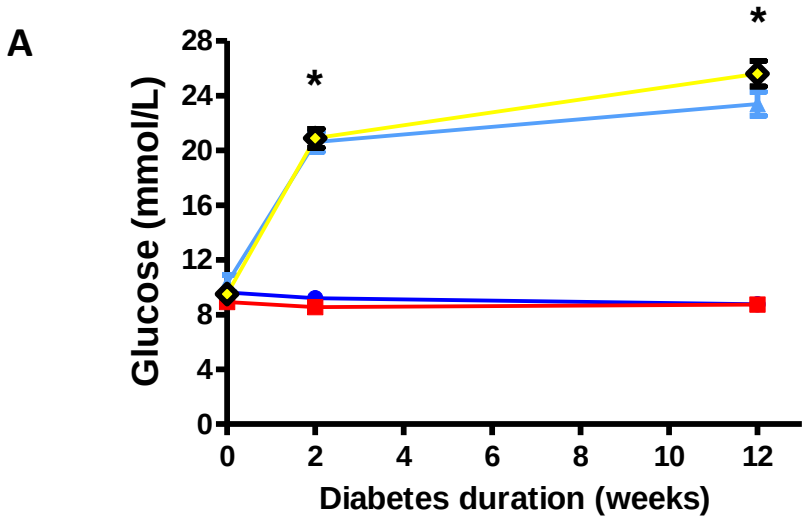
Prior to injection, mice in all 4 groups demonstrated normoglycaemia, with values ranging from 8-10mM. 2 weeks post-injection, STZ-treated animals already exhibited a significantly elevated blood glucose relative to citrate buffer-treated control mice (20.6 ± 0.7 in WT diabetic vs 9.2 ± 0.2 in WT; Figure 4.1A). Hyperglycaemia was then sustained for the remaining duration of the diabetes protocol and increased slightly further by the end of the 12 weeks (Figure 4.1). As expected, mGCH1 overexpression had no effect on blood glucose ranges in either control or diabetic mice.

Along with hyperglycaemia, some other classic signs of type 1 diabetes were observed. Mice exhibited polydipsia and polyuria, requiring more frequent exchange of cage bedding and water replenishment. Diabetic mice also demonstrated reductions in body weight compared to control, which were evident at 2 weeks, with the difference becoming even greater by 12 weeks (27.6 ± 0.5 in WT diabetic vs 32.7 ± 0.7 in WT; Figure 4.1B).

Hyperglycaemia is accompanied by insulin insufficiency

In line with hyperglycaemia and the other physical observations of T1D phenotype, plasma insulin levels after 12 weeks of diabetes were significantly decreased. In both WT and mGCH1-Tg mice, STZ treatment reduced insulin to 42% of those levels in control littermates (1.52 ± 0.37 in WT diabetic vs 3.67 ± 0.34 in WT; Figure 4.2A), confirming pancreatic β-cell damage. Paired glucose and insulin data demonstrated the corresponding level of glycaemia for each mouse given the relative degree of insulin insufficiency (Figure 4.2B). Again, unsurprisingly, mGCH1 overexpression produced no effect on plasma insulin concentrations in either control or diabetic mice.

Plasma glucose concentration and body weight



Glucose levels (mM)

	0 weeks	2 weeks	12 weeks
WT control	9.6±0.2	9.2±0.2	8.8±0.2
WT diabetic	10.3±0.6	20.6±0.7*	23.4±0.9*
Tg control	8.9±0.4	8.6±0.3	8.7±0.2
Tg diabetic	9.5±0.2	20.9±0.7*	25.6±0.9*

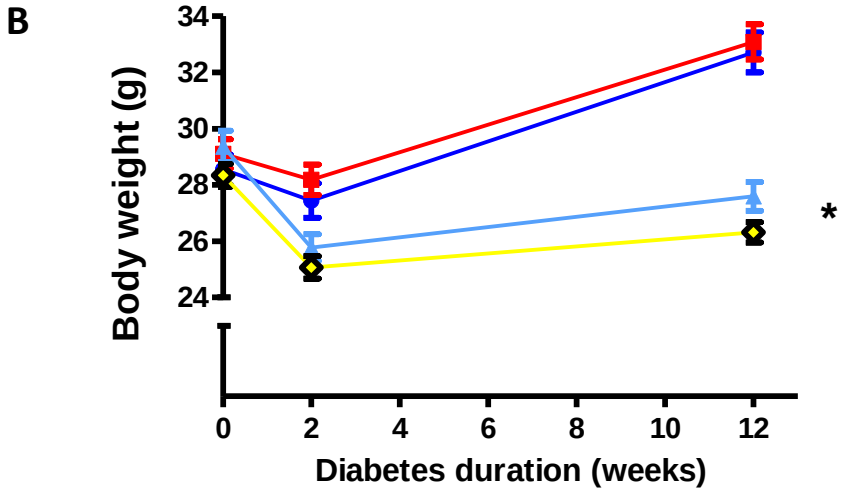


Figure 4.1 STZ-treated mice exhibit rapid and sustained hyperglycaemia, as well as reductions in body weight.

(A) As expected, diabetes induction with STZ caused elevated blood glucose levels in both WT and mGCH1-Tg mice, which was evident 2 weeks post-injection and continued for the remainder of the 12 week protocol. **(B)** Hyperglycaemia was consistent with reductions in body weight in STZ-treated mice compared to control littermates (2-way ANOVA; *P<0.05 for WT and Tg control vs WT and Tg diabetic; n = 15 per group).

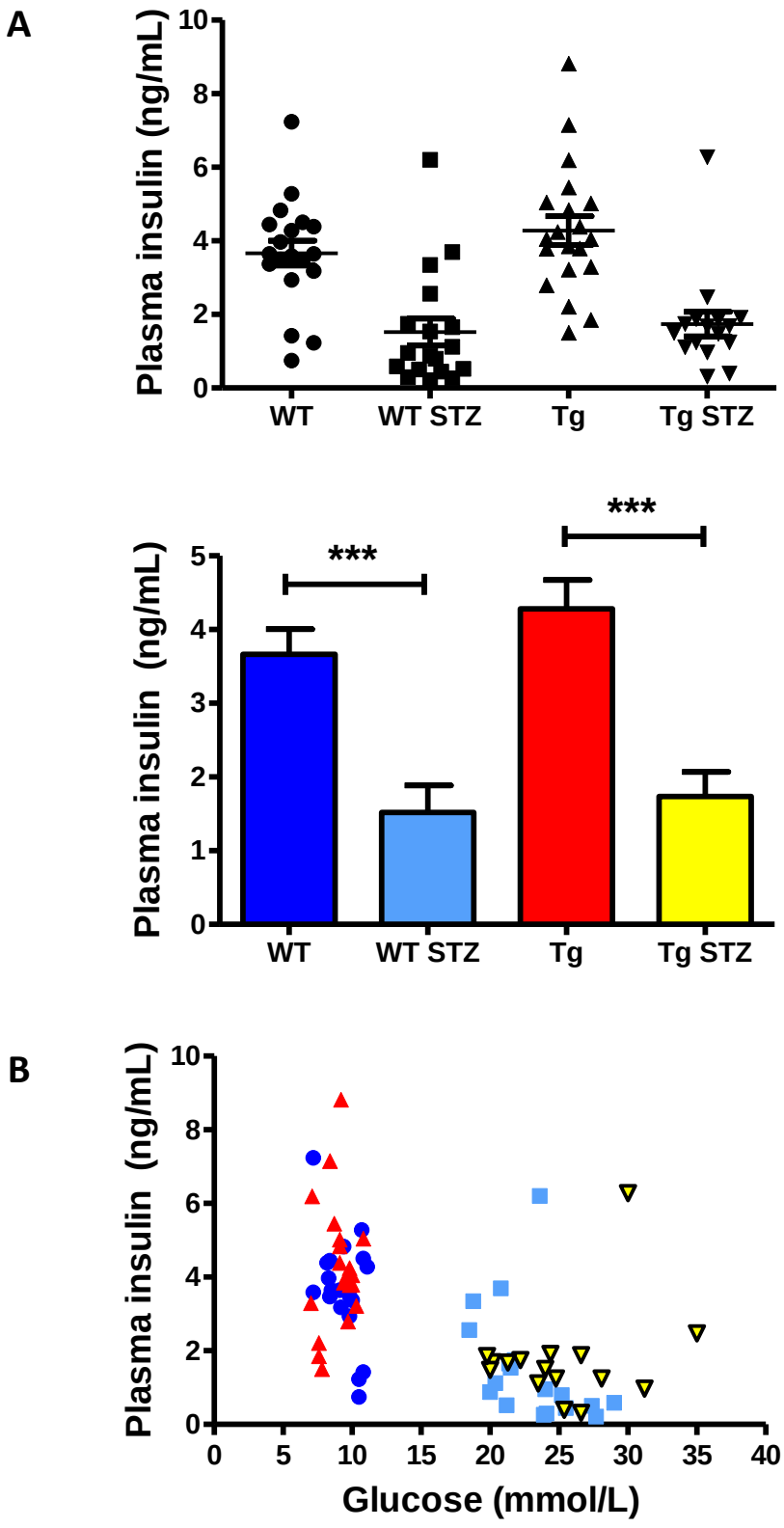


Figure 4.2 Insulin insufficiency accompanies hyperglycaemia in STZ-treated mice.

(A) 12 weeks after the final STZ injection, diabetic mice exhibited a significantly reduced plasma insulin levels compared to citrate-treated mice **(B)** Illustration of plasma insulin levels paired with blood glucose levels for each mouse (2-way ANOVA; ***P<0.001; n = 16-20).

Endothelial dysfunction in aorta is an early event in diabetes development

Organ bath studies of vasomotor function at 4 weeks demonstrated that aortas from diabetic mice had unchanged vasoconstrictor responses to PE compared to control littermates (Figure 4.3A). However, short term diabetes did induce endothelial dysfunction, with diabetic aortas exhibiting a significantly impaired endothelium-dependent vasodilatation to ACh (46% relaxation in WT diabetic vs 90% in WT; Figure 4.3B). Relaxation could be completely abolished in both groups in the presence of 100μM of the global NOS inhibitor L-NAME, highlighting the dependence of the aorta on NO as a primary mediator of endothelium-dependent vasodilatation (Figure 4.3C). Impaired relaxation could also be attributed to the endothelium because diabetes caused no difference in endothelium-independent vasodilatation to the NO donor SNP (Figure 4.3D). These data support the idea that the endothelium is especially vulnerable to hyperglycaemia, and that damage to these cells can occur as an early event in disease pathogenesis.

12 week diabetic mice exhibit endothelial dysfunction and enhanced vasoconstriction in aorta

12 weeks post-STZ injection, vascular reactivity was again assessed, also in both mGCH1-Tg groups. By 12 weeks, diabetic mice of both genotypes also now displayed an enhanced vasoconstriction to PE (187% in WT diabetic vs 146% in WT) (Figure 4.4A). As expected, endothelial dysfunction persisted in diabetic animals (in both WT and Tg) after 12 weeks, as evidenced again by impaired vasodilatation to ACh (60% in WT diabetic vs 90% in WT) (Figure 4.4B). This impairment in vasodilatation was also reproduced with the protease-activated receptor agonist SLIGRL, demonstrating that this effect was not due to a specific alteration in muscarinic receptor signalling (Figure 4.4C). Since the GCH1 transgene is myocardial-specific in its overexpression, unsurprisingly the PE, ACh and SLIGRL dose-response curves differed only by treatment and not by genotype. As with the short term responses, 12 weeks of diabetes caused no change in endothelium-independent vasodilatation to SNP (Figure 4.4D). These data suggest that as diabetes progresses beyond the short term, the aorta may also undergo further vascular remodelling that can predispose it to more severe vasoconstriction.

Resistance vessels are protected from diabetes-induced vascular dysfunction

In parallel to measurements in aorta, vasomotor experiments were also performed in mesenteric arteries from 12 week diabetic mice. Unlike the results from aorta, mesenteric arteries showed no difference in contractile responses to the constrictor U46619 (Figure 4.5A). Interestingly, mesenteric arteries also showed no evidence of endothelial dysfunction, with ACh-induced vasodilatation almost identical between groups (Figure 4.5B). This unexpected finding was not limited to ACh; the result was also replicated with the vasodilator SLIGRL (Figure 4.5C). Responses to SNP also revealed that endothelium-independent vasodilatation was preserved in all groups (Figure 4.5D). These data suggest that compared to the aorta, the mesenteric circulation is in some way protected from the detrimental effects of hyperglycaemia on the function of the vascular endothelium.

A subset of experiments was also performed to determine the contribution of NO and EDHF to the endothelium-dependent vasodilatation of the mesenteric artery. In the presence of 100µM L-NAME, mesenteric arteries from WT mice had a significantly blunted, but not abolished, response to ACh (49% relaxation). The simultaneous addition of 100µM L-NAME with 1µM TRAM and 50nM apamin to inhibit both NO- and EDHF-mediated dilatation caused a further reduction in relaxation to ACh (23%) (Figure 4.6A). These results were very similar in arterial rings from WT diabetic mice, which displayed 45% and 25% relaxation to ACh respectively, in the presence of L-NAME or the combination of L-NAME, TRAM-34 and apamin (Figure 4.6B). Together, these findings indicate that despite a contribution from EDHF, mesenteric arteries from both control and diabetic mice still rely considerably on NO-signalling in the activation of endothelium-dependent vasodilatation. However, these interpretations should be taken in the context of a small sample size and a relatively large standard deviation (SD). In fact, using the mean (36.8%) and SD (± 25.5%) at the EC_{50} from my current findings, for an 80% power to detect a 20% effect size (with a 5% margin for error) calculations currently dictate that very much larger sample sizes would be required. This is therefore a potential limitation of this subset of experiments and must be taken into consideration before making robust conclusions.

Vasomotor function: aorta 4 weeks

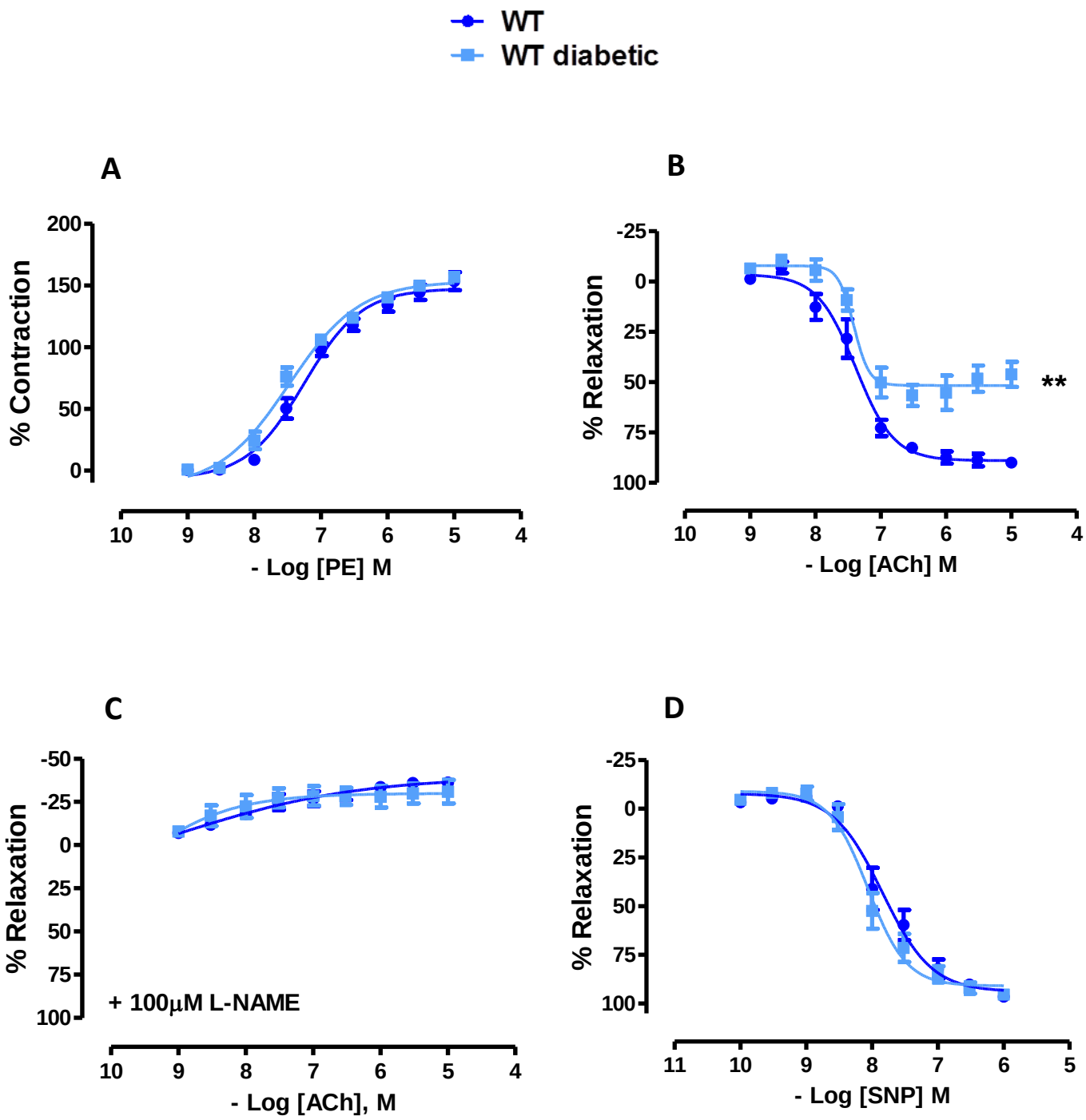


Figure 4.3. 4-week diabetic mice exhibit normal vasoconstrictor responses, but endothelial dysfunction in aorta

(A) Aortas from diabetic mice showed no difference in contractile responses to increasing doses of the vasoconstrictor PE. **(B)** Diabetic mice demonstrated impaired endothelium-dependent vasorelaxation to the vasodilator ACh. **(C)** Abolition of relaxation by 100µM L-NAME showed that dilator responses were NO-dependent. **(D)** However, 4 weeks of hyperglycaemia did not alter endothelium-independent smooth muscle relaxation in response to the NO donor SNP (2-way ANOVA; **P<0.01 for WT vs WT diabetic; n = 5-7).

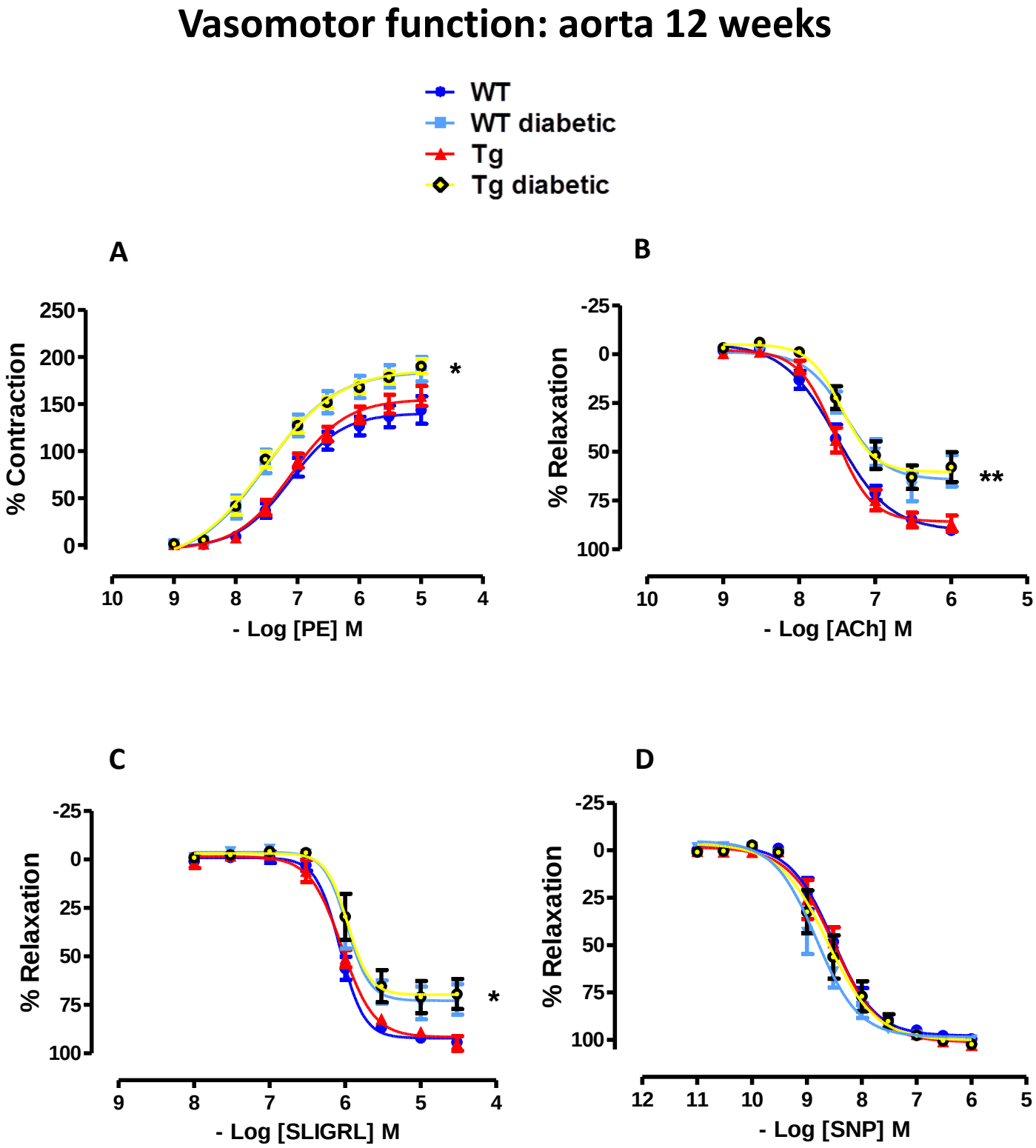


Figure 4.4. Enhanced vasoconstriction accompanies persistent endothelial dysfunction in aorta from 12 week diabetic mice.

(A) Aortas from both WT and mGCH1-Tg diabetic mice showed augmented contractility in response to PE. These mice also exhibited impaired endothelium-dependent vasodilatation to both **(B)** ACh and **(C)** SLIGRL. **(D)** 12 weeks of hyperglycaemia did not alter endothelium-independent smooth muscle relaxation to SNP (2-way ANOVA; *P<0.05; **P<0.01 for WT and Tg control vs WT and Tg diabetic; n = 7-9).

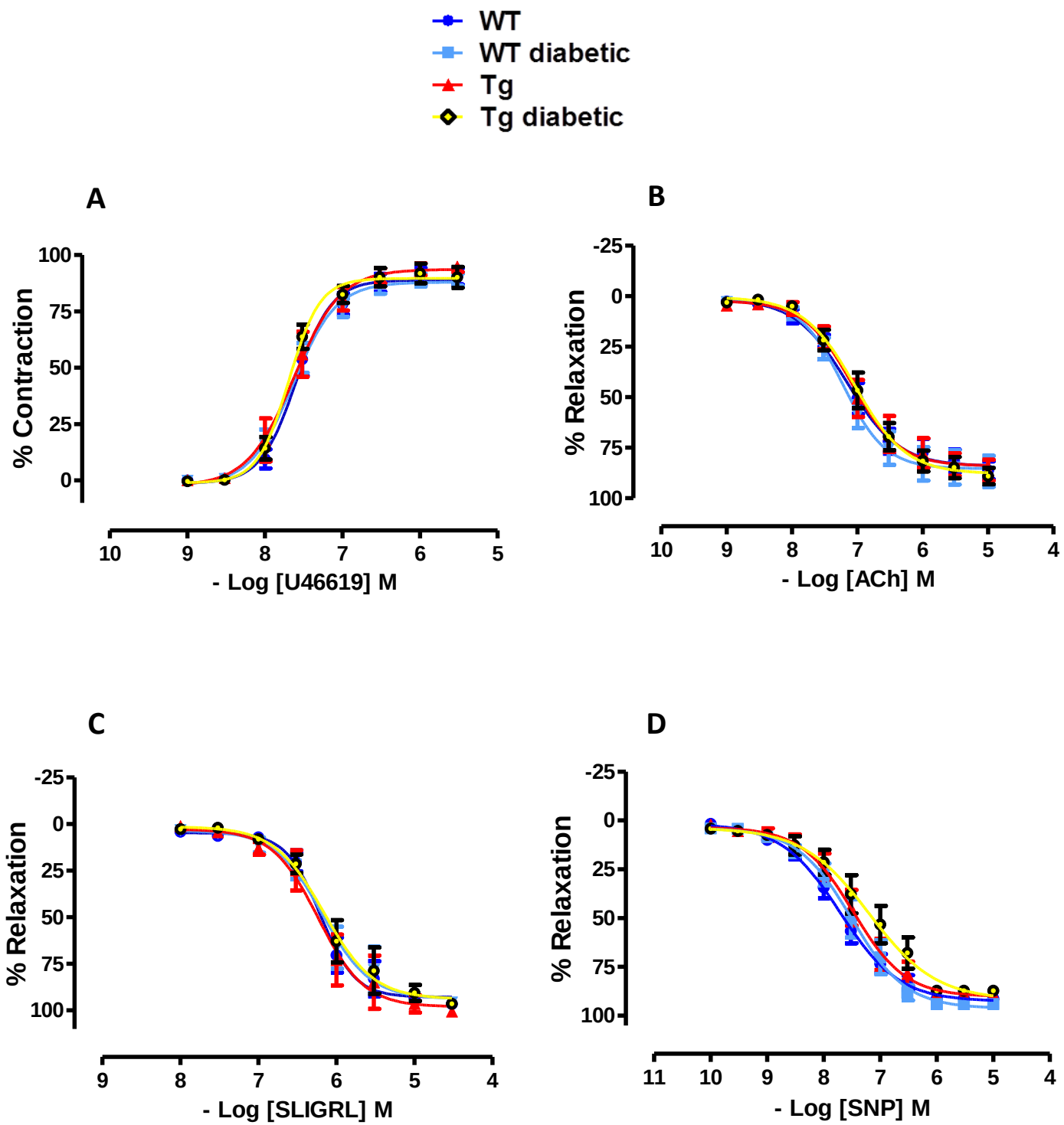


Figure 4.5 Mesenteric artery is protected from diabetes-induced vascular impairment.

(A) Vasoconstrictor responses to the prostaglandin analogue U46619 were not altered following 12 weeks of hyperglycaemia. Similarly, no dysfunction in endothelium-dependent vasodilatation was evident between groups in response to either **(B)** ACh or **(C)** SLIGRL. **(D)** As with the aorta, diabetes did not alter endothelium-independent smooth muscle relaxation to SNP (n= 8-12).

Vasomotor function: mesenteric artery 12 weeks

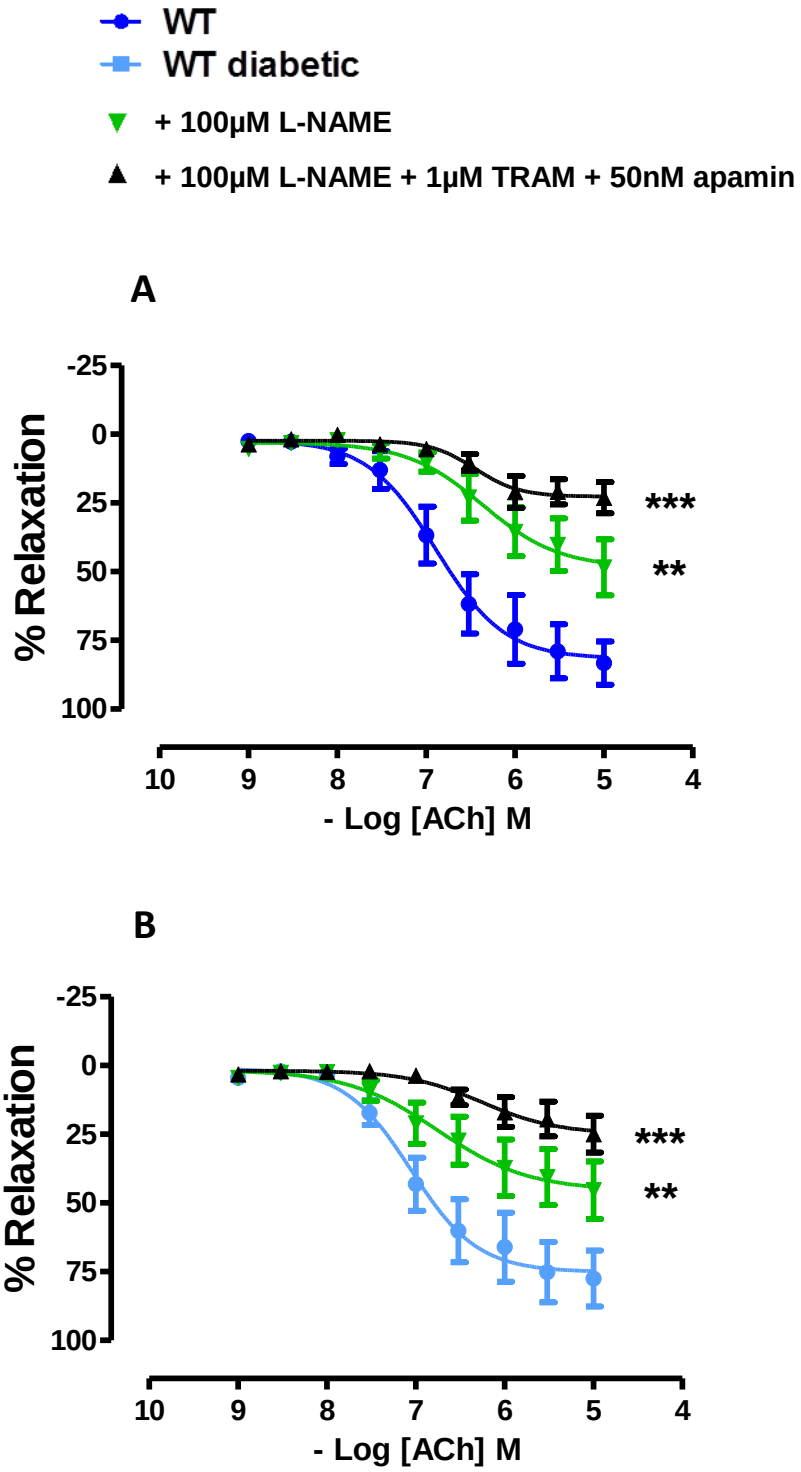


Figure 4.6. NO is still a major mediator of endothelium-dependent vasodilatation in the mesenteric artery.

(A) In WT control mice, L-NAME significantly blunted the relaxation response to ACh. The response was inhibited further by the addition of TRAM-34 and apamin to inhibit IK_{Ca} and SK_{Ca} conductance channels, respectively (2-Way ANOVA; **P<0.01; ***P<0.001 vs WT; n = 6). **(B)** The same pattern of responses was demonstrated in WT diabetic mice, revealing no alteration in NO-mediated or EDHF-mediated relaxation in the mesenteric artery as compared to control (2-Way ANOVA; **P<0.01; ***P<0.001 vs WT diabetic; n = 7).

Oxidative stress underlies the endothelial dysfunction in diabetes

To explore the potential mechanisms underlying the impairment in vascular function, O_2^- production was measured in whole sections of thoracic aorta. Consistent with the functional impairment, 12 week diabetic mice from both genotypes showed increases of 53% in vascular O_2^- production compared to WT and Tg control mice (26.4 ± 2.8 in WT diabetic vs 17.9 ± 1.8 in WT; Figure 4.7). Once again, myocardial overexpression of GCH1 had no impact on peripheral ROS production, with no apparent differences between genotypes. A subset of experiments conducted with prior incubation of aortas in 1mM L-NAME showed that the differences in O_2^- production between diabetics and controls were abolished after NOS inhibition (Figure 4.8). As well as increases in vascular ROS production, aortas from diabetic mice also exhibited alterations in biopterin levels. Both WT and Tg diabetic mice displayed a decrease in BH4 bioavailability, as evidenced by a significant reduction in the BH4:BH2 ratio (1.96 ± 0.3 in WT diabetic vs 3.2 ± 0.4 in WT; Figure 4.9). Taken together, these data indicate that in the type 1 diabetic state, hyperglycaemia leads to a decrease in the availability of the NOS cofactor BH4, which is accompanied by oxidative stress originating in part from NOS-derived O_2^- production.

O_2^- production: aorta 12 weeks

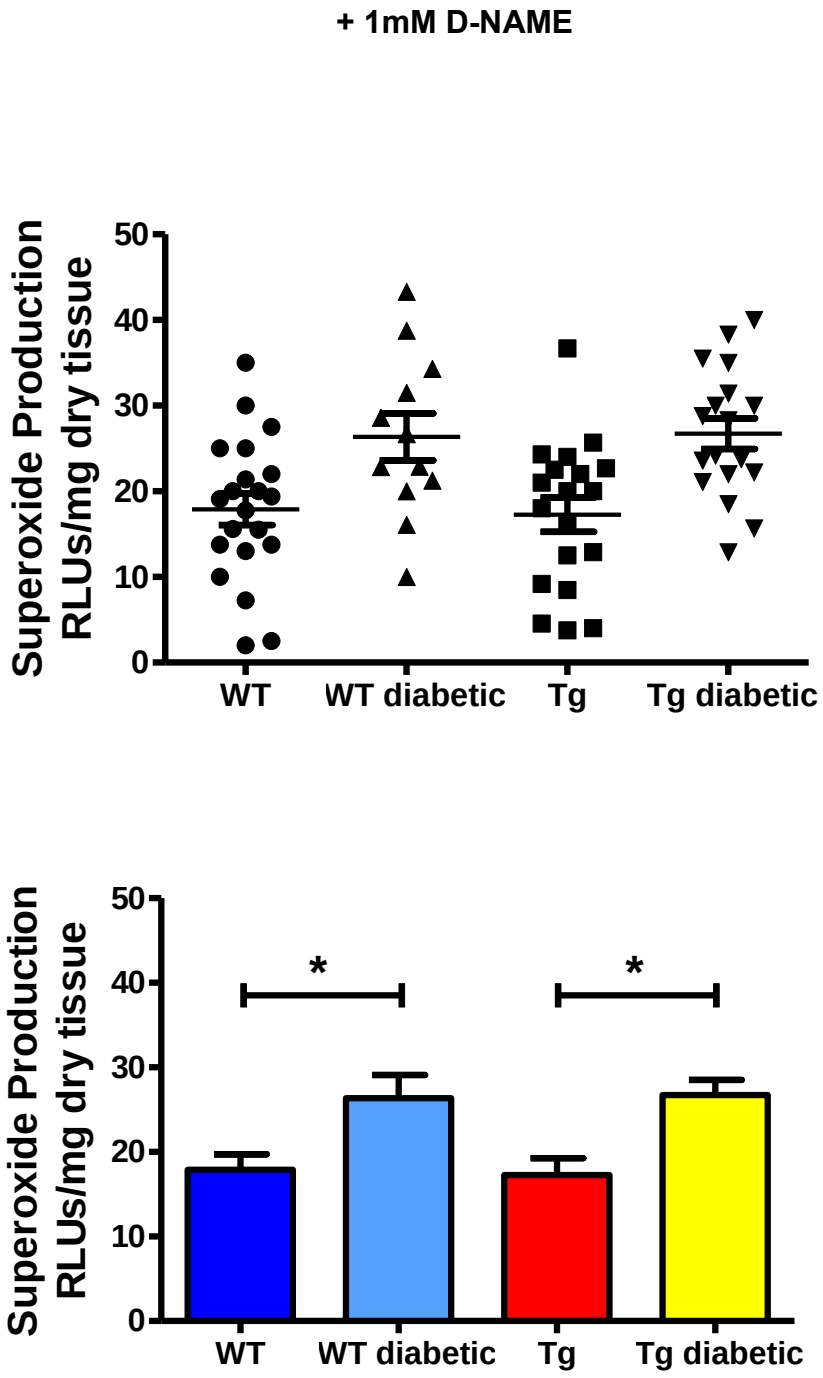


Figure 4.7. 12 weeks of hyperglycaemia causes increased O_2^- production in aorta.

Aortas from diabetic mice (pre-incubated in 1mM D-NAME) demonstrated increased levels of O_2^- compared to control animals, with no difference between genotypes (2-Way ANOVA; *P<0.05; n = 12-21).

O_2^- production: aorta 12 weeks

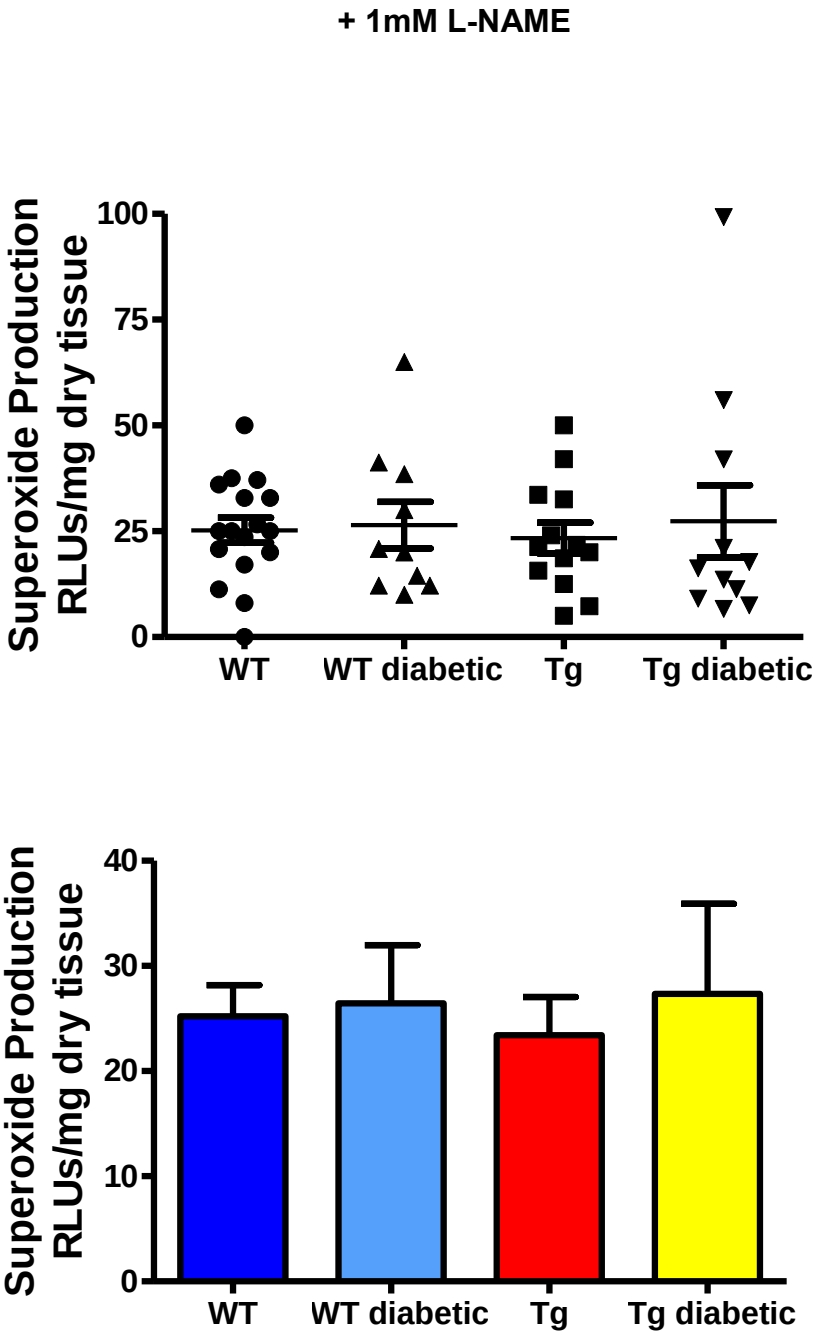


Figure 4.8. NOS inhibition abolishes the diabetes-induced increased in O_2^- production.

Acute NOS inhibition by pre-incubation with 1mM L-NAME eliminated the differences in O_2^- levels between diabetic and control mice.

Biopterin levels: aorta 12 weeks

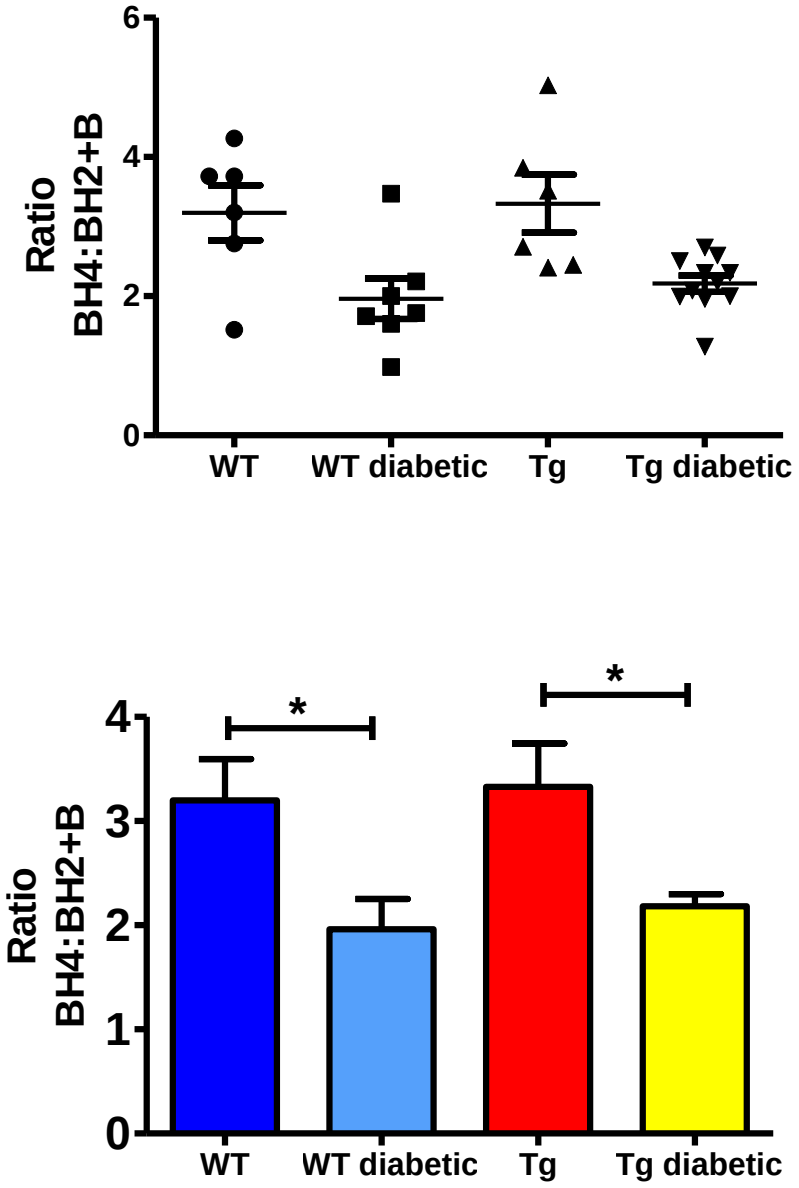


Figure 4.9. Hyperglycaemia is associated with decreased BH4 bioavailability in the aorta.

Aortas from diabetic mice showed a reduction in the ratio of the reduced BH4 cofactor to its oxidised form BH2, with comparable changes across genotypes (2-Way ANOVA; *P<0.05; n = 6-11).

Conclusions

The main findings presented in this chapter demonstrate that:

1. Hyperglycaemia causes impairments in endothelial-dependent vascular reactivity in the aorta, which occurs as an early event in diabetes development, and persists once the condition has progressed further.

2. The myocardial overexpression of mGCH1 does not influence vascular function, as predicted.

3. Diabetic aortas reveal increased oxidative stress, which is likely attributed to NOS uncoupling.

4. In contrary to the aorta, the mesenteric artery of the type 1 diabetic mouse is protected against endothelial dysfunction.

Discussion

The findings from this chapter on the vascular reactivity of the aorta are in line with several previous reports and conform to the unifying mechanism of hyperglycaemia-induced endothelial damage put forward by Brownlee and colleagues (299). Endothelial dysfunction is described as a complication that arises from diabetes in its broadest sense, often without reference to disease type. Although a key feature of type 2 diabetes is hyperglycaemia, the concurrent presence of hyperinsulinemia is also a strong force for the long-term progression of vascular damage. In our model of type 1 diabetes, mice instead experience hyperglycaemia on a background of insulin deficiency, thus there is good reason to believe that signalling pathways activated by high levels of glucose underlie the observed impairment in aortic function.

I have reported that mice begin to exhibit hyperglycaemia even after 1 week of diabetes, with endothelial dysfunction in the aorta evident as early as 4 weeks. Much of the work utilising the STZ rodent model of diabetes has focused on the rat, where vascular function is typically assessed at least

8 weeks after diabetes induction (300, 301). Early work by Hattori et al. showed that after 8-12 weeks of STZ-induced hyperglycaemia, aortas from these rats showed a reduction in the maximum level of vasodilatation to ACh, as well as increased fade of the response with a greater rebound constriction (300). With similar STZ doses, a later study showed that after 8 weeks the degree of endothelial dysfunction actually correlated with levels of glycaemia, as measured by HbA1c (302). In addition, Majithiya et al. showed that the degree of impairment in endothelium-dependent vasodilation of the aorta was comparable to that observed in this chapter, with the maximal relaxation of diabetic vessels being 55% vs 90% in control (303). Few studies in the rat have documented early and late time points, but those that have demonstrate no changes in endothelial function after 1 week of diabetes, yet a clear dysfunction after 8 weeks (293, 301). The suggestion that STZ-induced diabetes is not injurious to endothelial function after merely 1 week is contradicted by the results of Oak et al. in the mouse (304). Although these authors reported marked aortic endothelial dysfunction after only 7 days of hyperglycaemia, the findings come from a model using extremely severe doses of STZ (3x 100mg/kg), which has been shown to cause significant mortality and is unlikely to be representative of disease development (193). Similarly, single STZ administrations in the range of 140mg/kg have been tested previously in this laboratory, with behavioural deficits and excessive weight loss being observed.

My data describing endothelial dysfunction after 4 weeks of hyperglycaemia is consistent with some other reports of vascular reactivity in the aorta. The study by Alp et al. showed impaired endothelial-dependent vasodilation at 4 weeks with a single high dose (160mg/kg) STZ protocol (155), which although potentially severe, is also supported by findings from the Akita model of type 1 diabetes. As with my investigation, Toque et al. investigated the effects of hyperglycaemia on the aorta at multiple time points. These authors likewise described a decline in endothelial function at 4 weeks (more so in ACh potency rather than E_{max}), which progressed to an even more significant dysfunction at 12 and 24 weeks (305). In addition, diminished relaxation has been demonstrated between 4 and 12 weeks of diabetes, where Romero et al. observed the abnormality after 8 weeks of diabetes (306). The STZ protocol used here was also a lower dose regimen of 4 alternate day injections at 65mg/kg/day, which

could well produce a disease onset more akin to that which occurred during my own investigation. However, the reports of Romero et al., as well as many others, fail to include measurements of plasma insulin levels, thus it is difficult to compare type 1 diabetic phenotypes to help explain temporal differences.

Aside from the almost immediate endothelial dysfunction reported by some studies using severe diabetes models, the temporal effects of hyperglycaemia on NO-mediated dilatation in the literature (in both mouse and rat aorta) are largely supportive of my own findings reported in this chapter. One interesting difference to note is the progressive nature of the vascular impairment described by Toque et al. (305), as opposed to the comparable levels of dysfunction seen at 4 and 12 weeks in my own study. As well as obvious differences in mouse strain and disease model, some of this might also be explained by the nature of hyperglycaemia between the 4 week and 12 week period, which was far more incremental in the former study compared to my own (Figure 4.1A). What is consistent amongst all these previous and current findings is that the dilator response of the smooth muscle to NO donors remains completely intact in the diabetic state. These *ex vivo* animal studies are also mirrored by reports from insulin-dependent diabetic patients, where measures of flow-mediated dilatation in the periphery show endothelial dysfunction, but no differences in response to nitroprusside (307, 308). Taken together, the current data available indicates that both the ability of the vascular smooth muscle to respond to NO via the GC-cGMP pathway and the contractile machinery of the myocyte is preserved in the diabetic state. Rather, the abnormality lies upstream in either the generation or diffusion of NO, or a failure in maintaining its status as an intact diatomic molecule due to reactions with other pro-oxidant species.

My results presented here substantiate the cellular basis for impaired endothelial function, which is the onset of oxidative stress and NOS uncoupling. Although much of the work generating this hypothesis came from established endothelial cell lines *in vitro* (299), findings from diabetic animal models also now support this mechanism. In the STZ-treated rat Majithiya et al. suggested, though did

not measure directly, increased ROS production through depletion of catalase, SOD and glutathione, as well as increases in lipid peroxidation (303). In a similar model, Hattori suggested likewise, showing that exogenous SOD treatment could prevent the decline in ACh-mediated relaxation in the diabetic aorta (300). Elaborating on this with more direct measures, experiments in the mouse aorta have shown with independent methods that diabetes causes elevated O_2^- with concomitant decreases in NO (155, 304). This has been perhaps most extensively investigated by Alp et al., who not only showed that diabetic aortas displayed increased O_2^-, reduced NO and depleted glutathione, but also decreased BH4 bioavailability (155). My results corroborate these findings, where an increase in O_2^- was accompanied by a decreased BH4:BH2 ratio, indicative of oxidative stress. Moreover, the ability of NOS inhibition to abolish the difference in ROS production further supports NOS uncoupling as a driver for the observed endothelial dysfunction.

Interestingly, Toque et al. also reported additional mechanisms of reduced NO bioavailability in the diabetic mouse aorta that should be considered, namely decreased phosphorylation of eNOS at Ser^{1177} and increased arginase activity (305). Although Ser^{1177} phosphorylation alone may not be sufficient for stimulating NO production (309), this site still plays a key role in eNOS activation and is known to be a target of insulin through the PI3K/Akt cascade (269, 310). While reduced eNOS activation may therefore occur inherently from diminished insulin signalling in the type 1 diabetes setting, Du et al. have shown that hyperglycaemia itself is able to reduce Ser^{1177} phosphorylation, and that this effect can be prevented by inhibiting mitochondrial O_2^- production and the activation of the hexosamine pathway (311). Increases in arginase expression and activity depletes the pool of L-arginine available as a substrate for NOS, thereby also acting as a mechanism to reduce NO turnover. Heightened arginase activity has been associated with diabetes-induced endothelial dysfunction, moreover, treatment with arginase inhibitors was able to reverse the impairments in NO-mediated vasodilatation (305, 312, 313). Additional studies have also suggested that the ROS generated in response to hyperglycaemia may directly increase arginase activity, potentially through stimulation of Rho kinase (314). Although neither eNOS phosphorylation nor arginase status was assessed in my study, the

evidence from other studies suggests that these components may have contributed to the endothelial dysfunction, simply as a result of oxidative stress as the precipitating event. What is apparent from the findings of Alp et al. is that the coupling state of NOS may be the most important factor, where increased NO relative to O_2^- production by the NOS enzyme can prevent redox imbalance and any potentially destructive pathways downstream (155).

Reduced NO bioavailability has also been linked to the increased pressor response induced by the vasoconstrictor phenylephrine. Several studies in the aorta have shown that endothelium removal or NOS inhibition can increase the sensitivity of the vessel to α-adrenergic agonists (including PE), as well as increase the maximal level of vasoconstriction (315-318). It has therefore been proposed that NO release normally acts as a modulator of vasoconstriction in a system of negative feedback. The indication of vascular NOS uncoupling and impaired NO availability in diabetic aortas would therefore explain the enhanced pressor response observed both in my study and in previous reports with different experimental models (303-306).

Interestingly, after 4 weeks of diabetes, aortas did not show a significantly enhanced vasoconstriction, even though the degree of endothelial dysfunction at 4 and 12 weeks was comparable. This might suggest that changes to other vasoactive mediators, influenced by longer term hyperglycaemia, may be required to cause the hypercontractile response to PE. Xavier et al. have suggested that prostaglandin H2 (PGH_2) and thromboxane (TXA_2) are potential candidates, which may explain their own analogous time-dependent findings of normal pressor responses after 1 week of diabetes, yet abnormal after 4 weeks (319). Another possibility is that the increase in α-adrenergic constrictor responses was mediated through increased DAG-PKC signalling in the vascular smooth muscle, which may increase Ca^{2+} influx, as well as Ca^{2+} release from internal stores (320, 321). However, Chang and Stevens have shown in the STZ-treated rat that endothelium removal could abolish the augmented PE sensitivity of the aorta in diabetic animals compared to control (after 52 weeks), suggesting that vasoconstrictor/vasodilator imbalances in the endothelium are more likely to account for the long

term hypercontractility of the vessel, as opposed to direct changes to the vascular smooth muscle (322). Why this would be observed at 12 weeks and not 4 weeks in my study is still unclear, but the difference might be a summation of changes to various signalling pathways in the regulation of vascular tone, all of which become more apparent and severe throughout the course of diabetes. While the NOS dysfunction at 4 weeks would still likely affect the capacity of the vessel to suppress PE-induced vasoconstriction, NO availability is clearly not the sole factor influencing the contractility of the diabetic mouse aorta in response to α-adrenergic stimulation. The experimental data from vascular function, O_2^- production and BH4 bioavailability at 12 weeks reveal not only an effect of diabetes, but also the lack of an effect from the transgene. Indeed, these measurements show very similar results between genotypes, with differences arising only from STZ treatment. While this is to be expected in a model of myocardial-specific GCH1 overexpression, these functional and biochemical data provide verification that the transgene is not having significant pleiotropic effects at the level of the vasculature.

Perhaps the most interesting finding from this chapter is the lack of impairment in mesenteric arteries coming from the same diabetic mice that exhibited endothelial dysfunction in aorta. Since the aorta is a main conduit vessel and the mesenteric artery is a resistance vessel, this indicates heterogeneity in the responses of different vascular beds to the diabetic milieu. Despite previous reports highlighting a greater influence of non NO-mediated endothelium-dependent vasodilation in the mesenteric artery (281, 282, 323, 324), my results demonstrated that in control mice, there was still a significant component of the relaxation response that was inhibitable by L-NAME (albeit with considerable variability). 12 weeks of diabetes also did not appear to alter the nature of the response; inhibition of NOS and EDHF led to similar declines in vasodilatation in both diabetic and control vessels. In contrast, Matsumoto et al. described endothelial dysfunction in the mesenteric artery of STZ-treated mice which was attributed to a specific impairment in the EDHF pathway (283). Impaired EDHF-mediated responses were also reported by Fitzgerald et al., however, these authors also determined that their severe, short term diabetes protocol also led to a compensatory upregulation of NO function (281).

While EDHF dysfunction and NO compensation is an unlikely interpretation from my results, the maintenance of endothelial function in the diabetic state that was largely NO-dependent may suggest that this pathway is instead protected in some way in the mesenteric vascular bed. Evidence for this comes from a mouse model (hph-1) of inherited GCH1 deficiency, where d'Uscio et al. have shown that mice demonstrate a decrease in BH4:BH2 ratio in the aorta and yet not in mesenteric vessels, while the latter also exhibits an improved antioxidant profile (via CuZnSOD) and no elevation in O_2^- (325). An absence of oxidative stress in the resistance vasculature is an interesting possibility and would be a likely explanation for the maintained endothelial function observed *ex vivo* in my study, as well as the preservation of normal blood pressure reported in the hph-1 mouse (325). This is also supported by Takaki et al., who showed that the index of BH4 bioavailability tended to be increased in the mesenteric artery compared to the aorta, suggesting that eNOS uncoupling would be unlikely to contribute to O_2^- generation in resistance vessels (324). However, it might be necessary to distinguish between resistance vessels, since Kidokoro et al. have shown that type 1 diabetic Akita mice display increased ROS and eNOS uncoupling in the glomerulus, while endothelial-specific GCH1 overexpression can improve the BH4:BH2 index and prevent the development of diabetic nephropathy (326). Similar effects have been seen in skeletal muscle arterioles from the STZ-treated rat, showing impaired flow-mediated dilatation due to NO dysfunction, which could subsequently be restored by treatment with the BH4 precursor sepiapterin (327).

The extent to which NOS coupling is affected by diabetes, and the importance of this status to vascular function, may very well vary between vascular beds, specific arteries and even the arteriolar branch (i.e. vessel diameter) studied. While ROS generation may still be elevated by hyperglycaemia, certain vessels may also have varying activities of redox signalling pathways to compensate. This may well be the case in the mesenteric artery, where an increase in CuZnSOD function could convert O_2^- to H_2O_2/EDHF to facilitate vasodilatation (325, 328, 329). The extent to which this happens in human vessels though is not clear; Guzik et al. confirmed the importance of CuZnSOD as a buffer against oxidative stress, yet reported no differences in SOD activity between internal mammary arteries and

saphenous veins (330). However, specificity in the SOD isoenzyme and localisation should also be consideration, as Landmasser et al. have shown reduced activity of endothelium-bound SOD (EC-SOD) in the arteries of patients with coronary artery disease (CAD), even though CuZnSOD and MnSOD were unchanged (331). Taken together, one must overall consider the total sum of vasoactive mediators that could potentially contribute to changes in vascular reactivity in both the physiological and diabetic state, as well as the variation conferred by virtue of species/strain differences, diabetic model, the disease duration and its overall severity.

Chapter 5

The pathology of diabetes in the myocardium and effect of mGCH1 overexpression

Introduction

Studies of the circulation, both from my results and wider experimental findings, have revealed a similar diabetic phenotype (perhaps dependent on the vascular bed) of endothelial dysfunction, with many exploring the underlying cellular mechanisms. However, in the myocardium, the picture is far less clear, even for the functional definition of the diabetic cardiomyopathy.

Clinical cardiomyopathy phenotype

While a distinct cardiac dysfunction, independent of other cardiovascular risk factors, has been recognised in the diabetic state, reports vary in the structural and functional aberrations that may occur. The large Framingham study of male and female diabetic subjects showed that there was an increase in LV mass in women, but not men, in the presence of diabetes (332). The Strong Heart study later demonstrated that both men and women with T2D exhibited an increase in LV mass and wall thickness, although this did come from a completely different subject population (Native American Indians) (333). Structural changes in the myocardium during diabetes may well depend on the presence of other comorbidities. For example, in a study of a multi-ethnic population with T2D, the increase in LV mass could have been due to the interaction detected between diabetes and central obesity (334). In addition, Galvan et al. reported that insulin sensitivity alone was not an independent predictor of LV mass after taking body mass into account (335), which is also consistent with the observation that obesity itself, independent of blood pressure, can be a major cause of LV hypertrophy (336). Similarly, in T1D patients there have been some reports of LV hypertrophy, although this occurred with co-existing diabetic nephropathy, suggesting that dysregulation of the renin-angiotensin system and resulting hypertension could be the predominant factor (337, 338). The significance of an increase in LV mass has been considered by the findings of Rerpattanapipat et al., who showed that LV hypertrophy was observed in established diabetes, but not in a group of individuals with impaired fasting glucose, implicating hypertrophy as more of a long term consequence of diabetic complications instead of an initial event in the development of cardiomyopathy (339).

Functionally, diabetic cardiomyopathy has been associated with the development of LV diastolic dysfunction, as determined by both conventional echocardiography and tissue Doppler imaging (TDI). Boyer et al. examined asymptomatic, T2D patients with no history of cardiovascular disease, observing that up to 75% of patients exhibited diastolic dysfunction, which was most effectively detected with TDI (340). Similar findings were made in asymptomatic T1D subjects with a disease duration ranging from 2 to 36 years. Here Shivalkar et al. found that diastolic and systolic dysfunction (assessed from specific LV regional segments) was present within the first decade (accompanying endothelial dysfunction), but that the diastolic impairments preceded the changes in systolic parameters (341). The value of TDI in the assessment of diabetic cardiomyopathy has been further highlighted by di Bonito et al., who showed that a depressed E'/A' ratio (assessed by TDI) was present in 50% of non-obese, normotensive T2D patients that showed normal cardiac function using conventional echocardiography. Interestingly, these subjects all had a diabetes duration of less than 4 years, revealing just how rapidly diastolic dysfunction may develop in certain individuals with diabetes (342). This is consistent with the findings from children and adolescents with early T1D, where LV relaxation time was prolonged despite no observation of systolic dysfunction (343).

However, a definitive consensus on LV diastolic dysfunction as the preliminary indicator of diabetic cardiomyopathy still does not exist. Ernande et al. showed that some patients with T2D indeed had a normal systolic strain in the presence of diastolic dysfunction; a different subset showed both abnormal systolic and diastolic function; yet another group exhibited systolic strain alterations even with normal diastolic parameters (344). Similarly, measurements of myocardial strain in other studies using different methods have also described impaired contractility in diabetic subjects, even though traditional markers of systolic function (e.g. fractional shortening, ejection fraction) remained unchanged (345, 346).

Together, these patient studies have suggested that the selected parameters for best reflecting LV function may explain some of the uncertainty over the identity of diabetic cardiomyopathy, which has likely also been influenced by diabetes type, as well as disease severity and management.

Animal models of diabetic cardiomyopathy

Whereas the majority of clinical reports focus on T2D or a mixed diabetes cohort, a number of animal studies have attempted to recapitulate diabetic cardiomyopathy in selective models of T1D. In the STZ-treated rodent, available reports of structural changes in the development of cardiomyopathy have been variable. In the rat, Joffe et al. showed that after 10 weeks post-STZ treatment diabetic rats displayed a greater LV mass: body weight ratio (347). Although this is supported by other findings after 6 months, histological measurements indicated that diabetic rats exhibited thinner myocardial fibres (348), suggesting that aside from LV hypertrophy the results may be due to the significant drop in body weight over the study period. Furthermore, Yu et al. saw that 4 weeks of diabetes in the STZ-treated mouse did not alter the overall LV mass: body weight ratio, yet there was a decrease in LV mass in these animals (349).

In terms of the functional phenotype, Katare et al. have studied the evolution of diabetic cardiomyopathy using the 5-day low-dose STZ treatment protocol. They showed with *in vivo* echocardiography that diabetic mice displayed early diastolic dysfunction after 4 weeks, as evidenced by a reduced E/A ratio. This progressed after 12 weeks, at which point mice began to display decreases in fractional shortening and EF (176). A similar multi-time point (and STZ-dosing regimen) study by Thomas et al. evidenced progressive diastolic dysfunction beginning after 6 weeks of diabetes, while systolic performance was maintained until 10 weeks post-injection (350). This is also consistent with some other single time point echocardiography studies with the use of moderate STZ dosages, where diastolic dysfunction is not joined by systolic impairment until 12 weeks of hyperglycaemia (351, 352). Haemodynamic measures in the low-dose mouse model have suggested that systolic dysfunction may occur earlier in disease progression, where Westerman et al. showed that after 8 weeks the rate of

cardiac contraction and EF were decreased, accompanying the observed increase in cardiac stiffness and depressed rates of relaxation (353). Other studies using echocardiography, perfused hearts and isolated cardiomyocytes have described more overt systolic dysfunction, presenting as early as 4 weeks. However, these reports come from STZ protocols using dosages of 100-200mg/kg/day, therefore the sheer severity of this diabetes model may be accelerating the cardiac phenotype towards heart failure (349, 354, 355). Further phenotypic variation stems from the genetic models of T1D, where some isolated myocyte experiments have shown decreased contractility after 8-12 weeks of diabetes in Ove26 and Akita mice (356, 357). However, this is in contrast to Basu et al., who showed that after both 8 weeks and 20 weeks of diabetes, Akita mice displayed preserved systolic function, despite prolonged relaxation time with measures of echocardiography and haemodynamics (172).

Changes to cardiomyocyte physiology

Within these animal models, authors have attempted to dissect out the cellular mechanisms at play that explain aspects of the cardiomyopathy phenotype. In the STZ-treated rat, Lacombe et al. showed that diastolic dysfunction (but preserved systolic performance) *in vivo* was also accompanied by prolonged Ca^{2+} transient decay at the level of the cardiomyocyte, which may be explained by the decreased protein expression of SERCA and PLB-Ser^{16} (352). Similar findings have also been reported in the STZ mouse, albeit with severe dosage protocols (354, 358), where inducible overexpression of SERCA was shown to rescue the existing cardiomyopathy observed in both myocytes and the perfused whole heart (354). A reduction in the levels of SERCA have been consistent across other mouse models of type 1 diabetic cardiomyopathy, such as the Ove26 (356) and Akita mouse lines (172, 359), while reports vary in the degree to which PLB, RyR and NCX are changed, or indeed even measured (360-364).

However, while decreased expression and/or activity of the primary Ca^{2+}-handling machinery is certainly one potential arbiter of cardiac dysfunction in diabetes, alternative, or perhaps additional factors have been put forward. In a lower dose STZ model of T1D, Nielsen et al. showed that diabetic

cardiomyopathy was associated with increased accumulation of myocardial triglycerides (TAGs), while overexpression of apoB lipoprotein was able to prevent cardiac TAG accumulation and attenuate the cardiac dysfunction in the diabetic state (351). Potential lipotoxicity in the absence of fibrosis or hypertrophy has also been suggested in similar mouse models, where increases in TAGs are also accompanied by markers of increased fatty acid (FA) utilisation e.g. palmitoyl coA and the expression profiles of MCAD, PDK4 and UCP3 (172, 355). The type of TAG may also be important, where Finck et al. have shown that TAGs containing long-chain FA, but not medium-chain TAGs were associated with diabetic cardiomyopathy (365). However, the work of Listenberger et al. has suggested that in non-adipose tissues the formation of TAGs may actually be a protective mechanism against the potential toxicity of other lipid intermediates (366). Derivatives such as ceramide and DAG have been implicated in cardiac cytotoxicity and "lipoapoptosis" (367, 368), moreover, where there is TAG accumulation there is likely also a concomitant increase in these other metabolites, making the source of lipotoxicity hard to identify (172).

While the absence of fibrosis and hypertrophy has been reported in some of the rodent models of T1 diabetic cardiomyopathy (172, 350, 369), others have implicated these structural changes and an underlying inflammatory process as a primary factor in the development of LV cardiac dysfunction. In the STZ-treated rat, histological staining of LV tissue has shown increased collagen deposition, which is also supported by elevated expression profiles of collagen I and III, as well as TGF-β (370-372). Tschope et al. additionally showed that overexpression of kallikrein (to inhibit collagen synthesis) prevented collagen accumulation and prevented the diabetic cardiomyopathy (371). These studies have been expanded further in both the mouse and the rat, where investigators have demonstrated cardiac fibrosis in association with increased expression of pro-inflammatory markers TNFα, IFNγ and MMPs, as well as decreased levels of anti-inflammatory IL-4 and IL-10 (373, 374). The involvement of immune cells directly has been suggested by elevations in the density of CD3 T-lymphocytes and mast cells (373-375), while Becher et al. showed that the degree of collagen deposition and T-cell infiltration was correlated with the extent of LV impairment (374).

Much less evidence currently exists to convincingly implicate NO, and more specifically NOS uncoupling and biopterin status, to the LV cardiomyopathy in T1D. In the STZ-treated mouse Jo et al. did show that myocardial NO production was decreased with a reduction in the BH4:BH2 ratio, which has been attributed to an increase in iNOS expression. Despite some good experiments exploring the oxidative environment in the diabetic heart, the functional cardiomyopathy phenotype was not extensively characterised, moreover, the findings come from a severe diabetic model with extremely high mortality rates (75-85%) (193). Nagareddy et al. have also shown that iNOS expression is increased in the hearts of STZ-treated rats, in association with elevated nitrotyrosine levels as a marker of oxidative stress. However, no assessment of global cardiac performance or cardiomyocyte function was conducted, while the actual myocardial NOS activity went unmeasured (376). Interestingly, in the spontaneous diabetic BB rat, isolation and culture of coronary endothelial cells revealed that both BH4 and NO levels were decreased in the diabetic state. This has been attributed to an impairment in *de novo* BH4 biosynthesis, since GCH1 activity was decreased in diabetic cells, while sepiapterin treatment normalised BH4 levels (through the salvage pathway) (377). Although this is consistent with NOS uncoupling and reduced BH4 bioavailability in other parts of the vasculature, this has not been directly linked with LV dysfunction in the diabetic state. Overall, the available data have not produced a comprehensive phenotypic picture of diabetic cardiomyopathy combined with studies of NOS and BH4 signalling, nor have they indicated a possible causal link between the latter and the former.

The involvement of archetypal hyperglycaemia-induced mechanisms

In contrast to the vasculature, the same putative mechanisms activated by high intracellular glucose have been less well characterised in the myocardium. In terms of the alternative flux of glycolytic intermediates, Trueblood et al. have shown that hearts from BB diabetic rats exhibit impaired glycolysis with an accumulation of glyceraldehyde 3-phosphate (G3P). By inhibition of polyol pathway flux (with the aldose reductase inhibitor zopolrestat), G3P levels were normalised, which has been attributed to restored NAD+ levels and flux through GAPDH (378). This built on the earlier work of

Ramasamy et al., who showed in the same rat model that diabetic hearts had significantly elevated levels of sorbitol and fructose, which was prevented by inclusion of zopolrestat in the cardiac perfusate (379). While these findings suggest that excessive polyol pathway flux could occur in the myocardium as well as the vascular endothelium during hyperglycaemia, there was no association between this metabolic alteration and the diabetic cardiomyopathy per se. Indeed, in one instance Ramasamy and colleagues describe no LV dysfunction in the diabetic state (378), while in the other the focus lies predominantly on the responses to I/R injury (379). Interestingly zopolrestat has also been tested clinically in diabetic patients with impaired cardiac function and existing autonomic neuropathy. These patients were predominantly T2 diabetics of already long-standing duration, in which aldose reductase inhibition only produced a mild benefit on systolic function during exercise (380).

Currently, more substantial evidence exists for increased flux through the hexosamine pathway in the diabetic heart, again as a result of reduced GAPDH activity and impaired glycolysis. After 2 weeks of severe hyperglycaemia, Hu et al. demonstrated that hearts exhibited increased expression of the O-GlcNAcylation modification, as well as the enzyme catalysing its addition, O-linked GlcNAc transferase (OGT). These authors also used LV adenoviral gene delivery to overexpress N-acetylglucosaminidase (GCA), the enzyme responsible for removal of O-GlcNAc; the cardiomyocytes from these hearts showed accelerated decay of Ca^{2+} transients, while perfused hearts exhibited improvements in the velocities of shortening and relengthening. This reversal of the diabetic LV dysfunction may have been attributed to improved calcium reuptake since GCA gene delivery was able to restore the PLB-Ser^{16}/total PLB ratio (381). This is also supported by cell culture studies in high glucose conditions, which indicate that O-GlcNAcylation is sufficient to alter SERCA expression and reduce PLB phosphorylation (361, 382). Aside from EC-coupling, Ramirez-Correa et al. have identified O-GlcNAc-modified myofilament proteins by mass spectrometry, moreover, they showed that incubation of skinned fibres with GlcNAc caused a decrease in myofilament Ca^{2+}-sensitivity (383). In addition, increased levels of OGT have been observed in the cardiac mitochondrial matrix from T1D mice, as

well as the mislocalisation of both OGT and OGA (384). Whilst no functional assessment was made, Banerjee and colleagues propose that these alterations may initiate a cardioprotective cascade, shifting the cardiomyocyte to a glycolytic state to maintain cellular metabolism (384). However, whether this can be reconciled with the expected decrease in glycolytic flux (from reduced GAPDH activity) still remains unclear.

As with hexosamine addition, some studies have also demonstrated the presence of AGEs on cardiomyocyte proteins in the diabetic state. In a series of experiments Bidasee et al. found that after 6 weeks of STZ-induced diabetes, AGE modifications were identified on the cardiac RyR and SERCA, in association with impaired LV contractility and relaxation. These authors revealed that glycation products could alter RyR Ca^{2+} sensitivity, and suggest a disruption in the tertiary structure of SERCA, resulting in impaired Ca^{2+} translocation across the SR (385, 386). In a more severe STZ model, increased levels of the reactive AGE methylglyoxal were measured in diabetic hearts, which was also accompanied by collagen cross-linking and elevated RAGE expression. Most importantly, gene silencing of RAGE was able to prevent the abnormalities in relaxation time and peak shortening that had been noted in diabetic cardiomyocytes (387). Another line of evidence implicates a role for AGEs more specifically in the diastolic impairment in diabetes versus the systolic dysfunction, as suggested by Kranstuber et al. They showed that after 8 weeks, T1D rats exhibited more severe diastolic abnormalities *in vivo*, which was also consistent with prolonged Ca^{2+} transient decay in isolated myocytes. Interestingly, treatment with a breaker of AGE cross-links was able to prevent the diastolic decline and normalise transient decay, yet no improvements were observed in systolic function or transient amplitude (388). However, this may be contrary to some clinical findings, where Campbell et al. reported diastolic dysfunction in diabetic patients with preserved systolic function, yet no increase in AGE or RAGE expression from LV biopsies (389). This might suggest that although AGE modifications may be present in the diabetic milieu during established diabetic cardiomyopathy, the AGE-RAGE interaction itself may not be a primary driver of the LV diastolic dysfunction.

The most convincing evidence for excessive PKC signalling in the development of diabetic cardiomyopathy has come from Lei et al. in the STZ-treated rat 5 weeks after diabetes, these authors showed that diastolic dysfunction was evident with preserved systolic function, which was associated with increased cardiomyocyte PKCβII phosphorylation and a disruption to the caveolar Akt/NOS signalling cascade. Interestingly, PKCβII inhibition both prevented this disruption and attenuated the LV diastolic dysfunction with diabetes. Although the exact cellular mechanism underlying impaired LV relaxation was not investigated, a role for ROS has certainly been implicated, as shown by direct measurements of elevated LV O_2^- production and markers for nitrative stress (192). In combination with oxidative stress, PKCβII activation has also been linked with the increased expression of markers of inflammation and remodelling e.g. NF-κB and TGF-β, which is consistent with the cardiomyocyte hypertrophy observed in this model of diabetic cardiomyopathy (390). Furthermore, Arikawa et al. have made a case for the involvement of PKCβ in the alteration of cardiac metabolism in the diabetic state. After 8 weeks of T1D, these authors showed that PKCβ inhibition (as well as insulin treatment) could attenuate the diastolic dysfunction in STZ-treated rats. This was also associated with improved glucose utilisation in perfused hearts, concomitant with a normalisation of UCP3 and PDK4 protein expression, as well as several genes involved in fatty acid metabolism (391).

Is ROS the primary driver?

If some of these mechanisms induced by high intracellular glucose (as described by Brownlee and colleagues) underlie the LV dysfunction in diabetic cardiomyopathy, then one might also expect increased intracellular ROS, as with the vascular endothelial cell. These increased ROS levels might also persist over the long term through epigenetic imprinting and the notion of hyperglycaemic "memory;" a more recent mechanism proposed in the vasculature by Paneni et al. (70). Unfortunately, much of the abovementioned literature, which investigates diabetic changes to the cellular machinery involved in myocyte contractility and relaxation, often overlooks the direct involvement of oxidative stress. Similarly, some studies which focus on the assessment of cardiac ROS (through various

markers) in diabetes often fail to fully explore the putative pathways induced in the hyperglycaemic state.

Shen et al. have shown that myocardial-specific overexpression of the antioxidant MnSOD was able to prevent the decline in velocities of contraction and relaxation in the OVE26 diabetic mouse. No direct comparison of ROS levels was measured between diabetes and control, however, MnSOD-Tg mice showed improved mitochondrial respiratory control and GSH levels, the suggestion being that mitochondrial-derived ROS mediate the LV dysfunction in diabetes (392). In the same mouse model, Song et al. found that diabetic cardiomyocytes in culture had greater mitochondrial ROS production under high glucose conditions. However, in contrast to the experiments of Brownlee and colleagues, control myocytes showed no difference in ROS levels between normal and high glucose media. Another unusual finding is that these authors found no LV dysfunction *in vivo*, even though isolated myocytes displayed impaired rates of contractility and relaxation (393). Furthermore, Liang et al. documented disorganised mitochondria and reduced glutathione levels in OVE26 hearts, yet no diabetic cardiomyopathy was evident during the perfusion of these hearts at baseline (394). Whilst mitochondrial dysfunction and increased ROS production has been indicated in the OVE26 mouse, comprehensive work by Bugger et al. in the Akita diabetic mouse has suggested differently. Diastolic dysfunction (with preserved systolic function) was accompanied by increased FA oxidation, yet no observed increase in mitochondrial uncoupling or decline in cardiac efficiency. In addition, several independent markers of ROS demonstrated an absence of oxidative stress in diabetic hearts, potentially suggesting that elevated ROS levels may be necessary for the uncoupling of oxidative phosphorylation during the shift to FA metabolism in T1D (395).

Other studies in the STZ-treated mouse have yielded results which more directly associate ROS with LV dysfunction, in spite of no investigation of cardiac fuel metabolism. Turdi et al. have shown that cardiomyocytes isolated and cultured from diabetic mice displayed reduced rates of relengthening and prolonged relaxation time, which was also complemented by findings of defective calcium

handling. These impairments were attributed to increased ROS production and cardiomyocyte apoptosis; moreover, cardiac-specific overexpression of catalase was able to prevent oxidative stress and attenuate the functional impairment in diabetic cardiomyocytes (396). This is supported by the findings from similar experimental models, where comparable functional deficits and markers of ROS have been reported, as well as a reduction in SERCA and NCX protein expression (397, 398). While some of these studies have suggested that NADPH oxidase may underlie an elevation in cardiac O_2^- production in diabetes (398, 399), the involvement of NOS dysfunction in oxidative stress has not been determined.

This chapter investigates how type 1 diabetes impacts myocardial function at early and late time points, also then exploring the potential beneficial effects of BH4 augmentation, through both mGCH1 overexpression and BH4 supplementation.

Methods

Experimental protocols were performed as generally described in chapter 2.

Superoxide production

As with measurements in the vasculature, O_2^- production was measured by lucigenin-enhanced chemiluminescence. 300-400µg of sample protein from LV homogenates was incubated in a scintillation vial of KHB containing 5µM lucigenin. The effect of inhibiting NOS activity on O_2^- production was determined by the addition of 1mM L-NAME, with the inactive isomer D-NAME (1mM) used for control runs. 10mM of the specific O_2^- scavenger tiron was used to confirm the origin of the ROS signal was O_2^-. Chemiluminescence levels were assessed over the final 2 min of each period of recording and the values expressed as the tiron-inhibitable fraction, measured as relative light units, per mg protein, per second (RLUs/mg/s).

O_2^- production was also measured in LV homogenates by HPLC detection of dihydroethidium (DHE) conversion to 2-hydroxyethidium (2-OHE). LV homogenates were incubated with DHE (50µM) for 15

min at 37°C, after which the cells were lysed with methanol. Hydrochloric acid (100mM) was added and the samples were loaded into the autosampler for detection. Subsets of supernatants were pre-incubated with L-NAME (1mM) or the inactive isomer D-NAME (1mM), as well as the O_2^- scavenger tiron (10mM). The separation of DHE, 2-OHE and ethidium was performed using the gradient HPLC system with a reverse-phase column, and quantified using fluorescence detection set at 510nm (excitation) and 595nm (emission). All results were expressed as the tiron-inhibitable fraction of 2-OHE.

Cardiomyocyte isolation

LV myocytes were isolated using Langendorff perfusion followed by enzymatic dispersion. Hearts were perfused with Ca^{2+}-free isolation solution (oxygenated at 37˚C) for 3 min, followed by 9 min of perfusion with collagenase solution I. Hearts were removed and the LV excised and digested in collagenase solution II (shaken at 300 rpm, 37˚C). Digested LV myocytes were resuspended and centrifuged for 3 min at 400 rpm. The final myocyte pellet was resuspended in storage solution and used within 6 hours for shortening experiments.

Cell shortening and $[Ca^{2+}]_i$ transients

Single cell dimensions and shortening cycles were measured and recorded using a video-edge detection system in LV myocytes field-stimulated at 3Hz (continuously perfused at 35 ± 1.5 ˚C). $[Ca^{2+}]_i$ transients were measured in field-stimulated LV myocytes pre-loaded with the Ca^{2+}-sensitive probe Fura-2 (5 µM). The $[Ca^{2+}]_i$ transient was determined from the Fura-2 fluorescence ratio (excitation at 340nm compared with 380nm; baseline values were representative of diastolic $[Ca^{2+}]_i$, while peak values represented systolic $[Ca^{2+}]_i$. The amplitude of the $[Ca^{2+}]_i$ transient was then calculated by: peak $[Ca^{2+}]_i$ – baseline $[Ca^{2+}]_i$ fluorescence. The time constant for the decay of the $[Ca^{2+}]_i$ transient (tau) was calculated by fitting a curve with a bi-exponential function using Axon Clampfit 8.2 software. For both sets of experiments, values were determined from the average of at least 10 steady-state contractions and $[Ca^{2+}]_i$ transients per cell.

Echocardiography

Global cardiac function was studied *in vivo* using a high-resolution 2D-echocardiography system with an ultra-high frequency MS400 transducer probe (18-38 MHz). 2D images (standard B-mode) of the heart were obtained, as well as mitral blood inflow and tissue velocities by pulse-wave Doppler. LV wall dimensions were determined in the parasternal short-axis view (M-mode), from which measures of ejection fraction and fractional shortening were derived. Traces were analysed using the Vevo software and summary data comprised of at least 3 cardiac cycles for each parameter.

Creatine kinase (CK) activity

For assaying CK activity, LV samples (5mg) were homogenised using a pre-cooled glass homogenising rod (1300 revs/min) in ice buffer. 150µl of the homogenate solution was removed and split into triplicates for protein quantification. Sample homogenates were precipitated and the CK isoenzymes separated and quantified using a rapid gel electrophoresis (REP) unit. CK activity was assessed by the change in absorbance during catalysis, detected at 340nm and expressed as mIU/mgww. For mitochondrial CK, activity was normalised to citrate synthase activity as a marker of the sample's oxidative capacity.

Glutathione assay

Glutathione was measured using a commercially available assay kit, based on the method of enzymatic recycling. LV tissue was homogenised according to assay instructions using a manual glass dounce tissue grinder. Homogenates were centrifuged at 13 000 rpm for 10 min at 4°C and the supernatants transferred to fresh Eppendorf tubes and maintained on ice prior to the assay. Total glutathione was detected from absorbance values at 405nm, as compared to a GSSG standard curve. Oxidised glutathione was discerned with the use of 4-vinylpyridine to inhibit recycling by glutathione reductase. The concentration (pM) of oxidised glutathione in each sample was subtracted from the concentration of total glutathione, thereby also revealing the concentration of reduced glutathione.

Immunoblotting

LV samples were homogenised in 1x RIPA buffer containing protease inhibitors. Sample homogenates were quantified using a BCA protein assay; proteins were then separated by gel electrophoresis in criterion 4-15% gels and transferred to PVDF membrane. Expression was determined by Western blotting with primary antibodies directed to the target proteins (see table, page 19), made up in TBST containing 5% milk. Membranes were incubated in West Pico chemiluminescent substrate and developed using either an X-ograph or ChemiDoc MP system. Protein quantification was expressed relative to the house-keeping proteins GAPDH or TnI.

Quantitative real-time RT PCR

RT-PCR was used to assess the expression of mouse primary mRNA transcripts for IL-1β, MCP-1, MMP-2, MMP-9, collagen 1A1, GLUT1, GLUT4 and the house-keeping gene α-actin. Total RNAs were extracted with an RNeasy Mini Kit and cDNA synthesised with QuantiTect Reverse Transcription Kit. cDNA were amplified with TaqMan(R) Gene Expression Master Mix and the necessary sequence-specific TaqMan probes (see table, page 19).

Samples were loaded into 96-well optical plates and RT-PCR performed with an iCycler IQ real-time system. 13.5µl of cDNA (100ng/µl), 15µl TaqMan master mix, and 1.5µl TaqMan gene expression assays were mixed together per reaction. RT-PCR reactions proceeded under the following conditions: 10 min at 50°C, 10 min at 95°C, 50x cycles of 15 secs at 95°C and 1 min at 60°C. cDNA amplification was quantified via the Livak method and results were displayed as the fold change (ΔCt) as compared to the expression of the housekeeping gene, selected for normalisation.

Histology

Lipid content in the myocardium was assessed using oil red O (ORO) staining. LV tissue was collected in optimal cutting temperature (OCT) compound and flash-frozen in isopentane bathed in liquid nitrogen. ORO stock was prepared according to manufacturer's instructions and filtered to remove

any precipitates. Embedded LV tissue was quickly sectioned on a cryostat into 12µm-thick sections; 3 cross-sections were taken for each LV and incubated in ORO solution for 5 min. ORO was washed away with water intermittently for 30 min. Air-dried stained sections were imaged the same day using a bright-field light microscope (Nikon Eclipse TE2000U Inverted Microscope) with 20x magnification. Staining intensity was quantified using ImageJ software (v. 1.46r; National Institutes of Health, Bethesda, USA). Sections of liver were stained and visualised in parallel as a positive control.

Biopterin quantification

The detection of the different biopterins BH4, BH2 and B was achieved by separation and quantification by reverse phase HPLC. LV tissue was homogenised in ice cold re-suspension buffer, followed by 2 centrifugations (15min at 13 000 rpm and 4°C). A volume of 180ul of the supernatant was taken into a separate tube and 20ul of precipitation buffer was added, followed by a final spin (5min at 13 000 rpm and 4°C) Supernatants (100µl) were injected into an isocratic HPLC system; biopterins were separated using a Carbon-18 column and quantified by sequential electrochemical and fluorescence detection. Biopterin concentrations were quantified by comparison with injected BH4 and BH2 reference standards; the final concentrations were normalised to the sample protein content.

Myofilament mechanics

Ca^{2+} sensitivity, tension development and passive stiffness were assessed in LV demembranated trabeculae. Trabeculae (80-250µm in width; 1-3mm in length) were dissected from the LV wall and placed in skinning solution overnight at 4°C. Skinned trabeculae were attached via T-clips to a permeabilised fibre test system. Muscle fibres were initially equilibrated in relaxing solution of low calcium (pCa 9.0) and stretched to a sarcomere length of 2.3 µm, as detected by laser diffraction. Initial activation was performed at pCa 4.0, after which trabeculae were correctly repositioned and sarcomere length re-established. To determine force-Ca^{2+} sensitivity and tension development, fibres were placed in incremental pCa solutions (9.0 – 4.0) and the force production monitored in each pCa

solution until it reached equilibrium. For assessing passive stiffness fibres were stretched from their original length (L_0) and held at different lengths by performing a stretch and hold procedure. Fibres were stretched over a period of 15 sec, followed by a hold for 180 sec. This was performed to generate the following lengths: 1.05*L_0, 1.10*L_0, 1.15*L_0, 1.20*L_0, 1.25*L_0, and 1.30*L_0, with sarcomere length recorded after each stretch. A custom-built application was developed using Matlab software for the analysis of force-Ca^{2+} sensitivity and tension redevelopment; to determine Ca^{2+}-dependent force specifically, the measure of passive stiffness was subtracted from the force generated at each pCa. Ca^{2+}-dependent force was plotted against pCa to resolve the force-Ca^{2+} sensitivity relationship.

NOS activity

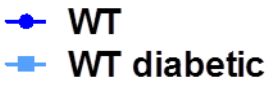
NOS activity was assayed by radiochemical detection of the conversion of L-arginine substrate to L-citrulline, as detailed previously. The metabolic products of L-arginine were separated by ion exchange HPLC and online radiochemical scintillation detection, with the analysis of recorded data performed using Azur software. LV tissue was homogenised in ice-cold KHB, also containing 5 µM of N-hydroxy-nor-L-arginine to inhibit arginase activity. Sample homogenates were centrifuged for 10 min at 13 000 rpm (4°C) and supernatants incubated on ice for 30 min with the addition of exogenous NOS cofactors: FMN 1mM, FAD 1µM, NADPH 1mM). This was performed in the absence or presence of the non-specific NOS inhibitor L-NAME (1mM), followed by 4 hour incubation at 37°C with 0.75µl of labelled ^{14}C L-arginine (1.85MBq/ml). 10% Trichloroacetic acid was added to de-proteinate the samples and the supernatants (700µl) were then loaded into the autosampler and cooled down to 4°C. Elution time was determined using standards of ^{14}C L-arginine (1µM). Chromatographic peaks were integrated and expressed in proportion to the total ^{14}C counts for each sample. The results were expressed as the L-NAME-inhibitable fraction of L-citrulline to represent the NOS-attributable component.

BH4 supplementation

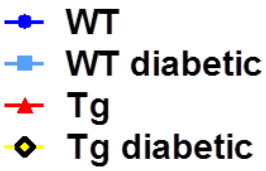
Oral BH4 was supplemented at 200mg/kg/day dose, implemented after 6 weeks of the diabetes protocol. Supplementation continued for the remaining 6 weeks until the 12 week terminal end point.

Results

For only WT vs WT diabetic comparisons, the following colours are assigned for each treatment group:



For comparisons between treatment and genotype (mGCH1-Tg), the following colours are assigned for each group:



For comparisons between WT, WT diabetic and WT diabetic mice supplemented with BH4, the following colours are assigned for each group:



No cardiomyopathy is evident after 4 weeks of diabetes

To assess whether LV dysfunction was an early event in the progression of T1D, global cardiac function was evaluated *in vivo.* Measures of fractional shortening and ejection fraction from the parasternal short-axis view demonstrated no differences in systolic performance between control and diabetic mice (Figure 5.1). Similarly, diastolic function also remained unaltered after 4 weeks of diabetes, as reflected by the early to late ratios of both transmitral and tissue Doppler velocities (Figure 5.2). This *in vivo* assessment was also consistent with findings at the cardiomyocyte level, where both control and diabetic mice showed similar degrees of cell shortening and relaxation times (Figures 5.3 and 5.4). This corresponded with measurements of calcium handling, which reflected equal amplitude of the Ca^{2+} transient, as well the same rate of transient decay in both groups (Figures 5.3 and 5.4). Despite no obvious abnormalities in diabetes, the presence of the mGCH1 transgene significantly accelerated relaxation time and calcium sequestration in cardiomyocytes from both control and diabetic mice

(Tau1: 0.095 ± 0.005 in Tg diabetic vs 0.120 ± 0.006 in WT diabetic; Figure 5.4 A and B). Together, these results illustrate that in the very early stages of T1D, there is no evidence of a disruption to cardiomyocyte EC-coupling, with cellular and global cardiac function being preserved. The alteration in EC-coupling with mGCH1 overexpression, but not with diabetes, was also accompanied by unchanged LV protein expression in all of the 3 NOS isoforms (Figure 5.5).

mGCH1 overexpression protects against the later onset of diabetic cardiomyopathy

LV function was measured again 12 weeks post-injection to determine whether cardiomyopathy developed later in the progression of T1D. Although relatively mild in severity and less evident throughout the course of experiments, WT diabetic mice displayed a significant decline in systolic function at this time point, as demonstrated by the decrease in ejection fraction (76.47 ± 1.67 in WT vs 68.57 ± 1.92 in WT diabetic; Figure 5.6). Echocardiography also revealed that WT diabetic mice exhibited a significant LV diastolic dysfunction, as evidenced by a decrease in the E'/A' ratio with tissue Doppler (1.37 ± 0.047 in WT vs 0.95 ± 0.084 in WT diabetic; Figure 5.7A and B), despite E/A remaining normal. This was also reflected in the ratio of the early diastolic mitral velocity to the early diastolic tissue Doppler velocity (E/E'), another clinical indicator for impaired diastolic performance (Figure 5.7C).

Non-diabetic mice overexpressing mGCH1 showed minor increases in EF and E'/A' ratio relative to WT control. But most importantly, mGCH1 overexpression in diabetic mice was able to completely prevent the diastolic and systolic dysfunction exhibited by WT diabetic mice. Indeed, Tg diabetic mice demonstrated an EF (77.55 ± 1.79 in Tg diabetic vs 68.57 ± 1.92 in WT diabetic; Figure 5.6) and E'/A' ratio (1.58 ± 0.087 in Tg diabetic vs 0.95 ± 0.084 in WT diabetic; Figure 5.7) that was at least equivalent to, or slightly greater than, those parameters in normal WT control mice. Interestingly, measurements of heart rate at the time of M-mode recording showed decreased rates in mice overexpressing mGCH1, even though no differences were detected between WT control and WT diabetic mice (Figure

5.8). Additionally, no differences were detected in heart rate across any of the groups during the assessment of diastolic function by tissue Doppler imaging (Figure 5.8)

The diabetic cardiomyopathy was also evident in isolated cells, where WT diabetic LV myocytes showed a prolonged time to reach 50% relaxation (0.037 ± 0.002 in WT vs 0.043 ± 0.002 in WT diabetic; Figure 5.9B), in line with a slower rate of decay in the Ca^{2+} transient, Tau1 (0.085 ± 0.002 in WT vs 0.096 ± 0.002 in WT diabetic; Figure 5.9C). Consistent with the results at 4 weeks, and as reported previously by Carnicer et al. (131), the presence of the mGCH1 transgene in healthy, non-diabetic mice, was able to accelerate Ca^{2+}-reuptake and hasten the relaxation time of LV myocytes (Tau1: 0.070 ± 0.003 in Tg vs 0.085 ± 0.002 in WT; t_{50}: 0.026 ± 0.001 in Tg vs 0.037 ± 0.002 in WT; Figure 5.9). Similar to *in vivo* measurements, mGCH1 overexpression in diabetes prevented the impairment in relaxation, improving calcium handling and relaxation time relative to both WT diabetic and WT control mice (Tau1: 0.072 ± 0.002 in Tg diabetic vs 0.096 ± 0.002 WT diabetic; t_{50}: 0.026 ± 0.001 in Tg diabetic vs 0.043 ± 0.002 in WT diabetic; Figure 5.9). In contrast to relaxation, WT diabetic myocytes did not show a decline in contractility, as evidenced by the extent of cell shortening and the amplitude of the Ca^{2+} transient (Figure 5.10). Despite a slight elevation in both mGCH1-Tg groups with these functional parameters, no significant differences were detected. (Figure 5.10).

Systolic Function: 4 weeks

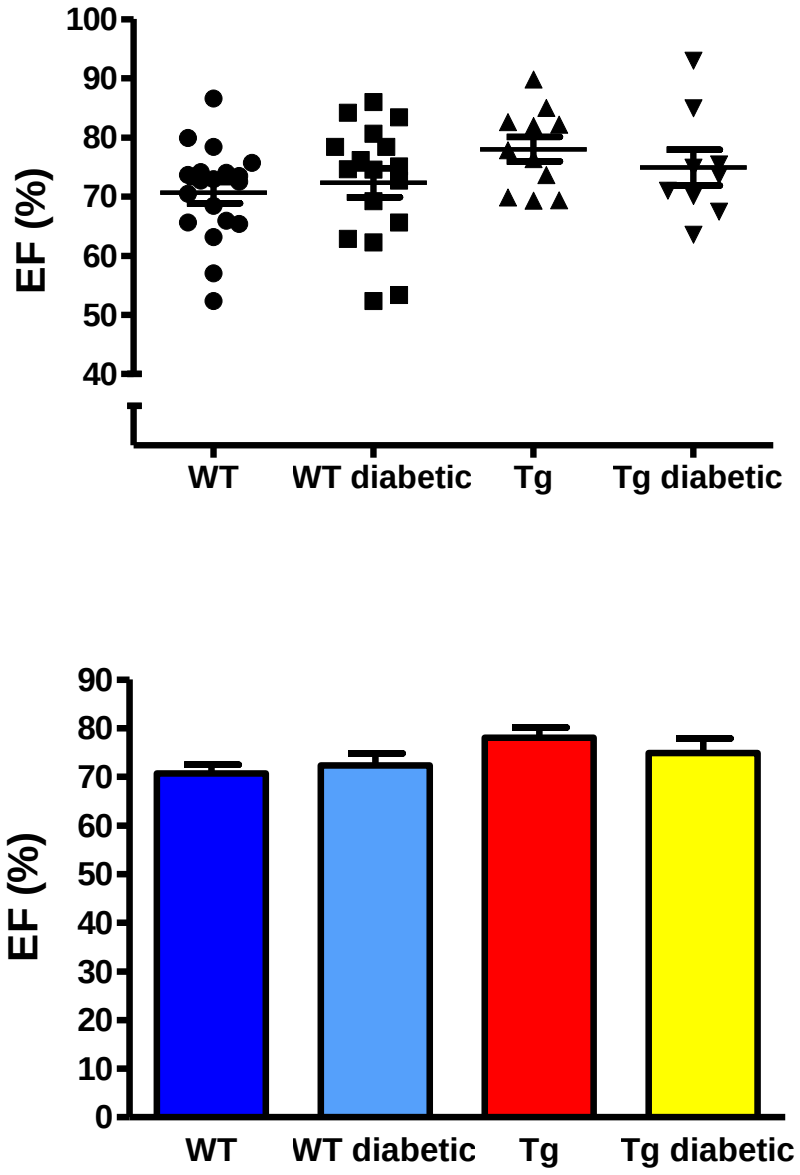


Figure 5.1. Systolic function remains normal after 4 weeks of diabetes.

From echocardiographic screening mice showed no evidence of impaired LV systolic function after short term diabetes (n = 9-19 mice).

Diastolic Function: 4 weeks

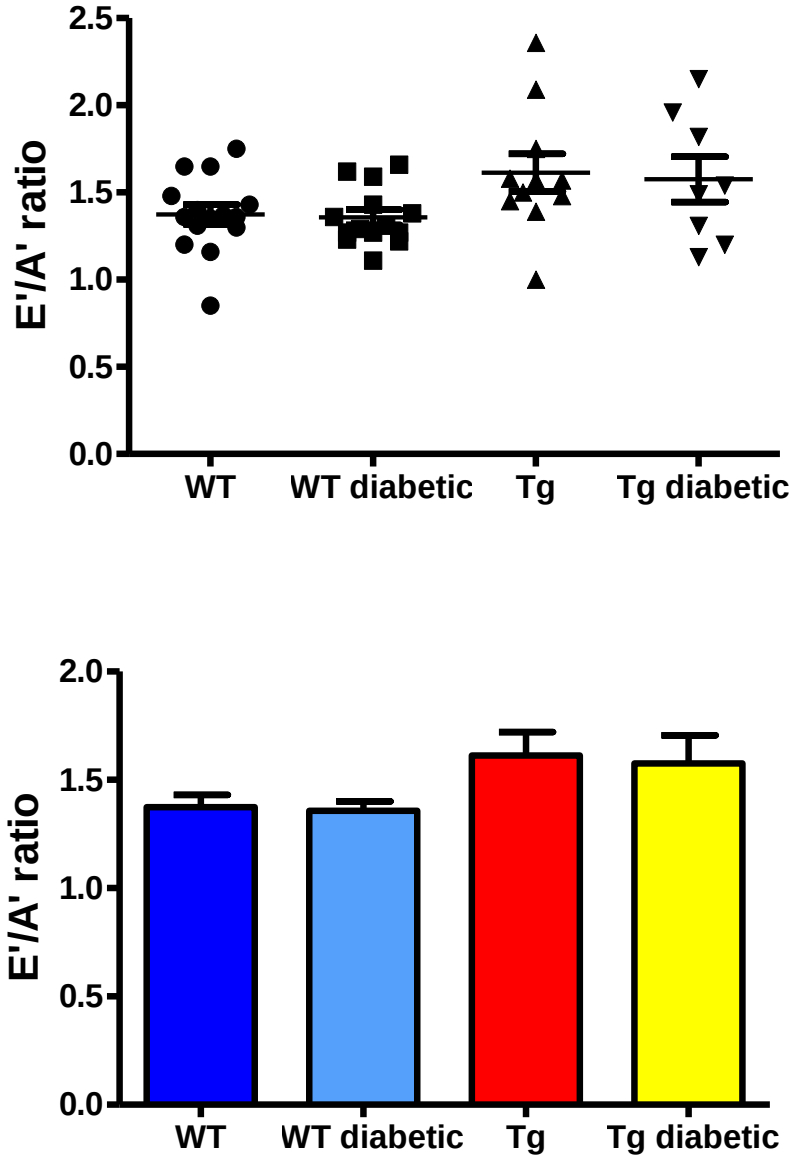


Figure 5.2. No defects in diastolic function are evident after 4 weeks of diabetes.

In vivo assessment detected no changes to LV diastolic performance in mice 4 weeks post-injection (n = 8-14 mice).

Cardiomyocyte Function: 4 weeks

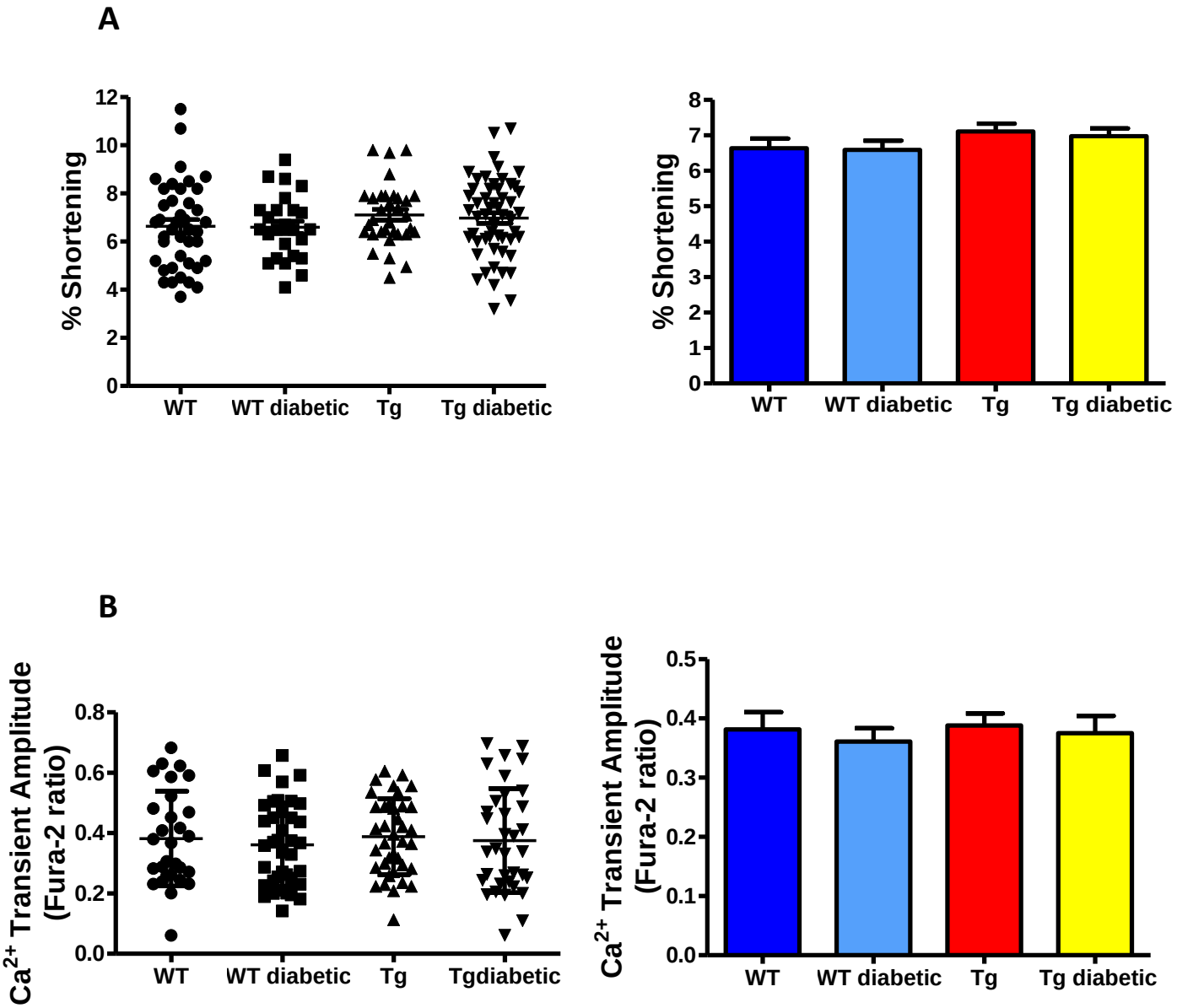


Figure 5.3. Cardiomyocyte contractility is not altered in short term diabetes.

(A) The degree of shortening in isolated cardiomyocytes showed no differences between groups. **(B)** Consistent with unaltered contractility, the Ca^{2+} transient amplitude released from the SR remained equivalent across experimental groups (n = 29-38 cells from 3 hearts per group).

Cardiomyocyte Function: 4 weeks

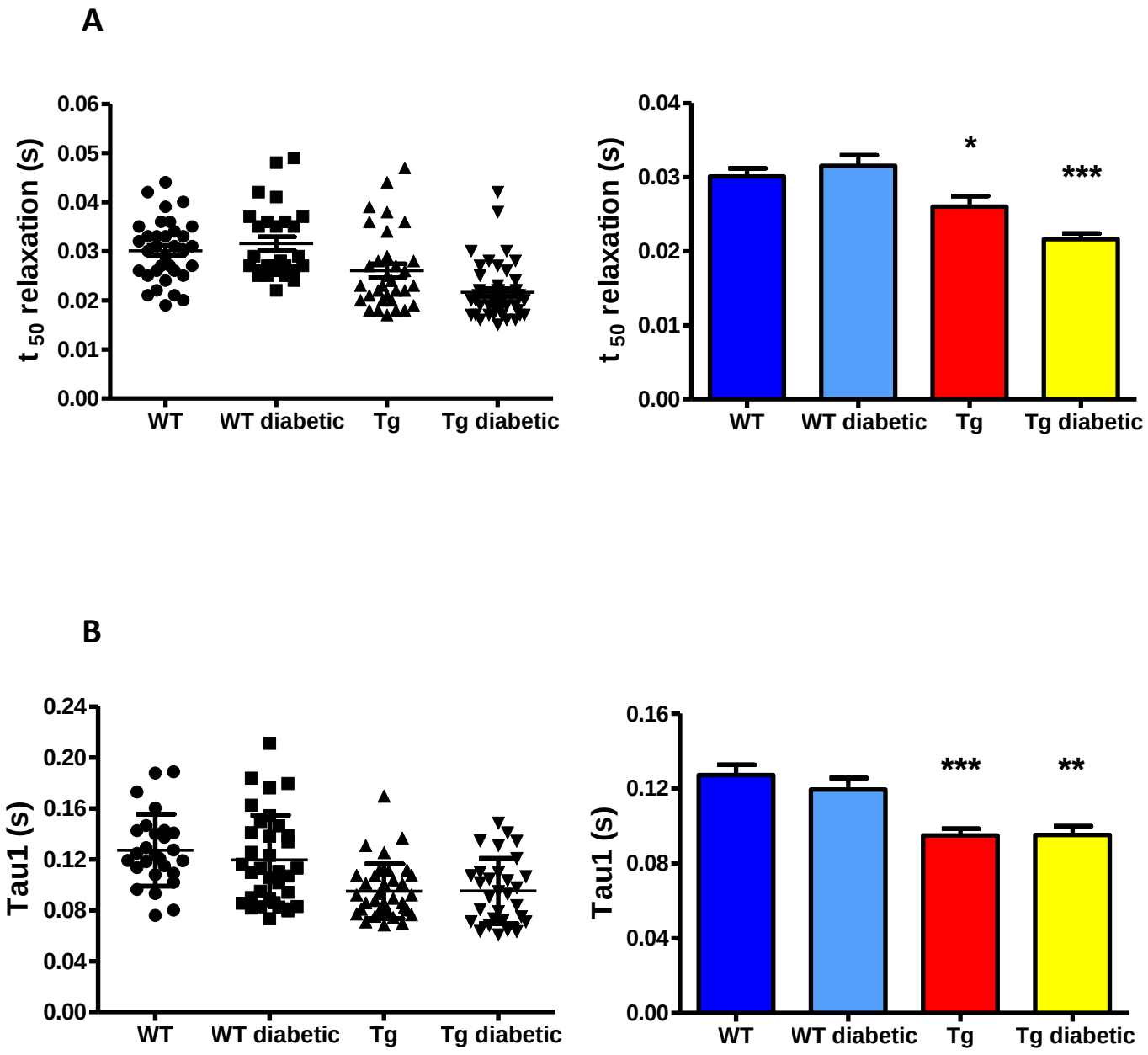


Figure 5.4. Cardiomyocyte relaxation remains normal after 4 weeks of diabetes.

(A) Myocytes from WT diabetic mice showed no prolongation in the time to reach 50% relaxation, yet relaxation time was accelerated in myocytes from mGCH1-Tg hearts, both in control and diabetic groups (2-way ANOVA; *P<0.05 vs WT; ***P<0.001 vs WT diabetic; P<0.05 for interaction between treatment and genotype). **(B)** The changes in relaxation time were mirrored by the rate of decay of the Ca^{2+} transient, which was faster in mGCH1-Tg cardiomyocytes. (2-way ANOVA; ***P<0.01 vs WT; **P<0.01 vs WT diabetic; n = 29-38 cells from 3 hearts per group).

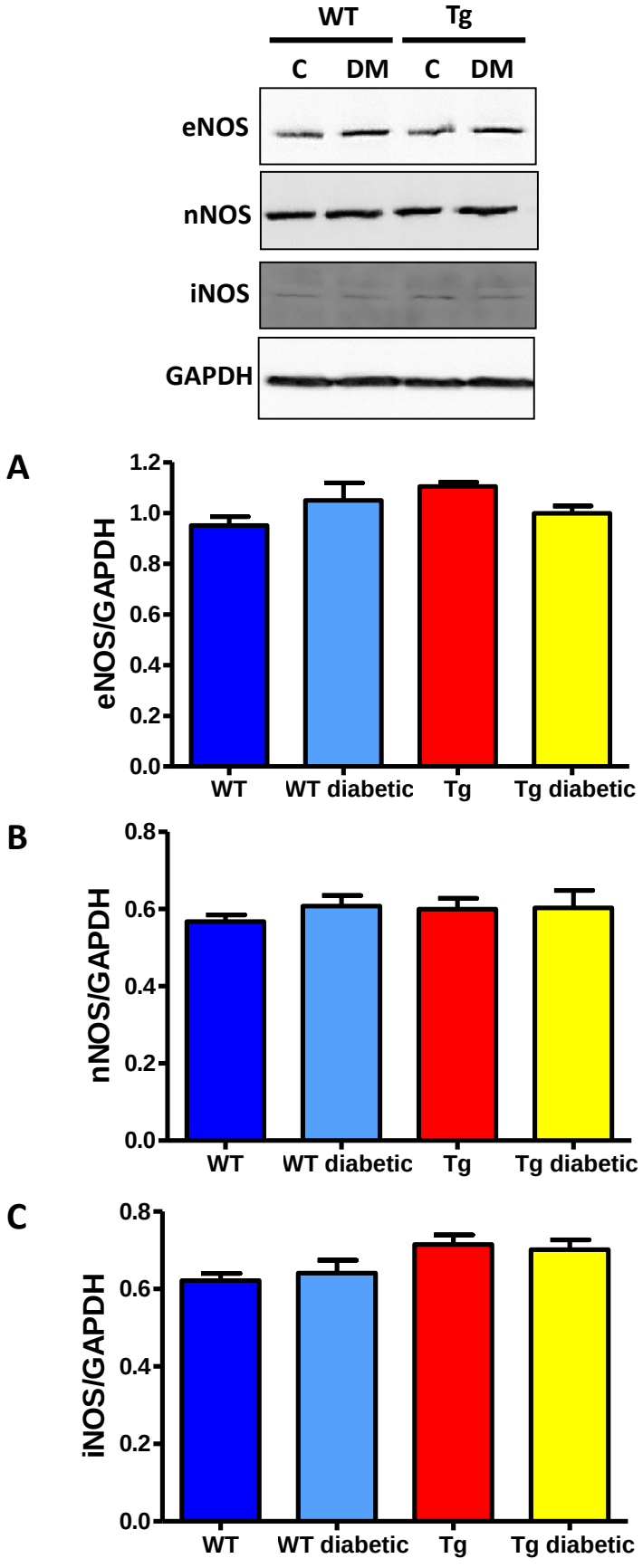


Figure 5.5. Myocardial NOS expression is unchanged in the early stages of T1D.

Immunoblots in LV homogenates after 4 weeks of diabetes demonstrated that there were no differences between groups in the expression of **(A)** eNOS, **(B)** nNOS or **(C)** iNOS isoforms (n = 4-6).

Systolic Function: 12 weeks

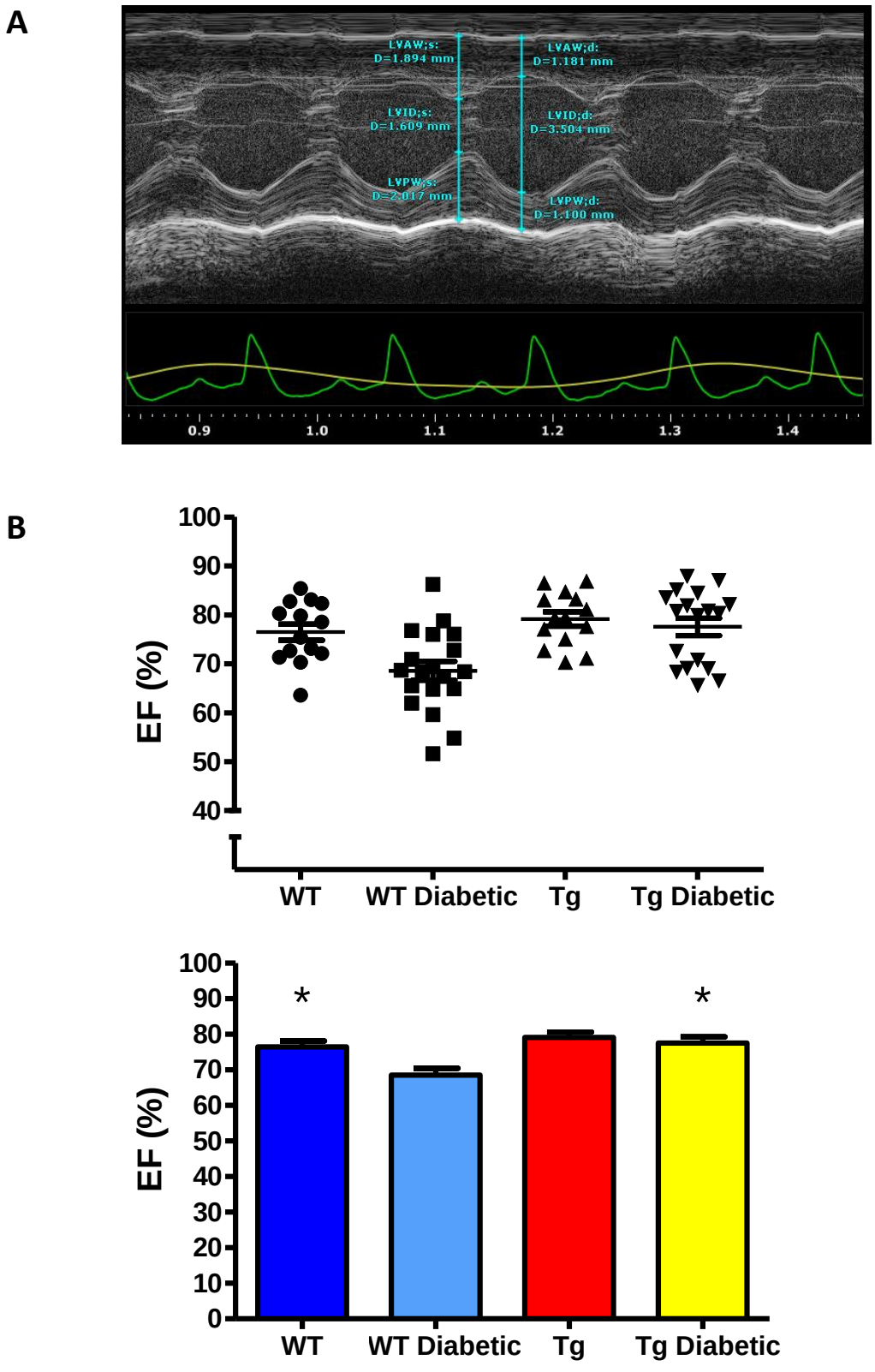


Figure 5.6. mGCH1-Tg mice are equally protected against systolic impairment after 12 weeks of diabetes.

(A) Representative M-mode image of LV wall motion over several cardiac cycles. Internal wall diameters during systole and diastole are used to calculate fractional shortening and EF. **(B)** WT diabetic mice exhibited a reduced EF, which was prevented by mGCH1 overexpression. (2-way ANOVA; *P<0.05 vs WT diabetic; n = 14-19 mice).

Diastolic Function: 12 weeks

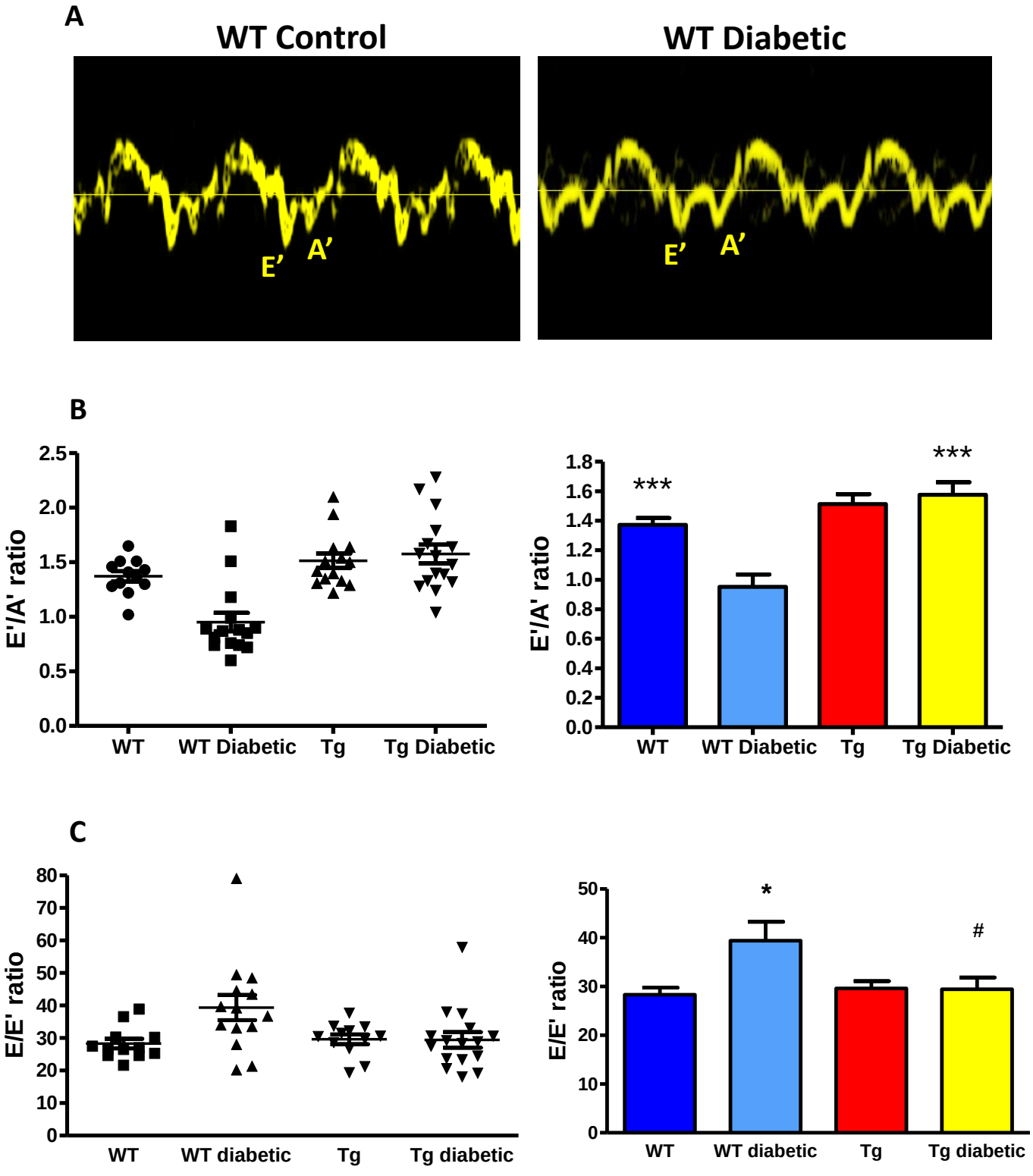


Figure 5.7. mGCH1 overexpression protects against the LV diastolic dysfunction in long term diabetes.

(A) Representative tissue Doppler imaging trace illustrating peaks of early and late atrial filling in WT control and WT diabetic mice. **(B)** E'/A' ratio was significantly diminished in WT diabetic mice, but was prevented in mice overexpressing the mGCH1 transgene. (2-way ANOVA; ***P<0.001 vs WT diabetic; P<0.01 for interaction between treatment and genotype). **(C)** The clinical marker of E/E' was elevated in WT diabetic mice, but normalised in mGCH1-Tg mice (2-Way ANOVA, *P<0.05 vs WT; #P<0.05 vs WT diabetic; n = 8-14 mice).

Echocardiography at 12 weeks: heart rate

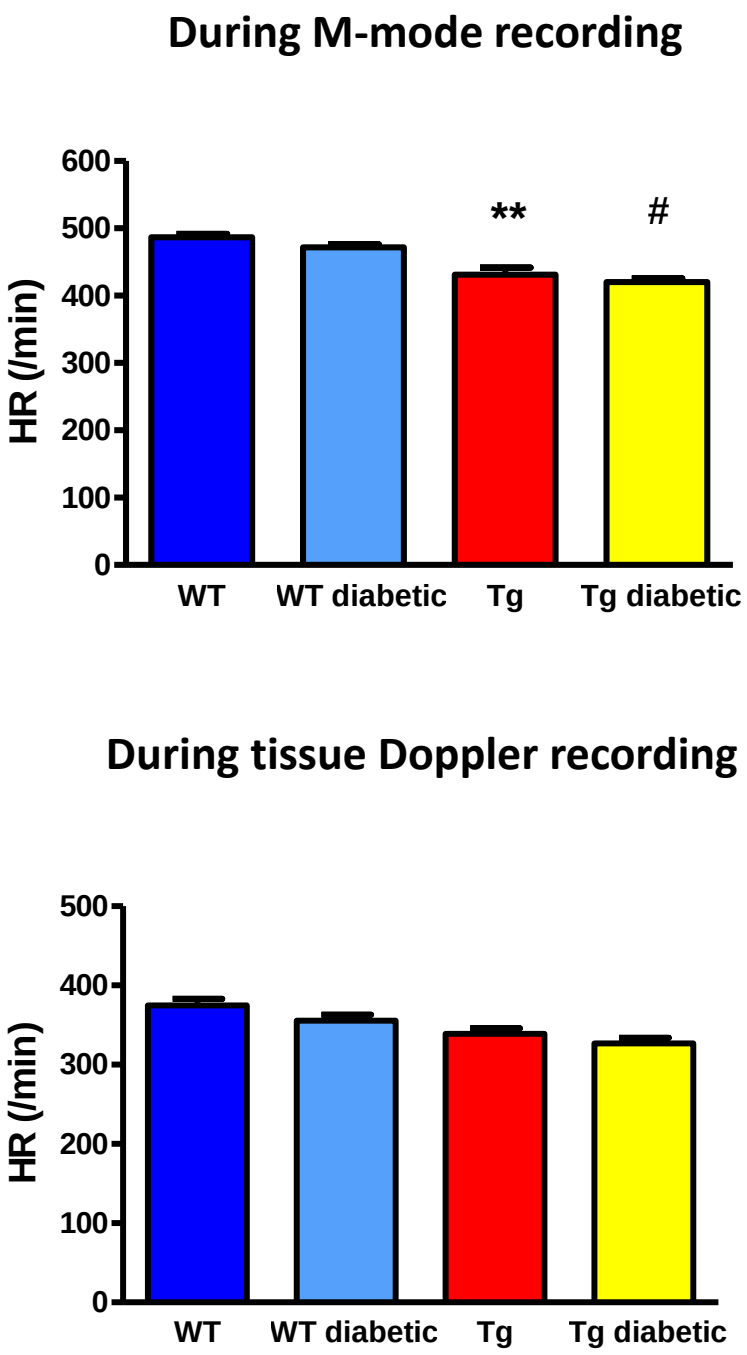


Figure 5.8. Heart rate is slower in mGCH1-Tg mice during the assessment of systolic function.

During *in vivo* assessment of cardiac function, heart rate was significantly lower in control and diabetic mice overexpressing mGCH1 at the time of M-mode recording (upper panel). However, heart rate was not different across experimental groups during tissue Doppler recording for the assessment of diastolic function (lower panel). (2-way ANOVA; **P<0.01 vs WT; # P<0.01 vs WT diabetic; n = 15-20 mice).

Cardiomyocyte Function: 12 weeks

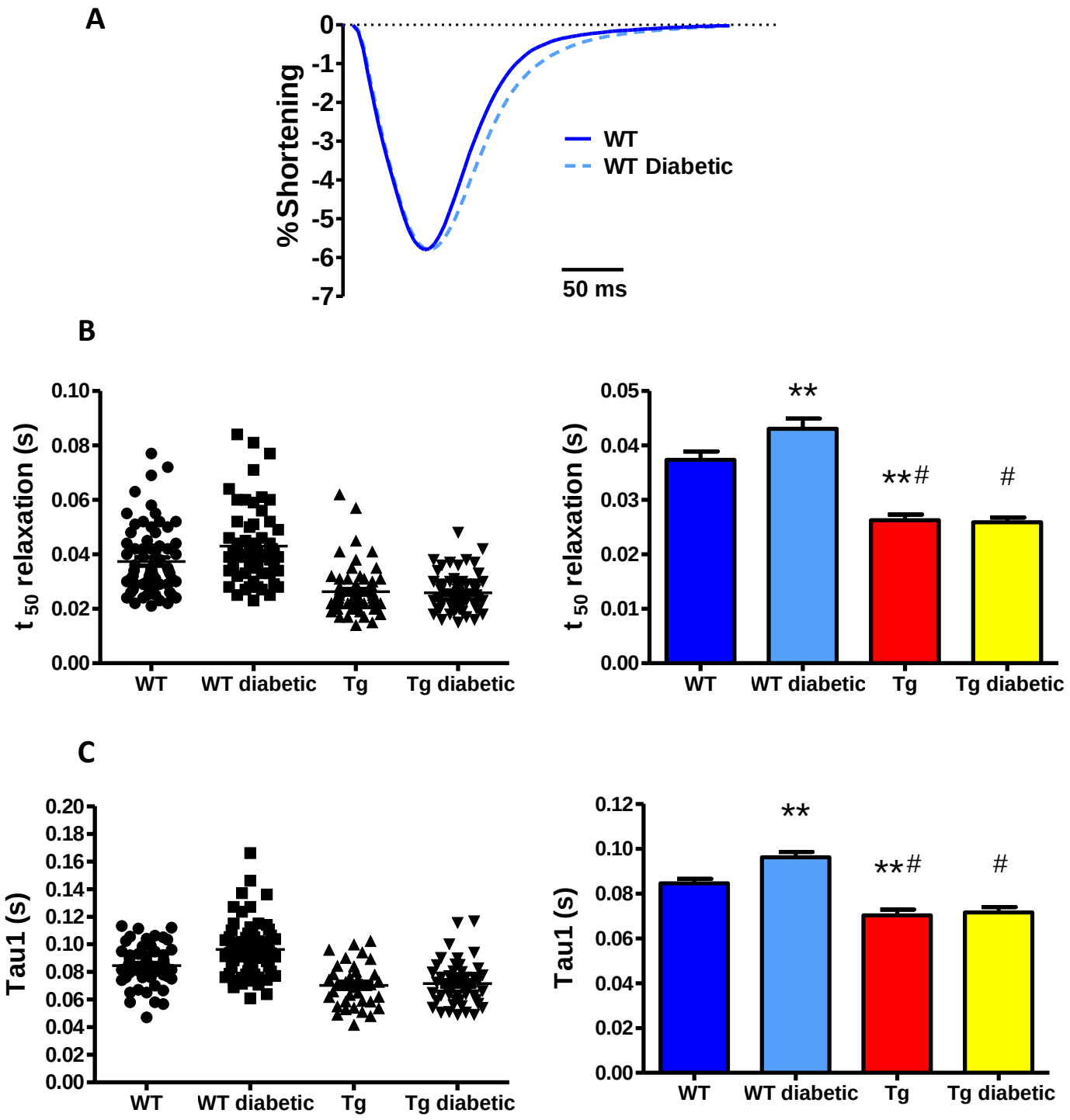


Figure 5.9. 12 week diabetic cardiomyopathy is also evident at the cardiomyocyte level.

(A) Representative schematic of relaxation dynamics in WT control and WT diabetic myocytes following contractile shortening. **(B)** Myocytes from WT diabetic mice showed prolongation in the time to reach 50% relaxation. Relaxation time was accelerated in myocytes from mGCH1-Tg hearts, not only preventing the dysfunction in diabetes, but also improving relaxation relative to WT control. **(C)** The same changes in relaxation time were also mirrored by the rate of Ca^{2+} transient decay, which was prolonged in WT diabetes, but hastened in mGCH1-Tg cardiomyocytes. (2-way ANOVA; **P<0.01 vs WT; # P<0.01 vs WT diabetic; P<0.05 for interaction between treatment and genotype; n = 57-73 cells from 5 hearts per group).

Cardiomyocyte Function: 12 weeks

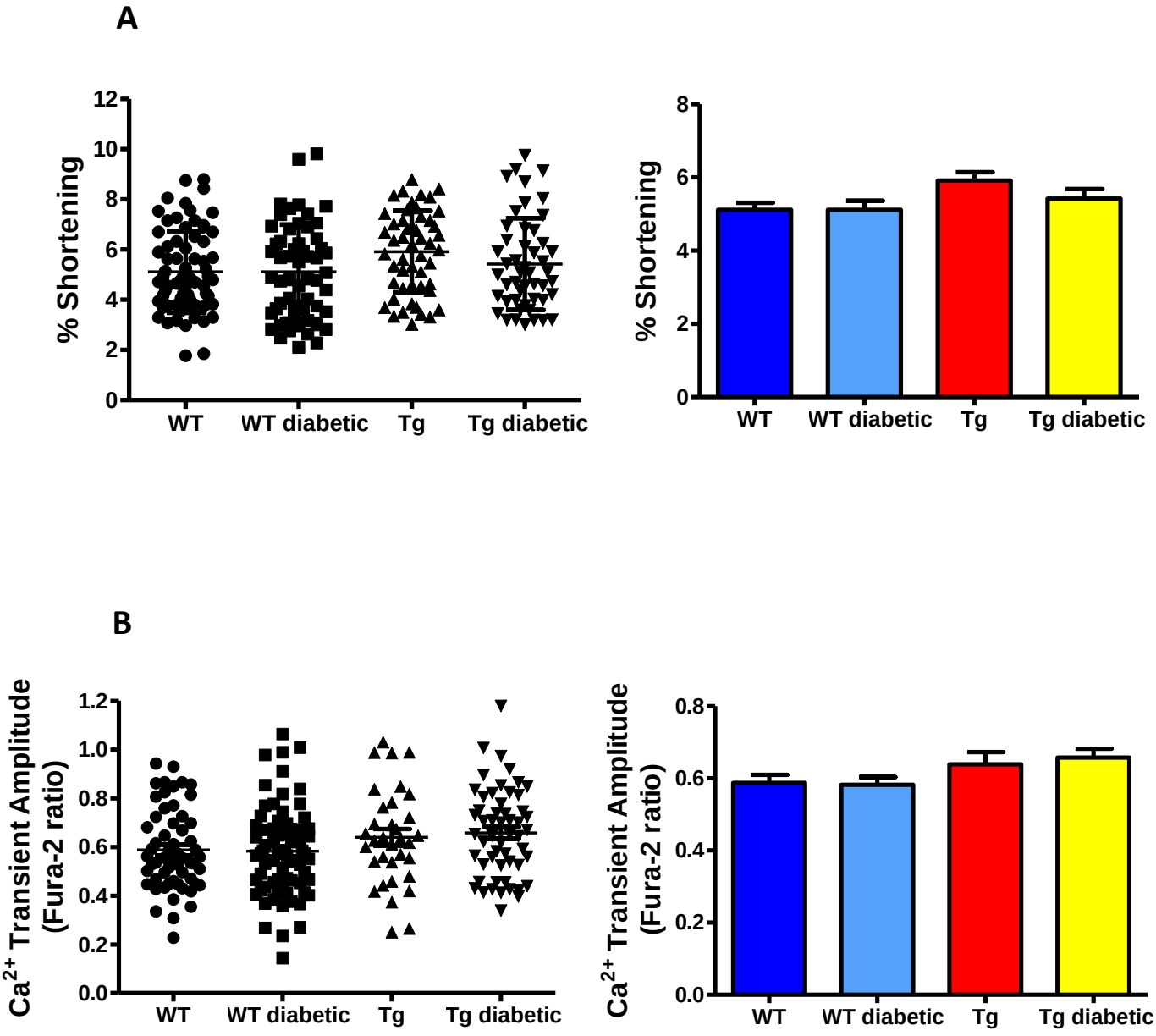


Figure 5.10. Cardiomyocytes from 12 weeks diabetic mice do not exhibit impaired contractility.

(A) The extent of shortening in isolated cardiomyocytes showed no differences between groups. **(B)** Consistent with unaltered contractility, the amplitude of the Ca^{2+} transient released from the SR remained equivalent across experimental groups. (n = 57-73 cells from 5 hearts per group).

Increased ROS production not underlie the LV dysfunction in diabetes

As with the aorta, the same markers of oxidative stress were determined in LV homogenates. However, unlike the vasculature, WT diabetic mice demonstrated no increase in LV O_2^- production compared to control mice, both with chemiluminescence and HPLC detection, either after D-NAME or L-NAME treatment (Figure 5.11). In addition, mGCH1 overexpression resulted in no significant changes to O_2^- levels in either treatment group (Figure 5.11). In line with these findings, WT diabetic hearts showed no decrease in BH4 levels or the ratio of BH4 to its oxidised form BH2 (Figure 5.12A). Similarly, the ratio was not different in the hearts of transgenic mice in either the diabetic or non-diabetic state, even though mGCH1 overexpression predictably resulted in a significant elevation in the absolute levels of BH4 present in the LV (397 ± 26.2 in Tg diabetic vs 3.74 ± 0.44 in WT diabetic; Figure 5.12B). As with the findings in early diabetes, NOS protein expression in the myocardium similarly remained unchanged between groups (Figure 5.13). Despite this, mGCH1 overexpression resulted in increased NOS activity in both control and diabetic hearts (1.03 ± 0.14 in Tg vs 0.46 ± 0.11 in WT; Figure 5.14A), consistent with the increase in biopterin levels in transgenic mice reported here and previously (131). In agreement with the measurements of BH4 bioavailability and ROS production, no changes in NOS activity were present between WT control and WT diabetic mice (Figure 5.14A). Glutathione status, another indicator of oxidative stress, also remained unchanged with diabetes in WT mice, as demonstrated by similar levels of both total glutathione, as well as the ratio of GSH to GSSG (Figure 5.14B). Interestingly, the overall levels of total glutathione were significantly higher in mGCH1-Tg hearts compared to WT. This was due to a specific increase in the reduced form (71.22 ± 7.25 in Tg vs 39.04 ± 5.36 in WT; Figure 5.14B), thereby improving the GSH:GSSG ratio. Together these findings demonstrate that T1D is not accompanied by oxidative stress and NOS uncoupling in the LV, and that the massively elevated biopterin levels with mGCH1 overexpression is able to enhance cardiac NOS activity and increase glutathione levels.

LV 12 weeks: O_2^- production

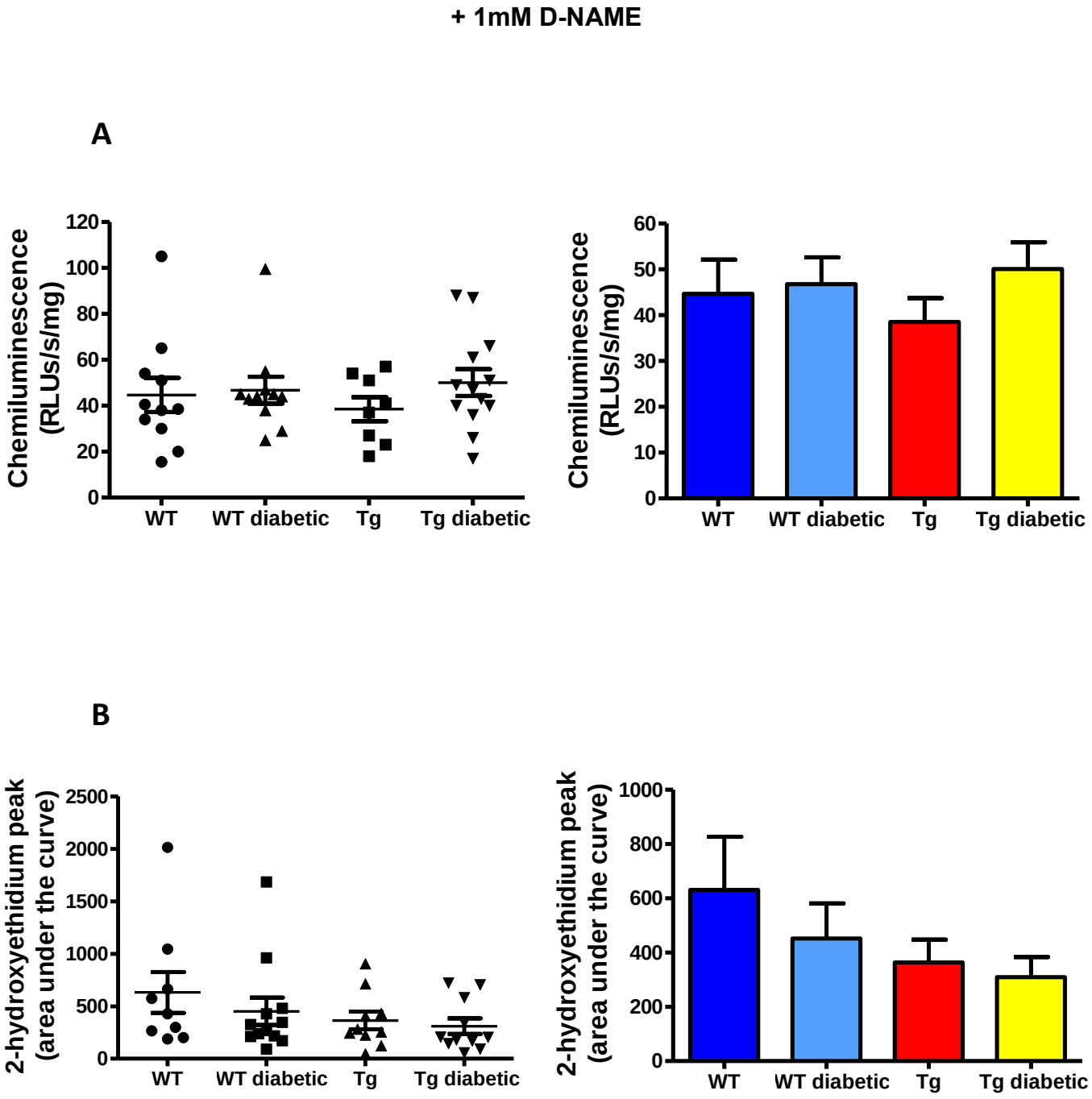


Figure 5.11. Diabetic hearts do not exhibit increased production of ROS.

(A) Chemiluminescence detection of O_2^- generation in LV homogenates demonstrated no oxidative stress after 12 weeks of diabetes (n = 8-12). **(B)** 2-hydroxyethidium peak detection by HPLC illustrated a non-significant trend towards decreased O_2^- production in diabetes and mGCH1-Tg hearts (n = 9-12). In both instances, samples were incubated in 1mM D-NAME; results are expressed as the tiron-inhibitable fraction.

LV 12 weeks: biopterin levels

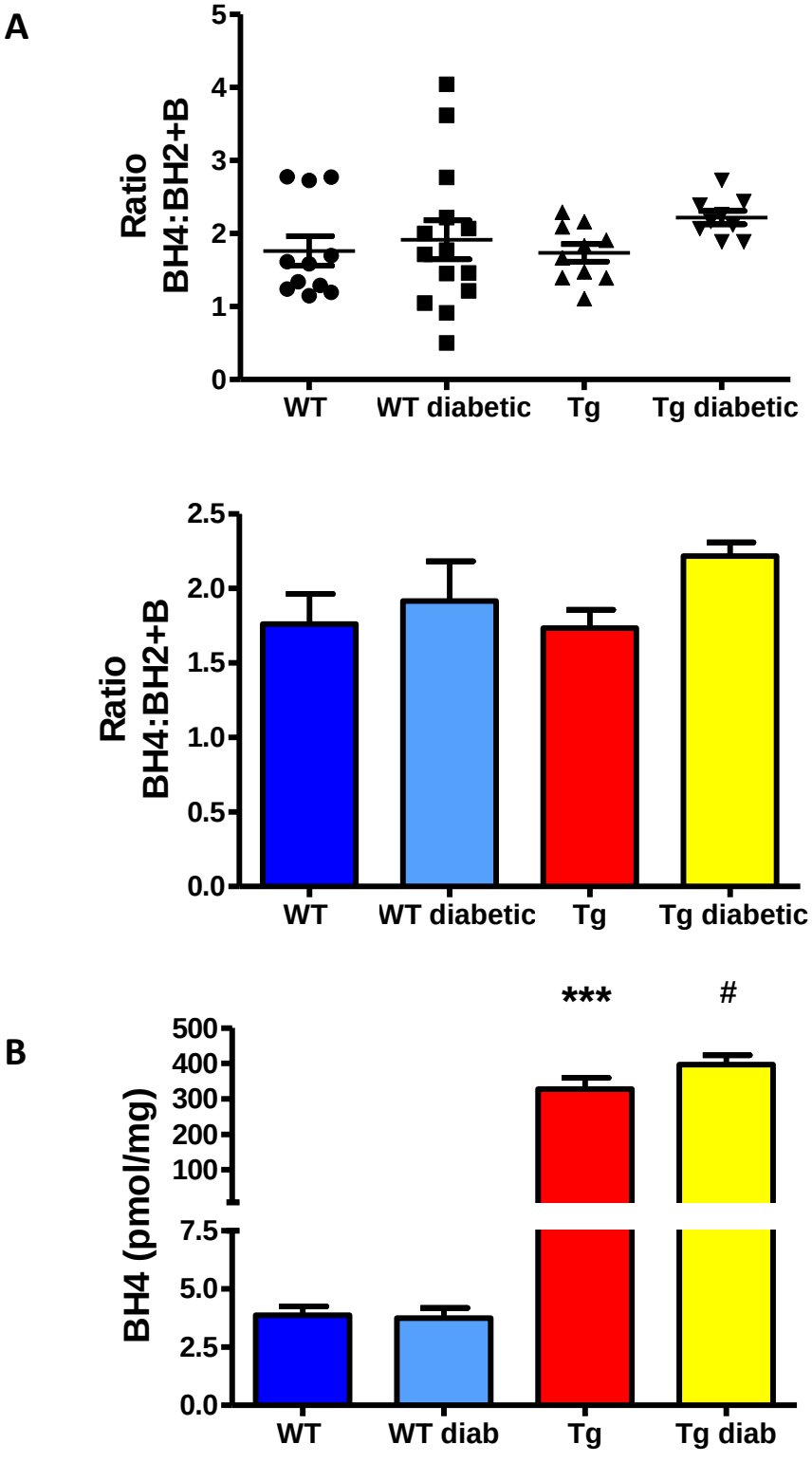


Figure 5.12. Diabetes does not result in reduced BH4 bioavailability.

(A) WT diabetic mice demonstrated no reduction in the ratio of reduced BH4 to the oxidised form BH2 in LV homogenates. **(B)** Despite unchanged BH4:BH2 ratios, mGCH1 overexpression caused a significant elevation in the absolute levels of BH4 in the myocardium of both control and diabetic mice (2-way ANOVA; ***P<0.001 vs WT; # P<0.001 vs WT diabetic; n = 8-12).

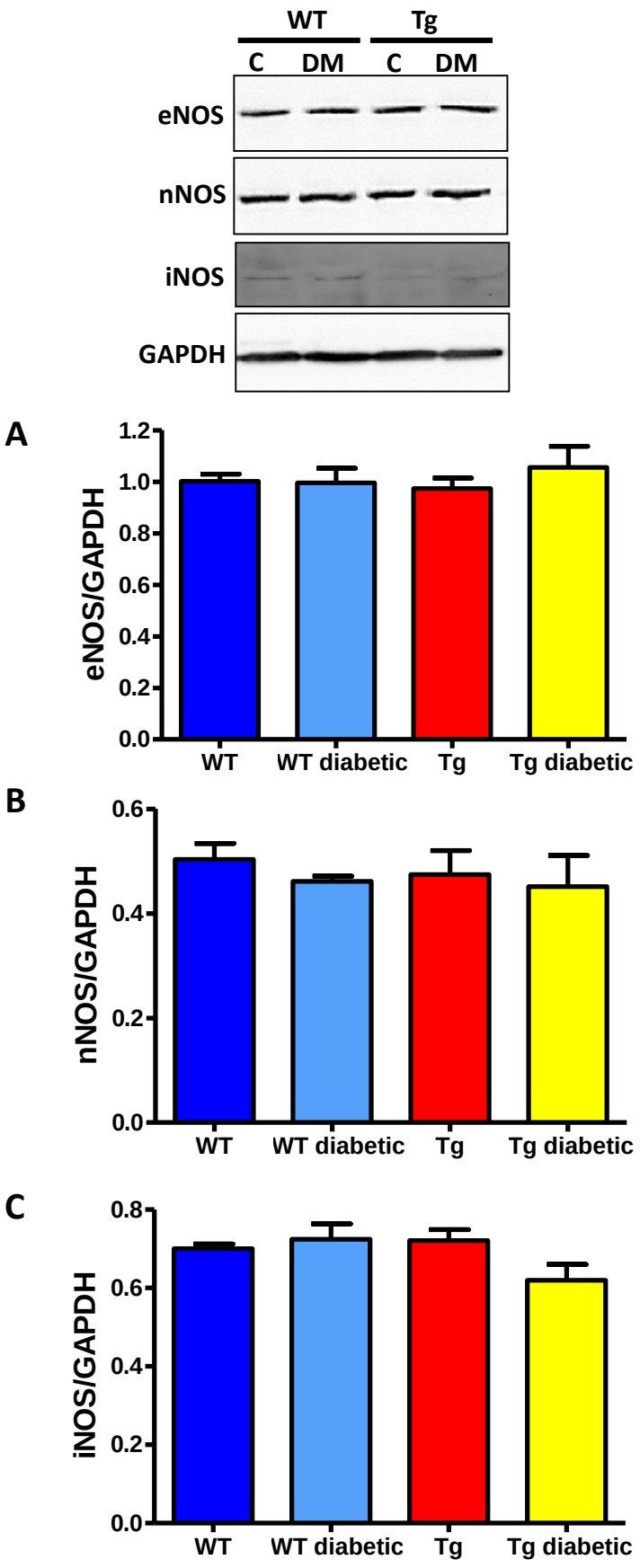


Figure 5.13. Myocardial NOS expression still remains unaltered in the later stages of T1D.

NOS immunoblots were repeated in LV homogenates after 12 weeks of diabetes. NO differences between groups were detected in the expression of **(A)** eNOS, **(B)** nNOS and **(C)** iNOS (n = 3-5).

LV 12 weeks: NOS activity, glutathione status

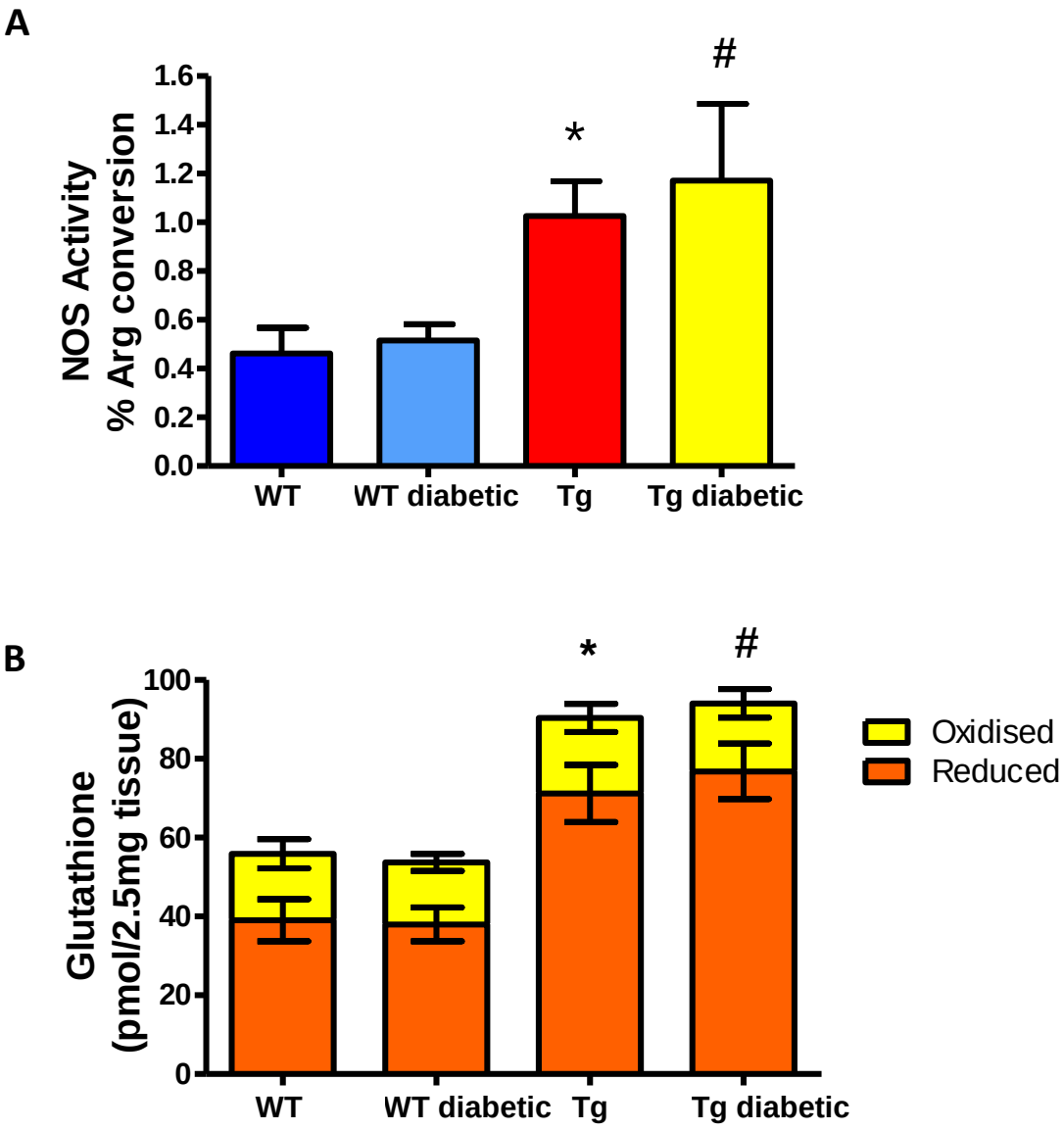


Figure 5.14. NOS activity and glutathione status is enhanced in hearts overexpressing mGCH1.

(A) mGCH1 overexpression resulted in significantly elevated myocardial NOS activity, both in control and diabetic mice. (2-way ANOVA; *P<0.05 vs WT; # P<0.05 vs WT diabetic; n = 4-5. **(B)** mGCH1-Tg hearts additionally showed increased levels of reduced glutathione, improving the GSH:GSSG ratio. (2-way ANOVA; *P<0.05 vs WT; # P<0.05 vs WT diabetic; n = 10).

EC-coupling protein expression and myofilament mechanics

Previous studies in the diabetic mouse have attributed cardiac dysfunction to disrupted EC-coupling, specifically associated with changes to the expression of proteins involved in regulating Ca^{2+} handling (172, 354, 386, 388, 398). After 12 weeks of diabetes, LV homogenates showed no alteration in the expression of SERCA, either in WT or mGCH1-Tg mice (Figure 5.15). Since phospholamban phosphorylation at serine^{16} (by cAMP-dependent PKA) and threonine^{17} (by CaMKII) regulates Ca^{2+} sequestration through SERCA, the phosphorylation status of PLB was determined relative to the total levels present. For both PLB-Ser^{16} and PLB-Thr^{17}, diabetes had no observed effect on protein expression, while mGCH1 overexpression caused a slight, but non-significant increase in non-diabetic mice (Figures 5.16 and 5.17). In addition to the SR calcium reuptake, reductions in NCX expression have also been reported in the diabetic heart (356, 398). However, in LV homogenates from 12 week diabetic mice, no apparent changes in NCX expression were detected. Both diabetic groups actually showed a small increase in protein levels, but these changes were not significant (Figure 5.18). Together these data suggest that impaired calcium handling, as a result of altered EC-coupling protein expression, is not a primary factor underlying the LV dysfunction in the WT diabetic mouse.

As well as the machinery involved in calcium handling, changes to LV relaxation can be influenced by the dynamics of the active myofilaments during the contractile cycle. Measurements of force-Ca^{2+} sensitivity in demembranated trabeculae revealed that diabetic mice exhibited no significant shift in myofilament Ca^{2+}-sensitivity compared to control mice (Figure 5.19A). Interestingly, mGCH1 overexpression in control mice resulted in a significant right shift in the force-Ca^{2+} curve, indicating a reduction in the Ca^{2+}-sensitivity of force development (1.28 ± 0.03 in Tg vs 1.17 ± 0.03 in WT; Figure 5.19A). However this effect was not consistent across treatments; in the presence of diabetes, the mGCH1 transgene produced the opposite effect on calcium sensitivity ($P<0.05$ for the interaction between genotype and treatment). Further evaluation of cardiac fibres demonstrated an increase in passive stiffness in hearts from WT diabetic mice, which was prevented in those hearts overexpressing

mGCH1 (56.65 ± 6.51 in WT diabetic vs 40.73 ± 3.90 in WT; Figure 5.19B). No differences across groups were observed in the active force generated by the myofilaments (Figure 5.19C), nor were there any alterations to the length and width of the fibres (Figure 5.20). These results indicate that increased stiffness of the myofilaments may contribute to the impaired LV relaxation in WT diabetic hearts, and that GCH1 overexpression may be protective in this regard, without a notably beneficial effect on Ca^{2+} responsiveness.

LV 12 weeks: SERCA protein expression

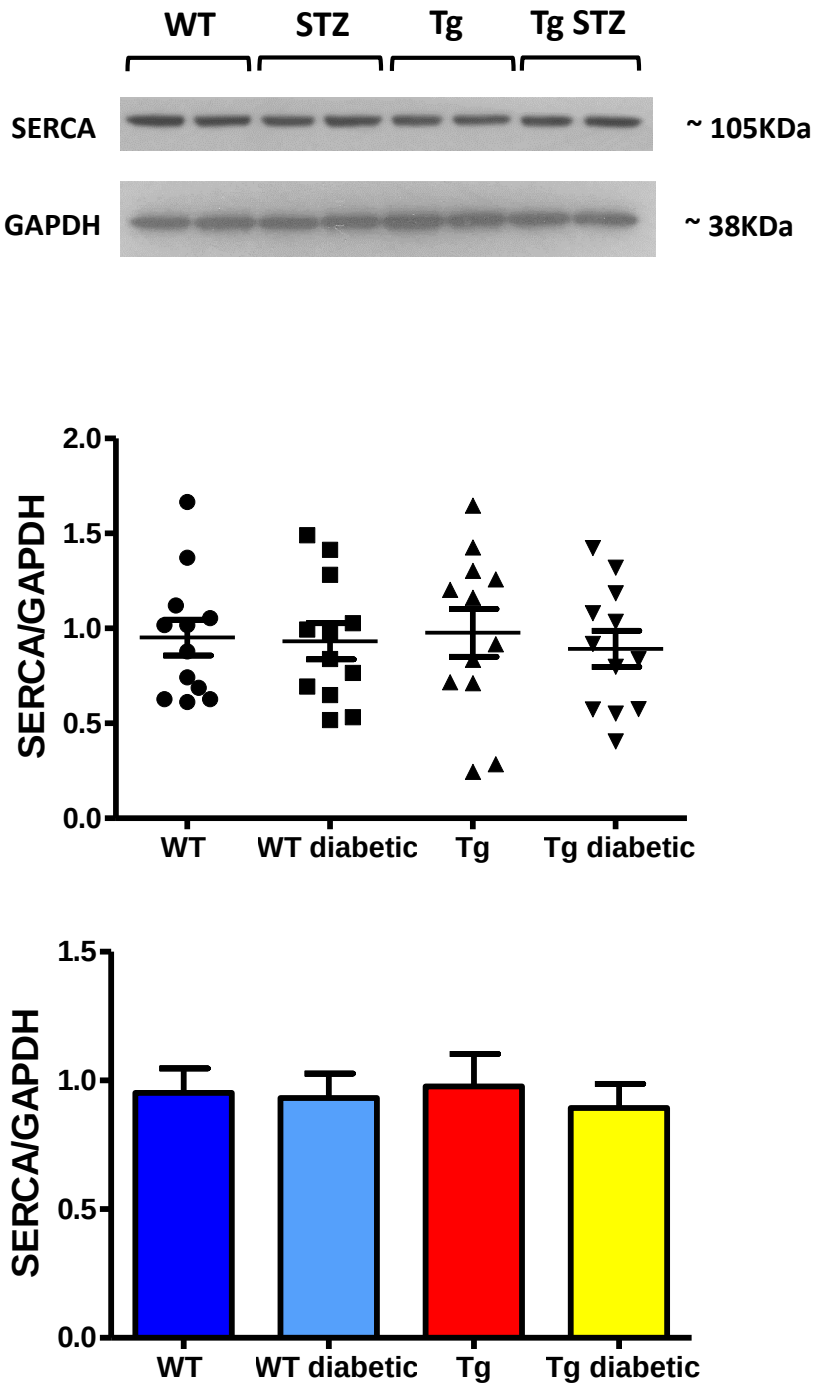


Figure 5.15. SERCA expression remains unchanged in diabetes.

Despite changes to relaxation and calcium handling, expression of SERCA protein was not different between experimental groups (n = 12).

LV 12 weeks: PLB-Ser^{16} protein expression

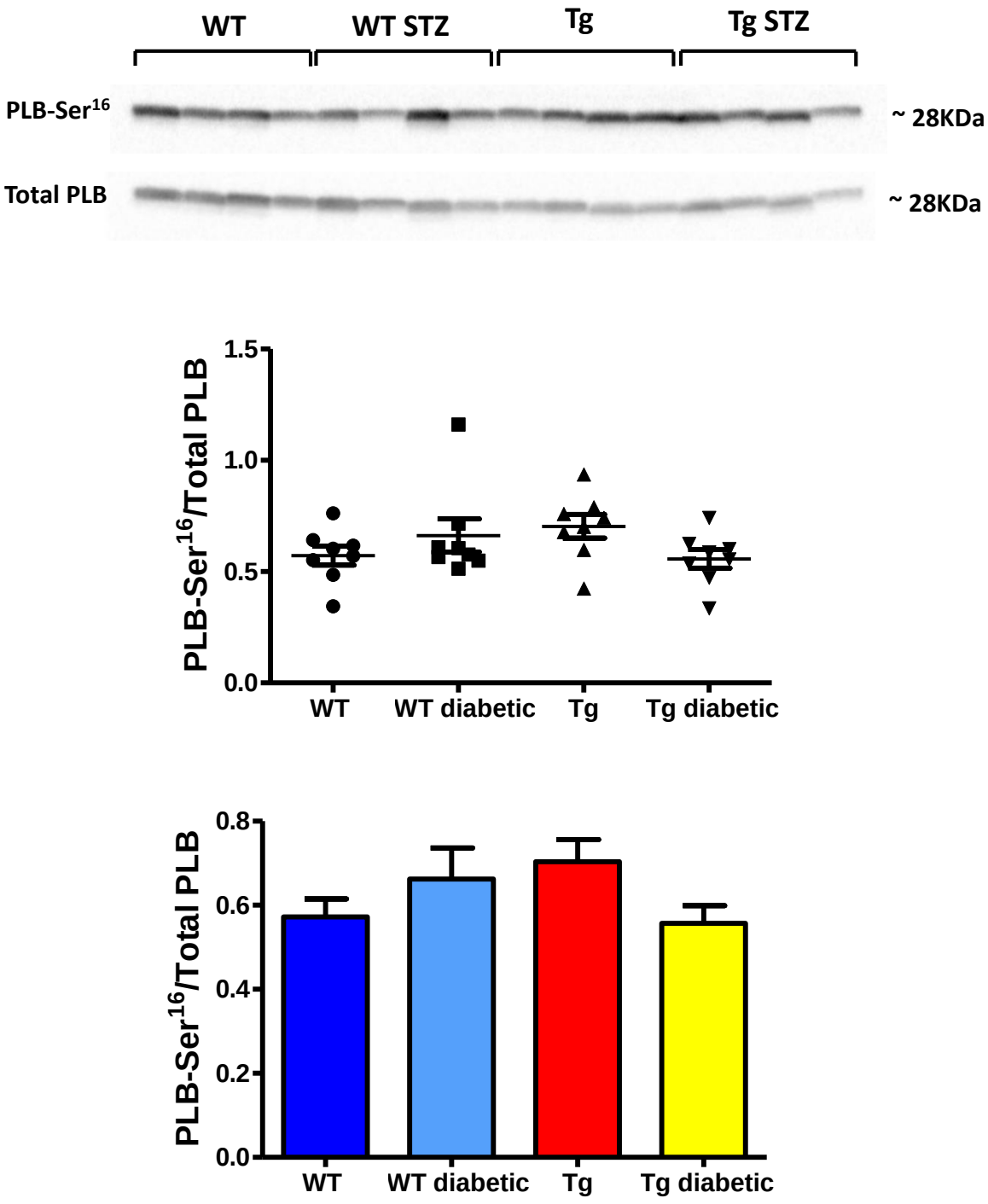


Figure 5.16. Diabetes does not alter the fraction of phosphorylated serine^{16} on PLB.

After 12 weeks of diabetes, no significant shift in the ratio of PLB-ser^{16}/total PLB protein expression was detected in LV homogenates between groups (n = 8).

LV 12 weeks: PLB-Thr^{17} protein expression

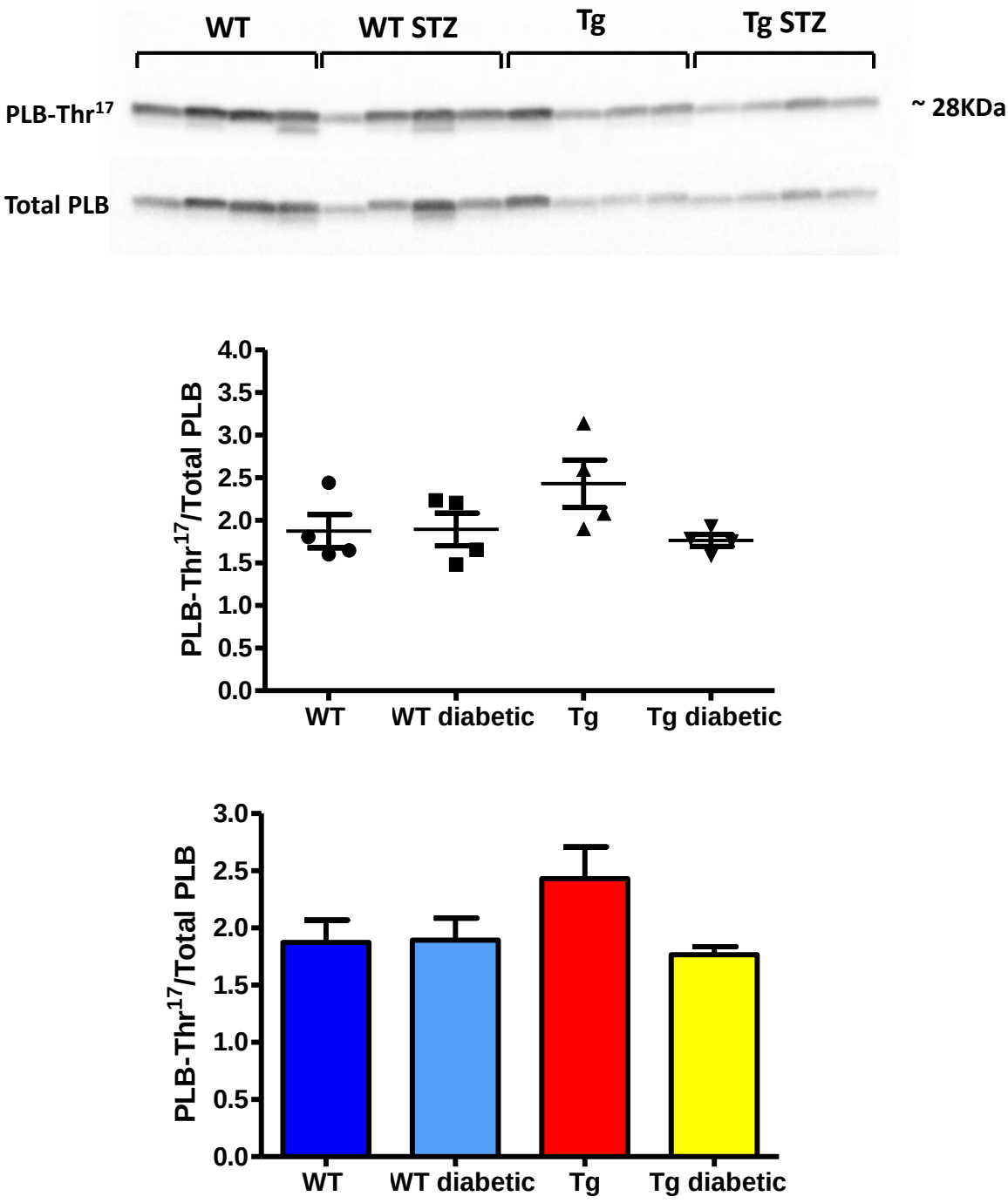


Figure 5.17. Phosphorylation status of PLB threonine^{17} is not reduced in diabetes.

While a small, non-significant increase in the ratio of PLB-thr^{17}/total PLB expression was observed in mGCH1-Tg control hearts, no changes were detected in either diabetic group (n = 4).

LV 12 weeks: NCX protein expression

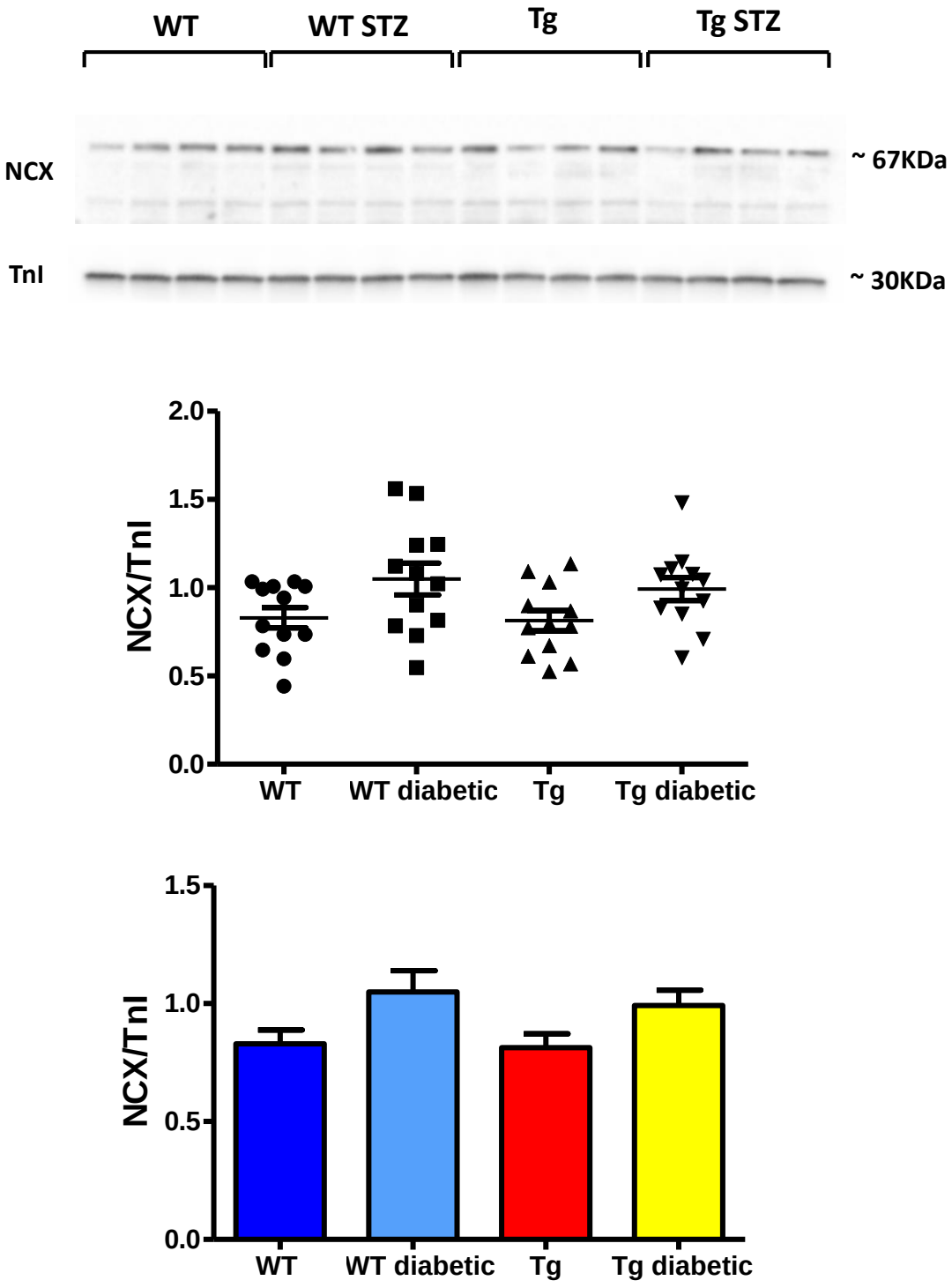


Figure 5.18. Levels of NCX expression remain unchanged in LV homogenates in long term diabetes.

After 12 weeks of hyperglycaemia, diabetic mice did not show significant alterations in the protein levels of the sodium-calcium exchanger (n = 12).

LV 12 weeks: myofilament mechanics

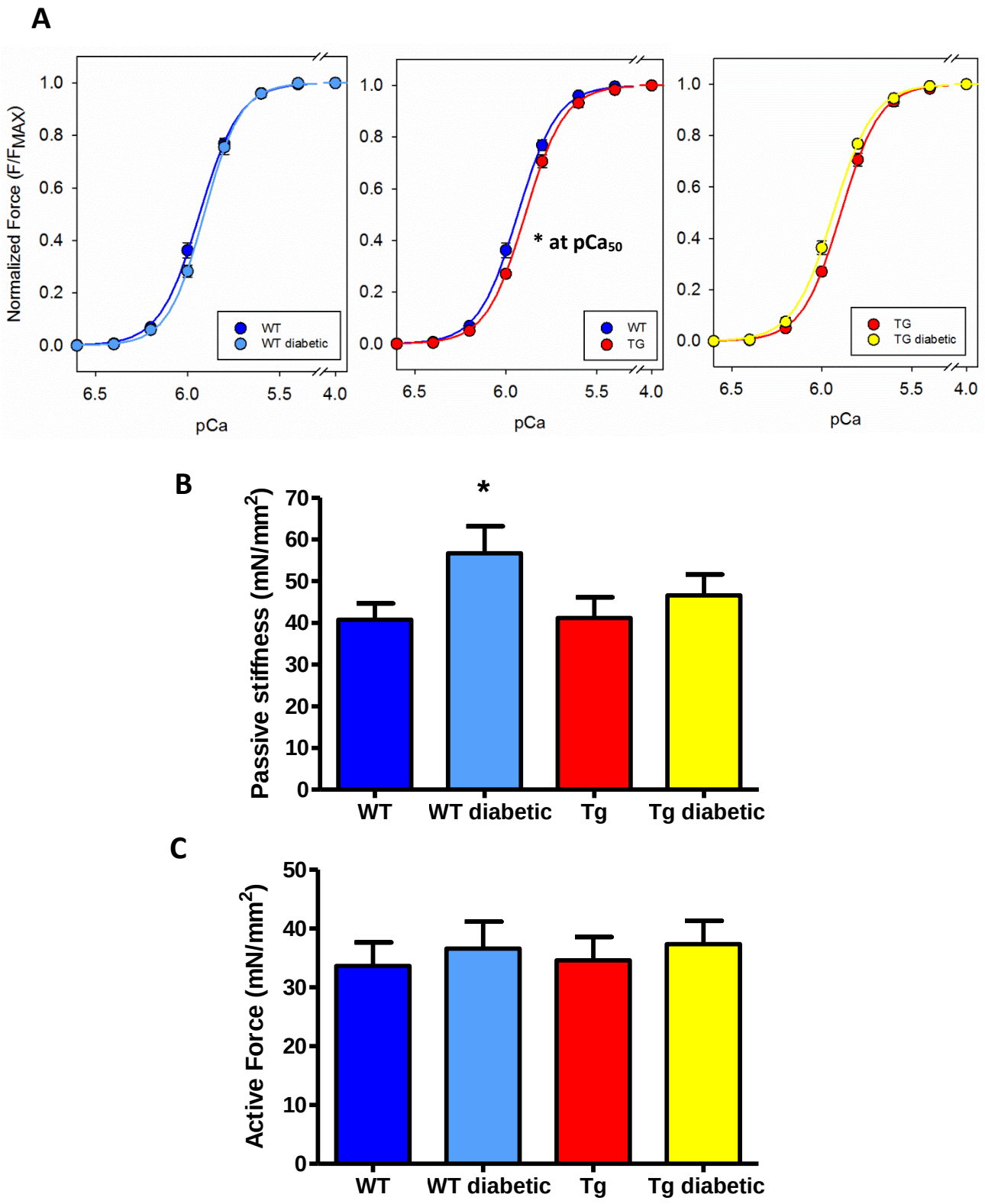


Figure 5.19. Myofilament mechanics in demembranated trabeculae.

(A) WT diabetic mice showed no changes to myofilament Ca^{2+} sensitivity in the development of force (left), whereas mGCH1 overexpression in control mice caused a desensitisation (middle), yet a sensitisation effect of the transgene in diabetes (right) (*P<0.05 at pCa_{50}; P<0.05 for interaction between treatment and genotype). **(B)** The relationship between force and sarcomere length demonstrated that WT diabetic mice had increased LV passive stiffness, which was prevented in mGCH1-Tg diabetic mice. **(C)** The generation of active force by LV fibres was not different between groups. (2-way ANOVA; *P<0.05 vs WT; n = 17-21 fibres from 4-5 hearts per group).

LV 12 weeks: myofilament dimensions

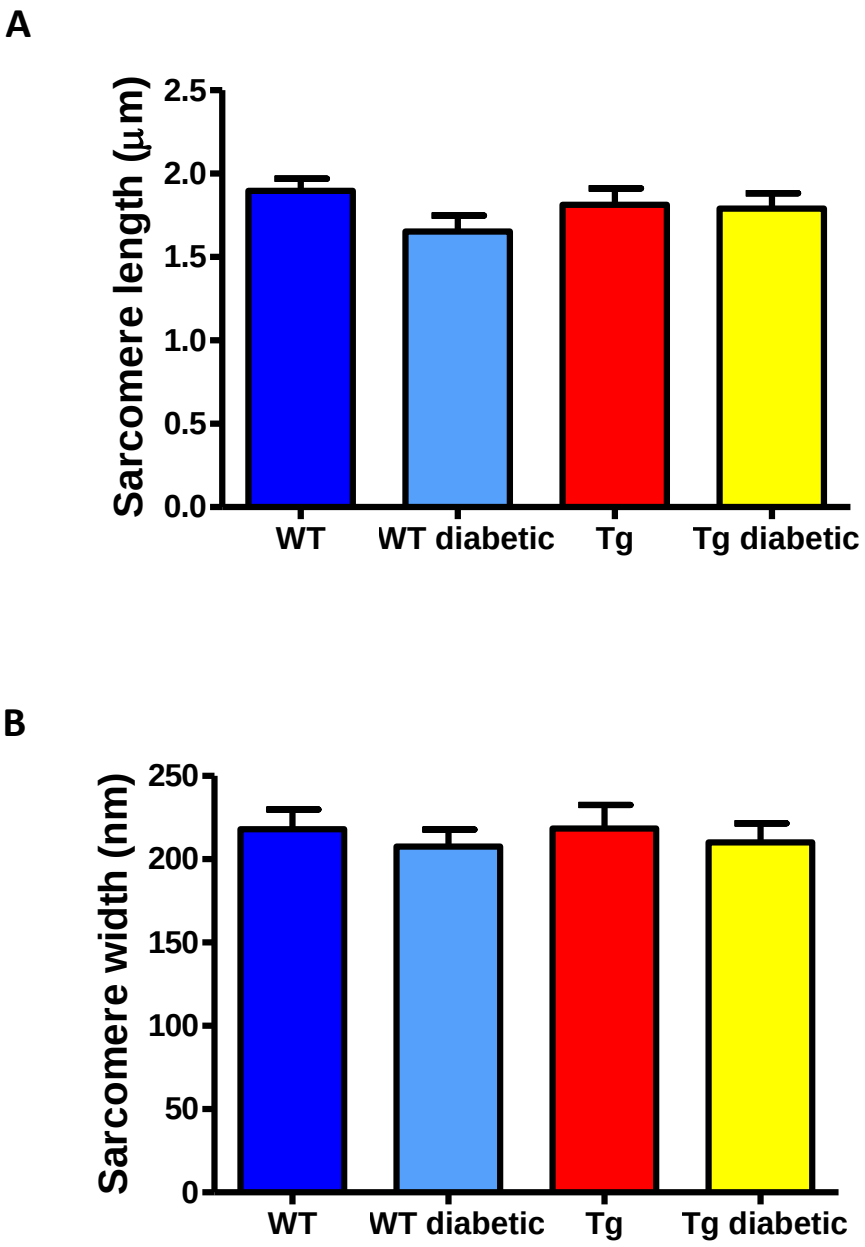


Figure 5.20. Myofilament dimensions in demembranated trabeculae.

Neither diabetic nor mGCH1-tg mice showed any differences in the **(A)** length or **(B)** width of sarcomeres isolated from LV demembranated trabeculae (n = 17-21 fibres from 4-5 hearts per group).

The role of fibrosis and markers of inflammation

To establish whether an underlying inflammatory process was a trigger in the development of diabetic cardiomyopathy, LVs were studied for the expression of inflammatory cytokines, as well as potential accompanying fibrosis. Analysis of collagen 1A1 gene expression in LV homogenates showed no differences between control and diabetic mice (Figure 5.21), however, an assay of hydroxyproline content in hydrolysed LV samples showed that both WT diabetic and mGCH1 diabetic mice had increased levels of total collagen compared to control mice, while the mere presence of the transgene had no effect (54.88 ± 7.87 in WT diabetic vs 28.77 ± 9.14 in WT; Figure 5.22).

Since AGE accumulation in diabetes has been associated with increased collagen cross-linking, LV homogenates were assessed for the expression of the receptor for AGEs, RAGE. Immunoblots using independent antibodies directed at both the N- and C-terminus of RAGE demonstrated no differences between any of the groups (Figure 5.23A). Another precipitator of fibrosis and tissue remodelling, inflammatory signalling, was explored with gene expression analysis. Compared to WT mice, diabetic mice showed no elevation in key mediators of the inflammatory response (Figure 5.23B). This included the inflammatory cytokine IL-1β, the macrophage chemokine MCP-1, as well as the metalloproteinases MMP-2 and MMP-9 involved in ECM remodelling.

Also associated with pro-inflammatory responses and tissue modification in the diabetic state is increased signalling from PKCβ. Moreover, in the vasculature, Paneni and colleagues have implicated PKCβII in tissue hyperglycaemic "memory", resulting in sustained ROS production due to epigenetic regulation through histone 3 acetylation (70). In LV homogenates, PKCβII protein expression was unchanged between groups (Figure 5.24). As a downstream target, the extent of acetylated histone 3, relative to total histone 3 levels, also reflected no apparent difference with diabetes (Figure 5.25), consistent with the absence of oxidative stress. Together these data illustrate that diabetic mice, irrespective of mGCH1 overexpression, have increased LV collagen deposition. However, evidence

suggests that any cardiac fibrosis is unlikely a downstream result of AGE-RAGE interactions or increased inflammatory signalling, inclusive of a role for PKCβ.

LV 12 weeks: collagen 1A1 gene expression

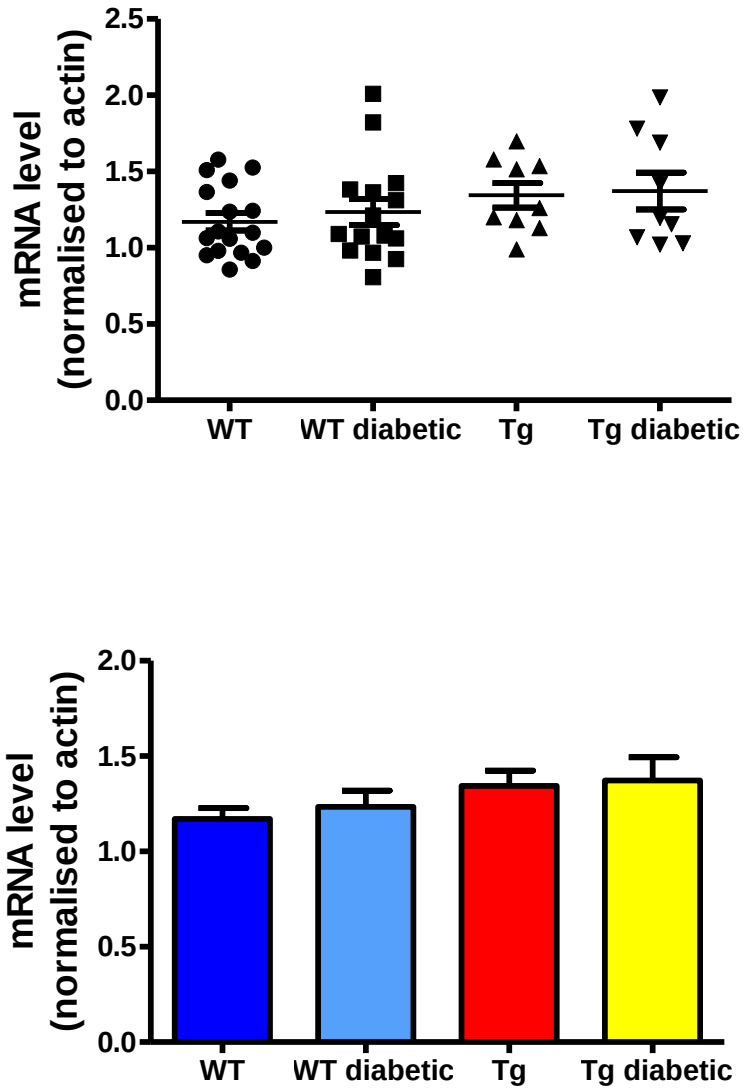


Figure 5.21. 12 weeks of diabetes is not associated with altered LV collagen 1A1 gene expression.

No differences in collagen 1A1 mRNA levels were detected in hearts between experimental groups (n = 9-17).

LV 12 weeks: collagen content

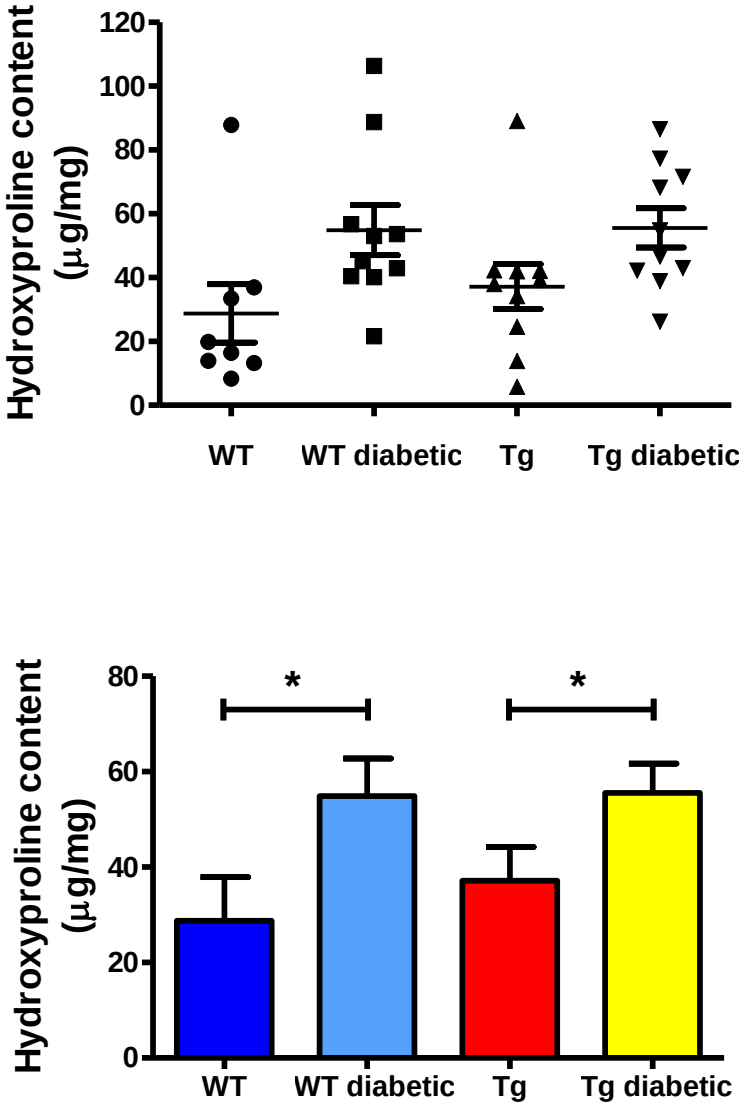
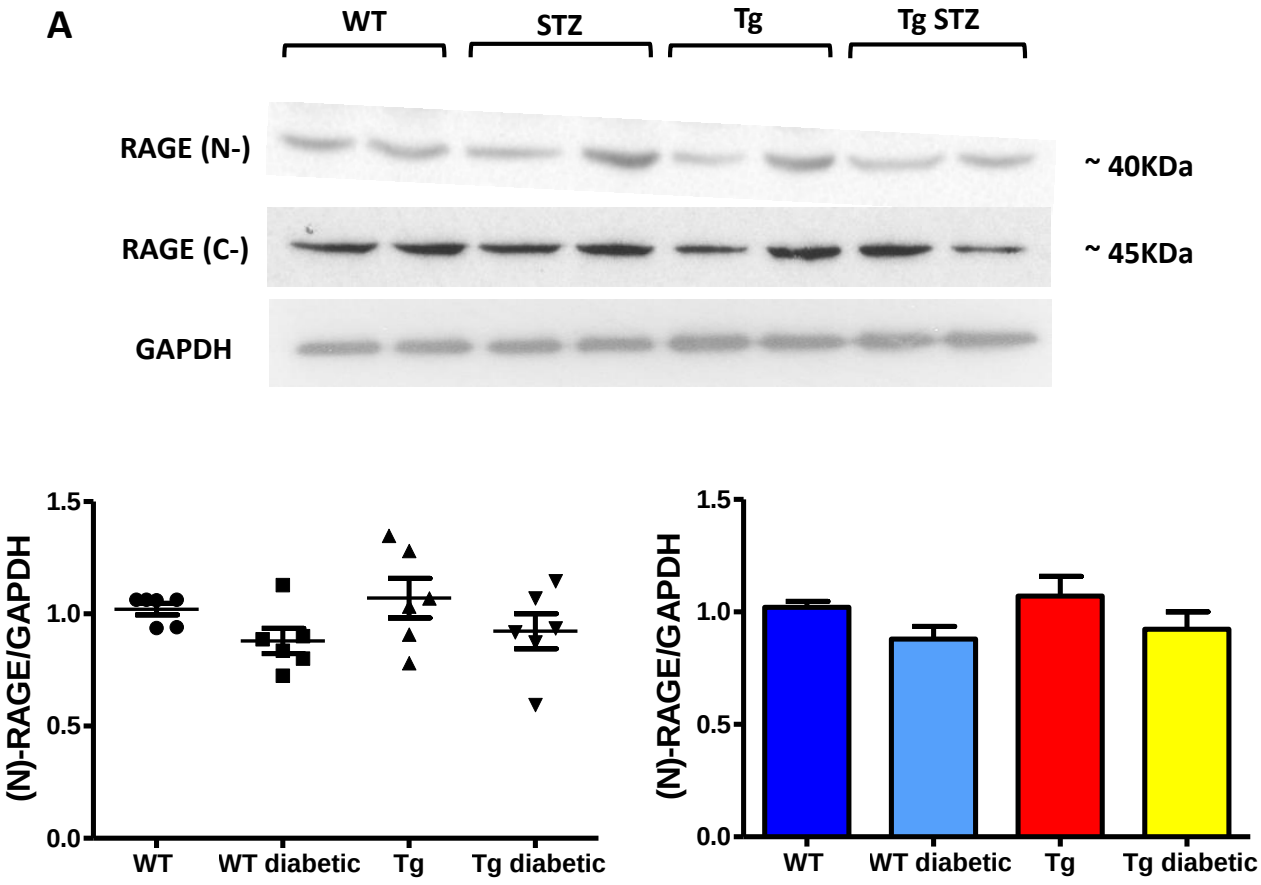


Figure 5.22. 12 week diabetic mice exhibit increased LV collagen content.

Long term diabetes was associated with increased levels of LV hydroxyproline, a major constituent of collagen. These increases in collagen were not prevented in hearts overexpressing mGCH1. (2-way ANOVA; *P<0.05; n = 8-10).

LV 12 weeks: inflammatory markers



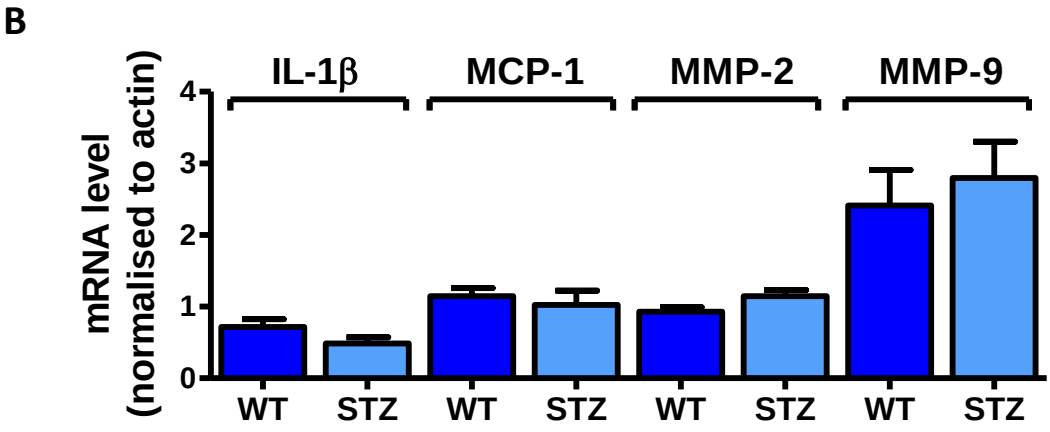


Figure 5.23. Inflammation is not implicated in the development of diabetic cardiomyopathy.

(A) LV homogenates from diabetic mice showed no elevation in the expression of the receptor for AGEs (n = 8). **(B)** In WT mice, diabetes was not associated with increased levels of various pro-inflammatory cytokines in the myocardium (n = 15-17).

LV 12 weeks: PKCβII protein expression

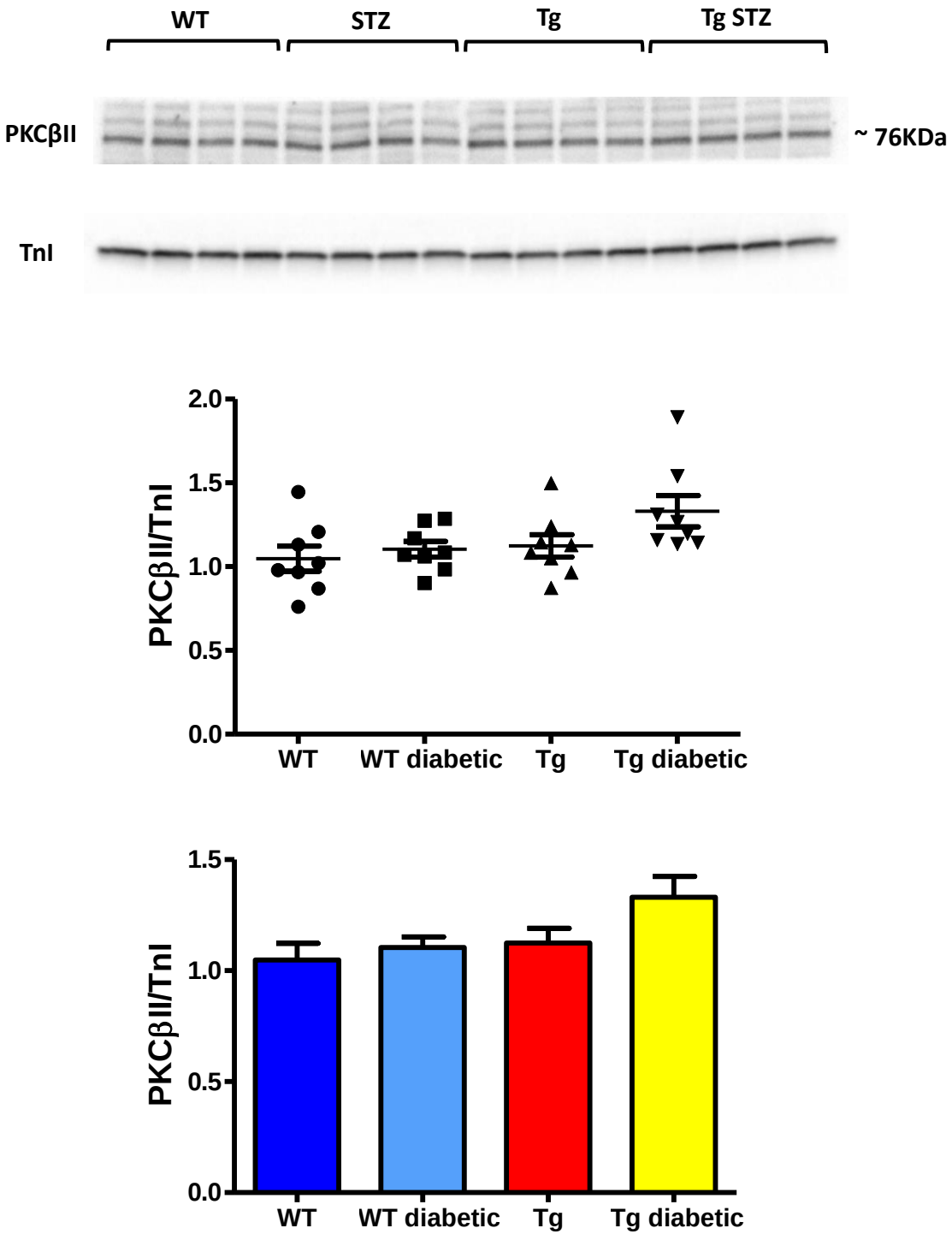


Figure 5.24 PKCβII expression is not upregulated in the LV of diabetic mice.

12 weeks of hyperglycaemia did not result in alterations to the levels of PKCβII (n = 8).

LV 12 weeks: AcH3 protein expression

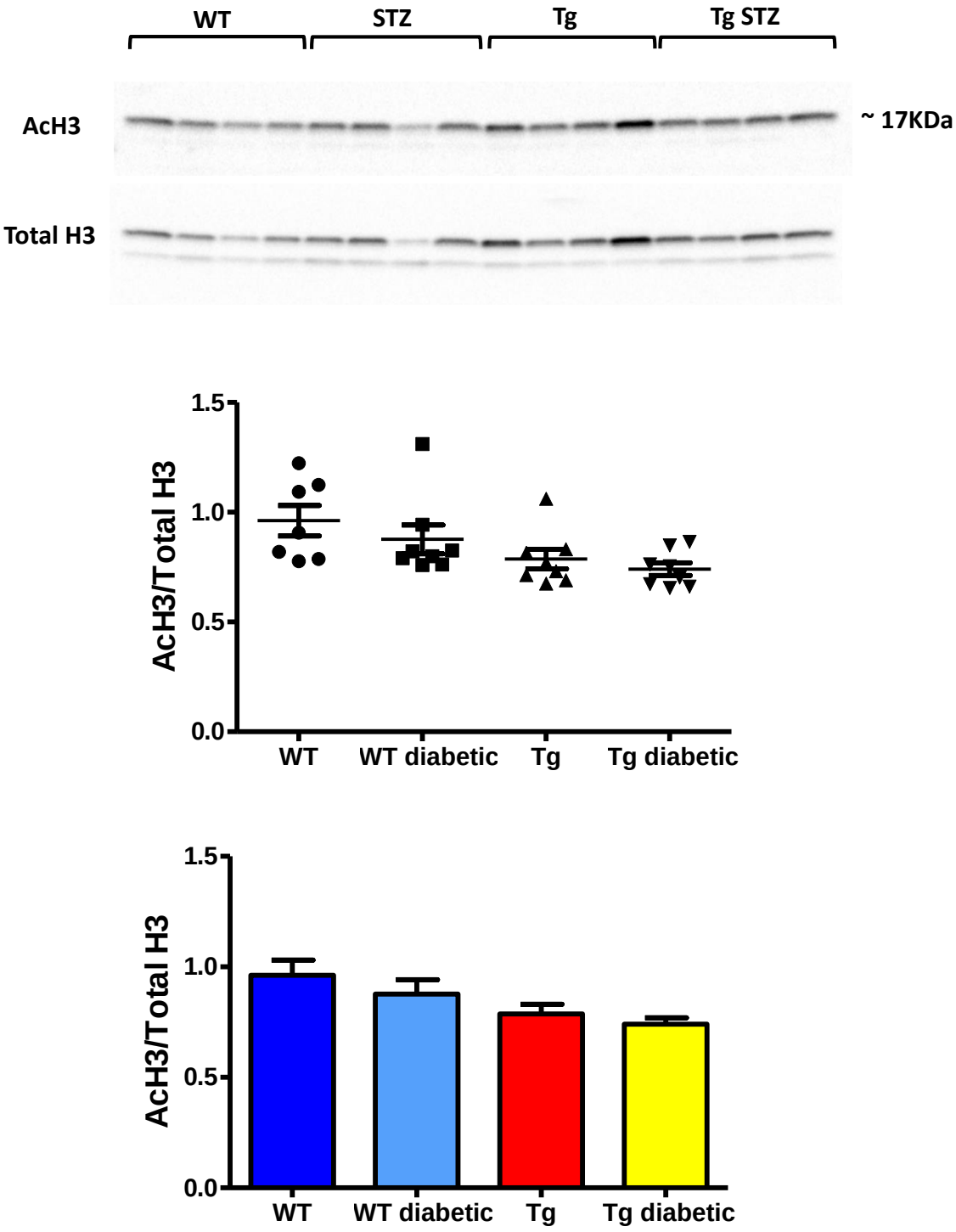


Figure 5.25. Diabetes is not associated with excessive acetylation of histone protein 3 in the myocardium.

No differences were observed in the ratio of acetylated H3 to total H3 levels expressed in LV homogenates (n = 8).

mGCH1 overexpression prevents altered energy metabolism in the diabetic heart

Impaired cardiac energetics has been proposed as a potential underlying mechanism of the cardiomyopathy observed in the diabetic state (177, 400). Appropriate shuttling of high energy phosphates via the creatine kinase (CK) enzyme is critical for normal myocardial performance (401-404). Furthermore, observations from both diabetes and heart failure have described reduced CK flux, altered isoenzyme content and disrupted PCr/ATP balance (177, 400, 405-409). With this in mind, the activity of creatine kinase isoforms was measured in LV homogenates to assess effective shuttling of high energy phosphates. There was a trend towards decreased global CK activity in WT diabetic mice, but this difference did not reach statistical significance (Figure 5.26A). However, the trend could be explained by the notable changes observed in the activity of the mitochondrial isoform of CK (CK-mt). CK-mt activity was significantly decreased in LV from WT diabetic mice, moreover, mGCH1 overexpression prevented this decline in diabetes (2.03 ± 0.07 in Tg diabetic vs 1.56 ± 0.13 in WT diabetic; Figure 5.26B). This metabolic change was specific to the mitochondria, as the activity of the muscle-specific (CK-mm) and brain-specific (CK-bb) isoforms of creatine kinase remained equivalent across all groups (Figure 5.27A and B). CK activity was normalised relative to the activity of citrate synthase, a key enzyme at the start of the TCA cycle, which similarly showed no significant differences between groups (Figure 5.27C).

Given the reduced energetics at the mitochondrial level in diabetic but not mGCH1-Tg hearts, LV homogenates were assessed for potential indicators of substrate switching and decreased ATP production, possibly through increased activity of the uncoupling proteins in the ETC, as previously described (410-413). Immunoblots for UCP3 expression demonstrated a pronounced increase in WT diabetic mice versus all other groups (2.73 ± 0.31 in WT diabetic vs 1.03 ± 0.08 in WT; Figure 5.28), suggestive of uncoupled Ox-Phos in WT diabetic, but not mGCH1-Tg hearts (0.95 ± 0.09). To confirm that the region of interest on the Western blot corresponded to UCP3 at that molecular weight, some blots were repeated in the presence of the UCP3-blocking peptide provided by the manufacturer,

which subsequently eliminated the predicted bands (Figure 5.28). Additionally, LV homogenates were evaluated for the voltage-dependent anion channel (VDAC), located on outer mitochondrial membrane. There was no evidence of altered VDAC expression between groups (Figure 5.29), demonstrating that UCP3 expression was not altered simply as a result of changes to mitochondrial number.

Increased expression of UCP3 in the mitochondrial chain is indicative of a shift in cardiac substrate utilisation, towards greater FA metabolism and reduced energy derived from glucose (414-419). Thus, expression levels of relevant glucose transporters were determined in LV homogenates as an indicator of potential differences in cardiomyocyte glucose uptake. Profiles of both gene and protein expression demonstrated that the insulin-mediated transporter GLUT4 remained unchanged between all groups, despite some considerable variability in gene expression data (Figure 5.30 and 5.31). However, both gene and protein expression of the insulin-independent transporter GLUT1 were significantly elevated in control and diabetic mice with mGCH1 overexpression (Figures 5.32 and 5.33). Together these results suggest that mGCH1 overexpression may confer improved basal glucose uptake into LV cardiomyocytes.

One potential mechanism by which increased myocardial BH4 and NOS activity in transgenic mice could increase glucose uptake is through the activation of the energy sensor AMPK and increased GLUT receptor translocation (420). Despite the labile nature of AMPK, the expression of its downstream phosphorylation target, acetyl CoA carboxylase (ACC), was examined as a marker for potential AMPK activity. However, immunoblots demonstrated no differences between experimental groups in the ratio of phosphorylated to total ACC expression (Figure 5.34).

Given the insulin insufficiency in T1D, a shift in cardiomyocyte fuel metabolism towards greater FA oxidation might be expected, as has been previously reported (181, 395). To determine whether WT diabetic hearts might be metabolising FA to a greater extent than glucose, expression levels of medium-chain acyl-CoA dehydrogenase (MCAD) were measured, the major enzyme responsible for

the β-oxidation of FA in the mitochondria. Despite the insulin insufficiency, WT diabetic mice showed no difference in the levels of MCAD in LV homogenates (Figure 5.35). The upregulation of FA substrate metabolism is normally associated with increased PPARα activation (365, 421, 422) and potentially expression (423, 424), yet immunoblots of LV PPARα levels similarly demonstrated no significant alterations (Figure 5.36). Furthermore, no changes were detected in the expression of pyruvate dehydrogenase kinase 4 (PDK4) (Figure 5.37), which normally mediates the inhibition of glucose metabolism by FA through the Randle cycle (for review see (425)). Finally, α-ketoglutarate dehydrogenase (αKGD) expression was studied as an indicator of adjusted metabolic flux through the TCA cycle. Consistent with the unaltered citrate synthase activity, no differences in αKGD were observed between groups. (Figure 5.38). As well as the analysis of enzymes involved in lipid metabolism, tissue sections were examined histologically for the presence of increased myocardial TAG deposition. In LV samples, the presence of lipids in all groups of mice was very low with oil red O staining. Sections of liver were used as positive controls, which interestingly demonstrated significantly decreased lipid content in both diabetic groups (17.16 ± 4.95 in WT diabetic vs 33.30 ± 6.13 in WT; Figure 5.39). Overall, these data suggest that WT diabetic mice do not experience cardiac lipotoxicity, and that there is no evident upregulation in the metabolic machinery involved in LV FA metabolism.

LV 12 weeks: creatine kinase activity

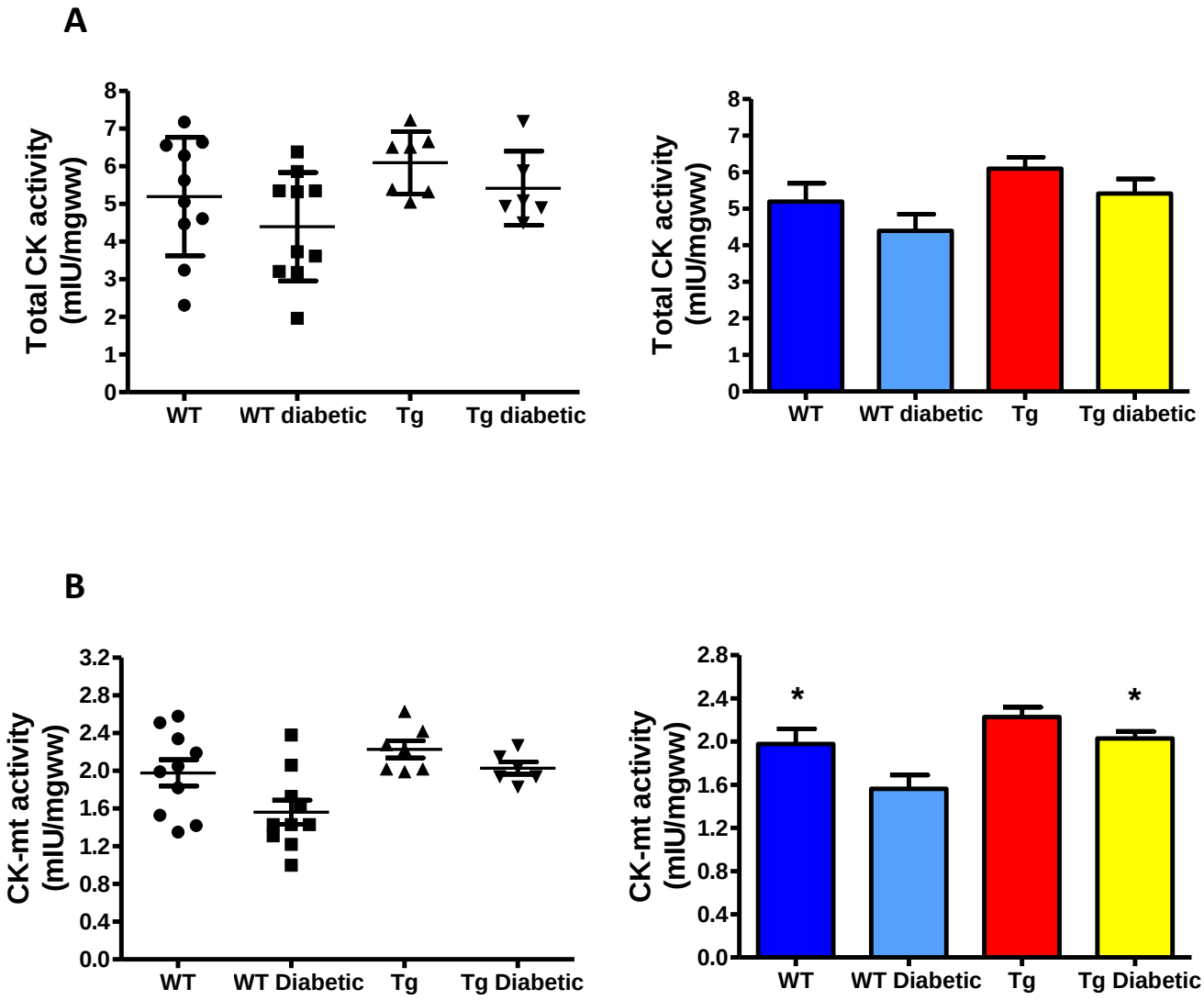


Figure 5.26. mGCH1 overexpression prevents the impairment in mitochondrial creatine kinase activity in diabetes.

(A) Diabetes resulted in a non-significant trend towards decreased total creatine kinase activity**. (B)** Activity of the mitochondrial isoform of creatine kinase was significantly reduced in WT diabetic hearts, but mGCH1-Tg hearts were protected against this effect (2-way ANOVA; *P<0.05 vs WT diabetes; n = 6-10).

LV 12 weeks: creatine kinase activity

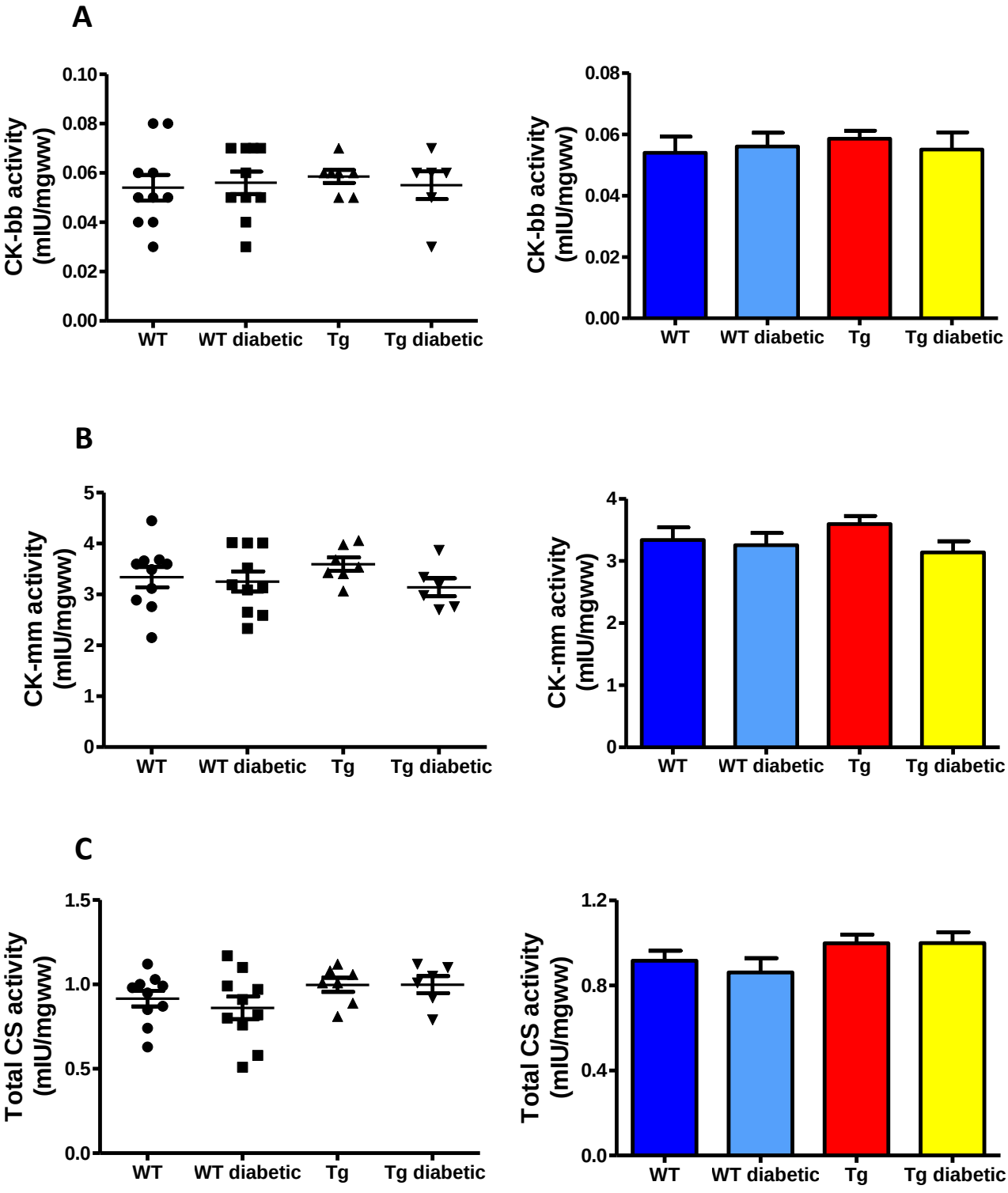


Figure 5.27. Non-mitochondrial isoforms of creatine kinase do not exhibit reduced activity in diabetic hearts.

(A) The brain-specific isoform of CK displayed minor activity in LV homogenates and showed no differences between groups. **(B)** The muscle-specific CK isoform showed greater activity than CK-bb, but this was not changed by either treatment or genotype. **(C)** CK activity was normalised to the total activity of citrate synthase, which remained the same across all groups (n = 6-10).

LV 12 weeks: UCP3 protein expression

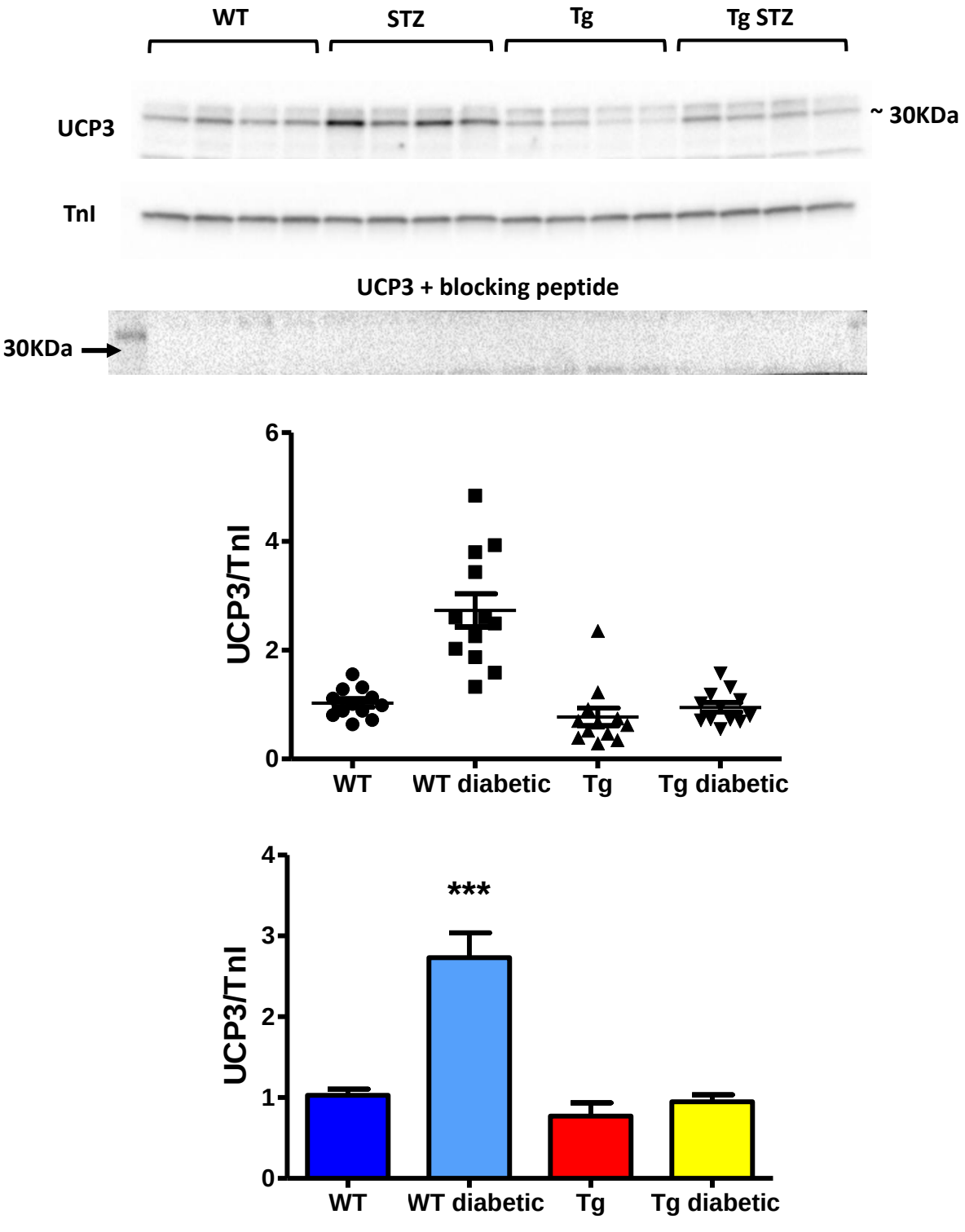


Figure 5.28. Diabetic hearts demonstrate increased expression of uncoupling protein 3.

WT diabetic mice showed significantly elevated levels of UCP3 in LV homogenates, which was prevented in diabetic mice overexpressing mGCH1. Incubation with the synthetic blocking peptide eradicated the bands predicted at the corresponding molecular weight (30KDa). (2-Way ANOVA; ***P<0.001 vs all groups; P<0.001 for interaction between treatment and genotype; n = 12).

LV 12 weeks: VDAC protein expression

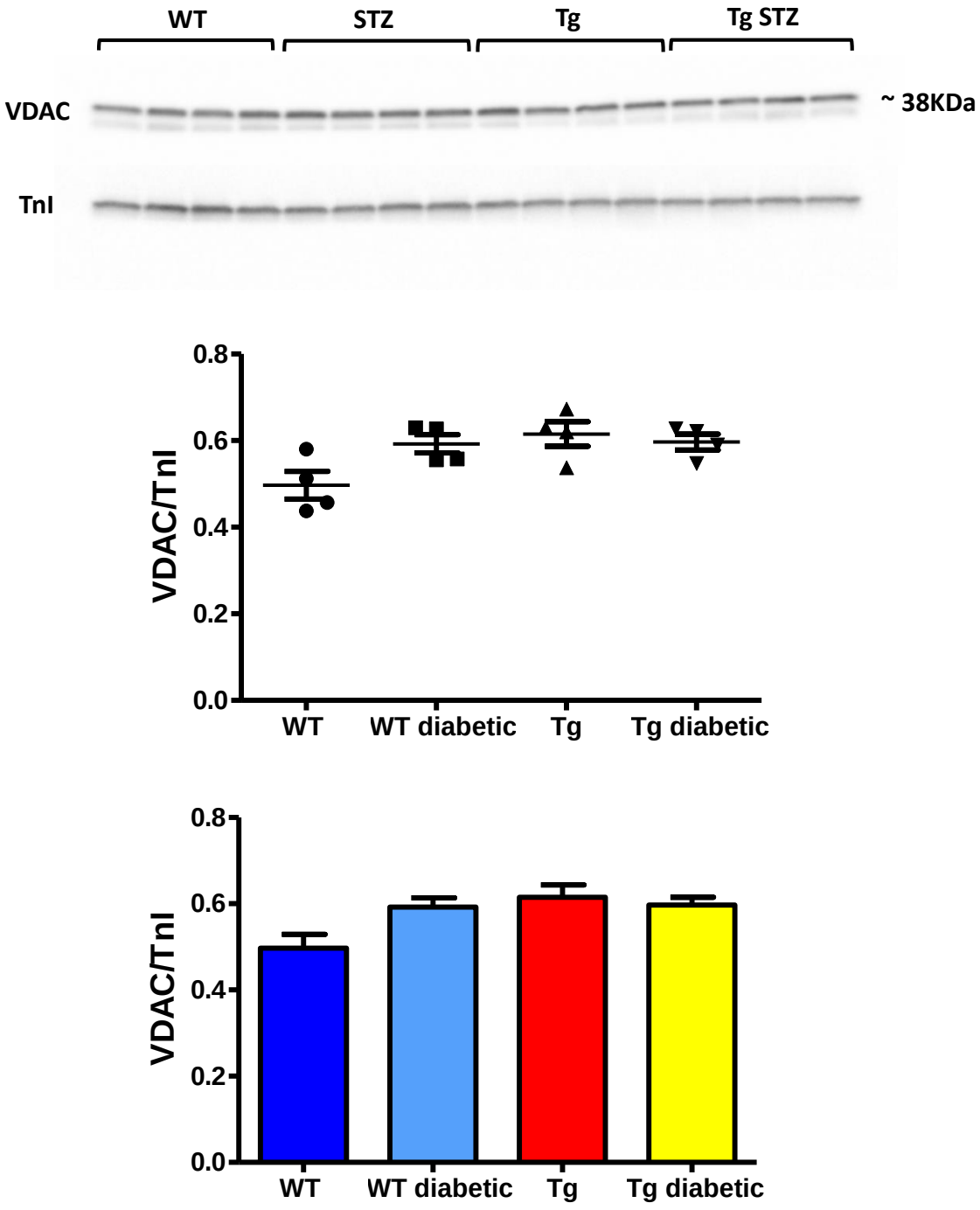
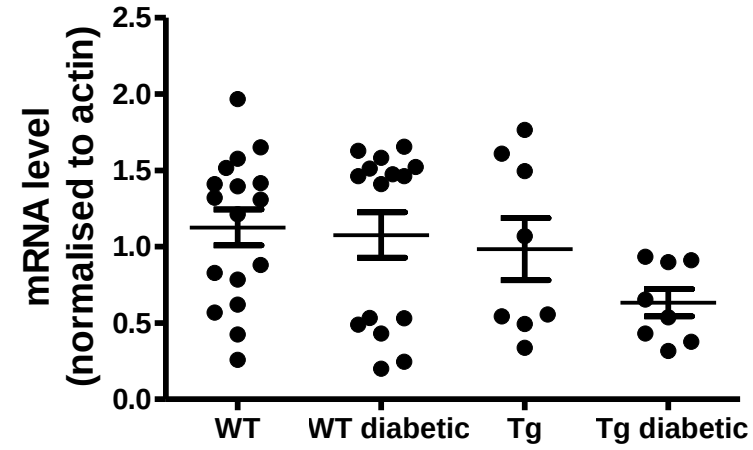


Figure 5.29. Long term diabetes is not associated with altered LV mitochondrial density.

Diabetic mice showed no evidence of altered VDAC expression, an indicator of mitochondrial number (n = 4).

LV 12 weeks: GLUT4 gene expression



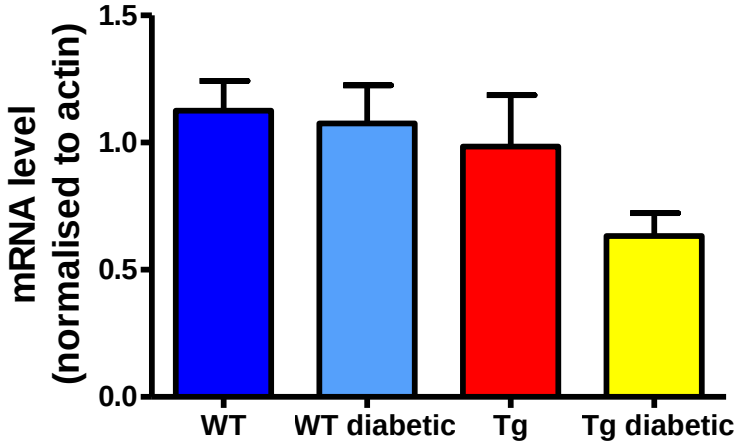


Figure 5.30. Long term diabetes is not associated with altered GLUT4 gene expression in the myocardium.

Levels of GLUT4 mRNA in LV homogenates showed no discernible change in the presence of diabetes in WT mice. Only in diabetic (but not control) mice overexpressing mGCH1 was there a non-significant decrease in gene expression observed (n = 8-17).

LV 12 weeks: GLUT4 protein expression

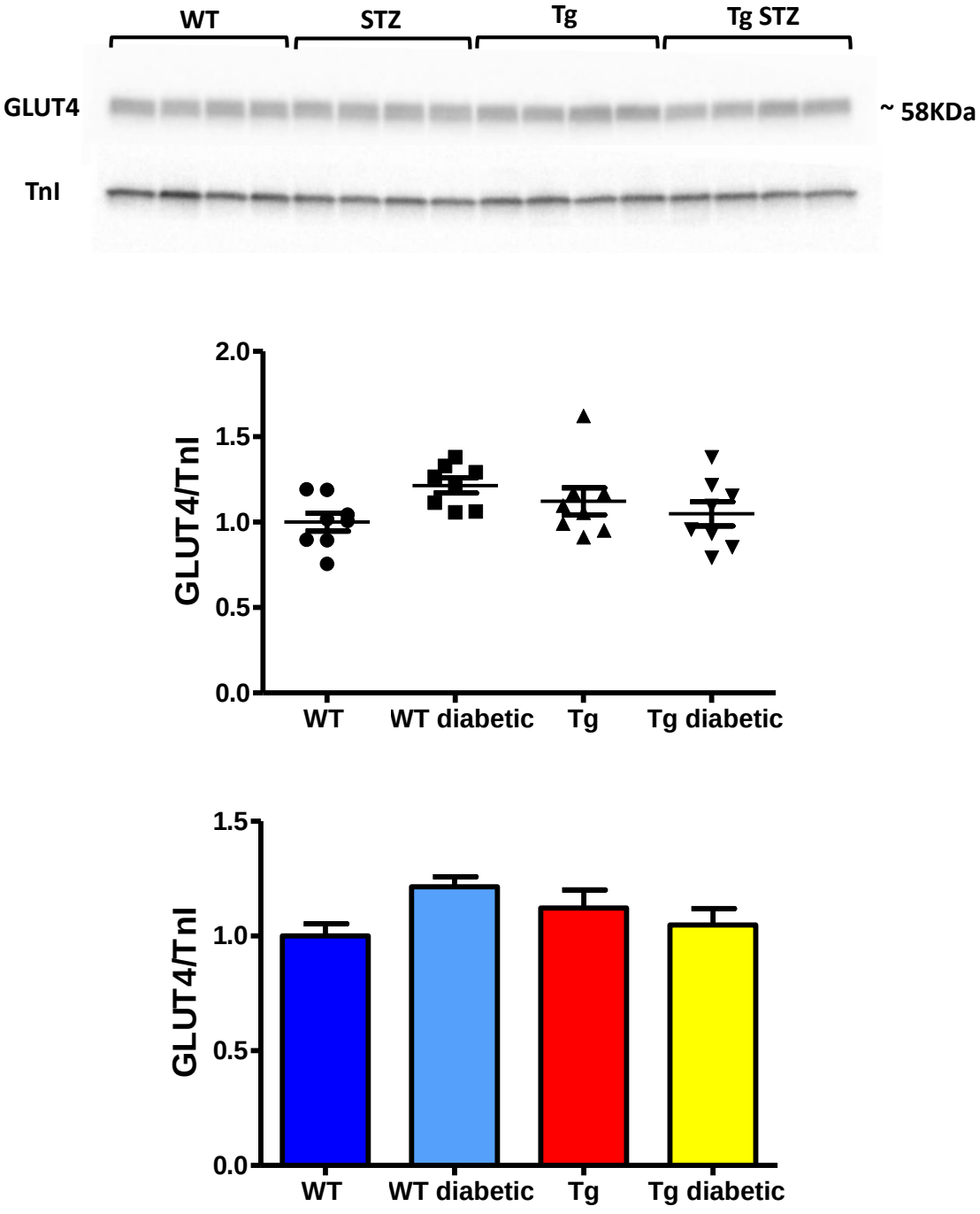


Figure 5.31. T1D does not alter LV expression of GLUT4 protein.

After 12 weeks, the diabetic milieu did not modify LV expression of the insulin-dependent GLUT4 transporter (n = 8).

LV 12 weeks: GLUT1 gene expression

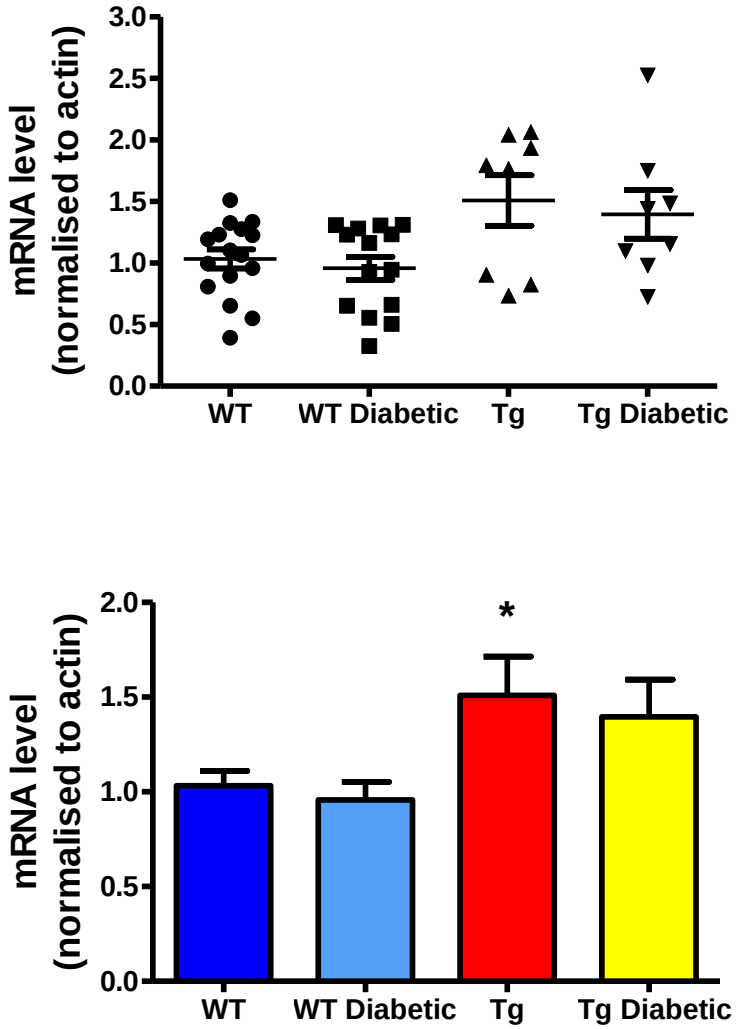


Figure 5.32. mGCH1-Tg hearts demonstrate upregulated GLUT1 gene expression.

mGCH1 overexpression resulted in an elevation in LV mRNA levels of the insulin-independent GLUT1 transporter. (2-way ANOVA; *P<0.05 vs WT; n = 8-16).

LV 12 weeks: GLUT1 protein expression

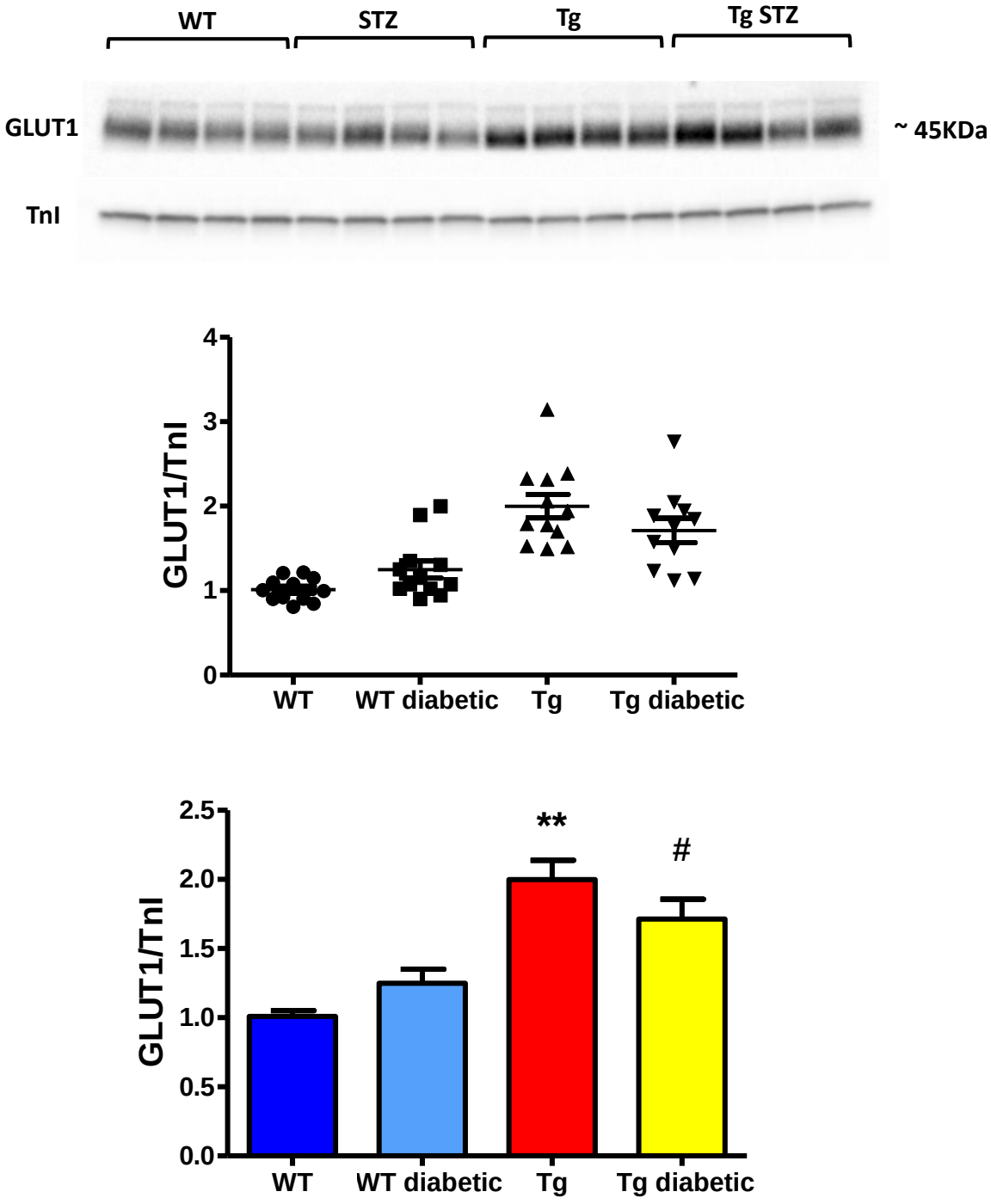


Figure 5.33. mGCH1 overexpression increases GLUT1 protein levels in the myocardium.

In both control and diabetic mice, mGCH1 expression resulted in significantly elevated expression of the GLUT1 protein. (2-way ANOVA; **P<0.01 vs WT; # P<0.05 vs WT diabetic; P<0.05 for interaction between treatment and genotype; n =12).

LV 12 weeks: ACC protein expression

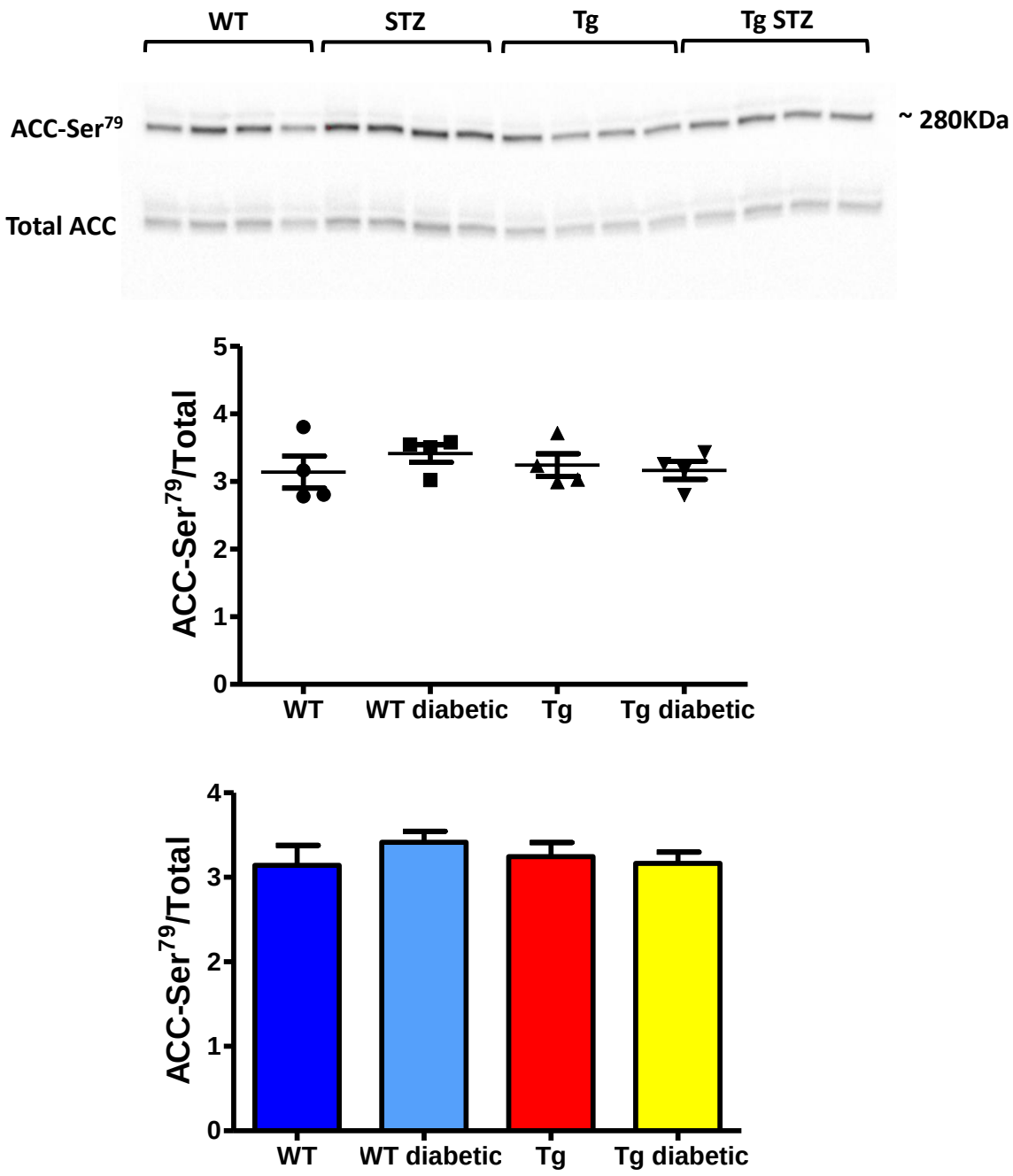


Figure 5.34. Neither diabetes nor mGCH1 overexpression is associated with AMPK activation.

Expression of phosphorylated ACC, a primary downstream target of AMPK, showed no differences between groups (n = 4).

LV 12 weeks: MCAD protein expression

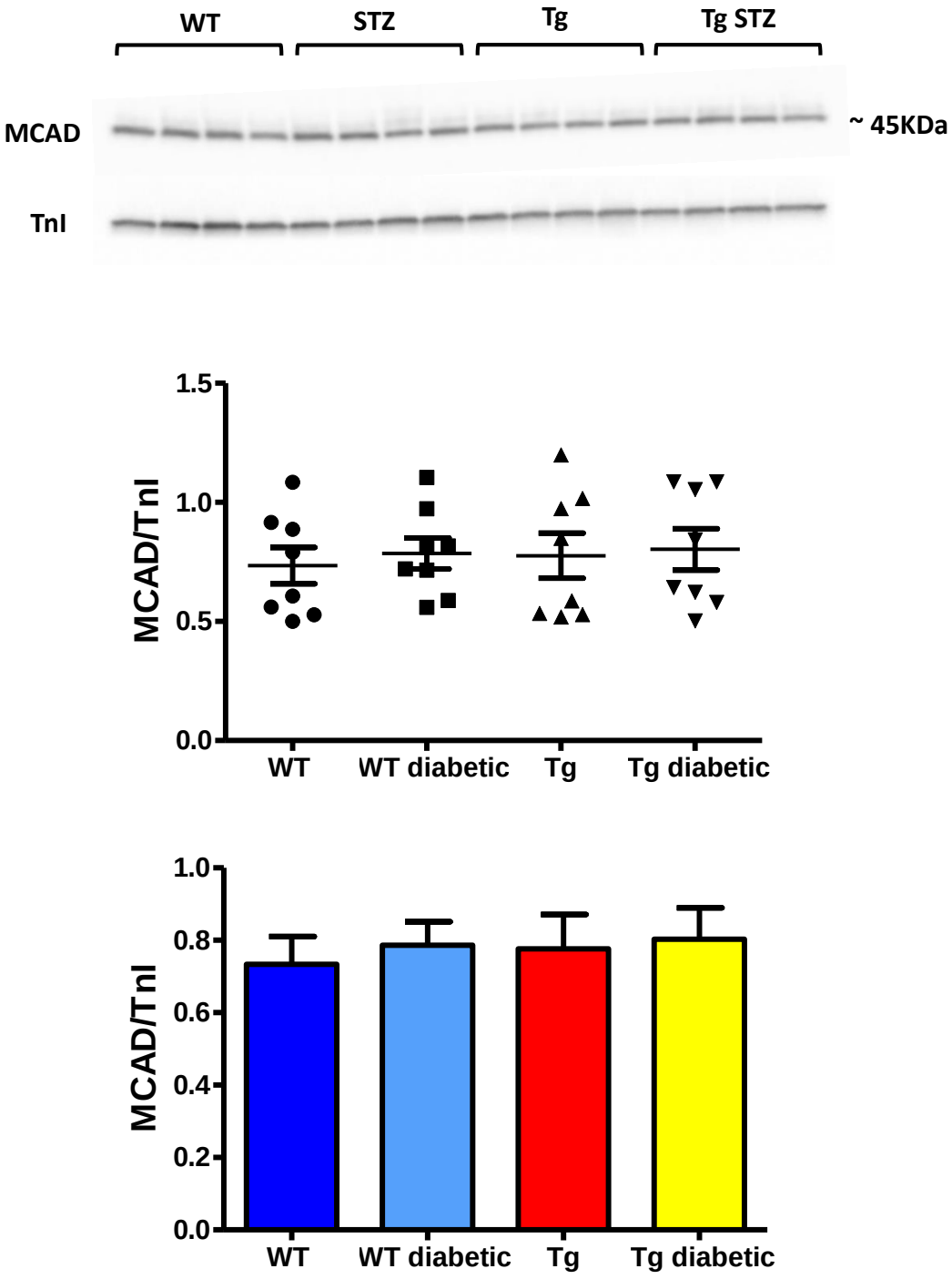


Figure 5.35. Myocardial expression of MCAD is not upregulated in diabetic mice.

Expression of MCAD, the enzyme primarily involved in fatty acid β-oxidation, showed no differences between experimental groups. (n = 8).

LV 12 weeks: PPARα protein expression

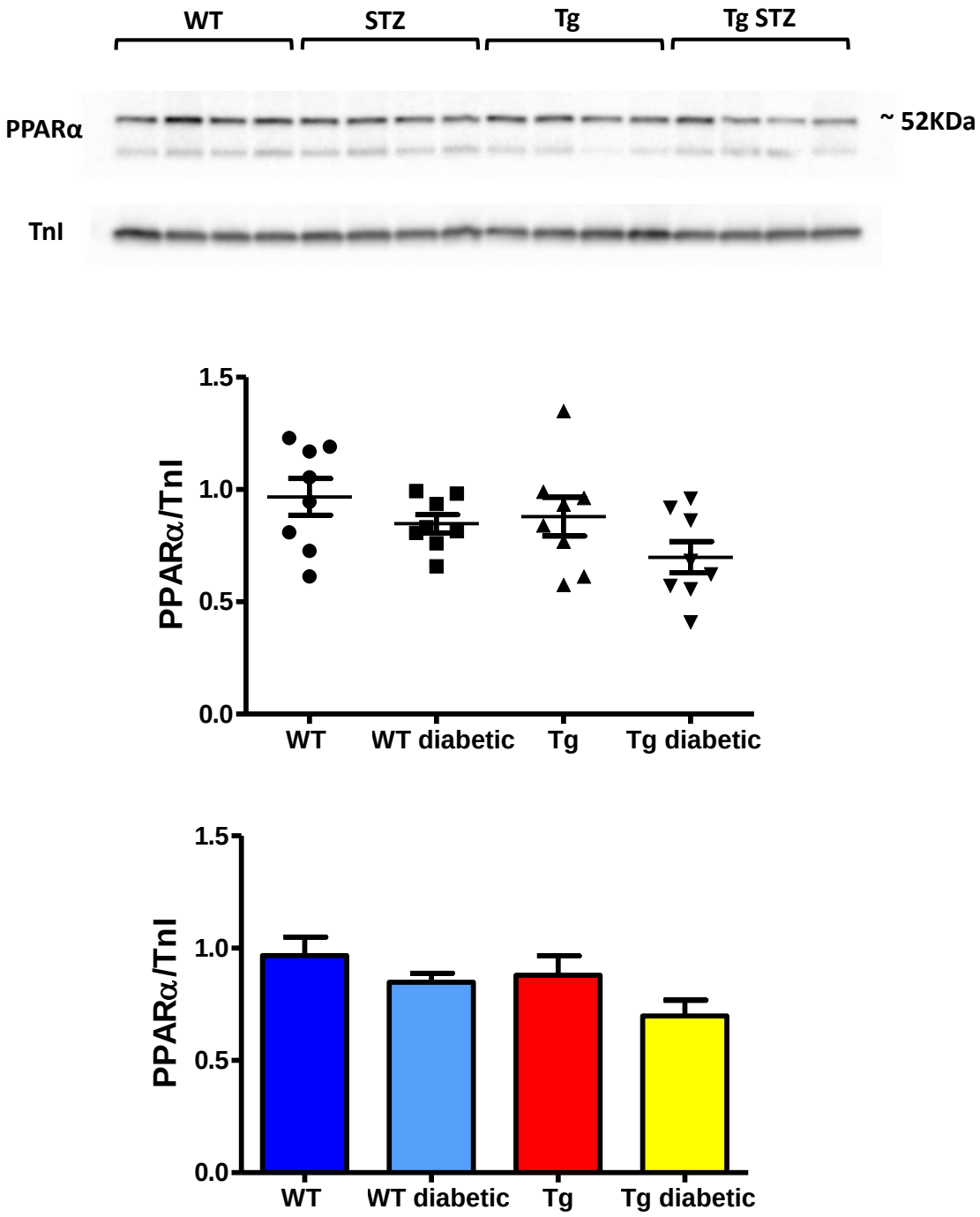


Figure 5.36. Long term diabetes does not upregulate myocardial PPARα expression.

No significant modifications to LV PPARα expression were evident in either diabetic or mGCH1-Tg mice (n = 8).

LV 12 weeks: PDK4 protein expression

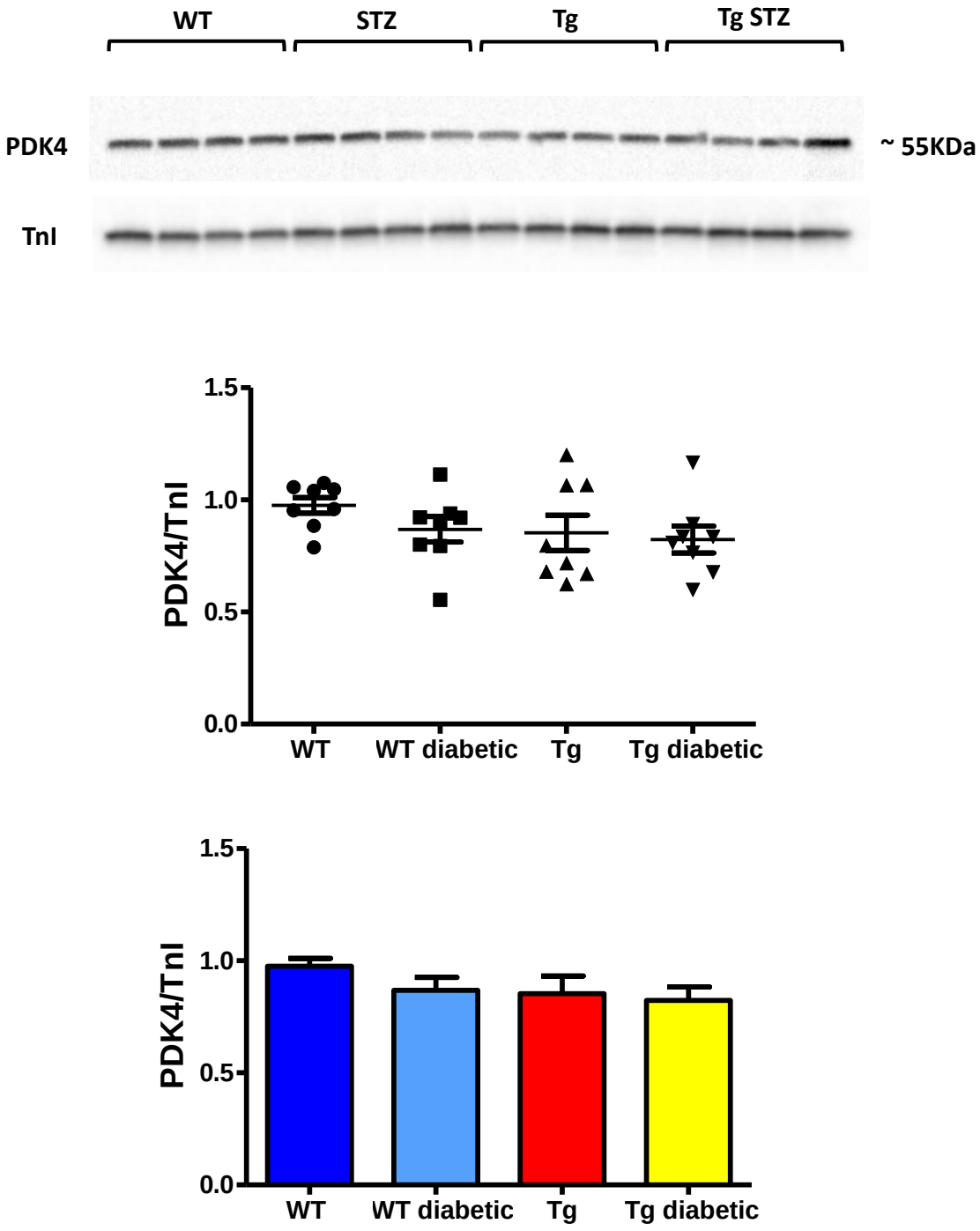


Figure 5.37. LV expression of PDK4 is not increased after 12 weeks of diabetes.

No changes to PDK4 levels were evident in either diabetic or mGCH1-Tg mice (n = 8).

LV 12 weeks: αKGD protein expression

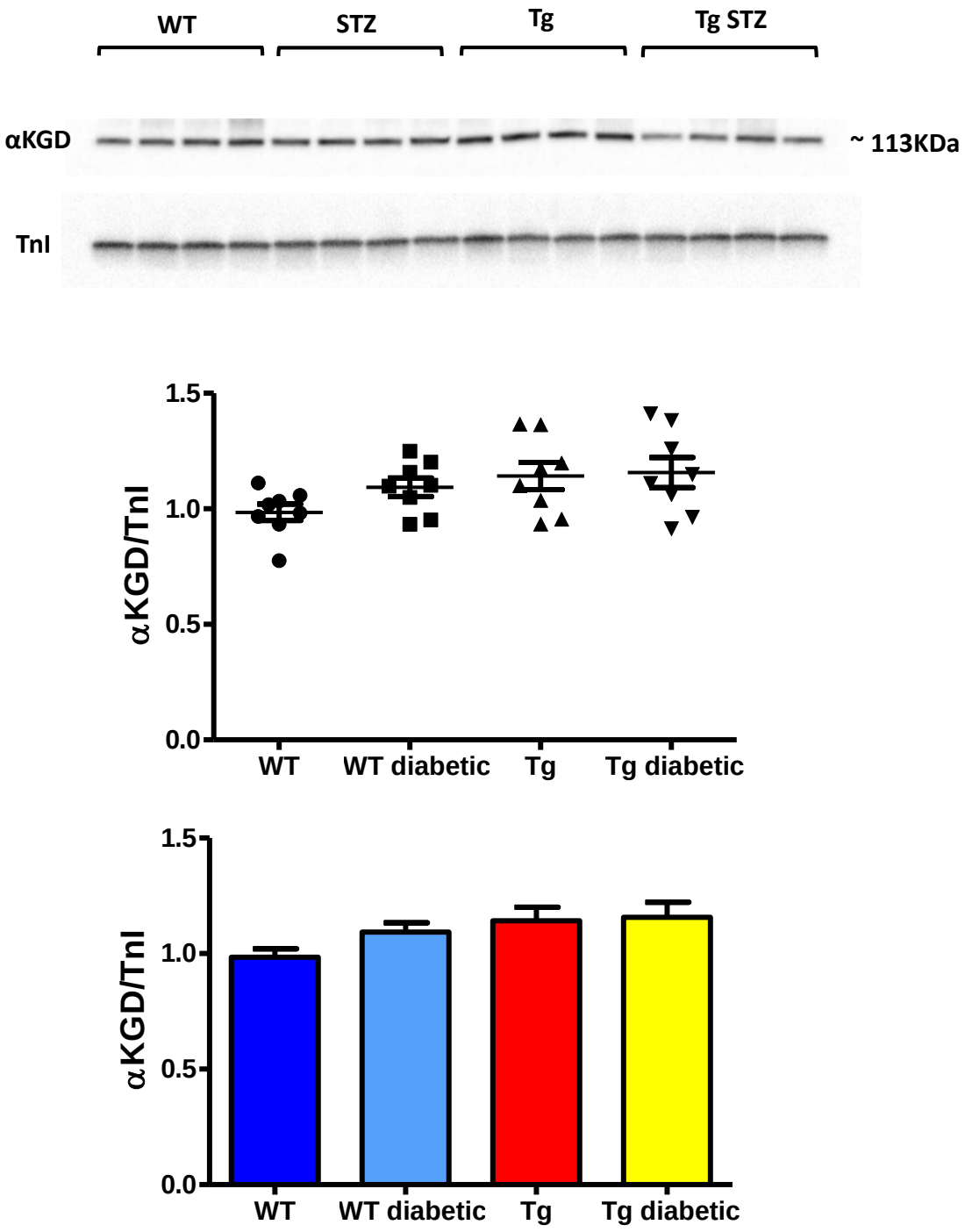


Figure 5.38. Diabetes does not change the myocardial expression of αKGD.

Diabetes was not associated with differences in the levels of the TCA cycle enzyme αKGD (n = 8).

Liver 12 weeks: lipid deposition

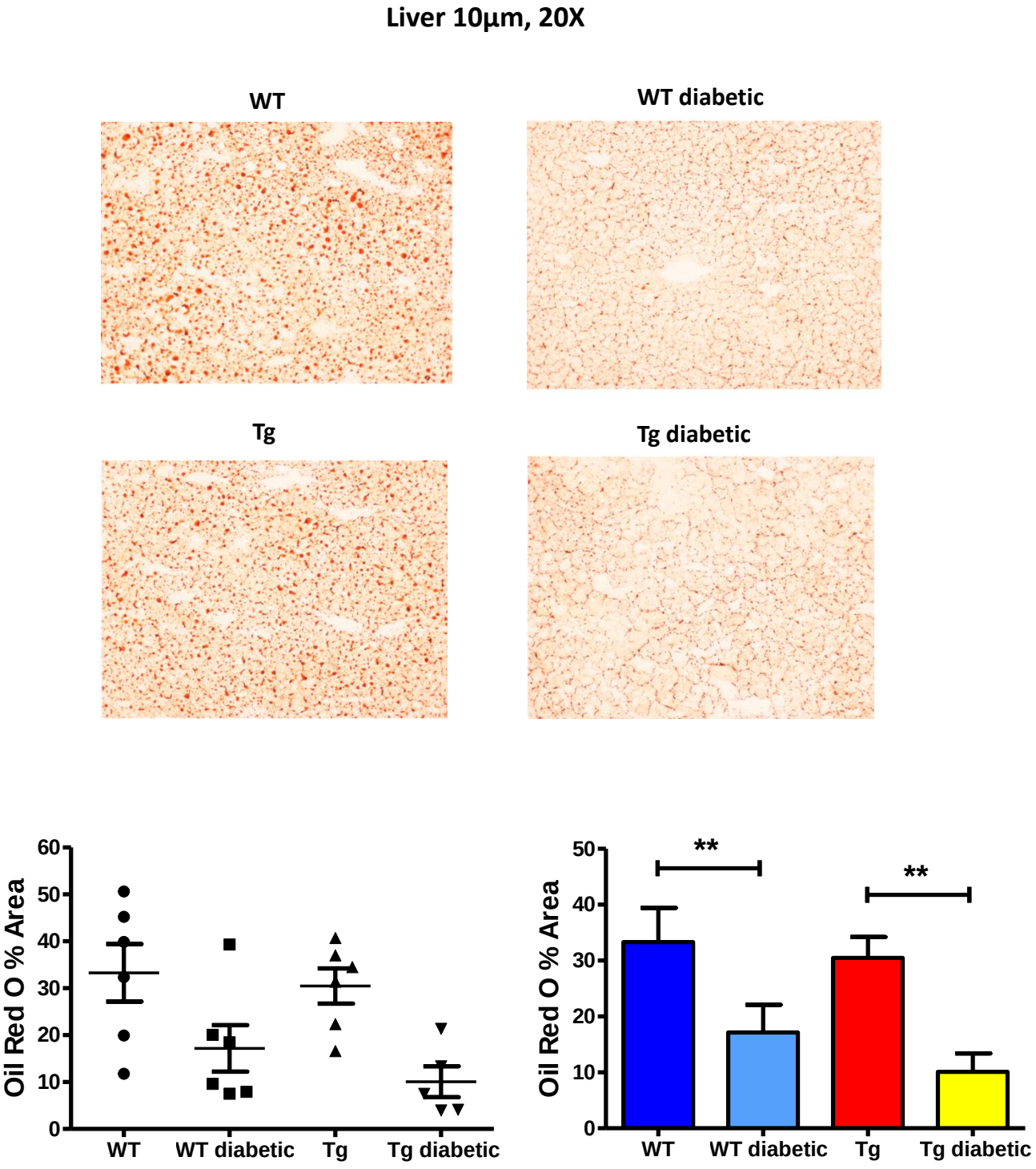


Figure 5.39. Lipid deposition is reduced in the liver of diabetic mice.

(A) Representative histological images of liver sections with oil red O staining for triglycerides and lipids. (B) Irrespective of genotype, diabetic mice demonstrated a significantly decreased fraction of oil red O staining. (2-way ANOVA; **P<0.01; n = 3 sections from 5-6 hearts per group).

Metabolic changes may precede the onset of diabetic cardiomyopathy

To investigate whether the potential changes to mitochondrial uncoupling preceded, and potentially contributed to, the onset of LV dysfunction in WT diabetic mice, UCP3 expression was evaluated in LV homogenates from mice after only 4 weeks of diabetes. At the early time point, UCP3 levels were already significantly elevated in WT diabetic mice only (Figure 5.40), analogous to the findings at 12 weeks. To determine whether the early changes in UCP3 were also accompanied by the same trend observed with glucose transporter expression, GLUT1 levels were similarly assessed in 4 week LV homogenates. Indeed, immunoblots demonstrated that mGCH1 overexpression resulted in upregulated myocardial GLUT1 expression in both control and diabetic mice (Figure 5.41). In the context of the findings at 12 weeks, these additional data suggest that early expressional changes may be related to shifts in LV cardiomyocyte metabolism, which may contribute to the development of, and protection against, diabetic cardiomyopathy.

LV 4 weeks: UCP3 protein expression

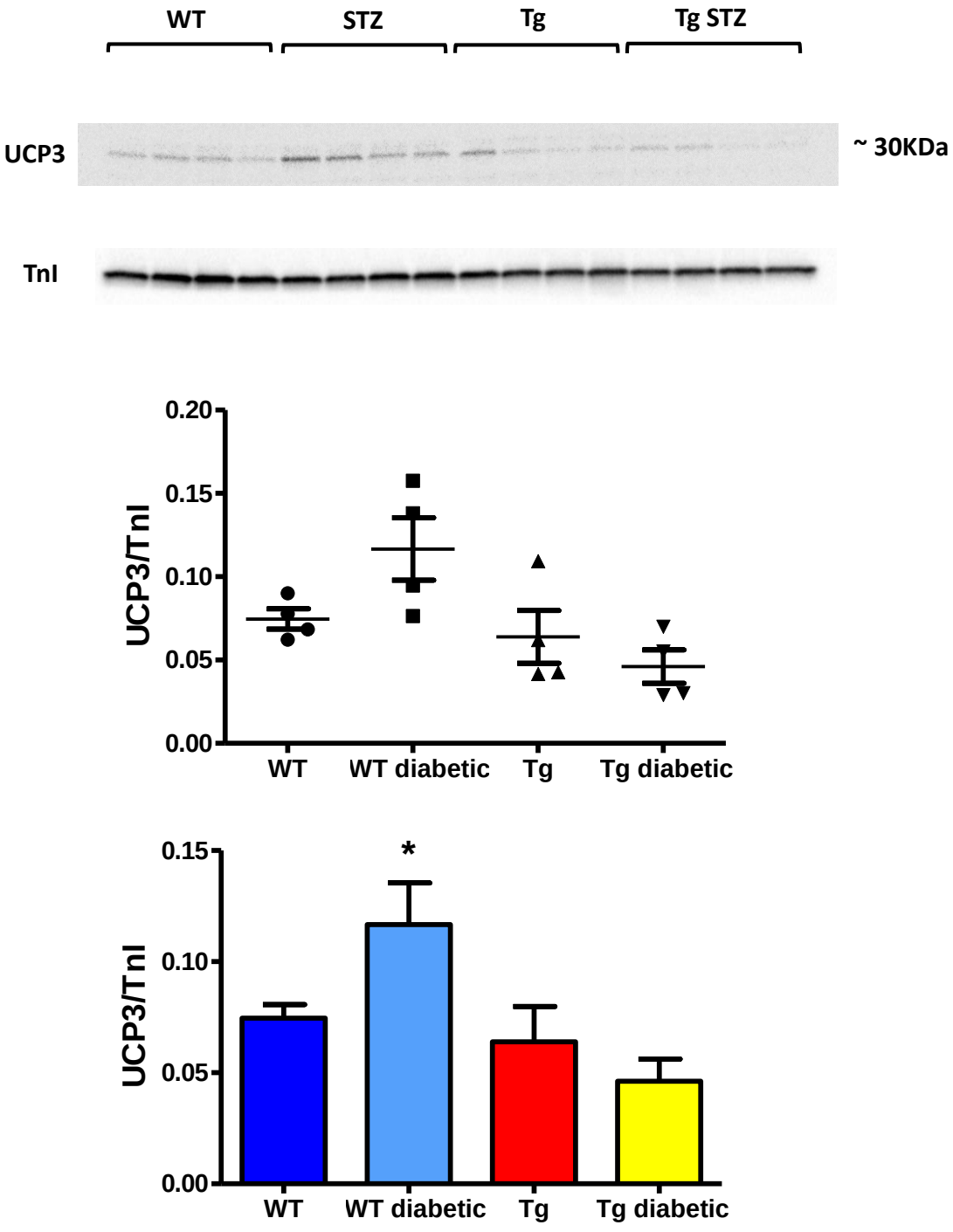


Figure 5.40. Mitochondrial UCP3 upregulation is an early event in the development of diabetic cardiomyopathy.

After only 4 weeks of diabetes, WT diabetic mice demonstrated significantly elevated UCP3 expression in LV homogenates, which was prevented in mice overexpressing mGCH1. (2-way ANOVA; *P<0.05 vs all groups; P<0.05 for interaction between treatment and genotype; n =4).

LV 4 weeks: GLUT1 protein expression

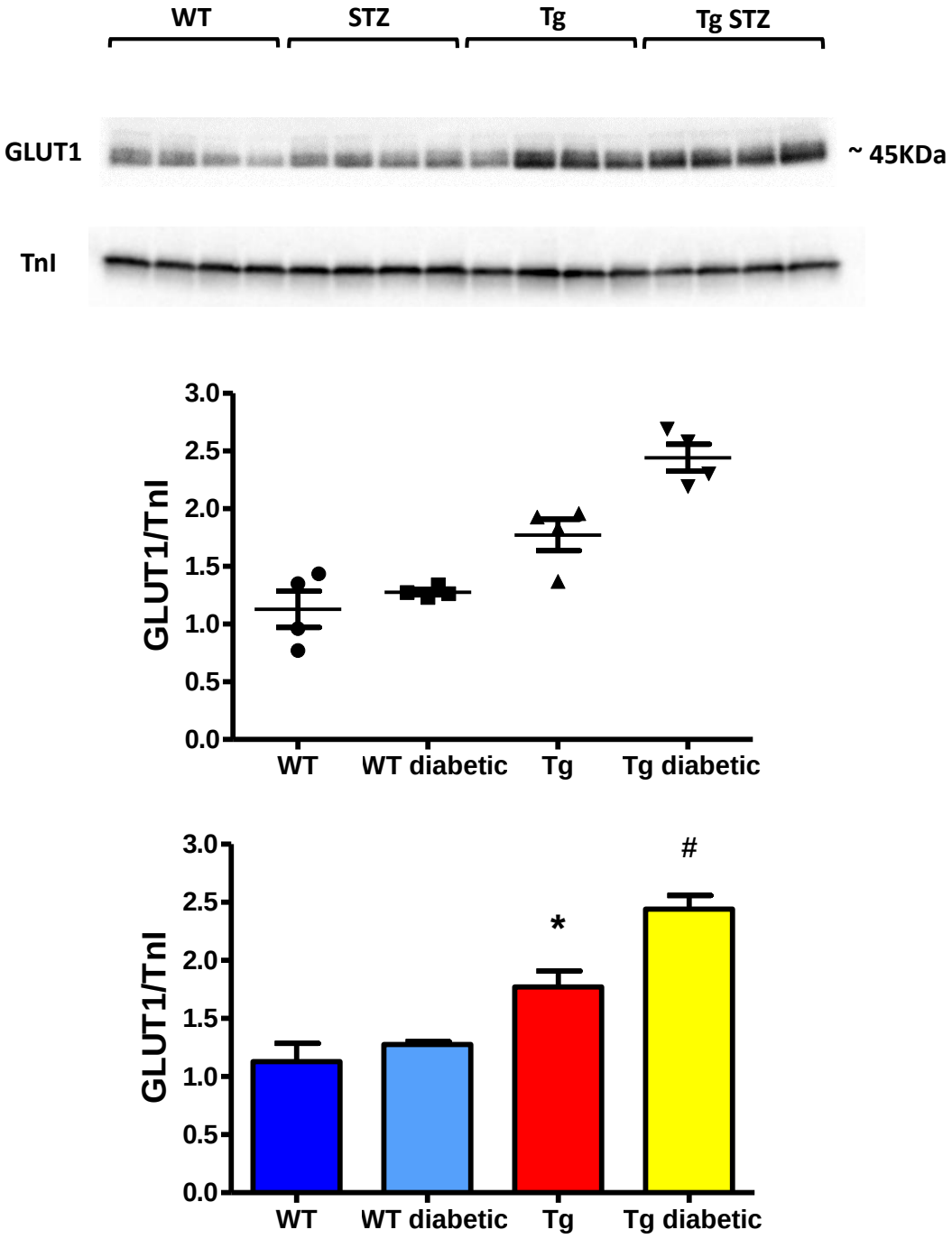


Figure 5.41. mGCH1 overexpression increases GLUT1 levels prior to the onset of diabetic LV dysfunction.

After 4 weeks, control and diabetic mice overexpressing mGCH1 showed upregulated GLUT1 expression in LV homogenates. (2-way ANOVA; *P<0.05 vs WT; # P<0.05 vs WT diabetic; P<0.05 for interaction between treatment and genotype; n = 4).

BH4 supplementation increases cardiac biopterins and improves LV NOS activity

The dose of 200mg/kg/day for oral BH4 supplementation was selected based on previous studies of NOS coupling status in cardiac hypertrophy, where 200mg/kg/day was demonstrated to be on the high end of the efficacious range (187, 426). To confirm that BH4 through oral supplementation was being transported effectively into the myocardium, both plasma samples and LV tissue was evaluated for biopterin concentrations. Dietary BH4 treatment in diabetic mice resulted in a substantial elevation in total biopterin levels compared to mice fed with placebo (Figure 5.42A); moreover, plasma samples from these mice exhibited significantly higher concentrations of BH4 specifically (Figure 5.42B). However, the BH4:BH2 ratio revealed that the dietary BH4 had largely oxidised after being assimilated from digestion, as reflected by a significantly decreased ratio in both diabetic groups (1.08 ± 0.16 in diabetes + BH4 vs 2.92 ± 0.23 in control; Figure 5.42C). Mirroring the results from the plasma, LV samples from BH4 fed diabetic mice similarly showed both increased total biopterins and a significantly increased concentration of BH4 (9.41 ± 1.28 in diabetes + BH4 vs 5.56 ± 0.58 in diabetes; Figure 5.43A and B). However, unlike the plasma, LV samples demonstrated no change in the ratio of reduced to oxidised BH4 between groups (Figure 5.43C). Additionally, the elevation in cardiac BH4 had favourable effects on LV NOS activity, which was significantly augmented in BH4 supplemented diabetic mice (0.56 ± 0.12 in diabetes + BH4 vs 0.32 ± 0.08 in diabetes; Figure 5.43D). Together these data show that dietary BH4 is successfully imported into the myocardium, where it can directly enhance NO production.

BH4 supplementation: plasma biopterins

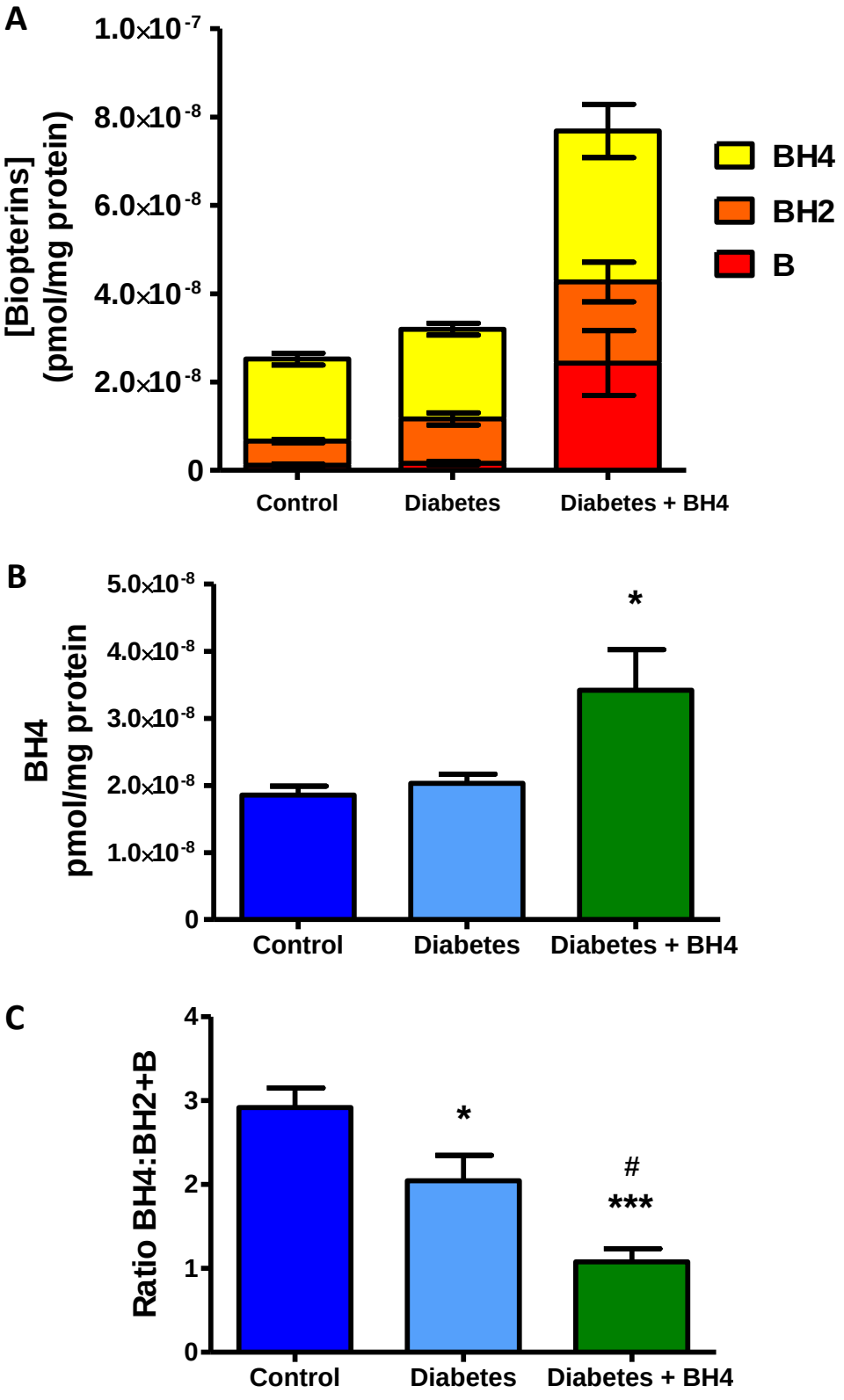


Figure 5.42. BH4 supplementation elevates plasma biopterins.

(A) Following 6 weeks of dietary BH4, diabetic fed mice exhibited increased levels of total biopterins (mg/plasma protein). **(B)** Along with overall biopterins, supplementation translated into elevated plasma concentrations of BH4 (1-way ANOVA; *P<0.05 vs diabetes and control). **(C)** Despite increases in plasma BH4, supplementation also resulted in significant oxidation of BH4, leading to a large decrease in the BH4:BH2 ratio (*P<0.05, ***P<0.001 vs control; # P<0.05 vs diabetes) (n = 9-10).

BH4 supplementation: LV biopterins and NOS activity

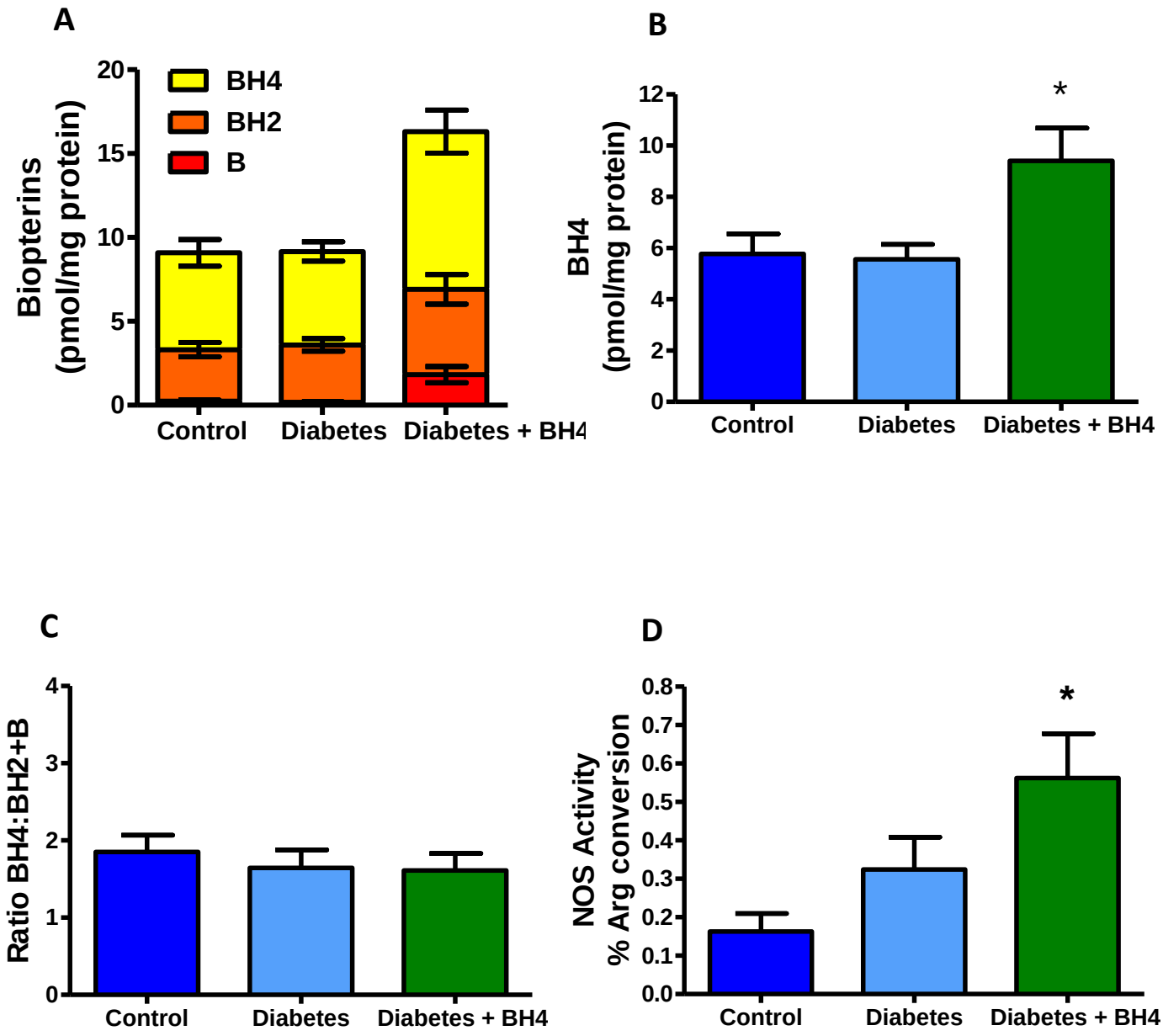


Figure 5.43. BH4 supplementation increases cardiac BH4 and improves NOS activity.

(A) Dietary BH4 was able to elevate the total biopterin levels in the myocardium. **(B)** LV concentrations of BH4 specifically were elevated in supplemented diabetic mice (1-way ANOVA; *P<0.05 vs control and diabetes; n = 7-11). **(C)** Biopterins imported into the myocardium did not increasingly oxidise from BH4 to BH2. **(D)** The increase in BH4 was sufficient to significantly enhance myocardial NOS activity (1-way ANOVA; *P<0.05 vs control; n = 6-8).

BH4 supplementation may not alter the same metabolic pathways as mGCH1 overexpression

Given the possibility that BH4 supplementation may confer similar improvements in cardiac function to those observed with mGCH1 overexpression (*experiments currently underway*), diabetic hearts from the BH4 fed group were likewise assessed for the expression of UCP3 and GLUT1, to establish if the same metabolic alterations might be responsible. Contrary to mGCH1-Tg mice, BH4 supplementation did not prevent the upregulation in UCP3 expression, which was significantly elevated in both diabetic groups (0.87 ± 0.07 in diabetes + BH4 vs 0.60 ± 0.06 in control; Figure 5.44). Unlike the transgene, BH4 supplementation additionally failed to result in an increased LV expression of GLUT1, which remained unchanged in all groups (Figure 5.45). These data suggest that dietary BH4 is unlikely to ameliorate diabetic cardiomyopathy through potential upregulation of basal glucose transport or improved mitochondrial energy production.

BH4 supplementation: LV UCP3 protein expression

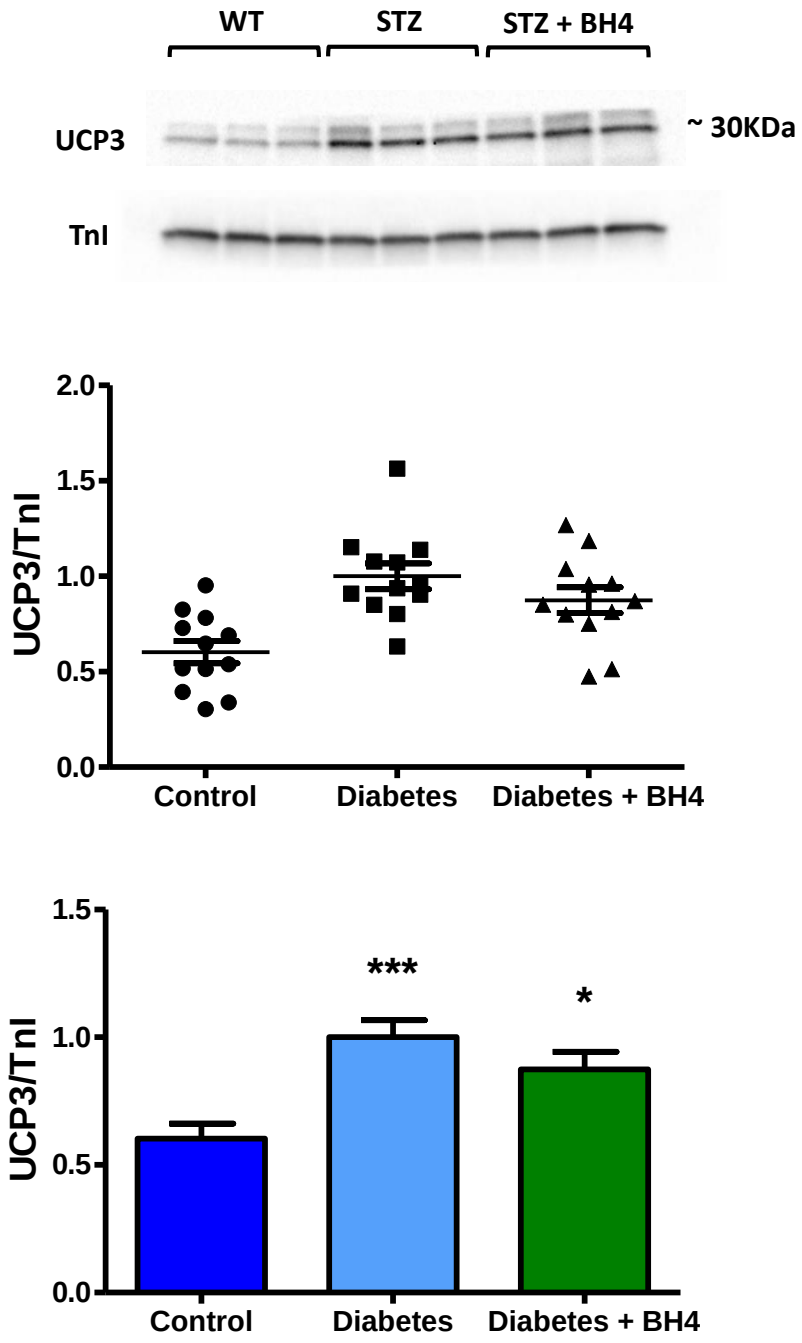


Figure 5.44. BH4 supplementation does not prevent the diabetes-induced increase in UCP3 expression.

As with WT diabetic mice, diabetic mice supplemented with BH4 still demonstrated significantly elevated levels of myocardial UCP3 compared to control mice (1-way ANOVA; *P<0.05 and ***P<0.001 vs control; n = 12).

BH4 supplementation: LV GLUT1 protein expression

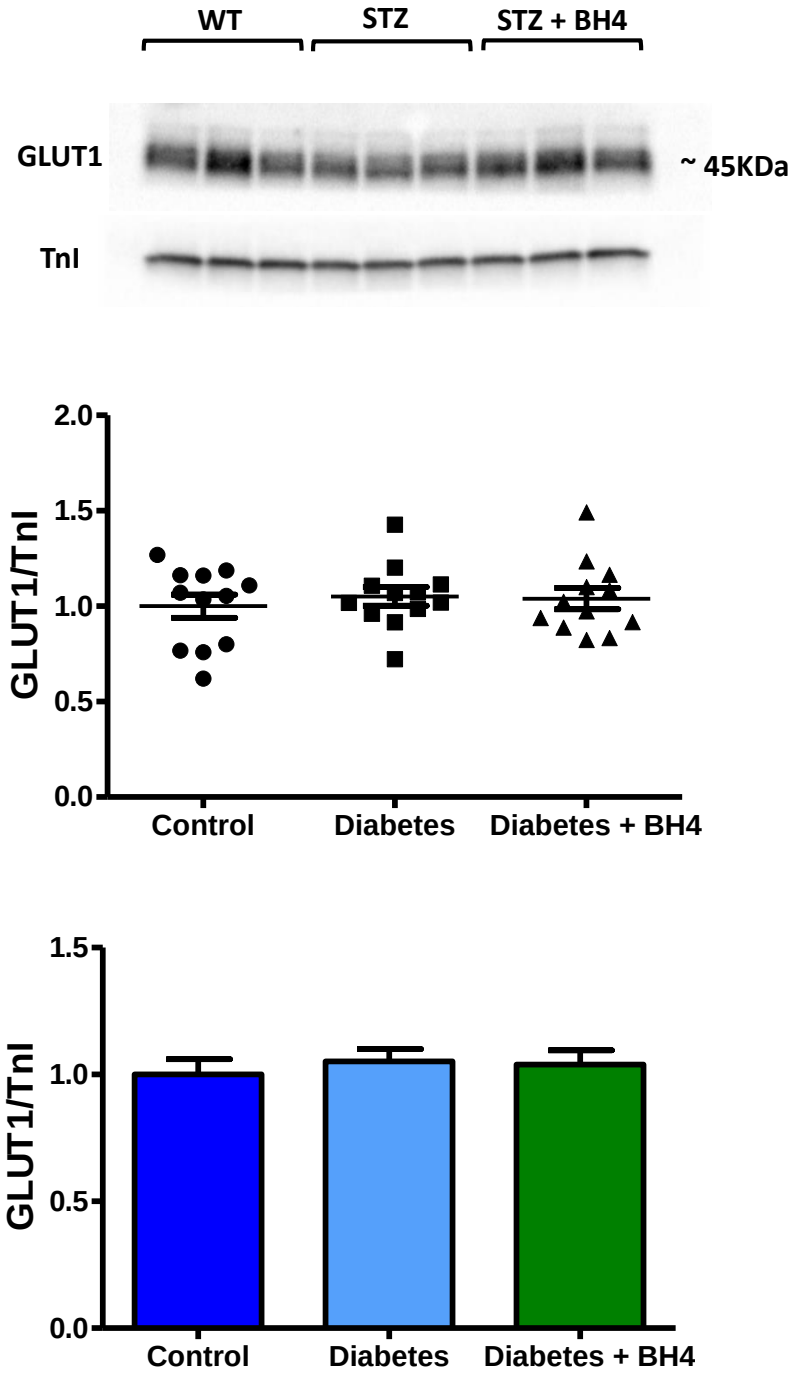


Figure 5.45. BH4 supplementation does not upregulate LV GLUT1 expression.

After 6 weeks of dietary BH4 supplementation in diabetic mice, GLUT1 expression levels remained unchanged compared to placebo-treated control and diabetic mice (n = 12).

Conclusions

The main findings presented in this chapter demonstrate that:

1. Cardiomyopathy is evident after 12 weeks, but not merely 4 weeks, of STZ-induced type 1 diabetes.

2. In contrast to the hyperglycaemic signalling in the vasculature, LV dysfunction in diabetes is not a result of increased ROS generation and NOS uncoupling.

3. Following 12 weeks of hyperglycaemia, altered cardiomyocyte and myofilament function was associated with changes to myocardial metabolism and collagen content.

4. Overexpression of the mGCH1 transgene protects against diabetic cardiomyopathy.

5. While mGCH1 overexpression improves mitochondrial energetics, BH4 supplementation would likely be protective via a mechanism independent from restoring metabolic flexibility.

Discussion

Few of the comprehensive studies of the phenotype and underlying mechanisms of STZ-induced diabetic cardiomyopathy investigate the temporal effects during the development of the disease. Studies that observe serious cardiomyopathy after only a few weeks may be confounded by the severity of the STZ dose and the potential for extra-pancreatic toxicity (427, 428). The fact that the model used in my study employed a low-dose STZ protocol with reduced severity and negligible mortality, may go some way to explaining why LV dysfunction was not observed until 12 weeks of sustained hyperglycaemia. These results do however, contrast the findings of Katare et al. using the same protocol and similar functional measurements (176). One reason for this disparity could be variation in the sensitivity of the 2 different mouse strains to STZ-induced diabetic complications, as has been suggested previously (429). In addition, only 2 time-points were investigated in my study, thus it is possible that the onset of diabetic cardiomyopathy may have occurred at some intermediate point between 4 and 12 weeks, as reported by Westerman et al. (353).

A particularly interesting finding was the lack of increased myocardial O_2^- production in diabetic mice, despite obvious LV functional impairment. Although some studies have implicated ROS as a possible driver of the cardiomyopathy observed in those diabetes models (396, 397), the reports and the underlying mechanisms are far less comprehensive as compared to those described in the vasculature. This may be due, in part, to the actual glucose concentration that the cardiomyocyte is exposed to i.e. does hyperglycaemia translate to high intracellular glucose in the setting of insulin insufficiency? Whilst glucose transport into vascular endothelial cells is largely unregulated through the action of GLUT1, cardiomyocytes rely more heavily on transport through GLUT4, a process which is insulin-mediated (182, 430). In this case, it is perhaps not surprising that the cardiomyocyte might be less vulnerable to the damaging effects of excess glucose originally described by Brownlee et al. in the endothelium (74, 311). This would be consistent with the results of my study, which indicate no diabetes-induced increase in hexosamine or polyol pathway flux; no pro-inflammatory response downstream of PKCβ activation; and no increase in AGE-RAGE signalling. This study also extensively investigated the underlying precipitator of these cellular events - oxidative stress. Direct measurements of ROS were consistent with maintained NOS coupling and glutathione status, suggesting that diabetic cardiomyopathy proceeded without a change to redox balance.

The lack of elevated myocardial O_2^- ROS observed here is consistent with some previous reports (395, 431), but not others (392, 432). This discrepancy may be explained by the T1D rodent model used, for example, STZ-triggered versus genetically determined. Even within the pool of literature on STZ-induced diabetes, dose varies significantly, thereby generating large potential differences in insulin levels, nutrient metabolism and ectopic drug toxicity. Another consideration is compartmentalised ROS signalling. Despite no obvious indications of increased ROS in LV homogenates, it is now increasingly clear that oxido-reductive modifications can be confined both temporally and spatially within the cell (433, 434). Of particular importance are mitochondria, which are not only a major source of intracellular ROS (435), but are also one of the most vulnerable sub-cellular compartments to oxidation (436-438). In the context of diabetic cardiomyopathy, some investigators have reported

an increase in stimulated mitochondrial ROS production in the Ove26 diabetic mouse, which could be prevented by antioxidant overexpression, additionally protecting against the LV dysfunction (392, 432). However, this is different to more recent findings in a model of pre-diabetes, using a low dose STZ protocol similar to that described in my study. Herlein et al. demonstrated that the hearts from STZ-treated animals showed no increase in mitochondrial ROS production (431, 439), which is also consistent with the findings from Bugger et al. in the long term diabetic Akita mouse (395). Furthermore, in contrast to those reports in the Ove26 mouse, these more recent studies measured H_2O_2 generated directly from the mitochondria. Taken together with my data, this evidence suggests that in the early (and potentially later) stages of T1D, there is no ROS imbalance, either at the whole tissue level or localised to the mitochondria. However, it should be noted that only immediate O_2^- production, as well as glutathione and biopterin status were measured in LV homogenates as a proxy of ROS balance. One can therefore not exclude the potential for longer term, cumulative oxidative stress without measurement of additional markers, such as protein carbonylation, lipid peroxidation and malondialdehyde.

Despite the diabetes-induced impairment in cardiomyocyte function and calcium handling, it was interesting to observe no expression changes in those relevant EC-coupling components, notably PLB, SERCA and NCX. Whilst reports of NCX downregulation in animal models of diabetic cardiomyopathy are few (356, 398), decreased SERCA expression has been described extensively (172, 352, 382, 386, 388), consistent with the dominant role of SERCA in rodents for cardiomyocyte Ca^{2+} extrusion (440). In addition, some of these studies report accompanying increases in PLB expression, or reduced PLB-Ser^{16} phosphorylated fractions, disrupting the SERCA:PLB ratio and similarly inhibiting calcium reuptake (352, 361, 381, 386).

The disparity between these reports and my results may be due to either the presence or absence of myocardial oxidative stress, as well as the potential onset of downstream mechanisms. For example, the downregulation in SERCA and NCX described by Wold et al. occurred on a background of increased

cardiomyocyte O_2^- production and reduced glutathione status (398). In other studies, Bidasee and colleagues attributed the abnormalities in RyR, SERCA and PLB expression and function to the intracellular AGE modifications brought on in the diabetic state (385, 386). Furthermore, some of these authors have shown that the alterations in PLB and SERCA expression are associated with increased O-GlcNAcylation (361, 381, 382); moreover, inhibition of hexosamine pathway flux normalised expression levels and attenuated the LV dysfunction in diabetes (381). It is also worth noting that in several of the other abovementioned studies, SERCA, NCX and PLB expression changes occur not in the absence of oxidative stress, but rather in the absence of measured oxidative stress (172, 352, 354, 356). It is possible that increased ROS was still a potential driver of diabetic cardiomyopathy in these studies, yet the authors simply prioritised other experimental assessments, namely the functional cardiac phenotype. Together, these data suggest that where altered expression profiles of EC-coupling proteins impact LV function in diabetes, the presence of oxidative stress may be required to influence that expression, potentially via the onset of pathways associated with high intracellular glucose. This would be consistent with my findings of both unchanged levels of these proteins and a lack of ROS imbalance, suggesting a different underlying mechanism for the observed cardiomyopathy.

Although normal EC-coupling was not limited by protein expression, calcium cycling during each cardiac cycle is heavily ATP dependent, making it vulnerable to limitations on energy supply. This is because SERCA reportedly requires a very high free energy (released from ATP hydrolysis) for Ca^{2+} transport (441), causing it to be sensitive to changes in the creatine kinase/phosphocreatine system. It is hypothesised that cytosolic CK activity, unlike mitochondrial CK activity, exists in a state near to equilibrium, making it less susceptible to fluctuations in energy metabolism (442, 443). In the context of my results, LVs from diabetic mice displayed normal cytosolic CK activity, yet reduced mitochondrial CK activity, indicating diminished mitochondrial shuttling of high energy phosphates. This could suggest reduced stimulation of oxidative phosphorylation in the ETC due to the decreased ability of CK to maintain an appropriate [ATP]/[ADP] ratio in the mitochondrial matrix. Similarly, Kupriyanov et

al. have shown that CK activity in the heart correlates with increased ATP synthesis rates, suggesting that defects in oxidative phosphorylation will translate to reduced available energy for use by the cytosolic machinery (444). This is in overall agreement with the purported role of the CK/PCr shuttle in the heart, acting more like an energetic transport system versus the buffer function required in fast-twitch, glycolytic tissues, namely skeletal muscle (442). My data is also consistent with earlier reports of diabetic cardiomyopathy in STZ-treated animals, where authors have described impaired CK/PCr shuttling in diabetic hearts, as well as decreases in cardiac efficiency (177-179).

Disrupted mitochondrial energetics, decreased cardiac efficiency and ultimately LV dysfunction may be elicited by a mismatch in fuel supply and demand. In clinical studies of both T1D and T2D it has been observed that the myocardium shifts substrate metabolism, away from glucose and towards increased FA utilisation (180, 181, 445). Although FA oxidation contributes up to 70% of the ATP produced by the heart at rest, increased workload under stress critically requires the utilisation of glucose (446, 447). Thus, in the setting of insulin insufficiency (including resistance) the heart is metabolically inflexible, unable to switch between available substrates to maintain stable ATP levels. This situation has been implicated in animal models of diabetic cardiomyopathy, where several studies have reported changes in the expression of genes and respective proteins involved in FA and glucose transport and oxidation (172, 176, 355, 391). It is interesting that the same modifications were not observed in my results, where key metabolic proteins such as MCAD, PDK4 and αKGD remained unaltered in diabetic state. This was perhaps less surprising in the case of PPARα, where activation rather than expression may be more heavily influenced by fatty acid ligands (365, 421, 422). Overall, this data might suggest that diabetic cardiomyopathy preceded without changes to β-oxidation, inhibition of glucose oxidation (via the Randle cycle) or TCA cycle flux. However, Bugger et al. equally showed in the Akita mouse that there were no changes to the cardiac expression of genes involved in FA metabolism, yet still increased FA oxidation (395). This indicates the possibility of a shift in cardiac fuel substrates and metabolic activity even in the absence of considerable changes in protein expression.

Many of the studies that refer to this loss of metabolic flexibility in T1D actually attribute the cardiomyopathy to excessive FA utilisation and ultimately lipotoxicity (172, 355, 365). However, consistent with the unchanged protein expression in my study, there were also no observations of increased lipid staining in diabetic hearts. On the contrary, diabetic mice actually exhibited undetectable levels of cardiac lipid deposition. This may be explained by considering the available lipid supply to the heart, i.e. the levels of circulating plasma FA. In STZ-treated mice, How et al. demonstrated decreases in cardiac efficiency which could not be explained by increases in FA oxidation (and the necessary increased oxygen requirement) (178). They detected no elevation in plasma lipids concomitant with no visible body fat, similar to those physical observations of mice in my study. This would also be consistent with the findings from STZ-treated sheep, where Ramanathan et al. did report impaired LV oxygen utilisation with the decrease in cardiac efficiency, in this case also observing increased plasma FA and FA uptake (179). Therefore, whilst insulin insufficiency may predispose the heart to metabolic inflexibility, the relative upregulation of lipid utilisation is likely still highly dependent on delivery. This has been highlighted in T1D patients, where Peterson et al. have shown that myocardial FA utilisation is the same in diabetic and control subjects when plasma FA levels are matched (448).

A switch in myocardial metabolic substrates is suggested in my data by the massively elevated expression of UCP3 in WT diabetic mice. While the role of UCP3 is still not fully understood, the clearest relationship demonstrates that UCP3 is upregulated in skeletal and cardiac muscle upon increases in FA levels (418, 449). This is supported by studies in starved mice almost exclusively metabolising FA, where cardiac mitochondria show increased UCP3 expression and reduced Ox-Phos efficiency, as illustrated by increased proton leak and a decreased ADP/O ratio (450). In the state of T1D cardiomyopathy, Arikawa et al. have shown reduced glucose utilisation in perfused hearts, in association with an upregulation of cardiac UCP3 gene and protein expression (391). Similar findings were reported in the mouse by Pulinilkunnil et al., who described increased UCP3 expression in association with a switch to FA utilisation and TAG accumulation (355). Metabolic dysregulation due

to excessive FA utilisation would be consistent with my results on impaired creatine kinase activity, together suggesting reduced phosphate shuttling out of the mitochondria. This would also be supported by several earlier reports in rodent models of T1D, which have described significant reductions in the levels of high energy phosphates in the myocardium (451-453).

It is particularly interesting that UCP3 expression was elevated even at the 4 week time point, before the onset of a functional cardiomyopathy. This suggests that a shift in metabolic substrates occurs relatively quickly and may precede the later development of LV dysfunction. Under this paradigm it is possible that the myocardium retains some metabolic headroom, able to tolerate some degree of excessive FA utilisation before the disruption in mitochondrial energetics becomes functionally limiting. While this is speculative, Herlein et al. have shown discordance between respiratory coupling and ATP production from the cardiac mitochondria of STZ-treated rats (431). Furthermore, in the insulin resistant ob/ob mouse, Buchanan et al. demonstrated that increased FA oxidation and decreased glucose oxidation occurred before any decline in cardiac function (454). This hypothesis may also be rationalised by returning to the consideration of substrate delivery. ATP synthesis may be maintained in the early stages of diabetes (4 weeks) when there is the capacity to increase FA delivery via lipolysis from available body fat. However, this may not be the case after longer term diabetes (12 weeks), at which point substrate demand exceeds supply (with potentially concomitant mitochondrial dysregulation), eventually leading to impaired ATP production.

Although a direct dissipation of mitochondrial membrane potential through UCP3 may still be possible, UCP3 upregulation in the context of diabetes is not necessarily indicative of uncoupled Ox-Phos. For example, in the Akita diabetic mouse Bugger et al. reported increased myocardial UCP3 gene and protein expression, despite no evidence of mitochondrial uncoupling or a decrease in cardiac efficiency (395). This was similarly reported by Herlein et al., who showed that respiratory coupling in cardiac mitochondria was not decreased in T1D, despite the increase in UCP3 (431). These studies, as well as others (455-457), have raised questions over the exact role of UCP3, while additional studies

in cardiac and skeletal muscle suggest that UCP3 is unlikely to be responsible for mitochondrial uncoupling (458-460).

However, it has also been proposed that UCP3 expression and activity may be elevated as a protective mechanism against oxidative stress. While UCP3 gene deletion appears to lead to elevated mitochondrial superoxide production (455, 461), Echtay et al. have shown that O_2^- is actually required to induce uncoupling through UCP3 (462). Additionally, Talbot et al. have suggested a negative feedback mechanism, in which endogenous ROS production activates UCP3, subsequently dissipating the mitochondrial membrane potential to reduce further ROS generation (namely from complex I). This is also supported by the work of Bugger et al., who have suggested that mitochondrial uncoupling in diabetes may require a coexistent increase in ROS production, as has been described in models of T2D (395, 463, 464). Whilst it is possible that a punctuated oxidative stressor in the onset of diabetic cardiomyopathy may have induced UCP3, other adaptive responses of the uncoupling protein should not be excluded. For example, some evidence suggests that UCP3 may prevent the accumulation of damaging lipid peroxides in the inner mitochondrial matrix (465), which would be consistent with the correlation between UCP3 levels and FA metabolism.

While an energy deficit may underlie the LV dysfunction observed in WT diabetic mice, improved energy availability may similarly contribute to the preserved LV performance in mGCH1-Tg mice. This is evident from the sustained mitochondrial CK activity in control and diabetic mice overexpressing mGCH1, suggesting that the transgene conferred improvements in metabolic flexibility of the myocardium. This is supported by the significant increases in the expression of the GLUT1 glucose transporter in mGCH1-Tg mice. GLUT4 has a higher affinity for glucose than GLUT1 and is the main mediator of glucose uptake in insulin-responsive tissues (466). Tian et al. have indeed shown that insulin stimulates a pronounced and rapid uptake of glucose into the myocardium; an effect that is abolished in those hearts with specific GLUT4 deficiency (430). These authors also showed that the loss of GLUT4-mediated transport led to compensatory increases in the role of GLUT1 to maintain

glucose uptake, as has been described in other cases of cardiac dysfunction (467, 468). In the case of diabetes, impaired glucose utilisation would correspond with the unchanged GLUT1 expression observed in WT diabetic mice. Unaltered basal glucose uptake in these mice would be consistent with the lack of metabolic flexibility in the myocardium, while improved GLUT1-mediated transport in mGCH1-Tg hearts may have subsequently helped to preserve mitochondrial function. In addition, Wheeler et al. have shown that stimulated mitochondrial uncoupling (with FCCP) causes a decrease in glucose uptake in perfused rat hearts, possibly due to rapid ATP depletion or a change to local redox state (469, 470). Together this suggests that uncoupling in WT diabetic hearts may have contributed further to reducing glucose utilisation; a process that was averted in mGCH1-Tg hearts by preventing the stringency in substrate use.

The mechanism of this GLUT1 upregulation in mGCH1-Tg hearts is still unclear, but it could potentially be attributed to the increase in NOS activity in transgenic mice and the role of the cellular energy sensor AMPK. Several studies have reported the influence of AMPK on glucose transport, through both improvements in GLUT translocation and activity, as well as preventing GLUT internalisation (471-477). While AMPK can activate eNOS and nNOS through serine phosphorylation (478-480), more recently Li et al. have shown that NO may be able to activate glucose uptake in cardiac papillary muscle through an effect on AMPK (420). This may be partially mediated through threonine^{172} phosphorylation of AMPK, as has been suggested in endothelial cells by Zhang et al. (481). Interestingly, Wang et al. have also explored a direct link between AMPK and BH4, demonstrating that AMPK can suppress the proteasomal degradation of GCH1 induced by high glucose exposure (482, 483). Together it is possible that BH4, NOS and AMPK could all exist within a positive feedback loop, upon which activation could lead to increased GLUT activity and improved glucose transport. LV homogenates from mGCH1-Tg mice showed no indication of altered ACC-ser^{79} phosphorylation, a primary downstream target of AMPK involved in the regulation of FA biosynthesis and oxidation. While this result might suggest no increase in AMPK activity, Park et al. have pointed out that there may be little correlation between AMPK and ACC activity under some circumstances (484). In addition,

Zordoky et al. recently demonstrated in the heart that abolition of ACC phosphorylation by AMPK (through an ACC double knock-in mouse) did not alter the extent of FA oxidation (485). While AMPK in itself may be difficult to measure due to its labile nature (486), these data reveal the possible limitations of ACC status as a surrogate marker for AMPK, suggesting that a shift in substrate utilisation in mGCH1-Tg hearts may not be dependent on the AMPK-mediated inhibition of ACC.

Improved energy availability in mGCH1-Tg hearts may have also been attributed to the observed enhancement in glutathione status, via post-translational glutathionylation of cysteine residues. For example, Zmijewski et al. have shown that (S-)glutathionylation can activate AMPK subunits (487), which could be another potential mechanism for an increase in glucose utilisation via AMPK. In addition, Vesce et al. showed that GSH depletion reduced ATP transport through adenine nucleotide translocase (ANT), which might suggest that increased GSH levels could augment ATP flux across the inner mitochondrial membrane (488). However, this is contradicted by the findings of Queiroga et al., who reported that it was in fact the oxidised form, GSSG, which stimulated the ADP/ATP exchange rate of ANT (489). An interesting study more recently has implicated glutathione status with the regulation of mitochondrial uncoupling. In isolated mitochondria Mailloux et al. have demonstrated glutathionylation of UCP3, acting as an “off-switch” to inhibit state 4 respiration (490). Independent of changes to protein expression, increased glutathionylation of UCP3 could represent a further way in which mGCH1-Tg mice were safeguarded against impaired mitochondrial ATP production.

Glutathionylation has also been identified recently as a modification on myofilaments, as reported by Mollica et al., who showed that glutathionylation of TnI increased the calcium sensitivity of skeletal muscle fibres (491). In the myocardium Lovelock et al. have revealed glutathionylation of a different myofilament protein, myosin binding protein C (MyBP-C), which was associated with enhanced Ca^{2+} responsiveness (possibly via altered cross-bridge kinetics) in a model of diastolic dysfunction (492, 493). Although each of these myofilament modifications cannot be ruled out in my study, it is unlikely to explain the improvement in cardiomyocyte performance. In the case of the former, mGCH1

overexpression actually caused Ca^{2+} desensitisation in control mice; in the case of the latter, there were no observed differences in the rates of cross-bridge cycling between groups.

Alternatively, glutathione may have modified available cysteines on components of the EC-coupling machinery, potentially increasing their activity and overall Ca^{2+} handling. This may have occurred through the reaction of increased available NO (in mGCH1-Tg hearts) with glutathione, to produce the modifying agent nitrosoglutathione (494). Regulation by both glutathione and the nitroxyl ion has been reported to increase the activity of SERCA, potentially also requiring the concomitant modification of PLB (495-497). However, what these studies have also highlighted is that the modifications are detectable in an environment that is already oxidative in nature, often stimulated by other agents of redox imbalance e.g. peroxynitrite (497). Furthermore, other authors have pointed out that target modification by glutathionylation, and even the generation of the nitroxyl ion itself, is heavily tied to the overall redox status of the cell (498, 499). Taking this into consideration, it might be difficult to suggest significant post-translational activity by glutathionylation in mGCH1-Tg hearts, where there is no evidence of oxidative stress and the increase in glutathione levels remains as GSH relative to GSSG.

If one is to accept that mGCH1 overexpression prevented the diabetes-induced energy deficit through increased BH4 bioavailability and NOS activity, then one might also expect any functional benefits of increased exogenous BH4 to act through the same mechanism. Interestingly however, in BH4-supplemented diabetic mice, immunoblots revealed no increase in GLUT1 expression, while UCP3 remained upregulated, as in those diabetic mice fed placebo. If the alterations to GLUT1 and UCP3 protein expression are consistent with the changes to mitochondrial energetics (through possible substrate utilisation and uncoupling), then these results suggest that direct BH4 supplementation may potentially act through a different pathway relative to enhanced *de novo* BH4 biosynthesis.

It is interesting to note that while BH4 levels were significantly elevated in both the plasma and the LV of supplemented mice, the BH4:BH2 ratio was reduced in the plasma and yet was normalised in

the LV. This suggests that the BH4 salvage pathway may be upregulated in the myocardium during increased import of oxidised BH2, possibly due to increased activity of dihydrofolate reductase (DHFR). The relative importance of this pathway has been explored in cultured endothelial cells by Crabtree et al., who showed that both pharmacological inhibition and genetic knockdown of DHFR led to the oxidation of BH4 to BH2 and subsequent eNOS uncoupling. This change in BH4:BH2 ratio was not observed in cells with knockdown of GCH1, despite the reduction in total biopterins, suggesting that the *de novo* pathway dictates overall BH4 biosynthesis, while DHFR is more important in maintaining the relative levels of reduced and oxidised BH4 (166). In addition, these authors have since observed the role of DHFR *in vivo*, where its inhibition with methotrexate instigated eNOS uncoupling in an experimental setting of BH4 deficiency (the hph-1 mouse) (156).

Despite no evidence for a role of NOS uncoupling in WT diabetic hearts (fed placebo), it is still possible that supplemented BH4 was incorporated into the heart through increased activity of DHFR. Both *in vitro* and *in vivo* studies by Hagesawa and colleagues have shown the salvage pathway precursors sepiapterin and BH2 actually elevated cell and tissue levels of BH4 more effectively than BH4 itself (500, 501). They demonstrated the greatest surge of blood BH2 concentration after BH4 administration, suggesting systemic oxidation of circulating BH4, which would also be consistent with the limited clinical efficacy or oral BH4 supplementation that has been observed in the treatment of coronary artery disease (502).

Another interesting finding from the work of Sawabe et al. is that methotrexate (to inhibit DHFR) significantly reduced the tissue BH4:BH2 ratio, even in the group administered BH4. Furthermore, in mice that received no pterin supplementation, methotrexate was still a major determinant of the proportion of endogenous BH4 relative to BH2 (501). While this builds on the work of Crabtree et al., it also highlights that the dynamic flux of biopterin intermediates varies between specific tissues, given that methotrexate affected BH2 levels least in the liver. Although the heart was not tested and much

of the available literature focuses on the vasculature, it is an interesting prospect that increased import of BH2 into the cardiomyocyte could itself upregulate DHFR activity to improve BH4 status.

Another possibility drawn from these studies, consistent with the differential observations on metabolic protein expression in mGCH1-Tg versus BH4 supplemented mice, is that there may be an alternative, direct signalling pathway from the DHFR enzyme itself. Aside from BH4 recycling, DHFR also plays a key role in folate metabolism, catalysing the reduction reaction of dihydrofolate to tetrahydrofolate. This reaction step is critical for both purine and pyrimidine nucleotide synthesis, and the generation of 5-methyl tetrahydrofolate, which is required for downstream target methylation (503). A hallmark of myocardial stress during ischemia is delayed repletion of ATP due to impaired purine regeneration (504). In addition, Moens et al. have shown that high dose folate treatment prevents I/R injury, attributing this to sustained purine and ATP homeostasis (505). It is therefore possible that BH4 supplementation may still improve energy availability in the diabetic heart, acting instead through upregulated folate metabolism, as a result of increased DHFR activity. As for methylation, studies in isolated cardiac SR and sarcolemma have shown that phospholipid N-methylation increases Ca^{2+} extrusion through ATPase activity (506, 507). Panagia et al. have also shown that the addition of a methyl donor to the subcellular membranes of STZ-treated hearts stimulated SR Ca^{2+} pump activity to a greater extent than control hearts (508). Taken together, these studies may suggest a mechanism by which enhanced DHFR signalling may improve downstream calcium handling in the diabetic heart. It might also be worth considering the emerging role of methylation as an epigenetic regulator of gene expression. Gene profiling studies in patients with type 1 diabetes (as well as coronary artery disease and atherosclerosis) have identified regions of the genome that have abnormal methylation patterns (509-511), but the distinct functional impact of these modifications during cardiomyopathy remains unclear.

Chapter 6

Conclusions and General Discussion

This chapter is designed to summarise the key findings from my experimental work, identify any limitations of the studies, as well as highlight future directions for this line of research and the wider clinical implications.

One of the major findings from this study is that the model of STZ-induced diabetes employed here results in clear endothelial dysfunction with impaired vasodilatation in the great vessels. Particularly interesting is that 12 weeks of hyperglycaemia differentially affects the function of conduit and resistance arteries. Whilst the aorta displays dysfunction after 4 weeks of T1D, which continues through to 12 weeks, the mesenteric artery is in some way protected against the detrimental effects of high blood glucose. The vascular dysfunction observed is consistent with previous studies of diabetes in animals and human patients (5, 264-267), as is the underlying mechanism, attributed to increased oxidative stress and NOS uncoupling. I have explored the possibility that the mesenteric circulation may be more resistant to oxidative damage, perhaps due to improved antioxidant status and maintained BH4 bioavailability (324, 325).

In my hands, I have confirmed a role for NO in the compensatory vasodilatation of mesenteric arteries, in response to peri-arterial stimulation of sympathetic nerves. SNS dysregulation has been commonly associated with diabetes, particularly hyperinsulinemia and insulin resistance (512-515). However, sympathetic neuropathy has also been described in T1D (516), moreover, Ganguly et al. has shown in STZ-treated rats that plasma norepinephrine levels were elevated after 8 weeks of diabetes (517). Whilst I did not observe any indication of increased sympathetic tone in mesenteric arteries of diabetic mice (e.g. increased basal tone, heightened vasoconstriction), the extent of SNS activity in this vascular bed remains unknown. If maintained redox balance in the mesenteric artery is a potential mechanism of conferred protection against hyperglycaemia, it is entirely plausible that this would preserve both eNOS and nNOS coupling. In this way, mesenteric arteries from T1D mice might exhibit not just typical endothelium-dependent vasorelaxation, but also a normal balance of constrictor and dilator responses evoked from the perivascular nerves.

Different temporal effects have been observed between the vasculature and the myocardium following STZ treatment. Although the endothelial dysfunction is an early event (4 weeks) in the progression of diabetes, cardiomyopathy does not develop until 12 weeks post-injection, despite sustained hyperglycaemia throughout. Despite varying previous reports on the time point of LV dysfunction in diabetes (176, 349, 353-355), the results from my study suggest that different cellular conditions dictate the vulnerability of the vascular endothelium to high blood glucose, compared with the possible resistance of the cardiomyocyte. This may be attributed to the unregulated transport of glucose into the endothelial cell, likely mediated via the GLUT1 transporter, whereby it can initiate the damaging downstream pathways that have been described in detail by Brownlee and colleagues (299). This would be in contrast to the cardiomyocyte, where glucose entry is predominantly insulin-dependent through the activity of GLUT4 (182, 430). It would also therefore explain the relatively smaller body of research that has characterised the activation of these pathways in the cardiomyocyte, as well as their actual role in the development of LV dysfunction in diabetes. The possibility that T1D hearts do not exhibit excessive glucose levels would be consistent with the observation that LV from WT diabetic mice showed no indication of polyol or hexosamine pathway flux with glutathione depletion; no increase in PKCβ signalling and the onset of pro-inflammatory responses; and no sign of increased exposure to AGEs.

More importantly, the LV from these mice directly showed no elevation in ROS production, accompanied by maintained BH4 bioavailability and NOS activity. While this contradicts suggestions of oxidative stress in some studies, it is at the same time consistent with other reports that describe similar findings. Some of this discrepancy could likely be attributed to the extent of the cardiomyopathy described, and moreover, the variability in the type of animal and diabetes model used. While this is an obvious limitation, the results from this study are consistent with recent preliminary findings in the lab from human cardiac samples. An assessment of superoxide production in the left atrial appendage (LAA) of insulin-treated diabetics (randomised; age and gender matched; STICs trial placebo group) has shown no difference compared to control subjects (Figure 6.1).

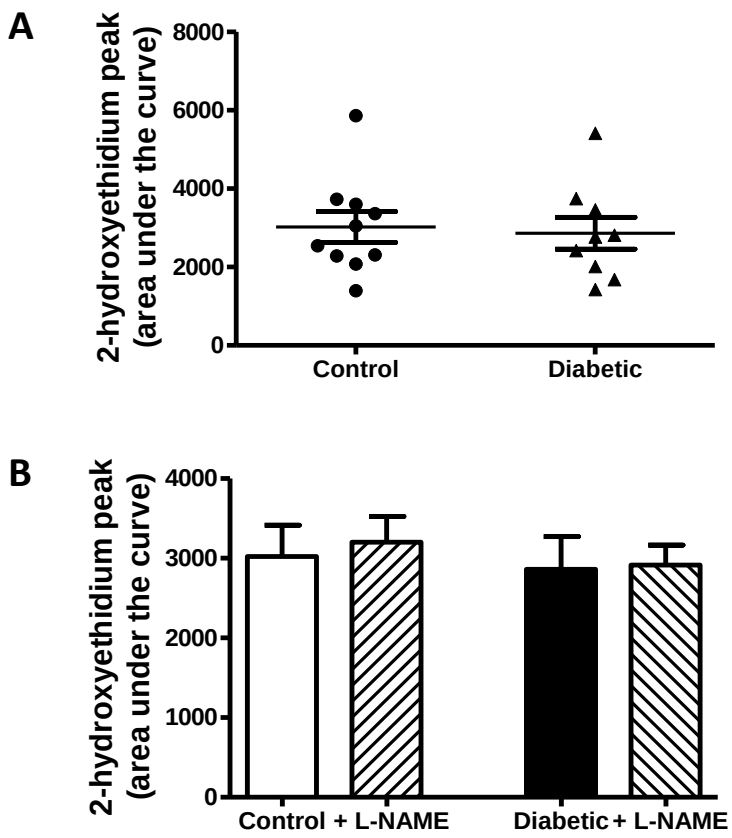


Figure 6.1. Hearts from diabetic patients show no evidence of increased oxidative stress or NOS uncoupling.

(A) Basal O_2^- production in LAA samples assessed by HPLC detection of DHE to 2-OHE conversion. **(B)** Samples from both control and diabetic subjects showed no decrease in O_2^- production upon incubation with L-NAME, indicative of the absence of NOS uncoupling (n = 10). *Experiment and data courtesy of Svetlana Reilly.*

Together these data suggest that the development of cardiac dysfunction in experimental and clinical diabetes is not synonymous with NOS uncoupling and an environment of oxidative stress. While this is in clear contrast to the pathology of the vasculature, it is not opposed by any compelling reports which extensively study the heart. The best available information has implicated iNOS uncoupling in the myocardium of STZ-treated animals, but the severity of these experimental models is high, the characterisation of the functional cardiomyopathy is limited and the measures of ROS production and NOS activity are indirect (193, 376). Overall, this might encourage us to re-evaluate our thinking of diabetes pathophysiology in different tissues and any supposition that ROS is the primary driver of dysfunction in all cell types.

The setting of insulin-deficiency may not promote high concentrations of intracellular glucose within the cardiomyocyte, rather, a lack of glucose and a loss of metabolic flexibility in the myocardium may underlie the LV dysfunction. In line with studies supporting this notion (180, 181, 445), my results have demonstrated that WT diabetic mice exhibit reduced energetic transfer within the mitochondria, potentially resulting in an energy deficit and preventing the EC-coupling machinery from normal calcium cycling. A reduction in ATP may arise from inflexibility in metabolic substrate use and possibly increased cycling of fatty acid anions away from the mitochondrial matrix via UCP3 (465). Significant increases in UCP3 expression were noted only in WT diabetic mice, an effect which was evident at 4 weeks, even prior to the development of cardiomyopathy. Given that insulin is such a primary regulator of energy storage and metabolism, it is entirely reasonable that β-cell destruction would result in a rapid change to cardiomyocyte substrate utilisation. Indeed this was shown by Chatham et al. with NMR spectroscopy, where glucose oxidation was depressed in the diabetic heart after only 1 week post-treatment with STZ (518, 519). The fact that LV dysfunction was not evident until 8 weeks after potential shifts in substrate consumption suggests that the myocyte may have some inherent redundancy in metabolic pathways; a reserve that suffices until substrate delivery and ATP production truly becomes limiting.

My findings suggest that early and sustained improvements to myocardial metabolism also underlie the short and long term improvements to LV function conferred by mGCH1 overexpression. The presence of the mGCH1 transgene prevented the upregulation in UCP3 and increased the expression of GLUT1, both at 4 weeks and 12 weeks. In the long term, this was associated with preserved mitochondrial CK activity, together suggesting that the mGCH1 transgene may augment basal glucose uptake in the cardiomyocyte, promoting metabolic flexibility and inhibiting energy depletion at the level of the mitochondria. While a detailed mechanism remains unclear, a role for increased NOS activity has been explored (potentially through AMPK), as well as an auxiliary effect of cellular modifications mediated by glutathione. If mGCH1 overexpression does augment myocardial glucose uptake, one might argue that this could actually lead to excessively high intracellular glucose,

triggering the same toxic pathways of glycaemic damage, as typically discussed in the vasculature. Whilst this is a temporal possibility, the normal insulin-dependency of myocardial glucose transport perhaps makes the cardiomyocyte less prone to the same level of glucose exposure compared to the vascular endothelial cell, even with a degree of improved GLUT1-mediated basal uptake.

Despite a case being made for altered mitochondrial energetics as a root cause for the diabetic dysfunction, it is interesting to note that diabetic hearts still displayed some degree of remodelling, as evidenced by increases in collagen content. Bollano et al. showed similar increases in total collagen in rat hearts following 12 weeks of diabetes, yet found no change to the PCr/ATP ratio, arguing against altered myocardial metabolism (520). Remodelling of the extracellular matrix has been described as a causal agent in diastolic dysfunction (521-523), thus it is possible that both energetic changes and a level of fibrosis contributed to the LV dysfunction seen in my study. Having said that, the onset of ECM alterations is typically associated with pro-inflammatory responses, oxidative stress and glycation (353, 373-375, 399, 524-529). Yet my results have demonstrated no evidence for any of these underlying mechanisms, thus the cellular trigger for the observed increase in collagen content remains unclear. Additionally, while excessive collagen and cardiac fibrosis would explain the rise in passive stiffness in LV trabeculae from WT diabetic mice, it would be inconsistent with those observations in Tg diabetic hearts, which showed equivalent hydroxyproline content, yet normal passive stiffness. These data suggest that mGCH1 overexpression may act through alternative cellular pathways to prevent the increase in LV stiffness in diabetes.

One potential candidate would be the elastic sarcomeric protein titin, which is estimated to be the largest contributor to passive force in rodent cardiac muscle (530, 531). Moreover, both the relative expression of the 2 titin isoforms, N2B and N2BA, as well as their phosphorylation status, have been shown to adjust myocardial passive stiffness (532-535). While a role for BH4 or NOS in titin modification is plausible (532, 536), Jeong et al. have shown that the improvements in diastolic function conferred by BH4 treatment were not due to any changes in titin phosphorylation status

(185). The glutathionylation of titin is another potential source of altered myocardial elasticity, however, as described by Cebollada et al., GSSG appears to be the effector of this modification, likely due to disturbances in redox homeostasis (537). It may therefore be less likely to explain my observations, where oxidative stress was absent and mGCH1 overexpression instead led to enhanced GSH. It is still possible that a shift in titin isoform expression may have occurred in mGCH1-Tg hearts, towards a more compliant N2BA phenotype, which is to be elucidated soon in further studies using qPCR. Provided there may be a switch in titin isoforms, it remains unclear as to whether this results from an influence of the transgene on cardiac development or via an as yet unidentified pathway involving BH4.

My findings indicate that in the diabetic heart there is a protective effect from that BH4 originating from intracellular *de novo* synthesis, via increased GCH1 activity. Whether the same protection is observed with a supplemented exogenous source remains to be seen, and is currently being investigated. The apparent oxidation of assimilated BH4 into BH2 within the circulation seems to be reversed upon entry to the myocardium, where an overall net increase in BH4 is observed. Whilst the availability of the cofactor is augmented under both experimental scenarios (GCH1 transgene versus exogenous), results from BH4 supplementation have highlighted the potential significance of the salvage pathway and not just the mainstream channel for freshly synthesised biopterins. Just as one should be cognisant of other transgene signalling pathways that are not directly related to BH4, it is possible that any derived benefits of oral supplementation may stem from distinct mechanisms mediated by the DHFR enzyme. If BH4 is still the primary protective component, my current observations with GLUT1 and UCP3 suggest that enzymatic regeneration leads to different cellular effects downstream. Given that DHFR can redistribute to the nucleus, cytosol or mitochondria depending on intracellular conditions (538), signalling from DHFR or its BH4 product may be highly specific to subcellular compartmentalisation. It remains to be seen whether the involvement of DHFR is critical to any benefits of BH4 in this model of T1D, and the precise mechanism(s) by which oral supplementation could improve LV function. Taking my findings in the context of the available

literature, the proposed action of mGCH1 overexpression and BH4 treatment can be incorporated into a condensed working model, illustrated below in Figure 6.2.

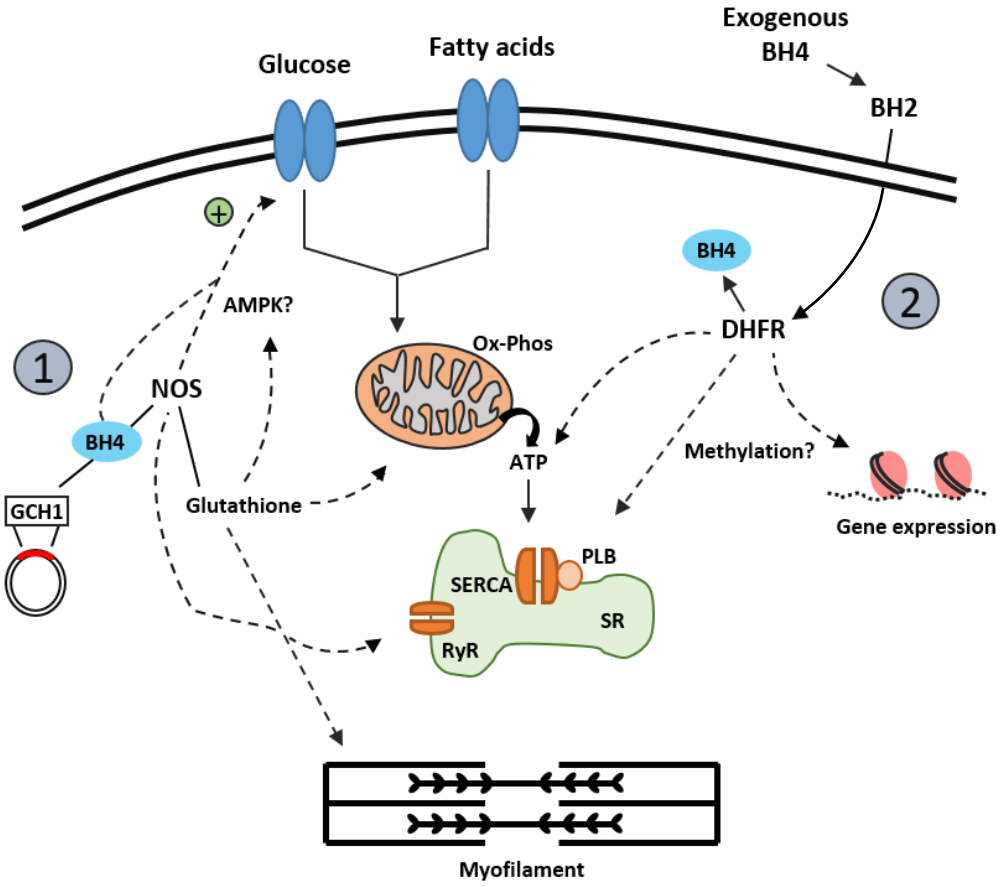


Figure 6.2. Proposed mechanisms by which mGCH1 overexpression and BH4 supplementation could prevent LV dysfunction in diabetes.

(1) BH4 augmentation through mGCH1 overexpression increases LV NOS activity, both of which may improve metabolic flexibility by increasing myocardial glucose utilisation. The capacity to switch between fuel substrates may prevent energy wastage due to mitochondrial uncoupling, overall maintaining ATP availability for the cell. Glutathionylation and nitrosylation may also play a role in the abovementioned mechanisms, as well as directly modulating the EC coupling machinery to improve contraction and relaxation. **(2)** Oral BH4 supplementation primarily oxidises to circulating BH2, which is recycled back into BH4 through DHFR. Enhanced DHFR activity could itself be a direct intracellular effector, enabling ATP repletion via folate metabolism, with additional possible effects on calcium handling and gene expression, mediated my methylation.

Limitations and areas for further study

Whilst my conclusions are based on the available findings, some experimental limitations from the study should be considered. One potential limitation would be the streptozotocin model of experimental T1D. STZ was chosen as it enables the easy induction of diabetes, which can be achieved

in mice of varying ages, as well as in genetically-altered mice. This prevents prolonged delays, which would be required if mGCH1-Tg mice were to be crossed with one of the genetic mouse models of diabetes. In addition, this model allows for the assessment of cardiovascular effects which are more specific to the state of hyperglycaemia and insulin insufficiency, without other confounding factors such as obesity, hypertension and dyslipidaemia, which normally accompany T2D.

STZ is a glucose analogue that is transported across the membrane by the GLUT2 transporter, a carrier which is primarily expressed in the pancreatic β-cell and the hepatocyte. Early studies showed that cells which did not express GLUT2 were resistant to the toxic effects of STZ (539, 540), suggesting that the liver would be the most vulnerable to any extra-pancreatic effects. Kume et al. have reported hepatotoxicity in the STZ-treated mouse, however, this occurred after an extremely high single dose of 200mg/kg (427); at this dose animal welfare is compromised and the rates of mortality severe (193). Despite being generally classified as specific to the β-cell, a few reports have described direct toxicity of STZ to cells of the kidney (541), and more importantly, the cardiomyocyte (428). It should be noted however, that Wold et al. only concluded cardiotoxicity from direct incubation of isolated LV myocytes in STZ, but not from hearts from STZ-treated rats (428). Furthermore, several studies of STZ-induced diabetes in both rats and mice have demonstrated prevention or reversal of cardiomyopathy upon treatment with insulin, suggesting that LV dysfunction is the result of the diabetic state and not from STZ toxicity directly, even at high doses (513, 542-545). Nevertheless, the Animal Models of Diabetic Complications Consortium (AMDCC) still recommends a low dose STZ-regimen with 5 consecutive daily injections of ~50mg/kg/day (194), very much consistent with the protocol used in this study.

While it is acknowledged that other T1D models could have been used in this study, the other available methods are also not without their own drawbacks. Similar to STZ, alloxan can be used for β-cell destruction, but high mortality has been reported in animals receiving diabetogenic doses, as well as inconsistencies in diabetes development in animals of the same species (546). Moreover, extra-pancreatic toxicity has been described after even light overdoses, particularly in hepatocytes and renal

tubular cells (547, 548). Within the available genetic strains, the Ove26 mouse is one of the best characterised. However, diabetes onset occurs at a very early age in the post-natal period, potentially leading to confounding myocardial adaptations from interference with cardiac development. Although this is not a disadvantage of the Akita mouse, which develops diabetes at 5-6 weeks of age, this is a more recently (*circa* 1997) created model that is generally less well characterised. It may not necessarily be a reliable model of diabetic cardiomyopathy either, as evidenced by Bugger et al., who demonstrated no overt LV dysfunction or change to cardiac efficiency (395). Perhaps more physiologically relevant would be the NOD mouse, which develops autoimmune T1D spontaneously, as a result of lymphocyte infiltration and destruction of pancreatic islets. As well as the delayed onset of overt diabetes (usually not until 10-14 weeks), incidence is highly dependent on the microbial environment. Mice therefore need to be housed in specific pathogen-free (SPF) cages, which is both expensive and logistically challenging when maintaining large colonies (549).

It is recognised that the earlier study of perivascular nerves has been conducted on the mesenteric artery of the rat and not the mouse. It is therefore difficult to infer a role for nNOS in the mesenteric circulation of the mouse given the wide inter- and intra-species variability. To build upon the work assessing vascular reactivity in the diabetic and mGCH1-Tg mouse, it would be interesting to perform peri-arterial nerve stimulation also in the setting of diabetes. These experiments could highlight whether oxidative stress occurs in both the vascular endothelial cell and the perivascular neuron, compromising nNOS as well as eNOS function, ultimately leading to impaired neurogenic vasodilatation.

A limitation of this study, as well as many others assessing isolated cardiomyocyte function, is that measurements were conducted in mechanically unloaded cells. Since cardiac mechanics is dependent on the spatial organisation of contractile and structural elements (550-552), findings in isolated myocytes may not accurately reflect *in vivo* conditions, which are also subject to preload and afterload. While my results in cardiomyocytes did largely mimic the echocardiographic assessment of

diabetic and mGCH1-Tg mice, the unloading may explain the less considerable effect of diabetes on myocyte contractile function. Another potential imperfection of these cardiomyocyte experiments was the glucose concentration of the storage buffer, which remained fixed at 5mM for both control and diabetic mice. While these conditions may more accurately reflect the levels of glucose that control cells would be exposed to *in vivo*, they may not be as representative of the glycaemic environment in the diabetic heart. While experiments could be repeated under hyperglycaemic conditions (~20mM), it is possible that cardiomyocytes from the T1D mouse do not experience this intracellular glucose concentration due to more strictly regulated membrane transport, as discussed earlier. Therefore, while the pre-set levels of glycaemia are unlikely to fully replicate those in the working diabetic heart, the true extent of this limitation still remains unclear.

Also limited at this time is available data outside of *in vitro* mitochondrial CK activity and LV immunoblots for the supposition of altered cardiac energetics in diabetic and mGCH1-Tg mice. Despite changes to energetic transfer in LV homogenates, the results do not necessarily assure that energy availability is altered *in vivo*. To substantiate this, experiments are currently underway in the perfused working heart to determine the PCr/ATP ratio and the free energy (ΔG) released from ATP hydrolysis, which are to be assessed using magnetic resonance spectroscopy. To accompany these experiments, oxygen consumption is being measured in isolated cardiomyocytes to investigate mitochondrial function and establish whether Ox-Phos truly is uncoupled in diabetic hearts. Finally, to connect the indications of altered metabolic function to substrate utilisation, arrangements have been made to measure radioactively-labelled 2-deoxyglucose uptake; ultimately this should confirm if GLUT1 upregulation translates to enhanced cardiomyocyte glucose transport.

In terms of diabetes pathophysiology, another area for general investigation in this model would be the role of other factors within the hormonal milieu that regulate blood glucose control, specifically glucagon. Since the early work of Banting and Best (553) and the subsequent Nobel Prize for its discovery, insulin has been depicted as the principal governor of cellular metabolism. Moreover, the

metabolic dysfunction that arises in the state of T1D is specifically ascribed to the lack of said insulin. From the perspective of evolution and survival, it is of far greater immediate danger that the body become *hypo*glycaemic versus *hyper*glycaemic. Hence, mammalian physiology has developed with a bias towards hormonal pathways that raise blood glucose levels e.g. glucagon, cortisol, adrenaline, thyroid and growth hormone. Although glucagon is indeed released in response to low blood glucose levels, interestingly, in the absence of insulin secretion, an increase in blood glucose also further stimulates glucagon release (554, 555). Consistent with this response, hyperglucagonaemia is a recognised phenomenon in patients with T1D (556), suggesting that glucagon dysregulation in itself may contribute significantly to disease pathogenesis. This has since been explored in the STZ model, where experiments by Lee and colleagues have demonstrated that the metabolic and physical manifestations of total β-cell destruction are absent in glucagon receptor-KO mice (557). Equally, these authors showed that restoration of the glucagon receptor (via adenoviral delivery) subsequently led to the same hyperglycaemia observed in WT mice treated with STZ (558). While these collective findings do not necessarily help explain how BH4 augmentation may prevent LV dysfunction in diabetes, they do encourage the further exploration of excessive glucagon signalling (and not just deficient insulin signalling) as a factor in the development of cardiomyopathy.

Final summary and clinical implications

This study has extensively evaluated the vascular and cardiac phenotype during the onset of T1D in the low-dose STZ mouse model. Early endothelial dysfunction is only accompanied by LV impairment after 12 weeks of hyperglycaemia, underlining the relative resistance of the myocardium over the peripheral circulation to diabetic complications. Through transgenic overexpression, BH4 is able to augment LV performance and prevent the development of cardiomyopathy. At the mechanistic level, preliminary evidence is pointing to exciting novel effects of BH4 in this experimental model, which could hold future translational potential.

The therapeutic potential of BH4 has already been recognised in the clinical setting, but so far, its overall efficacy in the treatment of cardiovascular disease still remains limited, attributed in part to its oxidation into the cofactor-null BH2 (502). Whilst optimisation of biopterin therapy remains a difficult challenge on the backdrop of oxidative stress, my results highlight the potential benefits of BH4 to LV dysfunction whereby ROS may not be the primary initial driver. This may very well be the case for those individuals afflicted with diabetic cardiomyopathy, yet who are asymptomatic and have not yet developed the vascular complications typical of redox imbalance.

Although cardiomyopathy in diabetes will likely continue to be linked with oxidative stress, the distinction between T1D and T2D should be paramount for the elucidation of underlying mechanisms, both in human patients and animal models. The build-up of damaging mitochondrial ROS is indeed a plausible mechanism in an environment of nutrient excess and forced cellular uptake, due to accompanying hyperinsulinemia. This may not necessarily be the case for T1D however, where LV impairment can instead develop during conditions of insulin deficiency. Nevertheless, hormonal imbalances and blood glucose dysregulation will ultimately still impact nutrient uptake, substrate utilisation and cellular energy flux, implicating a key role for the mitochondria, as reinforced in this study. More than its antioxidant effects or role as a cofactor, BH4 supplementation may positively influence the “powerhouse” of the cell, helping to fulfil the myocytes’ ubiquitous ATP requirement and safeguard against the functional decline in diabetes. Further studies in cells, animals and from patients should help to illuminate the way in which BH4 may confer benefit to the myocardium, provided research is not solely focussed on its classical mechanism of action, but also openly considers the wider reaches of biopterin signalling.

References

1. 2014. Available from: https://www.idf.org/worlddiabetesday/toolkit/gp/facts-figures.
2. Yancy WS, Jr., Foy M, Chalecki AM, Vernon MC, Westman EC. A low-carbohydrate, ketogenic diet to treat type 2 diabetes. Nutr Metab (Lond). 2005;2:34-41.
3. Westman EC, Yancy WS, Jr., Mavropoulos JC, Marquart M, McDuffie JR. The effect of a low-carbohydrate, ketogenic diet versus a low-glycemic index diet on glycemic control in type 2 diabetes mellitus. Nutr Metab (Lond). 2008;5:36-45.
4. Tay J, Luscombe-Marsh ND, Thompson CH, Noakes M, Buckley JD, Wittert GA, et al. A very low-carbohydrate, low-saturated fat diet for type 2 diabetes management: a randomized trial. Diabetes Care. 2014;37(11):2909-18.
5. Fowler MJ. Microvascular and Macrovascular Complications of Diabetes. Clincal Diabetes. 2008;26(2):77-82.
6. Hers HG. [The mechanism of the transformation of glucose in fructose in the seminal vesicles]. Biochim Biophys Acta. 1956;22(1):202-3.
7. Lee AY, Chung SS. Contributions of polyol pathway to oxidative stress in diabetic cataract. FASEB J. 1999;13(1):23-30.
8. Hale PJ, Nattrass M, Silverman SH, Sennit C, Perkins CM, Uden A, et al. Peripheral nerve concentrations of glucose, fructose, sorbitol and myoinositol in diabetic and non-diabetic patients. Diabetologia. 1987;30(7):464-7.
9. Gabbay KH, Merola LO, Field RA. Sorbitol pathway: presence in nerve and cord with substrate accumulation in diabetes. Science. 1966;151(3707):209-10.
10. van Heyningen R. Formation of Polyols by the Lens of the Rat with 'Sugar' Cataract. Nature. 1959;184:194-5.
11. Engerman RL, Kern TS, Larson ME. Nerve conduction and aldose reductase inhibition during 5 years of diabetes or galactosaemia in dogs. Diabetologia. 1994;37(2):141-4.
12. Chung SS, Ho EC, Lam KS, Chung SK. Contribution of polyol pathway to diabetes-induced oxidative stress. J Am Soc Nephrol. 2003;14(8 Suppl 3):S233-6.
13. Maillard LC. Action of amino acids on sugars. Formation of melanoidins in a methodical way. Compt Rend. 1912;154:66-8.
14. Thornalley PJ, Battah S, Ahmed N, Karachalias N, Agalou S, Babaei-Jadidi R, et al. Quantitative screening of advanced glycation endproducts in cellular and extracellular proteins by tandem mass spectrometry. Biochem J. 2003;375(Pt 3):581-92.
15. Giardino I, Edelstein D, Brownlee M. Nonenzymatic glycosylation in vitro and in bovine endothelial cells alters basic fibroblast growth factor activity. A model for intracellular glycosylation in diabetes. J Clin Invest. 1994;94(1):110-7.
16. Shinohara M, Thornalley PJ, Giardino I, Beisswenger P, Thorpe SR, Onorato J, et al. Overexpression of glyoxalase-I in bovine endothelial cells inhibits intracellular advanced glycation endproduct formation and prevents hyperglycemia-induced increases in macromolecular endocytosis. J Clin Invest. 1998;101(5):1142-7.
17. Portero-Otin M, Pamplona R, Ruiz MC, Cabiscol E, Prat J, Bellmunt MJ. Diabetes induces an impairment in the proteolytic activity against oxidized proteins and a heterogeneous effect in nonenzymatic protein modifications in the cytosol of rat liver and kidney. Diabetes. 1999;48(11):2215-20.
18. Vlassara H, Striker LJ, Teichberg S, Fuh H, Li YM, Steffes M. Advanced glycation end products induce glomerular sclerosis and albuminuria in normal rats. Proc Natl Acad Sci U S A. 1994;91(24):11704-8.
19. Charonis AS, Reger LA, Dege JE, Kouzi-Koliakos K, Furcht LT, Wohlhueter RM, et al. Laminin alterations after in vitro nonenzymatic glycosylation. Diabetes. 1990;39(7):807-14.
20. Charonis AS, Tsilbary EC. Structural and functional changes of laminin and type IV collagen after nonenzymatic glycation. Diabetes. 1992;41 Suppl 2:49-51.

21. Duran-Jimenez B, Dobler D, Moffatt S, Rabbani N, Streuli CH, Thornalley PJ, et al. Advanced glycation end products in extracellular matrix proteins contribute to the failure of sensory nerve regeneration in diabetes. Diabetes. 2009;58(12):2893-903.
22. Takata K, Horiuchi S, Araki N, Shiga M, Saitoh M, Morino Y. Endocytic uptake of nonenzymatically glycosylated proteins is mediated by a scavenger receptor for aldehyde-modified proteins. J Biol Chem. 1988;263(29):14819-25.
23. Vlassara H, Li YM, Imani F, Wojciechowicz D, Yang Z, Liu FT, et al. Identification of galectin-3 as a high-affinity binding protein for advanced glycation end products (AGE): a new member of the AGE-receptor complex. Mol Med. 1995;1(6):634-46.
24. Ma K, Xu Y, Wang C, Li N, Li K, Zhang Y, et al. A cross talk between class A scavenger receptor and receptor for advanced glycation end-products contributes to diabetic retinopathy. Am J Physiol Endocrinol Metab. 2014;307(12):E1153-65.
25. Pugliese G, Pricci F, Iacobini C, Leto G, Amadio L, Barsotti P, et al. Accelerated diabetic glomerulopathy in galectin-3/AGE receptor 3 knockout mice. FASEB J. 2001;15(13):2471-9.
26. Feng L, Matsumoto C, Schwartz A, Schmidt AM, Stern DM, Pile-Spellman J. Chronic vascular inflammation in patients with type 2 diabetes: endothelial biopsy and RT-PCR analysis. Diabetes Care. 2005;28(2):379-84.
27. Nin JW, Ferreira I, Schalkwijk CG, Prins MH, Chaturvedi N, Fuller JH, et al. Levels of soluble receptor for AGE are cross-sectionally associated with cardiovascular disease in type 1 diabetes, and this association is partially mediated by endothelial and renal dysfunction and by low-grade inflammation: the EURODIAB Prospective Complications Study. Diabetologia. 2009;52(4):705-14.
28. Yamamoto Y, Kato I, Doi T, Yonekura H, Ohashi S, Takeuchi M, et al. Development and prevention of advanced diabetic nephropathy in RAGE-overexpressing mice. J Clin Invest. 2001;108(2):261-8.
29. Wendt TM, Tanji N, Guo J, Kislinger TR, Qu W, Lu Y, et al. RAGE drives the development of glomerulosclerosis and implicates podocyte activation in the pathogenesis of diabetic nephropathy. Am J Pathol. 2003;162(4):1123-37.
30. Hammes HP, Martin S, Federlin K, Geisen K, Brownlee M. Aminoguanidine treatment inhibits the development of experimental diabetic retinopathy. Proc Natl Acad Sci U S A. 1991;88(24):11555-8.
31. Li J, Schmidt AM. Characterization and functional analysis of the promoter of RAGE, the receptor for advanced glycation end products. J Biol Chem. 1997;272(26):16498-506.
32. Bierhaus A, Schiekofer S, Schwaninger M, Andrassy M, Humpert PM, Chen J, et al. Diabetes-associated sustained activation of the transcription factor nuclear factor-kappaB. Diabetes. 2001;50(12):2792-808.
33. Chen Y, Akirav EM, Chen W, Henegariu O, Moser B, Desai D, et al. RAGE ligation affects T cell activation and controls T cell differentiation. J Immunol. 2008;181(6):4272-8.
34. Dunlop ME, Larkins RG. Pancreatic islets synthesize phospholipids de novo from glucose via acyl-dihydroxyacetone phosphate. Biochem Biophys Res Commun. 1985;132(2):467-73.
35. Xia P, Inoguchi T, Kern TS, Engerman RL, Oates PJ, King GL. Characterization of the mechanism for the chronic activation of diacylglycerol-protein kinase C pathway in diabetes and hypergalactosemia. Diabetes. 1994;43(9):1122-9.
36. Shiba T, Inoguchi T, Sportsman JR, Heath WF, Bursell S, King GL. Correlation of diacylglycerol level and protein kinase C activity in rat retina to retinal circulation. Am J Physiol. 1993;265(5 Pt 1):E783-93.
37. Craven PA, Davidson CM, DeRubertis FR. Increase in diacylglycerol mass in isolated glomeruli by glucose from de novo synthesis of glycerolipids. Diabetes. 1990;39(6):667-74.
38. Koya D, Jirousek MR, Lin YW, Ishii H, Kuboki K, King GL. Characterization of protein kinase C beta isoform activation on the gene expression of transforming growth factor-beta, extracellular matrix components, and prostanoids in the glomeruli of diabetic rats. J Clin Invest. 1997;100(1):115-26.

39. Koya D, King GL. Protein kinase C activation and the development of diabetic complications. Diabetes. 1998;47(6):859-66.
40. Thallas-Bonke V, Lindschau C, Rizkalla B, Bach LA, Boner G, Meier M, et al. Attenuation of extracellular matrix accumulation in diabetic nephropathy by the advanced glycation end product cross-link breaker ALT-711 via a protein kinase C-alpha-dependent pathway. Diabetes. 2004;53(11):2921-30.
41. Thallas-Bonke V, Thorpe SR, Coughlan MT, Fukami K, Yap FY, Sourris KC, et al. Inhibition of NADPH oxidase prevents advanced glycation end product-mediated damage in diabetic nephropathy through a protein kinase C-alpha-dependent pathway. Diabetes. 2008;57(2):460-9.
42. Cai W, Torreggiani M, Zhu L, Chen X, He JC, Striker GE, et al. AGER1 regulates endothelial cell NADPH oxidase-dependent oxidant stress via PKC-delta: implications for vascular disease. Am J Physiol Cell Physiol. 2010;298(3):C624-34.
43. Adamis AP, Miller JW, Bernal MT, D'Amico DJ, Folkman J, Yeo TK, et al. Increased vascular endothelial growth factor levels in the vitreous of eyes with proliferative diabetic retinopathy. Am J Ophthalmol. 1994;118(4):445-50.
44. Faries PL, Rohan DI, Takahara H, Wyers MC, Contreras MA, Quist WC, et al. Human vascular smooth muscle cells of diabetic origin exhibit increased proliferation, adhesion, and migration. J Vasc Surg. 2001;33(3):601-7.
45. Yamamoto T, Nakamura T, Noble NA, Ruoslahti E, Border WA. Expression of transforming growth factor beta is elevated in human and experimental diabetic nephropathy. Proc Natl Acad Sci U S A. 1993;90(5):1814-8.
46. Iwano M, Kubo A, Nishino T, Sato H, Nishioka H, Akai Y, et al. Quantification of glomerular TGF-beta 1 mRNA in patients with diabetes mellitus. Kidney Int. 1996;49(4):1120-6.
47. Lee HS, Moon KC, Song CY, Kim BC, Wang S, Hong HK. Glycated albumin activates PAI-1 transcription through Smad DNA binding sites in mesangial cells. Am J Physiol Renal Physiol. 2004;287(4):F665-72.
48. Ziyadeh FN, Hoffman BB, Han DC, Iglesias-De La Cruz MC, Hong SW, Isono M, et al. Long-term prevention of renal insufficiency, excess matrix gene expression, and glomerular mesangial matrix expansion by treatment with monoclonal antitransforming growth factor-beta antibody in db/db diabetic mice. Proc Natl Acad Sci U S A. 2000;97(14):8015-20.
49. Sayeski PP, Kudlow JE. Glucose metabolism to glucosamine is necessary for glucose stimulation of transforming growth factor-alpha gene transcription. J Biol Chem. 1996;271(25):15237-43.
50. McClain DA, Paterson AJ, Roos MD, Wei X, Kudlow JE. Glucose and glucosamine regulate growth factor gene expression in vascular smooth muscle cells. Proc Natl Acad Sci U S A. 1992;89(17):8150-4.
51. Akimoto Y, Kreppel LK, Hirano H, Hart GW. Hyperglycemia and the O-GlcNAc transferase in rat aortic smooth muscle cells: elevated expression and altered patterns of O-GlcNAcylation. Arch Biochem Biophys. 2001;389(2):166-75.
52. Daniels MC, Kansal P, Smith TM, Paterson AJ, Kudlow JE, McClain DA. Glucose regulation of transforming growth factor-alpha expression is mediated by products of the hexosamine biosynthesis pathway. Mol Endocrinol. 1993;7(8):1041-8.
53. Nerlich AG, Sauer U, Kolm-Litty V, Wagner E, Koch M, Schleicher ED. Expression of glutamine:fructose-6-phosphate amidotransferase in human tissues: evidence for high variability and distinct regulation in diabetes. Diabetes. 1998;47(2):170-8.
54. Ray PD, Huang BW, Tsuji Y. Reactive oxygen species (ROS) homeostasis and redox regulation in cellular signaling. Cell Signal. 2012;24(5):981-90.
55. Trachootham D, Alexandre J, Huang P. Targeting cancer cells by ROS-mediated mechanisms: a radical therapeutic approach? Nat Rev Drug Discov. 2009;8(7):579-91.
56. Andersen JK. Oxidative stress in neurodegeneration: cause or consequence? Nat Med. 2004;10 Suppl:S18-25.

57. Paravicini TM, Touyz RM. Redox signaling in hypertension. Cardiovasc Res. 2006;71(2):247-58.
58. Sugamura K, Keaney JF, Jr. Reactive oxygen species in cardiovascular disease. Free Radic Biol Med. 2011;51(5):978-92.
59. Korshunov SS, Skulachev VP, Starkov AA. High protonic potential actuates a mechanism of production of reactive oxygen species in mitochondria. FEBS Lett. 1997;416(1):15-8.
60. Chen Q, Vazquez EJ, Moghaddas S, Hoppel CL, Lesnefsky EJ. Production of reactive oxygen species by mitochondria: central role of complex III. J Biol Chem. 2003;278(38):36027-31.
61. St-Pierre J, Buckingham JA, Roebuck SJ, Brand MD. Topology of superoxide production from different sites in the mitochondrial electron transport chain. J Biol Chem. 2002;277(47):44784-90.
62. Mobbs CV, Mastaitis JW, Zhang M, Isoda F, Cheng H, Yen K. Secrets of the lac operon. Glucose hysteresis as a mechanism in dietary restriction, aging and disease. Interdiscip Top Gerontol. 2007;35:39-68.
63. Nishikawa T, Edelstein D, Du XL, Yamagishi S, Matsumura T, Kaneda Y, et al. Normalizing mitochondrial superoxide production blocks three pathways of hyperglycaemic damage. Nature. 2000;404(6779):787-90.
64. Vikramadithyan RK, Hu Y, Noh HL, Liang CP, Hallam K, Tall AR, et al. Human aldose reductase expression accelerates diabetic atherosclerosis in transgenic mice. J Clin Invest. 2005;115(9):2434-43.
65. Bravi MC, Pietrangeli P, Laurenti O, Basili S, Cassone-Faldetta M, Ferri C, et al. Polyol pathway activation and glutathione redox status in non-insulin-dependent diabetic patients. Metabolism. 1997;46(10):1194-8.
66. Lou MF, Dickerson JE, Jr., Garadi R, York BM, Jr. Glutathione depletion in the lens of galactosemic and diabetic rats. Exp Eye Res. 1988;46(4):517-30.
67. Wu G, Haynes TE, Li H, Yan W, Meininger CJ. Glutamine metabolism to glucosamine is necessary for glutamine inhibition of endothelial nitric oxide synthesis. Biochem J. 2001;353(Pt 2):245-52.
68. Kaneto H, Xu G, Song KH, Suzuma K, Bonner-Weir S, Sharma A, et al. Activation of the hexosamine pathway leads to deterioration of pancreatic beta-cell function through the induction of oxidative stress. J Biol Chem. 2001;276(33):31099-104.
69. Koya D, Lee IK, Ishii H, Kanoh H, King GL. Prevention of glomerular dysfunction in diabetic rats by treatment with d-alpha-tocopherol. J Am Soc Nephrol. 1997;8(3):426-35.
70. Paneni F, Mocharla P, Akhmedov A, Costantino S, Osto E, Volpe M, et al. Gene silencing of the mitochondrial adaptor p66(Shc) suppresses vascular hyperglycemic memory in diabetes. Circ Res. 2012;111(3):278-89.
71. Cerami A. Accumulation of advanced glycosylation endproducts on proteins and nucleic acids: role in ageing. Prog Clin Biol Res. 1985;195:79-90.
72. Scivittaro V, Ganz MB, Weiss MF. AGEs induce oxidative stress and activate protein kinase C-beta(II) in neonatal mesangial cells. Am J Physiol Renal Physiol. 2000;278(4):F676-83.
73. Yan SD, Schmidt AM, Anderson GM, Zhang J, Brett J, Zou YS, et al. Enhanced cellular oxidant stress by the interaction of advanced glycation end products with their receptors/binding proteins. J Biol Chem. 1994;269(13):9889-97.
74. Du X, Matsumura T, Edelstein D, Rossetti L, Zsengeller Z, Szabo C, et al. Inhibition of GAPDH activity by poly(ADP-ribose) polymerase activates three major pathways of hyperglycemic damage in endothelial cells. J Clin Invest. 2003;112(7):1049-57.
75. Sawa A, Khan AA, Hester LD, Snyder SH. Glyceraldehyde-3-phosphate dehydrogenase: nuclear translocation participates in neuronal and nonneuronal cell death. Proc Natl Acad Sci U S A. 1997;94(21):11669-74.
76. Madsen-Bouterse S, Mohammad G, Kowluru RA. Glyceraldehyde-3-phosphate dehydrogenase in retinal microvasculature: implications for the development and progression of diabetic retinopathy. Invest Ophthalmol Vis Sci. 2010;51(3):1765-72.

77. Garcia Soriano F, Virag L, Jagtap P, Szabo E, Mabley JG, Liaudet L, et al. Diabetic endothelial dysfunction: the role of poly(ADP-ribose) polymerase activation. Nat Med. 2001;7(1):108-13.
78. Ding H, Aljofan M, Triggle CR. Oxidative stress and increased eNOS and NADPH oxidase expression in mouse microvessel endothelial cells. J Cell Physiol. 2007;212(3):682-9.
79. Balteau M, Tajeddine N, de Meester C, Ginion A, Des Rosiers C, Brady NR, et al. NADPH oxidase activation by hyperglycaemia in cardiomyocytes is independent of glucose metabolism but requires SGLT1. Cardiovasc Res. 2011;92(2):237-46.
80. Chen F, Qian LH, Deng B, Liu ZM, Zhao Y, Le YY. Resveratrol protects vascular endothelial cells from high glucose-induced apoptosis through inhibition of NADPH oxidase activation-driven oxidative stress. CNS Neurosci Ther. 2013;19(9):675-81.
81. Inoguchi T, Li P, Umeda F, Yu HY, Kakimoto M, Imamura M, et al. High glucose level and free fatty acid stimulate reactive oxygen species production through protein kinase C--dependent activation of NAD(P)H oxidase in cultured vascular cells. Diabetes. 2000;49(11):1939-45.
82. Rueckschloss U, Galle J, Holtz J, Zerkowski HR, Morawietz H. Induction of NAD(P)H oxidase by oxidized low-density lipoprotein in human endothelial cells: antioxidative potential of hydroxymethylglutaryl coenzyme A reductase inhibitor therapy. Circulation. 2001;104(15):1767-72.
83. Rehman AU, Dugic E, Benham C, Lione L, Mackenzie LS. Selective inhibition of NADPH oxidase reverses the over contraction of diabetic rat aorta. Redox Biol. 2013;2C:61-4.
84. Asaba K, Tojo A, Onozato ML, Goto A, Quinn MT, Fujita T, et al. Effects of NADPH oxidase inhibitor in diabetic nephropathy. Kidney Int. 2005;67(5):1890-8.
85. Zhang M, Kho AL, Anilkumar N, Chibber R, Pagano PJ, Shah AM, et al. Glycated proteins stimulate reactive oxygen species production in cardiac myocytes: involvement of Nox2 (gp91phox)-containing NADPH oxidase. Circulation. 2006;113(9):1235-43.
86. Wautier MP, Chappey O, Corda S, Stern DM, Schmidt AM, Wautier JL. Activation of NADPH oxidase by AGE links oxidant stress to altered gene expression via RAGE. Am J Physiol Endocrinol Metab. 2001;280(5):E685-94.
87. Adachi T, Fukushima T, Usami Y, Hirano K. Binding of human xanthine oxidase to sulphated glycosaminoglycans on the endothelial-cell surface. Biochem J. 1993;289 (Pt 2):523-7.
88. Desco MC, Asensi M, Marquez R, Martinez-Valls J, Vento M, Pallardo FV, et al. Xanthine oxidase is involved in free radical production in type 1 diabetes: protection by allopurinol. Diabetes. 2002;51(4):1118-24.
89. Matsumoto S, Koshiishi I, Inoguchi T, Nawata H, Utsumi H. Confirmation of superoxide generation via xanthine oxidase in streptozotocin-induced diabetic mice. Free Radic Res. 2003;37(7):767-72.
90. Lao-ong T, Chatuphonprasert W, Nemoto N, Jarukamjorn K. Alteration of hepatic glutathione peroxidase and superoxide dismutase expression in streptozotocin-induced diabetic mice by berberine. Pharm Biol. 2012;50(8):1007-12.
91. Kitada M, Kume S, Imaizumi N, Koya D. Resveratrol improves oxidative stress and protects against diabetic nephropathy through normalization of Mn-SOD dysfunction in AMPK/SIRT1-independent pathway. Diabetes. 2011;60(2):634-43.
92. Kamata K, Kobayashi T. Changes in superoxide dismutase mRNA expression by streptozotocin-induced diabetes. Br J Pharmacol. 1996;119(3):583-9.
93. Pieper GM, Langenstroer P, Siebeneich W. Diabetic-induced endothelial dysfunction in rat aorta: role of hydroxyl radicals. Cardiovasc Res. 1997;34(1):145-56.
94. Majithiya JB, Balaraman R. Time-dependent changes in antioxidant enzymes and vascular reactivity of aorta in streptozotocin-induced diabetic rats treated with curcumin. J Cardiovasc Pharmacol. 2005;46(5):697-705.
95. Kikuchi C, Kajikuri J, Hori E, Nagami C, Matsunaga T, Kimura K, et al. Aortic superoxide production at the early hyperglycemic stage in a rat type 2 diabetes model and the effects of pravastatin. Biol Pharm Bull. 2014;37(6):996-1002.

96. Tiedge M, Steffeck H, Elsner M, Lenzen S. Metabolic regulation, activity state, and intracellular binding of glucokinase in insulin-secreting cells. Diabetes. 1999;48(3):514-23.
97. Hamanishi T, Furuta H, Kato H, Doi A, Tamai M, Shimomura H, et al. Functional variants in the glutathione peroxidase-1 (GPx-1) gene are associated with increased intima-media thickness of carotid arteries and risk of macrovascular diseases in japanese type 2 diabetic patients. Diabetes. 2004;53(9):2455-60.
98. Kornhauser C, Garcia-Ramirez JR, Wrobel K, Perez-Luque EL, Garay-Sevilla ME, Wrobel K. Serum selenium and glutathione peroxidase concentrations in type 2 diabetes mellitus patients. Prim Care Diabetes. 2008;2(2):81-5.
99. Lewis P, Stefanovic N, Pete J, Calkin AC, Giunti S, Thallas-Bonke V, et al. Lack of the antioxidant enzyme glutathione peroxidase-1 accelerates atherosclerosis in diabetic apolipoprotein E-deficient mice. Circulation. 2007;115(16):2178-87.
100. Wang X, Phelan SA, Forsman-Semb K, Taylor EF, Petros C, Brown A, et al. Mice with targeted mutation of peroxiredoxin 6 develop normally but are susceptible to oxidative stress. J Biol Chem. 2003;278(27):25179-90.
101. Fatma N, Singh P, Chhunchha B, Kubo E, Shinohara T, Bhargavan B, et al. Deficiency of Prdx6 in lens epithelial cells induces ER stress response-mediated impaired homeostasis and apoptosis. Am J Physiol Cell Physiol. 2011;301(4):C954-67.
102. Hu X, Weng Z, Chu CT, Zhang L, Cao G, Gao Y, et al. Peroxiredoxin-2 protects against 6-hydroxydopamine-induced dopaminergic neurodegeneration via attenuation of the apoptosis signal-regulating kinase (ASK1) signaling cascade. J Neurosci. 2011;31(1):247-61.
103. Pacifici F, Arriga R, Sorice GP, Capuani B, Scioli MG, Pastore D, et al. Peroxiredoxin 6, a novel player in the pathogenesis of diabetes. Diabetes. 2014;63(10):3210-20.
104. Tocchetti CG, Caceres V, Stanley BA, Xie C, Shi S, Watson WH, et al. GSH or palmitate preserves mitochondrial energetic/redox balance, preventing mechanical dysfunction in metabolically challenged myocytes/hearts from type 2 diabetic mice. Diabetes. 2012;61(12):3094-105.
105. Palmer RM, Ferrige AG, Moncada S. Nitric oxide release accounts for the biological activity of endothelium-derived relaxing factor. Nature. 1987;327(6122):524-6.
106. Ignarro LJ, Buga GM, Wood KS, Byrns RE, Chaudhuri G. Endothelium-derived relaxing factor produced and released from artery and vein is nitric oxide. Proc Natl Acad Sci U S A. 1987;84(24):9265-9.
107. Hemmens B, Mayer B. Enzymology of nitric oxide synthases. Methods Mol Biol. 1998;100:1-32.
108. Matsuoka A, Stuehr DJ, Olson JS, Clark P, Ikeda-Saito M. L-arginine and calmodulin regulation of the heme iron reactivity in neuronal nitric oxide synthase. J Biol Chem. 1994;269(32):20335-9.
109. Bogdan C. Nitric oxide and the immune response. Nat Immunol. 2001;2(10):907-16.
110. Carrier GO, Fuchs LC, Winecoff AP, Giulumian AD, White RE. Nitrovasodilators relax mesenteric microvessels by cGMP-induced stimulation of Ca-activated K channels. Am J Physiol. 1997;273(1 Pt 2):H76-84.
111. Rapoport RM. Cyclic guanosine monophosphate inhibition of contraction may be mediated through inhibition of phosphatidylinositol hydrolysis in rat aorta. Circ Res. 1986;58(3):407-10.
112. Cornwell TL, Pryzwansky KB, Wyatt TA, Lincoln TM. Regulation of sarcoplasmic reticulum protein phosphorylation by localized cyclic GMP-dependent protein kinase in vascular smooth muscle cells. Mol Pharmacol. 1991;40(6):923-31.
113. Draznin MB, Rapoport RM, Murad F. Myosin light chain phosphorylation in contraction and relaxation of intact rat thoracic aorta. Int J Biochem. 1986;18(10):917-28.
114. Vallance P, Collier J, Moncada S. Effects of endothelium-derived nitric oxide on peripheral arteriolar tone in man. Lancet. 1989;2(8670):997-1000.
115. Ichihara A, Inscho EW, Imig JD, Navar LG. Neuronal nitric oxide synthase modulates rat renal microvascular function. Am J Physiol. 1998;274(3 Pt 2):F516-24.

116. Seddon M, Melikian N, Dworakowski R, Shabeeh H, Jiang B, Byrne J, et al. Effects of neuronal nitric oxide synthase on human coronary artery diameter and blood flow in vivo. Circulation. 2009;119(20):2656-62.
117. Seddon MD, Chowienczyk PJ, Brett SE, Casadei B, Shah AM. Neuronal nitric oxide synthase regulates basal microvascular tone in humans in vivo. Circulation. 2008;117(15):1991-6.
118. Gros R, Afroze T, You XM, Kabir G, Van Wert R, Kalair W, et al. Plasma membrane calcium ATPase overexpression in arterial smooth muscle increases vasomotor responsiveness and blood pressure. Circ Res. 2003;93(7):614-21.
119. Kellogg DL, Jr., Zhao JL, Wu Y. Neuronal nitric oxide synthase control mechanisms in the cutaneous vasculature of humans in vivo. J Physiol. 2008;586(3):847-57.
120. Feron O, Belhassen L, Kobzik L, Smith TW, Kelly RA, Michel T. Endothelial nitric oxide synthase targeting to caveolae. Specific interactions with caveolin isoforms in cardiac myocytes and endothelial cells. J Biol Chem. 1996;271(37):22810-4.
121. Vaniotis G, Glazkova I, Merlen C, Smith C, Villeneuve LR, Chatenet D, et al. Regulation of cardiac nitric oxide signaling by nuclear beta-adrenergic and endothelin receptors. J Mol Cell Cardiol. 2013;62:58-68.
122. Martin SR, Emanuel K, Sears CE, Zhang YH, Casadei B. Are myocardial eNOS and nNOS involved in the beta-adrenergic and muscarinic regulation of inotropy? A systematic investigation. Cardiovasc Res. 2006;70(1):97-106.
123. Wang H, Kohr MJ, Wheeler DG, Ziolo MT. Endothelial nitric oxide synthase decreases beta-adrenergic responsiveness via inhibition of the L-type Ca2+ current. Am J Physiol Heart Circ Physiol. 2008;294(3):H1473-80.
124. Godecke A, Heinicke T, Kamkin A, Kiseleva I, Strasser RH, Decking UK, et al. Inotropic response to beta-adrenergic receptor stimulation and anti-adrenergic effect of ACh in endothelial NO synthase-deficient mouse hearts. J Physiol. 2001;532(Pt 1):195-204.
125. Takimoto E, Champion HC, Belardi D, Moslehi J, Mongillo M, Mergia E, et al. cGMP catabolism by phosphodiesterase 5A regulates cardiac adrenergic stimulation by NOS3-dependent mechanism. Circ Res. 2005;96(1):100-9.
126. Xu KY, Huso DL, Dawson TM, Bredt DS, Becker LC. Nitric oxide synthase in cardiac sarcoplasmic reticulum. Proc Natl Acad Sci U S A. 1999;96(2):657-62.
127. Khan SA, Lee K, Minhas KM, Gonzalez DR, Raju SV, Tejani AD, et al. Neuronal nitric oxide synthase negatively regulates xanthine oxidoreductase inhibition of cardiac excitation-contraction coupling. Proc Natl Acad Sci U S A. 2004;101(45):15944-8.
128. Williams JC, Armesilla AL, Mohamed TM, Hagarty CL, McIntyre FH, Schomburg S, et al. The sarcolemmal calcium pump, alpha-1 syntrophin, and neuronal nitric-oxide synthase are parts of a macromolecular protein complex. J Biol Chem. 2006;281(33):23341-8.
129. Oceandy D, Stanley PJ, Cartwright EJ, Neyses L. The regulatory function of plasma-membrane Ca(2+)-ATPase (PMCA) in the heart. Biochem Soc Trans. 2007;35(Pt 5):927-30.
130. Sears CE, Bryant SM, Ashley EA, Lygate CA, Rakovic S, Wallis HL, et al. Cardiac neuronal nitric oxide synthase isoform regulates myocardial contraction and calcium handling. Circ Res. 2003;92(5):e52-9.
131. Carnicer R, Hale AB, Suffredini S, Liu X, Reilly S, Zhang MH, et al. Cardiomyocyte GTP cyclohydrolase 1 and tetrahydrobiopterin increase NOS1 activity and accelerate myocardial relaxation. Circ Res. 2012;111(6):718-27.
132. Gonzalez DR, Beigi F, Treuer AV, Hare JM. Deficient ryanodine receptor S-nitrosylation increases sarcoplasmic reticulum calcium leak and arrhythmogenesis in cardiomyocytes. Proc Natl Acad Sci U S A. 2007;104(51):20612-7.
133. Wang H, Viatchenko-Karpinski S, Sun J, Gyorke I, Benkusky NA, Kohr MJ, et al. Regulation of myocyte contraction via neuronal nitric oxide synthase: role of ryanodine receptor S-nitrosylation. J Physiol. 2010;588(Pt 15):2905-17.

134. Hart JD, Dulhunty AF. Nitric oxide activates or inhibits skeletal muscle ryanodine receptors depending on its concentration, membrane potential and ligand binding. J Membr Biol. 2000;173(3):227-36.
135. Xu L, Eu JP, Meissner G, Stamler JS. Activation of the cardiac calcium release channel (ryanodine receptor) by poly-S-nitrosylation. Science. 1998;279(5348):234-7.
136. Sanchez G, Pedrozo Z, Domenech RJ, Hidalgo C, Donoso P. Tachycardia increases NADPH oxidase activity and RyR2 S-glutathionylation in ventricular muscle. J Mol Cell Cardiol. 2005;39(6):982-91.
137. Dulce RA, Yiginer O, Gonzalez DR, Goss G, Feng N, Zheng M, et al. Hydralazine and organic nitrates restore impaired excitation-contraction coupling by reducing calcium leak associated with nitroso-redox imbalance. J Biol Chem. 2013;288(9):6522-33.
138. Aracena-Parks P, Goonasekera SA, Gilman CP, Dirksen RT, Hidalgo C, Hamilton SL. Identification of cysteines involved in S-nitrosylation, S-glutathionylation, and oxidation to disulfides in ryanodine receptor type 1. J Biol Chem. 2006;281(52):40354-68.
139. Zhang YH, Zhang MH, Sears CE, Emanuel K, Redwood C, El-Armouche A, et al. Reduced phospholamban phosphorylation is associated with impaired relaxation in left ventricular myocytes from neuronal NO synthase-deficient mice. Circ Res. 2008;102(2):242-9.
140. Niederwieser A, Blau N, Wang M, Joller P, Atares M, Cardesa-Garcia J. GTP cyclohydrolase I deficiency, a new enzyme defect causing hyperphenylalaninemia with neopterin, biopterin, dopamine, and serotonin deficiencies and muscular hypotonia. Eur J Pediatr. 1984;141(4):208-14.
141. Hauer CR, Rebrin I, Thony B, Neuheiser F, Curtius HC, Hunziker P, et al. Phenylalanine hydroxylase-stimulating protein/pterin-4 alpha-carbinolamine dehydratase from rat and human liver. Purification, characterization, and complete amino acid sequence. J Biol Chem. 1993;268(7):4828-31.
142. Crane BR, Arvai AS, Ghosh DK, Wu C, Getzoff ED, Stuehr DJ, et al. Structure of nitric oxide synthase oxygenase dimer with pterin and substrate. Science. 1998;279(5359):2121-6.
143. Klatt P, Schmid M, Leopold E, Schmidt K, Werner ER, Mayer B. The pteridine binding site of brain nitric oxide synthase. Tetrahydrobiopterin binding kinetics, specificity, and allosteric interaction with the substrate domain. J Biol Chem. 1994;269(19):13861-6.
144. Klatt P, Schmidt K, Lehner D, Glatter O, Bachinger HP, Mayer B. Structural analysis of porcine brain nitric oxide synthase reveals a role for tetrahydrobiopterin and L-arginine in the formation of an SDS-resistant dimer. EMBO J. 1995;14(15):3687-95.
145. Wei CC, Wang ZQ, Wang Q, Meade AL, Hemann C, Hille R, et al. Rapid kinetic studies link tetrahydrobiopterin radical formation to heme-dioxy reduction and arginine hydroxylation in inducible nitric-oxide synthase. J Biol Chem. 2001;276(1):315-9.
146. Bec N, Gorren AFC, Mayer B, Schmidt PP, Andersson KK, Lange R. The role of tetrahydrobiopterin in the activation of oxygen by nitric-oxide synthase. J Inorg Biochem. 2000;81(3):207-11.
147. Hevel JM, Marletta MA. Macrophage nitric oxide synthase: relationship between enzyme-bound tetrahydrobiopterin and synthase activity. Biochemistry. 1992;31(31):7160-5.
148. Werner ER, Pitters E, Schmidt K, Wachter H, Werner-Felmayer G, Mayer B. Identification of the 4-amino analogue of tetrahydrobiopterin as a dihydropteridine reductase inhibitor and a potent pteridine antagonist of rat neuronal nitric oxide synthase. Biochem J. 1996;320 (Pt 1):193-6.
149. Stuehr D, Pou S, Rosen GM. Oxygen reduction by nitric-oxide synthases. J Biol Chem. 2001;276(18):14533-6.
150. Stroes E, Hijmering M, van Zandvoort M, Wever R, Rabelink TJ, van Faassen EE. Origin of superoxide production by endothelial nitric oxide synthase. FEBS Lett. 1998;438(3):161-4.
151. Zou MH, Shi C, Cohen RA. Oxidation of the zinc-thiolate complex and uncoupling of endothelial nitric oxide synthase by peroxynitrite. J Clin Invest. 2002;109(6):817-26.

152. Kuzkaya N, Weissmann N, Harrison DG, Dikalov S. Interactions of peroxynitrite, tetrahydrobiopterin, ascorbic acid, and thiols: implications for uncoupling endothelial nitric-oxide synthase. J Biol Chem. 2003;278(25):22546-54.
153. Crabtree MJ, Smith CL, Lam G, Goligorsky MS, Gross SS. Ratio of 5,6,7,8-tetrahydrobiopterin to 7,8-dihydrobiopterin in endothelial cells determines glucose-elicited changes in NO vs. superoxide production by eNOS. Am J Physiol Heart Circ Physiol. 2008;294(4):H1530-40.
154. Vasquez-Vivar J, Martasek P, Whitsett J, Joseph J, Kalyanaraman B. The ratio between tetrahydrobiopterin and oxidized tetrahydrobiopterin analogues controls superoxide release from endothelial nitric oxide synthase: an EPR spin trapping study. Biochem J. 2002;362(Pt 3):733-9.
155. Alp NJ, Mussa S, Khoo J, Cai S, Guzik T, Jefferson A, et al. Tetrahydrobiopterin-dependent preservation of nitric oxide-mediated endothelial function in diabetes by targeted transgenic GTP-cyclohydrolase I overexpression. J Clin Invest. 2003;112(5):725-35.
156. Crabtree MJ, Hale AB, Channon KM. Dihydrofolate reductase protects endothelial nitric oxide synthase from uncoupling in tetrahydrobiopterin deficiency. Free Radic Biol Med. 2011;50(11):1639-46.
157. Ren J, Duan J, Thomas DP, Yang X, Sreejayan N, Sowers JR, et al. IGF-I alleviates diabetes-induced RhoA activation, eNOS uncoupling, and myocardial dysfunction. Am J Physiol Regul Integr Comp Physiol. 2008;294(3):R793-802.
158. Chen CA, Wang TY, Varadharaj S, Reyes LA, Hemann C, Talukder MA, et al. S-glutathionylation uncouples eNOS and regulates its cellular and vascular function. Nature. 2010;468(7327):1115-8.
159. Heitzer T, Krohn K, Albers S, Meinertz T. Tetrahydrobiopterin improves endothelium-dependent vasodilation by increasing nitric oxide activity in patients with Type II diabetes mellitus. Diabetologia. 2000;43(11):1435-8.
160. Guzik TJ, Mussa S, Gastaldi D, Sadowski J, Ratnatunga C, Pillai R, et al. Mechanisms of increased vascular superoxide production in human diabetes mellitus: role of NAD(P)H oxidase and endothelial nitric oxide synthase. Circulation. 2002;105(14):1656-62.
161. Maier W, Cosentino F, Lutolf RB, Fleisch M, Seiler C, Hess OM, et al. Tetrahydrobiopterin improves endothelial function in patients with coronary artery disease. J Cardiovasc Pharmacol. 2000;35(2):173-8.
162. Tiefenbacher CP, Bleeke T, Vahl C, Amann K, Vogt A, Kubler W. Endothelial dysfunction of coronary resistance arteries is improved by tetrahydrobiopterin in atherosclerosis. Circulation. 2000;102(18):2172-9.
163. Pannirselvam M, Simon V, Verma S, Anderson T, Triggle CR. Chronic oral supplementation with sepiapterin prevents endothelial dysfunction and oxidative stress in small mesenteric arteries from diabetic (db/db) mice. Br J Pharmacol. 2003;140(4):701-6.
164. Huraux C, Makita T, Kurz S, Yamaguchi K, Szlam F, Tarpey MM, et al. Superoxide production, risk factors, and endothelium-dependent relaxations in human internal mammary arteries. Circulation. 1999;99(1):53-9.
165. Vasquez-Vivar J, Duquaine D, Whitsett J, Kalyanaraman B, Rajagopalan S. Altered tetrahydrobiopterin metabolism in atherosclerosis: implications for use of oxidized tetrahydrobiopterin analogues and thiol antioxidants. Arterioscler Thromb Vasc Biol. 2002;22(10):1655-61.
166. Crabtree MJ, Tatham AL, Hale AB, Alp NJ, Channon KM. Critical role for tetrahydrobiopterin recycling by dihydrofolate reductase in regulation of endothelial nitric-oxide synthase coupling: relative importance of the de novo biopterin synthesis versus salvage pathways. J Biol Chem. 2009;284(41):28128-36.
167. Rubler S, Dlugash J, Yuceoglu YZ, Kumral T, Branwood AW, Grishman A. New type of cardiomyopathy associated with diabetic glomerulosclerosis. Am J Cardiol. 1972;30(6):595-602.
168. Garcia MJ, McNamara PM, Gordon T, Kannel WB. Morbidity and mortality in diabetics in the Framingham population. Sixteen year follow-up study. Diabetes. 1974;23(2):105-11.

169. Brooks BA, Franjic B, Ban CR, Swaraj K, Yue DK, Celermajer DS, et al. Diastolic dysfunction and abnormalities of the microcirculation in type 2 diabetes. Diabetes Obes Metab. 2008;10(9):739-46.
170. Liu JE, Palmieri V, Roman MJ, Bella JN, Fabsitz R, Howard BV, et al. The impact of diabetes on left ventricular filling pattern in normotensive and hypertensive adults: the Strong Heart Study. J Am Coll Cardiol. 2001;37(7):1943-9.
171. Schannwell CM, Schneppenheim M, Perings S, Plehn G, Strauer BE. Left ventricular diastolic dysfunction as an early manifestation of diabetic cardiomyopathy. Cardiology. 2002;98(1-2):33-9.
172. Basu R, Oudit GY, Wang X, Zhang L, Ussher JR, Lopaschuk GD, et al. Type 1 diabetic cardiomyopathy in the Akita (Ins2WT/C96Y) mouse model is characterized by lipotoxicity and diastolic dysfunction with preserved systolic function. Am J Physiol Heart Circ Physiol. 2009;297(6):H2096-108.
173. Di Bonito P, Cuomo S, Moio N, Sibilio G, Sabatini D, Quattrin S, et al. Diastolic dysfunction in patients with non-insulin-dependent diabetes mellitus of short duration. Diabet Med. 1996;13(4):321-4.
174. Beljic T, Miric M. Improved metabolic control does not reverse left ventricular filling abnormalities in newly diagnosed non-insulin-dependent diabetes patients. Acta Diabetol. 1994;31(3):147-50.
175. Regan TJ, Lyons MM, Ahmed SS, Levinson GE, Oldewurtel HA, Ahmad MR, et al. Evidence for cardiomyopathy in familial diabetes mellitus. J Clin Invest. 1977;60(4):884-99.
176. Katare RG, Caporali A, Oikawa A, Meloni M, Emanueli C, Madeddu P. Vitamin B1 analog benfotiamine prevents diabetes-induced diastolic dysfunction and heart failure through Akt/Pim-1-mediated survival pathway. Circ Heart Fail. 2010;3(2):294-305.
177. Matsumoto Y, Kaneko M, Kobayashi A, Fujise Y, Yamazaki N. Creatine kinase kinetics in diabetic cardiomyopathy. Am J Physiol. 1995;268(6 Pt 1):E1070-6.
178. How OJ, Aasum E, Severson DL, Chan WY, Essop MF, Larsen TS. Increased myocardial oxygen consumption reduces cardiac efficiency in diabetic mice. Diabetes. 2006;55(2):466-73.
179. Ramanathan T, Shirota K, Morita S, Nishimura T, Huang Y, Zheng X, et al. Left ventricular oxygen utilization efficiency is impaired in chronic streptozotocin-diabetic sheep. Cardiovasc Res. 2002;55(4):749-56.
180. Herrero P, McGill J, Lesniak DS, Dence CS, Scott SW, Kisrieva-Ware Z, et al. PET detection of the impact of dobutamine on myocardial glucose metabolism in women with type 1 diabetes mellitus. J Nucl Cardiol. 2008;15(6):791-9.
181. Herrero P, Peterson LR, McGill JB, Matthew S, Lesniak D, Dence C, et al. Increased myocardial fatty acid metabolism in patients with type 1 diabetes mellitus. J Am Coll Cardiol. 2006;47(3):598-604.
182. Montessuit C, Lerch R. Regulation and dysregulation of glucose transport in cardiomyocytes. Biochim Biophys Acta. 2013;1833(4):848-56.
183. Simon JN, Duglan D, Casadei B, Carnicer R. Nitric oxide synthase regulation of cardiac excitation-contraction coupling in health and disease. J Mol Cell Cardiol. 2014;73:80-91.
184. Silberman GA, Fan TH, Liu H, Jiao Z, Xiao HD, Lovelock JD, et al. Uncoupled cardiac nitric oxide synthase mediates diastolic dysfunction. Circulation. 2010;121(4):519-28.
185. Jeong EM, Monasky MM, Gu L, Taglieri DM, Patel BG, Liu H, et al. Tetrahydrobiopterin improves diastolic dysfunction by reversing changes in myofilament properties. J Mol Cell Cardiol. 2013;56:44-54.
186. Patel BG, Wilder T, Solaro RJ. Novel control of cardiac myofilament response to calcium by S-glutathionylation at specific sites of myosin binding protein C. Front Physiol. 2013;4:336.
187. Moens AL, Takimoto E, Tocchetti CG, Chakir K, Bedja D, Cormaci G, et al. Reversal of cardiac hypertrophy and fibrosis from pressure overload by tetrahydrobiopterin: efficacy of recoupling nitric oxide synthase as a therapeutic strategy. Circulation. 2008;117(20):2626-36.

188. Takimoto E, Champion HC, Li M, Ren S, Rodriguez ER, Tavazzi B, et al. Oxidant stress from nitric oxide synthase-3 uncoupling stimulates cardiac pathologic remodeling from chronic pressure load. J Clin Invest. 2005;115(5):1221-31.
189. Dumitrescu C, Biondi R, Xia Y, Cardounel AJ, Druhan LJ, Ambrosio G, et al. Myocardial ischemia results in tetrahydrobiopterin (BH4) oxidation with impaired endothelial function ameliorated by BH4. Proc Natl Acad Sci U S A. 2007;104(38):15081-6.
190. Yamashiro S, Noguchi K, Matsuzaki T, Miyagi K, Nakasone J, Sakanashi M, et al. Beneficial effect of tetrahydrobiopterin on ischemia-reperfusion injury in isolated perfused rat hearts. J Thorac Cardiovasc Surg. 2002;124(4):775-84.
191. Ge ZD, Ionova IA, Vladic N, Pravdic D, Hirata N, Vasquez-Vivar J, et al. Cardiac-specific overexpression of GTP cyclohydrolase 1 restores ischaemic preconditioning during hyperglycaemia. Cardiovasc Res. 2011;91(2):340-9.
192. Lei S, Li H, Xu J, Liu Y, Gao X, Wang J, et al. Hyperglycemia-induced protein kinase C beta2 activation induces diastolic cardiac dysfunction in diabetic rats by impairing caveolin-3 expression and Akt/eNOS signaling. Diabetes. 2013;62(7):2318-28.
193. Jo H, Otani H, Jo F, Shimazu T, Okazaki T, Yoshioka K, et al. Inhibition of nitric oxide synthase uncoupling by sepiapterin improves left ventricular function in streptozotocin-induced diabetic mice. Clin Exp Pharmacol Physiol. 2011;38(8):485-93.
194. AMDCC. Low-Dose Streptozotocin Induction Protocol (Mouse). Found online at: https://www.diacomp.org/shared/showFile.aspx?doctypeid=3&docid=19.
195. Truett GE, Heeger P, Mynatt RL, Truett AA, Walker JA, Warman ML. Preparation of PCR-quality mouse genomic DNA with hot sodium hydroxide and tris (HotSHOT). Biotechniques. 2000;29(1):52, 4.
196. Kim YM, Guzik TJ, Zhang YH, Zhang MH, Kattach H, Ratnatunga C, et al. A myocardial Nox2 containing NAD(P)H oxidase contributes to oxidative stress in human atrial fibrillation. Circ Res. 2005;97(7):629-36.
197. Vasquez-Vivar J, Hogg N, Pritchard KA, Jr., Martasek P, Kalyanaraman B. Superoxide anion formation from lucigenin: an electron spin resonance spin-trapping study. FEBS Lett. 1997;403(2):127-30.
198. Fink B, Laude K, McCann L, Doughan A, Harrison DG, Dikalov S. Detection of intracellular superoxide formation in endothelial cells and intact tissues using dihydroethidium and an HPLC-based assay. Am J Physiol Cell Physiol. 2004;287(4):C895-902.
199. de Bono JP, Warrick N, Bendall JK, Channon KM, Alp NJ. Radiochemical HPLC detection of arginine metabolism: measurement of nitric oxide synthesis and arginase activity in vascular tissue. Nitric Oxide. 2007;16(1):1-9.
200. Halpern W, Mulvany MJ, Warshaw DM. Mechanical properties of smooth muscle cells in the walls of arterial resistance vessels. J Physiol. 1978;275:85-101.
201. Mulvany MJ, Halpern W. Mechanical properties of vascular smooth muscle cells in situ. Nature. 1976;260(5552):617-9.
202. Osol G, Cipolla M, Knutson S. A new method for mechanically denuding the endothelium of small (50-150 microns) arteries with a human hair. Blood Vessels. 1989;26(5):320-4.
203. Grossman SH. Electrophoresis of creatine kinase: A laboratory experiment in isoenzymes. Biochemical Education. 1982;10(1):8-10.
204. Grande P, Christiansen C, Naestoft J. Creatine kinase isoenzyme MB assay by electrophoresis. Scand J Clin Lab Invest. 1979;39(7):607-12.
205. Murthy VV. Adenylate kinase mimics creatine kinase-MM isoenzyme in a CK isoenzyme electrophoresis assay. J Clin Lab Anal. 1994;8(3):140-3.
206. Abbott BC, Lowy J. Stress relaxation in muscle. Proc R Soc Lond B Biol Sci. 1956;146(923):281-8.
207. Brophy CM, Knoepp L, Xin J, Pollock JS. Functional expression of NOS 1 in vascular smooth muscle. Am J Physiol Heart Circ Physiol. 2000;278(3):H991-7.

208. Huang A, Sun D, Shesely EG, Levee EM, Koller A, Kaley G. Neuronal NOS-dependent dilation to flow in coronary arteries of male eNOS-KO mice. Am J Physiol Heart Circ Physiol. 2002;282(2):H429-36.
209. Sander M, Chavoshan B, Harris SA, Iannaccone ST, Stull JT, Thomas GD, et al. Functional muscle ischemia in neuronal nitric oxide synthase-deficient skeletal muscle of children with Duchenne muscular dystrophy. Proc Natl Acad Sci U S A. 2000;97(25):13818-23.
210. Koyama T, Hatanaka Y, Jin X, Yokomizo A, Fujiwara H, Goda M, et al. Altered function of nitrergic nerves inhibiting sympathetic neurotransmission in mesenteric vascular beds of renovascular hypertensive rats. Hypertens Res. 2010;33(5):485-91.
211. Hatanaka Y, Hobara N, Honghua J, Akiyama S, Nawa H, Kobayashi Y, et al. Neuronal nitric-oxide synthase inhibition facilitates adrenergic neurotransmission in rat mesenteric resistance arteries. J Pharmacol Exp Ther. 2006;316(2):490-7.
212. Barnes RD, Ward LE, Frank KP, Tyce GM, Hunter LW, Rorie DK. Nitric oxide modulates evoked catecholamine release from canine adrenal medulla. Neuroscience. 2001;104(4):1165-73.
213. Kolo LL, Westfall TC, Macarthur H. Nitric oxide decreases the biological activity of norepinephrine resulting in altered vascular tone in the rat mesenteric arterial bed. Am J Physiol Heart Circ Physiol. 2004;286(1):H296-303.
214. Legros E, Tirapelli CR, Carrier E, Brochu I, Fournier A, D'Orleans-Juste P. Characterization of the non-adrenergic/non-cholinergic response to perivascular nerve stimulation in the double-perfused mesenteric bed of the mouse. Br J Pharmacol. 2007;152(7):1049-59.
215. Hah JM, Roman LJ, Martasek P, Silverman RB. Reduced amide bond peptidomimetics. (4S)-N-(4-amino-5-[aminoakyl]aminopentyl)-N'-nitroguanidines, potent and highly selective inhibitors of neuronal nitric oxide synthase. J Med Chem. 2001;44(16):2667-70.
216. Babu BR, Griffith OW. N5-(1-Imino-3-butenyl)-L-ornithine. A neuronal isoform selective mechanism-based inactivator of nitric oxide synthase. J Biol Chem. 1998;273(15):8882-9.
217. Ashley EA, Sears CE, Bryant SM, Watkins HC, Casadei B. Cardiac nitric oxide synthase 1 regulates basal and beta-adrenergic contractility in murine ventricular myocytes. Circulation. 2002;105(25):3011-6.
218. Ho GP, Selvakumar B, Mukai J, Hester LD, Wang Y, Gogos JA, et al. S-nitrosylation and S-palmitoylation reciprocally regulate synaptic targeting of PSD-95. Neuron. 2011;71(1):131-41.
219. Hopper RA, Garthwaite J. Tonic and phasic nitric oxide signals in hippocampal long-term potentiation. J Neurosci. 2006;26(45):11513-21.
220. Pigott B, Bartus K, Garthwaite J. On the selectivity of neuronal NOS inhibitors. Br J Pharmacol. 2013;168(5):1255-65.
221. Garvey EP, Oplinger JA, Furfine ES, Kiff RJ, Laszlo F, Whittle BJ, et al. 1400W is a slow, tight binding, and highly selective inhibitor of inducible nitric-oxide synthase in vitro and in vivo. J Biol Chem. 1997;272(8):4959-63.
222. Alderton WK, Cooper CE, Knowles RG. Nitric oxide synthases: structure, function and inhibition. Biochem J. 2001;357(Pt 3):593-615.
223. Brzozowski MJ, Alcantara SL, Iravani MM, Rose S, Jenner P. The effect of nNOS inhibitors on toxin-induced cell death in dopaminergic cell lines depends on the extent of enzyme expression. Brain Res. 2011;1404:21-30.
224. Castagnoli K, Palmer S, Anderson A, Bueters T, Castagnoli N, Jr. The neuronal nitric oxide synthase inhibitor 7-nitroindazole also inhibits the monoamine oxidase-B-catalyzed oxidation of 1-methyl-4-phenyl-1,2,3,6-tetrahydropyridine. Chem Res Toxicol. 1997;10(4):364-8.
225. Flavahan NA, Cooke JP, Shepherd JT, Vanhoutte PM. Human postjunctional alpha-1 and alpha-2 adrenoceptors: differential distribution in arteries of the limbs. J Pharmacol Exp Ther. 1987;241(2):361-5.
226. Han C, Li J, Minneman KP. Subtypes of alpha 1-adrenoceptors in rat blood vessels. Eur J Pharmacol. 1990;190(1-2):97-104.

227. Dunn WR, Brock JA, Hardy TA. Electrochemical and electrophysiological characterization of neurotransmitter release from sympathetic nerves supplying rat mesenteric arteries. Br J Pharmacol. 1999;128(1):174-80.
228. Sneddon P, Burnstock G. ATP as a co-transmitter in rat tail artery. Eur J Pharmacol. 1984;106(1):149-52.
229. Lundberg JM, Hokfelt T. Multiple co-existence of peptides and classical transmitters in peripheral autonomic and sensory neurons--functional and pharmacological implications. Prog Brain Res. 1986;68:241-62.
230. Li YJ, Duckles SP. Effect of endothelium on the actions of sympathetic and sensory nerves in the perfused rat mesentery. Eur J Pharmacol. 1992;210(1):23-30.
231. Boric MP, Figueroa XF, Donoso MV, Paredes A, Poblete I, Huidobro-Toro JP. Rise in endothelium-derived NO after stimulation of rat perivascular sympathetic mesenteric nerves. Am J Physiol. 1999;277(3 Pt 2):H1027-35.
232. Oroszi G, Szilvassy Z, Nemeth J, Tosaki A, Szolcsanyi J. Interplay between nitric oxide and CGRP by capsaicin in isolated guinea-pig heart. Pharmacol Res. 1999;40(2):125-8.
233. Kawasaki H, Nuki C, Saito A, Takasaki K. Role of calcitonin gene-related peptide-containing nerves in the vascular adrenergic neurotransmission. J Pharmacol Exp Ther. 1990;252(1):403-9.
234. Gray DW, Marshall I. Nitric oxide synthesis inhibitors attenuate calcitonin gene-related peptide endothelium-dependent vasorelaxation in rat aorta. Eur J Pharmacol. 1992;212(1):37-42.
235. Takahashi T, Nakamura K, Itoh H, Sima AA, Owyang C. Impaired expression of nitric oxide synthase in the gastric myenteric plexus of spontaneously diabetic rats. Gastroenterology. 1997;113(5):1535-44.
236. Oliveira RB, Troncon LE, Meneghelli UG, Dantas RO, Godoy RA. Gastric accommodation to distension and early gastric emptying in diabetics with neuropathy. Braz J Med Biol Res. 1984;17(1):49-53.
237. Cellek S, Anderson PN, Foxwell NA. Nitrergic neurodegeneration in cerebral arteries of streptozotocin-induced diabetic rats: a new insight into diabetic stroke. Diabetes. 2005;54(1):212-9.
238. Cellek S, Qu W, Schmidt AM, Moncada S. Synergistic action of advanced glycation end products and endogenous nitric oxide leads to neuronal apoptosis in vitro: a new insight into selective nitrergic neuropathy in diabetes. Diabetologia. 2004;47(2):331-9.
239. Sanchez A, Contreras C, Martinez MP, Climent B, Benedito S, Garcia-Sacristan A, et al. Role of neural NO synthase (nNOS) uncoupling in the dysfunctional nitrergic vasorelaxation of penile arteries from insulin-resistant obese Zucker rats. PLoS One. 2012;7(4):e36027.
240. Zhao FQ, Keating AF. Functional properties and genomics of glucose transporters. Curr Genomics. 2007;8(2):113-28.
241. Wright EM, Loo DD, Hirayama BA. Biology of human sodium glucose transporters. Physiol Rev. 2011;91(2):733-94.
242. James DE, Burleigh KM, Kraegen EW. Time dependence of insulin action in muscle and adipose tissue in the rat in vivo. An increasing response in adipose tissue with time. Diabetes. 1985;34(10):1049-54.
243. Simpson IA, Cushman SW. Hormonal regulation of mammalian glucose transport. Annu Rev Biochem. 1986;55:1059-89.
244. Stenbit AE, Tsao TS, Li J, Burcelin R, Geenen DL, Factor SM, et al. GLUT4 heterozygous knockout mice develop muscle insulin resistance and diabetes. Nat Med. 1997;3(10):1096-101.
245. Rossetti L, Stenbit AE, Chen W, Hu M, Barzilai N, Katz EB, et al. Peripheral but not hepatic insulin resistance in mice with one disrupted allele of the glucose transporter type 4 (GLUT4) gene. J Clin Invest. 1997;100(7):1831-9.
246. Tsao TS, Stenbit AE, Factor SM, Chen W, Rossetti L, Charron MJ. Prevention of insulin resistance and diabetes in mice heterozygous for GLUT4 ablation by transgenic complementation of GLUT4 in skeletal muscle. Diabetes. 1999;48(4):775-82.

247. Garvey WT, Maianu L, Zhu JH, Brechtel-Hook G, Wallace P, Baron AD. Evidence for defects in the trafficking and translocation of GLUT4 glucose transporters in skeletal muscle as a cause of human insulin resistance. J Clin Invest. 1998;101(11):2377-86.
248. Andreasson K, Galuska D, Thorne A, Sonnenfeld T, Wallberg-Henriksson H. Decreased insulin-stimulated 3-0-methylglucose transport in in vitro incubated muscle strips from type II diabetic subjects. Acta Physiol Scand. 1991;142(2):255-60.
249. Takata K, Kasahara T, Kasahara M, Ezaki O, Hirano H. Erythrocyte/HepG2-type glucose transporter is concentrated in cells of blood-tissue barriers. Biochem Biophys Res Commun. 1990;173(1):67-73.
250. Gould GW, Bell GI. Facilitative glucose transporters: an expanding family. Trends Biochem Sci. 1990;15(1):18-23.
251. Uldry M, Ibberson M, Hosokawa M, Thorens B. GLUT2 is a high affinity glucosamine transporter. FEBS Lett. 2002;524(1-3):199-203.
252. Burant CF, Bell GI. Mammalian facilitative glucose transporters: evidence for similar substrate recognition sites in functionally monomeric proteins. Biochemistry. 1992;31(42):10414-20.
253. Kasahara T, Kasahara M. Expression of the rat GLUT1 glucose transporter in the yeast Saccharomyces cerevisiae. Biochem J. 1996;315 (Pt 1):177-82.
254. Kaiser N, Sasson S, Feener EP, Boukobza-Vardi N, Higashi S, Moller DE, et al. Differential regulation of glucose transport and transporters by glucose in vascular endothelial and smooth muscle cells. Diabetes. 1993;42(1):80-9.
255. Heilig CW, Liu Y, England RL, Freytag SO, Gilbert JD, Heilig KO, et al. D-glucose stimulates mesangial cell GLUT1 expression and basal and IGF-I-sensitive glucose uptake in rat mesangial cells: implications for diabetic nephropathy. Diabetes. 1997;46(6):1030-9.
256. Chen SH. Diabetes increases glomerular GLUT1, and antisense-GLUT1 protects against diabetic glomerulosclerosis (Abstract). J Am Soc Nephrol. 2003;14.
257. Marshall BA, Ren JM, Johnson DW, Gibbs EM, Lillquist JS, Soeller WC, et al. Germline manipulation of glucose homeostasis via alteration of glucose transporter levels in skeletal muscle. J Biol Chem. 1993;268(25):18442-5.
258. Heilig CW, Concepcion LA, Riser BL, Freytag SO, Zhu M, Cortes P. Overexpression of glucose transporters in rat mesangial cells cultured in a normal glucose milieu mimics the diabetic phenotype. J Clin Invest. 1995;96(4):1802-14.
259. Weigert C, Brodbeck K, Brosius FC, 3rd, Huber M, Lehmann R, Friess U, et al. Evidence for a novel TGF-beta1-independent mechanism of fibronectin production in mesangial cells overexpressing glucose transporters. Diabetes. 2003;52(2):527-35.
260. Wang Y, Heilig K, Saunders T, Minto A, Deb DK, Chang A, et al. Transgenic overexpression of GLUT1 in mouse glomeruli produces renal disease resembling diabetic glomerulosclerosis. Am J Physiol Renal Physiol. 2010;299(1):F99-F111.
261. Zhang JZ, Gao L, Widness M, Xi X, Kern TS. Captopril inhibits glucose accumulation in retinal cells in diabetes. Invest Ophthalmol Vis Sci. 2003;44(9):4001-5.
262. Fernandes R, Carvalho AL, Kumagai A, Seica R, Hosoya K, Terasaki T, et al. Downregulation of retinal GLUT1 in diabetes by ubiquitinylation. Mol Vis. 2004;10:618-28.
263. Lu L, Seidel CP, Iwase T, Stevens RK, Gong YY, Wang X, et al. Suppression of GLUT1; a new strategy to prevent diabetic complications. J Cell Physiol. 2013;228(2):251-7.
264. Hink U, Li H, Mollnau H, Oelze M, Matheis E, Hartmann M, et al. Mechanisms underlying endothelial dysfunction in diabetes mellitus. Circ Res. 2001;88(2):E14-22.
265. Sena CM, Matafome P, Louro T, Nunes E, Fernandes R, Seica RM. Metformin restores endothelial function in aorta of diabetic rats. Br J Pharmacol. 2011;163(2):424-37.
266. Zhang H, Zhang J, Ungvari Z, Zhang C. Resveratrol improves endothelial function: role of TNF{alpha} and vascular oxidative stress. Arterioscler Thromb Vasc Biol. 2009;29(8):1164-71.

267. Cai S, Khoo J, Mussa S, Alp NJ, Channon KM. Endothelial nitric oxide synthase dysfunction in diabetic mice: importance of tetrahydrobiopterin in eNOS dimerisation. Diabetologia. 2005;48(9):1933-40.
268. Montagnani M, Chen H, Barr VA, Quon MJ. Insulin-stimulated activation of eNOS is independent of Ca2+ but requires phosphorylation by Akt at Ser(1179). J Biol Chem. 2001;276(32):30392-8.
269. Dimmeler S, Fleming I, Fisslthaler B, Hermann C, Busse R, Zeiher AM. Activation of nitric oxide synthase in endothelial cells by Akt-dependent phosphorylation. Nature. 1999;399(6736):601-5.
270. Kuboki K, Jiang ZY, Takahara N, Ha SW, Igarashi M, Yamauchi T, et al. Regulation of endothelial constitutive nitric oxide synthase gene expression in endothelial cells and in vivo : a specific vascular action of insulin. Circulation. 2000;101(6):676-81.
271. Murphy C, Kanaganayagam GS, Jiang B, Chowienczyk PJ, Zbinden R, Saha M, et al. Vascular dysfunction and reduced circulating endothelial progenitor cells in young healthy UK South Asian men. Arterioscler Thromb Vasc Biol. 2007;27(4):936-42.
272. Walker AB, Chattington PD, Buckingham RE, Williams G. The thiazolidinedione rosiglitazone (BRL-49653) lowers blood pressure and protects against impairment of endothelial function in Zucker fatty rats. Diabetes. 1999;48(7):1448-53.
273. Montagnani M, Golovchenko I, Kim I, Koh GY, Goalstone ML, Mundhekar AN, et al. Inhibition of phosphatidylinositol 3-kinase enhances mitogenic actions of insulin in endothelial cells. J Biol Chem. 2002;277(3):1794-9.
274. Cardillo C, Nambi SS, Kilcoyne CM, Choucair WK, Katz A, Quon MJ, et al. Insulin stimulates both endothelin and nitric oxide activity in the human forearm. Circulation. 1999;100(8):820-5.
275. Shinozaki K, Kashiwagi A, Nishio Y, Okamura T, Yoshida Y, Masada M, et al. Abnormal biopterin metabolism is a major cause of impaired endothelium-dependent relaxation through nitric oxide/O2- imbalance in insulin-resistant rat aorta. Diabetes. 1999;48(12):2437-45.
276. Shimokawa H, Yasutake H, Fujii K, Owada MK, Nakaike R, Fukumoto Y, et al. The importance of the hyperpolarizing mechanism increases as the vessel size decreases in endothelium-dependent relaxations in rat mesenteric circulation. J Cardiovasc Pharmacol. 1996;28(5):703-11.
277. Chuaiphichai S, McNeill E, Douglas G, Crabtree MJ, Bendall JK, Hale AB, et al. Cell-autonomous role of endothelial GTP cyclohydrolase 1 and tetrahydrobiopterin in blood pressure regulation. Hypertension. 2014;64(3):530-40.
278. Parsons SJ, Hill A, Waldron GJ, Plane F, Garland CJ. The relative importance of nitric oxide and nitric oxide-independent mechanisms in acetylcholine-evoked dilatation of the rat mesenteric bed. Br J Pharmacol. 1994;113(4):1275-80.
279. Hwa JJ, Ghibaudi L, Williams P, Chatterjee M. Comparison of acetylcholine-dependent relaxation in large and small arteries of rat mesenteric vascular bed. Am J Physiol. 1994;266(3 Pt 2):H952-8.
280. Garland CJ. Compromised vascular endothelial cell SK(Ca) activity: a fundamental aspect of hypertension? Br J Pharmacol. 2010;160(4):833-5.
281. Fitzgerald SM, Kemp-Harper BK, Parkington HC, Head GA, Evans RG. Endothelial dysfunction and arterial pressure regulation during early diabetes in mice: roles for nitric oxide and endothelium-derived hyperpolarizing factor. Am J Physiol Regul Integr Comp Physiol. 2007;293(2):R707-13.
282. Morikawa K, Matoba T, Kubota H, Hatanaka M, Fujiki T, Takahashi S, et al. Influence of diabetes mellitus, hypercholesterolemia, and their combination on EDHF-mediated responses in mice. J Cardiovasc Pharmacol. 2005;45(5):485-90.
283. Matsumoto T, Miyamori K, Kobayashi T, Kamata K. Specific impairment of endothelium-derived hyperpolarizing factor-type relaxation in mesenteric arteries from streptozotocin-induced diabetic mice. Vascul Pharmacol. 2006;44(6):450-60.

284. Pannirselvam M, Ding H, Anderson TJ, Triggle CR. Pharmacological characteristics of endothelium-derived hyperpolarizing factor-mediated relaxation of small mesenteric arteries from db/db mice. Eur J Pharmacol. 2006;551(1-3):98-107.
285. Pannirselvam M, Verma S, Anderson TJ, Triggle CR. Cellular basis of endothelial dysfunction in small mesenteric arteries from spontaneously diabetic (db/db -/-) mice: role of decreased tetrahydrobiopterin bioavailability. Br J Pharmacol. 2002;136(2):255-63.
286. Nacci C, Tarquinio M, De Benedictis L, Mauro A, Zigrino A, Carratu MR, et al. Endothelial dysfunction in mice with streptozotocin-induced type 1 diabetes is opposed by compensatory overexpression of cyclooxygenase-2 in the vasculature. Endocrinology. 2009;150(2):849-61.
287. Ce GV, Rohde LE, da Silva AM, Punales MK, de Castro AC, Bertoluci MC. Endothelial dysfunction is related to poor glycemic control in adolescents with type 1 diabetes under 5 years of disease: evidence of metabolic memory. J Clin Endocrinol Metab. 2011;96(5):1493-9.
288. Hurks R, Eisinger MJ, Goovaerts I, van Gaal L, Vrints C, Weyler J, et al. Early endothelial dysfunction in young type 1 diabetics. Eur J Vasc Endovasc Surg. 2009;37(5):611-5.
289. Hein TW, Potts LB, Xu W, Yuen JZ, Kuo L. Temporal development of retinal arteriolar endothelial dysfunction in porcine type 1 diabetes. Invest Ophthalmol Vis Sci. 2012;53(13):7943-9.
290. Horio N, Clermont AC, Abiko A, Abiko T, Shoelson BD, Bursell SE, et al. Angiotensin AT(1) receptor antagonism normalizes retinal blood flow and acetylcholine-induced vasodilatation in normotensive diabetic rats. Diabetologia. 2004;47(1):113-23.
291. Orie NN, Aloamaka CP, Iyawe VI. Duration-dependent attenuation of acetylcholine--but not histamine--induced relaxation of the aorta in diabetes mellitus. Gen Pharmacol. 1993;24(2):329-32.
292. Mulhern M, Docherty JR. Effects of experimental diabetes on the responsiveness of rat aorta. Br J Pharmacol. 1989;97(4):1007-12.
293. Pieper GM. Enhanced, unaltered and impaired nitric oxide-mediated endothelium-dependent relaxation in experimental diabetes mellitus: importance of disease duration. Diabetologia. 1999;42(2):204-13.
294. Kiff RJ, Gardiner SM, Compton AM, Bennett T. Selective impairment of hindquarters vasodilator responses to bradykinin in conscious Wistar rats with streptozotocin-induced diabetes mellitus. Br J Pharmacol. 1991;103(2):1357-62.
295. Heygate KM, Davies J, Holmes M, James RF, Thurston H. The effect of insulin treatment and of islet transplantation on the resistance artery function in the STZ-induced diabetic rat. Br J Pharmacol. 1996;119(3):495-504.
296. Waldron GJ, Garland CJ. Contribution of both nitric oxide and a change in membrane potential to acetylcholine-induced relaxation in the rat small mesenteric artery. Br J Pharmacol. 1994;112(3):831-6.
297. Gluais P, Edwards G, Weston AH, Falck JR, Vanhoutte PM, Feletou M. Role of SK(Ca) and IK(Ca) in endothelium-dependent hyperpolarizations of the guinea-pig isolated carotid artery. Br J Pharmacol. 2005;144(4):477-85.
298. Ding H, Kubes P, Triggle C. Potassium- and acetylcholine-induced vasorelaxation in mice lacking endothelial nitric oxide synthase. Br J Pharmacol. 2000;129(6):1194-200.
299. Brownlee M. The pathobiology of diabetic complications: a unifying mechanism. Diabetes. 2005;54(6):1615-25.
300. Hattori Y, Kawasaki H, Abe K, Kanno M. Superoxide dismutase recovers altered endothelium-dependent relaxation in diabetic rat aorta. Am J Physiol. 1991;261(4 Pt 2):H1086-94.
301. Kobayashi T, Oishi K, Hayashi Y, Matsumoto T, Kamata K. Changes in aortic endothelial gene expressions and relaxation responses following chronic short-term insulin treatment in diabetic rats. Atherosclerosis. 2006;185(1):47-57.
302. Rodriguez-Manas L, Angulo J, Peiro C, Llergo JL, Sanchez-Ferrer A, Lopez-Doriga P, et al. Endothelial dysfunction and metabolic control in streptozotocin-induced diabetic rats. Br J Pharmacol. 1998;123(8):1495-502.

303. Majithiya JB, Paramar AN, Balaraman R. Pioglitazone, a PPARgamma agonist, restores endothelial function in aorta of streptozotocin-induced diabetic rats. Cardiovasc Res. 2005;66(1):150-61.
304. Oak JH, Youn JY, Cai H. Aminoguanidine inhibits aortic hydrogen peroxide production, VSMC NOX activity and hypercontractility in diabetic mice. Cardiovasc Diabetol. 2009;8:65.
305. Toque HA, Nunes KP, Yao L, Xu Z, Kondrikov D, Su Y, et al. Akita spontaneously type 1 diabetic mice exhibit elevated vascular arginase and impaired vascular endothelial and nitrergic function. PLoS One. 2013;8(8):e72277.
306. Romero MJ, Iddings JA, Platt DH, Ali MI, Cederbaum SD, Stepp DW, et al. Diabetes-induced vascular dysfunction involves arginase I. Am J Physiol Heart Circ Physiol. 2012;302(1):H159-66.
307. Saenz de Tejada I, Goldstein I, Azadzoi K, Krane RJ, Cohen RA. Impaired neurogenic and endothelium-mediated relaxation of penile smooth muscle from diabetic men with impotence. N Engl J Med. 1989;320(16):1025-30.
308. Johnstone MT, Creager SJ, Scales KM, Cusco JA, Lee BK, Creager MA. Impaired endothelium-dependent vasodilation in patients with insulin-dependent diabetes mellitus. Circulation. 1993;88(6):2510-6.
309. Salt IP, Morrow VA, Brandie FM, Connell JM, Petrie JR. High glucose inhibits insulin-stimulated nitric oxide production without reducing endothelial nitric-oxide synthase Ser1177 phosphorylation in human aortic endothelial cells. J Biol Chem. 2003;278(21):18791-7.
310. Michell BJ, Griffiths JE, Mitchelhill KI, Rodriguez-Crespo I, Tiganis T, Bozinovski S, et al. The Akt kinase signals directly to endothelial nitric oxide synthase. Curr Biol. 1999;9(15):845-8.
311. Du XL, Edelstein D, Dimmeler S, Ju Q, Sui C, Brownlee M. Hyperglycemia inhibits endothelial nitric oxide synthase activity by posttranslational modification at the Akt site. J Clin Invest. 2001;108(9):1341-8.
312. Romero MJ, Platt DH, Tawfik HE, Labazi M, El-Remessy AB, Bartoli M, et al. Diabetes-induced coronary vascular dysfunction involves increased arginase activity. Circ Res. 2008;102(1):95-102.
313. Elms SC, Toque HA, Rojas M, Xu Z, Caldwell RW, Caldwell RB. The role of arginase I in diabetes-induced retinal vascular dysfunction in mouse and rat models of diabetes. Diabetologia. 2013;56(3):654-62.
314. Chandra S, Romero MJ, Shatanawi A, Alkilany AM, Caldwell RB, Caldwell RW. Oxidative species increase arginase activity in endothelial cells through the RhoA/Rho kinase pathway. Br J Pharmacol. 2012;165(2):506-19.
315. Martin W, Furchgott RF, Villani GM, Jothianandan D. Depression of contractile responses in rat aorta by spontaneously released endothelium-derived relaxing factor. J Pharmacol Exp Ther. 1986;237(2):529-38.
316. Kaneko K, Sunano S. Involvement of alpha-adrenoceptors in the endothelium-dependent depression of noradrenaline-induced contraction in rat aorta. Eur J Pharmacol. 1993;240(2-3):195-200.
317. Novella S, Dantas AP, Segarra G, Vidal-Gomez X, Mompeon A, Garabito M, et al. Aging-related endothelial dysfunction in the aorta from female senescence-accelerated mice is associated with decreased nitric oxide synthase expression. Exp Gerontol. 2013;48(11):1329-37.
318. van Langen J, Fransen P, Van Hove CE, Schrijvers DM, Martinet W, De Meyer GR, et al. Selective loss of basal but not receptor-stimulated relaxation by endothelial nitric oxide synthase after isolation of the mouse aorta. Eur J Pharmacol. 2012;696(1-3):111-9.
319. Xavier FE, Davel AP, Rossoni LV, Vassallo DV. Time-dependent hyperreactivity to phenylephrine in aorta from untreated diabetic rats: role of prostanoids and calcium mobilization. Vascul Pharmacol. 2003;40(1):67-76.
320. Abebe W, MacLeod KM. Protein kinase C-mediated contractile responses of arteries from diabetic rats. Br J Pharmacol. 1990;101(2):465-71.

321. Kunisaki M, Bursell SE, Umeda F, Nawata H, King GL. Normalization of diacylglycerol-protein kinase C activation by vitamin E in aorta of diabetic rats and cultured rat smooth muscle cells exposed to elevated glucose levels. Diabetes. 1994;43(11):1372-7.
322. Chang KS, Stevens WC. Endothelium-dependent increase in vascular sensitivity to phenylephrine in long-term streptozotocin diabetic rat aorta. Br J Pharmacol. 1992;107(4):983-90.
323. Chataigneau T, Feletou M, Huang PL, Fishman MC, Duhault J, Vanhoutte PM. Acetylcholine-induced relaxation in blood vessels from endothelial nitric oxide synthase knockout mice. Br J Pharmacol. 1999;126(1):219-26.
324. Takaki A, Morikawa K, Tsutsui M, Murayama Y, Tekes E, Yamagishi H, et al. Crucial role of nitric oxide synthases system in endothelium-dependent hyperpolarization in mice. J Exp Med. 2008;205(9):2053-63.
325. d'Uscio LV, Smith LA, Katusic ZS. Differential effects of eNOS uncoupling on conduit and small arteries in GTP-cyclohydrolase I-deficient hph-1 mice. Am J Physiol Heart Circ Physiol. 2011;301(6):H2227-34.
326. Kidokoro K, Satoh M, Channon KM, Yada T, Sasaki T, Kashihara N. Maintenance of endothelial guanosine triphosphate cyclohydrolase I ameliorates diabetic nephropathy. J Am Soc Nephrol. 2013;24(7):1139-50.
327. Bagi Z, Koller A. Lack of nitric oxide mediation of flow-dependent arteriolar dilation in type I diabetes is restored by sepiapterin. J Vasc Res. 2003;40(1):47-57.
328. Matoba T, Shimokawa H, Nakashima M, Hirakawa Y, Mukai Y, Hirano K, et al. Hydrogen peroxide is an endothelium-derived hyperpolarizing factor in mice. J Clin Invest. 2000;106(12):1521-30.
329. Matoba T, Shimokawa H, Kubota H, Morikawa K, Fujiki T, Kunihiro I, et al. Hydrogen peroxide is an endothelium-derived hyperpolarizing factor in human mesenteric arteries. Biochem Biophys Res Commun. 2002;290(3):909-13.
330. Guzik TJ, Olszanecki R, Sadowski J, Kapelak B, Rudzinski P, Jopek A, et al. Superoxide dismutase activity and expression in human venous and arterial bypass graft vessels. J Physiol Pharmacol. 2005;56(2):313-23.
331. Landmesser U, Merten R, Spiekermann S, Buttner K, Drexler H, Hornig B. Vascular extracellular superoxide dismutase activity in patients with coronary artery disease: relation to endothelium-dependent vasodilation. Circulation. 2000;101(19):2264-70.
332. Galderisi M, Anderson KM, Wilson PW, Levy D. Echocardiographic evidence for the existence of a distinct diabetic cardiomyopathy (the Framingham Heart Study). Am J Cardiol. 1991;68(1):85-9.
333. Devereux RB, Roman MJ, Paranicas M, O'Grady MJ, Lee ET, Welty TK, et al. Impact of diabetes on cardiac structure and function: the strong heart study. Circulation. 2000;101(19):2271-6.
334. Eguchi K, Boden-Albala B, Jin Z, Rundek T, Sacco RL, Homma S, et al. Association between diabetes mellitus and left ventricular hypertrophy in a multiethnic population. Am J Cardiol. 2008;101(12):1787-91.
335. Galvan AQ, Galetta F, Natali A, Muscelli E, Sironi AM, Cini G, et al. Insulin resistance and hyperinsulinemia: No independent relation to left ventricular mass in humans. Circulation. 2000;102(18):2233-8.
336. Woodiwiss AJ, Libhaber CD, Majane OH, Libhaber E, Maseko M, Norton GR. Obesity promotes left ventricular concentric rather than eccentric geometric remodeling and hypertrophy independent of blood pressure. Am J Hypertens. 2008;21(10):1144-51.
337. Sato A, Tarnow L, Parving HH. Increased left ventricular mass in normotensive type 1 diabetic patients with diabetic nephropathy. Diabetes Care. 1998;21(9):1534-9.
338. Weinrauch LA, Berger AJ, Aronson D, Gleason RE, Lee AT, D'Elia JA. Regression of left ventricular hypertrophy in diabetic nephropathy: loss of parasympathetic function predicts response to treatment. J Clin Hypertens (Greenwich). 2006;8(5):330-5.
339. Rerkpattanapipat P, D'Agostino RB, Jr., Link KM, Shahar E, Lima JA, Bluemke DA, et al. Location of arterial stiffening differs in those with impaired fasting glucose versus diabetes:

implications for left ventricular hypertrophy from the Multi-Ethnic Study of Atherosclerosis. Diabetes. 2009;58(4):946-53.
340. Boyer JK, Thanigaraj S, Schechtman KB, Perez JE. Prevalence of ventricular diastolic dysfunction in asymptomatic, normotensive patients with diabetes mellitus. Am J Cardiol. 2004;93(7):870-5.
341. Shivalkar B, Dhondt D, Goovaerts I, Van Gaal L, Bartunek J, Van Crombrugge P, et al. Flow mediated dilatation and cardiac function in type 1 diabetes mellitus. Am J Cardiol. 2006;97(1):77-82.
342. Di Bonito P, Moio N, Cavuto L, Covino G, Murena E, Scilla C, et al. Early detection of diabetic cardiomyopathy: usefulness of tissue Doppler imaging. Diabet Med. 2005;22(12):1720-5.
343. Suys BE, Katier N, Rooman RP, Matthys D, Op De Beeck L, Du Caju MV, et al. Female children and adolescents with type 1 diabetes have more pronounced early echocardiographic signs of diabetic cardiomyopathy. Diabetes Care. 2004;27(8):1947-53.
344. Ernande L, Bergerot C, Rietzschel ER, De Buyzere ML, Thibault H, Pignonblanc PG, et al. Diastolic dysfunction in patients with type 2 diabetes mellitus: is it really the first marker of diabetic cardiomyopathy? J Am Soc Echocardiogr. 2011;24(11):1268-75 e1.
345. Fang ZY, Yuda S, Anderson V, Short L, Case C, Marwick TH. Echocardiographic detection of early diabetic myocardial disease. J Am Coll Cardiol. 2003;41(4):611-7.
346. Andersen NH, Poulsen SH, Eiskjaer H, Poulsen PL, Mogensen CE. Decreased left ventricular longitudinal contraction in normotensive and normoalbuminuric patients with Type II diabetes mellitus: a Doppler tissue tracking and strain rate echocardiography study. Clin Sci (Lond). 2003;105(1):59-66.
347. Joffe, II, Travers KE, Perreault-Micale CL, Hampton T, Katz SE, Morgan JP, et al. Abnormal cardiac function in the streptozotocin-induced non-insulin-dependent diabetic rat: noninvasive assessment with doppler echocardiography and contribution of the nitric oxide pathway. J Am Coll Cardiol. 1999;34(7):2111-9.
348. Cosyns B, Droogmans S, Weytjens C, Lahoutte T, Van Camp G, Schoors D, et al. Effect of streptozotocin-induced diabetes on left ventricular function in adult rats: an in vivo Pinhole Gated SPECT study. Cardiovasc Diabetol. 2007;6:30.
349. Yu X, Tesiram YA, Towner RA, Abbott A, Patterson E, Huang S, et al. Early myocardial dysfunction in streptozotocin-induced diabetic mice: a study using in vivo magnetic resonance imaging (MRI). Cardiovasc Diabetol. 2007;6:6-14.
350. Thomas CM, Yong QC, Seqqat R, Chandel N, Feldman DL, Baker KM, et al. Direct renin inhibition prevents cardiac dysfunction in a diabetic mouse model: comparison with an angiotensin receptor antagonist and angiotensin-converting enzyme inhibitor. Clin Sci (Lond). 2013;124(8):529-41.
351. Nielsen LB, Bartels ED, Bollano E. Overexpression of apolipoprotein B in the heart impedes cardiac triglyceride accumulation and development of cardiac dysfunction in diabetic mice. J Biol Chem. 2002;277(30):27014-20.
352. Lacombe VA, Viatchenko-Karpinski S, Terentyev D, Sridhar A, Emani S, Bonagura JD, et al. Mechanisms of impaired calcium handling underlying subclinical diastolic dysfunction in diabetes. Am J Physiol Regul Integr Comp Physiol. 2007;293(5):R1787-97.
353. Westermann D, Rutschow S, Jager S, Linderer A, Anker S, Riad A, et al. Contributions of inflammation and cardiac matrix metalloproteinase activity to cardiac failure in diabetic cardiomyopathy: the role of angiotensin type 1 receptor antagonism. Diabetes. 2007;56(3):641-6.
354. Suarez J, Scott B, Dillmann WH. Conditional increase in SERCA2a protein is able to reverse contractile dysfunction and abnormal calcium flux in established diabetic cardiomyopathy. Am J Physiol Regul Integr Comp Physiol. 2008;295(5):R1439-45.
355. Pulinilkunnil T, Kienesberger PC, Nagendran J, Waller TJ, Young ME, Kershaw EE, et al. Myocardial adipose triglyceride lipase overexpression protects diabetic mice from the development of lipotoxic cardiomyopathy. Diabetes. 2013;62(5):1464-77.

356. Duan J, Zhang HY, Adkins SD, Ren BH, Norby FL, Zhang X, et al. Impaired cardiac function and IGF-I response in myocytes from calmodulin-diabetic mice: role of Akt and RhoA. Am J Physiol Endocrinol Metab. 2003;284(2):E366-76.
357. Lu Z, Jiang YP, Xu XH, Ballou LM, Cohen IS, Lin RZ. Decreased L-type Ca2+ current in cardiac myocytes of type 1 diabetic Akita mice due to reduced phosphatidylinositol 3-kinase signaling. Diabetes. 2007;56(11):2780-9.
358. Zhang Y, Babcock SA, Hu N, Maris JR, Wang H, Ren J. Mitochondrial aldehyde dehydrogenase (ALDH2) protects against streptozotocin-induced diabetic cardiomyopathy: role of GSK3beta and mitochondrial function. BMC Med. 2012;10:40.
359. LaRocca TJ, Fabris F, Chen J, Benhayon D, Zhang S, McCollum L, et al. Na+/Ca2+ exchanger-1 protects against systolic failure in the Akitains2 model of diabetic cardiomyopathy via a CXCR4/NF-kappaB pathway. Am J Physiol Heart Circ Physiol. 2012;303(3):H353-67.
360. Zhao SM, Wang YL, Guo CY, Chen JL, Wu YQ. Progressive decay of Ca2+ homeostasis in the development of diabetic cardiomyopathy. Cardiovasc Diabetol. 2014;13:75-85.
361. Yokoe S, Asahi M, Takeda T, Otsu K, Taniguchi N, Miyoshi E, et al. Inhibition of phospholamban phosphorylation by O-GlcNAcylation: implications for diabetic cardiomyopathy. Glycobiology. 2010;20(10):1217-26.
362. Trost SU, Belke DD, Bluhm WF, Meyer M, Swanson E, Dillmann WH. Overexpression of the sarcoplasmic reticulum Ca(2+)-ATPase improves myocardial contractility in diabetic cardiomyopathy. Diabetes. 2002;51(4):1166-71.
363. Norby FL, Wold LE, Duan J, Hintz KK, Ren J. IGF-I attenuates diabetes-induced cardiac contractile dysfunction in ventricular myocytes. Am J Physiol Endocrinol Metab. 2002;283(4):E658-66.
364. Tian C, Shao CH, Moore CJ, Kutty S, Walseth T, DeSouza C, et al. Gain of function of cardiac ryanodine receptor in a rat model of type 1 diabetes. Cardiovasc Res. 2011;91(2):300-9.
365. Finck BN, Han X, Courtois M, Aimond F, Nerbonne JM, Kovacs A, et al. A critical role for PPARalpha-mediated lipotoxicity in the pathogenesis of diabetic cardiomyopathy: modulation by dietary fat content. Proc Natl Acad Sci U S A. 2003;100(3):1226-31.
366. Listenberger LL, Han X, Lewis SE, Cases S, Farese RV, Jr., Ory DS, et al. Triglyceride accumulation protects against fatty acid-induced lipotoxicity. Proc Natl Acad Sci U S A. 2003;100(6):3077-82.
367. Zhou YT, Grayburn P, Karim A, Shimabukuro M, Higa M, Baetens D, et al. Lipotoxic heart disease in obese rats: implications for human obesity. Proc Natl Acad Sci U S A. 2000;97(4):1784-9.
368. Ussher JR. The role of cardiac lipotoxicity in the pathogenesis of diabetic cardiomyopathy. Expert Rev Cardiovasc Ther. 2014;12(3):345-58.
369. Weytjens C, Franken PR, D'Hooge J, Droogmans S, Cosyns B, Lahoutte T, et al. Doppler myocardial imaging in the diagnosis of early systolic left ventricular dysfunction in diabetic rats. Eur J Echocardiogr. 2008;9(3):326-33.
370. Li CJ, Lv L, Li H, Yu DM. Cardiac fibrosis and dysfunction in experimental diabetic cardiomyopathy are ameliorated by alpha-lipoic acid. Cardiovasc Diabetol. 2012;11:73-83.
371. Tschope C, Walther T, Koniger J, Spillmann F, Westermann D, Escher F, et al. Prevention of cardiac fibrosis and left ventricular dysfunction in diabetic cardiomyopathy in rats by transgenic expression of the human tissue kallikrein gene. FASEB J. 2004;18(7):828-35.
372. Miric G, Dallemagne C, Endre Z, Margolin S, Taylor SM, Brown L. Reversal of cardiac and renal fibrosis by pirfenidone and spironolactone in streptozotocin-diabetic rats. Br J Pharmacol. 2001;133(5):687-94.
373. Huang ZG, Jin Q, Fan M, Cong XL, Han SF, Gao H, et al. Myocardial remodeling in diabetic cardiomyopathy associated with cardiac mast cell activation. PLoS One. 2013;8(3):e60827: 1-8.
374. Becher PM, Lindner D, Frohlich M, Savvatis K, Westermann D, Tschope C. Assessment of cardiac inflammation and remodeling during the development of streptozotocin-induced diabetic cardiomyopathy in vivo: a time course analysis. Int J Mol Med. 2013;32(1):158-64.

375. Li Z, Abdullah CS, Jin ZQ. Inhibition of PKC-theta preserves cardiac function and reduces fibrosis in streptozotocin-induced diabetic cardiomyopathy. Br J Pharmacol. 2014;171(11):2913-24.
376. Nagareddy PR, McNeill JH, MacLeod KM. Chronic inhibition of inducible nitric oxide synthase ameliorates cardiovascular abnormalities in streptozotocin diabetic rats. Eur J Pharmacol. 2009;611(1-3):53-9.
377. Meininger CJ, Marinos RS, Hatakeyama K, Martinez-Zaguilan R, Rojas JD, Kelly KA, et al. Impaired nitric oxide production in coronary endothelial cells of the spontaneously diabetic BB rat is due to tetrahydrobiopterin deficiency. Biochem J. 2000;349(Pt 1):353-6.
378. Trueblood N, Ramasamy R. Aldose reductase inhibition improves altered glucose metabolism of isolated diabetic rat hearts. Am J Physiol. 1998;275(1 Pt 2):H75-83.
379. Ramasamy R, Oates PJ, Schaefer S. Aldose reductase inhibition protects diabetic and nondiabetic rat hearts from ischemic injury. Diabetes. 1997;46(2):292-300.
380. Johnson BF, Nesto RW, Pfeifer MA, Slater WR, Vinik AI, Chyun DA, et al. Cardiac abnormalities in diabetic patients with neuropathy: effects of aldose reductase inhibitor administration. Diabetes Care. 2004;27(2):448-54.
381. Hu Y, Belke D, Suarez J, Swanson E, Clark R, Hoshijima M, et al. Adenovirus-mediated overexpression of O-GlcNAcase improves contractile function in the diabetic heart. Circ Res. 2005;96(9):1006-13.
382. Clark RJ, McDonough PM, Swanson E, Trost SU, Suzuki M, Fukuda M, et al. Diabetes and the accompanying hyperglycemia impairs cardiomyocyte calcium cycling through increased nuclear O-GlcNAcylation. J Biol Chem. 2003;278(45):44230-7.
383. Ramirez-Correa GA, Jin W, Wang Z, Zhong X, Gao WD, Dias WB, et al. O-linked GlcNAc modification of cardiac myofilament proteins: a novel regulator of myocardial contractile function. Circ Res. 2008;103(12):1354-8.
384. Banerjee PS, Ma J, Hart GW. Diabetes-associated dysregulation of O-GlcNAcylation in rat cardiac mitochondria. Proc Natl Acad Sci U S A. 2015;112(19):6050-5.
385. Bidasee KR, Nallani K, Yu Y, Cocklin RR, Zhang Y, Wang M, et al. Chronic diabetes increases advanced glycation end products on cardiac ryanodine receptors/calcium-release channels. Diabetes. 2003;52(7):1825-36.
386. Bidasee KR, Zhang Y, Shao CH, Wang M, Patel KP, Dincer UD, et al. Diabetes increases formation of advanced glycation end products on Sarco(endo)plasmic reticulum Ca2+-ATPase. Diabetes. 2004;53(2):463-73.
387. Ma H, Li SY, Xu P, Babcock SA, Dolence EK, Brownlee M, et al. Advanced glycation endproduct (AGE) accumulation and AGE receptor (RAGE) up-regulation contribute to the onset of diabetic cardiomyopathy. J Cell Mol Med. 2009;13(8B):1751-64.
388. Kranstuber AL, Del Rio C, Biesiadecki BJ, Hamlin RL, Ottobre J, Gyorke S, et al. Advanced glycation end product cross-link breaker attenuates diabetes-induced cardiac dysfunction by improving sarcoplasmic reticulum calcium handling. Front Physiol. 2012;3:292: 1-10.
389. Campbell DJ, Somaratne JB, Jenkins AJ, Prior DL, Yii M, Kenny JF, et al. Impact of type 2 diabetes and the metabolic syndrome on myocardial structure and microvasculature of men with coronary artery disease. Cardiovasc Diabetol. 2011;10:80.
390. Soetikno V, Sari FR, Sukumaran V, Lakshmanan AP, Mito S, Harima M, et al. Curcumin prevents diabetic cardiomyopathy in streptozotocin-induced diabetic rats: possible involvement of PKC-MAPK signaling pathway. Eur J Pharm Sci. 2012;47(3):604-14.
391. Arikawa E, Ma RC, Isshiki K, Luptak I, He Z, Yasuda Y, et al. Effects of insulin replacements, inhibitors of angiotensin, and PKCbeta's actions to normalize cardiac gene expression and fuel metabolism in diabetic rats. Diabetes. 2007;56(5):1410-20.
392. Shen X, Zheng S, Metreveli NS, Epstein PN. Protection of cardiac mitochondria by overexpression of MnSOD reduces diabetic cardiomyopathy. Diabetes. 2006;55(3):798-805.

393. Song Y, Du Y, Prabhu SD, Epstein PN. Diabetic Cardiomyopathy in OVE26 Mice Shows Mitochondrial ROS Production and Divergence Between In Vivo and In Vitro Contractility. Rev Diabet Stud. 2007;4(3):159-68.
394. Liang Q, Carlson EC, Donthi RV, Kralik PM, Shen X, Epstein PN. Overexpression of metallothionein reduces diabetic cardiomyopathy. Diabetes. 2002;51(1):174-81.
395. Bugger H, Boudina S, Hu XX, Tuinei J, Zaha VG, Theobald HA, et al. Type 1 diabetic akita mouse hearts are insulin sensitive but manifest structurally abnormal mitochondria that remain coupled despite increased uncoupling protein 3. Diabetes. 2008;57(11):2924-32.
396. Turdi S, Li Q, Lopez FL, Ren J. Catalase alleviates cardiomyocyte dysfunction in diabetes: role of Akt, Forkhead transcriptional factor and silent information regulator 2. Life Sci. 2007;81(11):895-905.
397. Kajstura J, Fiordaliso F, Andreoli AM, Li B, Chimenti S, Medow MS, et al. IGF-1 overexpression inhibits the development of diabetic cardiomyopathy and angiotensin II-mediated oxidative stress. Diabetes. 2001;50(6):1414-24.
398. Wold LE, Ceylan-Isik AF, Fang CX, Yang X, Li SY, Sreejayan N, et al. Metallothionein alleviates cardiac dysfunction in streptozotocin-induced diabetes: role of Ca2+ cycling proteins, NADPH oxidase, poly(ADP-Ribose) polymerase and myosin heavy chain isozyme. Free Radic Biol Med. 2006;40(8):1419-29.
399. Thandavarayan RA, Watanabe K, Ma M, Gurusamy N, Veeraveedu PT, Konishi T, et al. Dominant-negative p38alpha mitogen-activated protein kinase prevents cardiac apoptosis and remodeling after streptozotocin-induced diabetes mellitus. Am J Physiol Heart Circ Physiol. 2009;297(3):H911-9.
400. Popovich BK, Boheler KR, Dillmann WH. Diabetes decreases creatine kinase enzyme activity and mRNA level in the rat heart. Am J Physiol. 1989;257(4 Pt 1):E573-7.
401. Zweier JL, Jacobus WE, Korecky B, Brandejs-Barry Y. Bioenergetic consequences of cardiac phosphocreatine depletion induced by creatine analogue feeding. J Biol Chem. 1991;266(30):20296-304.
402. Hamman BL, Bittl JA, Jacobus WE, Allen PD, Spencer RS, Tian R, et al. Inhibition of the creatine kinase reaction decreases the contractile reserve of isolated rat hearts. Am J Physiol. 1995;269(3 Pt 2):H1030-6.
403. Nascimben L, Friedrich J, Liao R, Pauletto P, Pessina AC, Ingwall JS. Enalapril treatment increases cardiac performance and energy reserve via the creatine kinase reaction in myocardium of Syrian myopathic hamsters with advanced heart failure. Circulation. 1995;91(6):1824-33.
404. Tian R, Nascimben L, Kaddurah-Daouk R, Ingwall JS. Depletion of energy reserve via the creatine kinase reaction during the evolution of heart failure in cardiomyopathic hamsters. J Mol Cell Cardiol. 1996;28(4):755-65.
405. Savabi F, Kirsch A. Alteration of the phosphocreatine energy shuttle components in diabetic rat heart. J Mol Cell Cardiol. 1991;23(11):1323-33.
406. Bashir A, Coggan AR, Gropler RJ. In vivo creatine kinase reaction kinetics at rest and stress in type II diabetic rat heart. Physiol Rep. 2015;3(1).
407. Neubauer S, Horn M, Naumann A, Tian R, Hu K, Laser M, et al. Impairment of energy metabolism in intact residual myocardium of rat hearts with chronic myocardial infarction. J Clin Invest. 1995;95(3):1092-100.
408. Liao R, Nascimben L, Friedrich J, Gwathmey JK, Ingwall JS. Decreased energy reserve in an animal model of dilated cardiomyopathy. Relationship to contractile performance. Circ Res. 1996;78(5):893-902.
409. Khuchua ZA, Ventura-Clapier R, Kuznetsov AV, Grishin MN, Saks VA. Alterations in the creatine kinase system in the myocardium of cardiomyopathic hamsters. Biochem Biophys Res Commun. 1989;165(2):748-57.

410. Clapham JC, Arch JR, Chapman H, Haynes A, Lister C, Moore GB, et al. Mice overexpressing human uncoupling protein-3 in skeletal muscle are hyperphagic and lean. Nature. 2000;406(6794):415-8.
411. Chan CB, De Leo D, Joseph JW, McQuaid TS, Ha XF, Xu F, et al. Increased uncoupling protein-2 levels in beta-cells are associated with impaired glucose-stimulated insulin secretion: mechanism of action. Diabetes. 2001;50(6):1302-10.
412. Zhang CY, Hagen T, Mootha VK, Slieker LJ, Lowell BB. Assessment of uncoupling activity of uncoupling protein 3 using a yeast heterologous expression system. FEBS Lett. 1999;449(2-3):129-34.
413. Jaburek M, Varecha M, Gimeno RE, Dembski M, Jezek P, Zhang M, et al. Transport function and regulation of mitochondrial uncoupling proteins 2 and 3. J Biol Chem. 1999;274(37):26003-7.
414. Wojtczak L, Wieckowski MR. The mechanisms of fatty acid-induced proton permeability of the inner mitochondrial membrane. J Bioenerg Biomembr. 1999;31(5):447-55.
415. Bernardi P, Penzo D, Wojtczak L. Mitochondrial energy dissipation by fatty acids. Mechanisms and implications for cell death. Vitam Horm. 2002;65:97-126.
416. Cole MA, Murray AJ, Cochlin LE, Heather LC, McAleese S, Knight NS, et al. A high fat diet increases mitochondrial fatty acid oxidation and uncoupling to decrease efficiency in rat heart. Basic Res Cardiol. 2011;106(3):447-57.
417. Boehm EA, Jones BE, Radda GK, Veech RL, Clarke K. Increased uncoupling proteins and decreased efficiency in palmitate-perfused hyperthyroid rat heart. Am J Physiol Heart Circ Physiol. 2001;280(3):H977-83.
418. Vettor R, Fabris R, Serra R, Lombardi AM, Tonello C, Granzotto M, et al. Changes in FAT/CD36, UCP2, UCP3 and GLUT4 gene expression during lipid infusion in rat skeletal and heart muscle. Int J Obes Relat Metab Disord. 2002;26(6):838-47.
419. Weigle DS, Selfridge LE, Schwartz MW, Seeley RJ, Cummings DE, Havel PJ, et al. Elevated free fatty acids induce uncoupling protein 3 expression in muscle: a potential explanation for the effect of fasting. Diabetes. 1998;47(2):298-302.
420. Li J, Hu X, Selvakumar P, Russell RR, 3rd, Cushman SW, Holman GD, et al. Role of the nitric oxide pathway in AMPK-mediated glucose uptake and GLUT4 translocation in heart muscle. Am J Physiol Endocrinol Metab. 2004;287(5):E834-41.
421. Murray AJ, Panagia M, Hauton D, Gibbons GF, Clarke K. Plasma free fatty acids and peroxisome proliferator-activated receptor alpha in the control of myocardial uncoupling protein levels. Diabetes. 2005;54(12):3496-502.
422. Mochizuki K, Suruga K, Fukami H, Kiso Y, Takase S, Goda T. Selectivity of fatty acid ligands for PPARalpha which correlates both with binding to cis-element and DNA binding-independent transactivity in Caco-2 cells. Life Sci. 2006;80(2):140-5.
423. Finck BN, Lehman JJ, Leone TC, Welch MJ, Bennett MJ, Kovacs A, et al. The cardiac phenotype induced by PPARalpha overexpression mimics that caused by diabetes mellitus. J Clin Invest. 2002;109(1):121-30.
424. Asayama K, Sandhir R, Sheikh FG, Hayashibe H, Nakane T, Singh I. Increased peroxisomal fatty acid beta-oxidation and enhanced expression of peroxisome proliferator-activated receptor-alpha in diabetic rat liver. Mol Cell Biochem. 1999;194(1-2):227-34.
425. Hue L, Taegtmeyer H. The Randle cycle revisited: a new head for an old hat. Am J Physiol Endocrinol Metab. 2009;297(3):E578-91.
426. Moens AL, Ketner EA, Takimoto E, Schmidt TS, O'Neill CA, Wolin MS, et al. Bi-modal dose-dependent cardiac response to tetrahydrobiopterin in pressure-overload induced hypertrophy and heart failure. J Mol Cell Cardiol. 2011;51(4):564-9.
427. Kume E, Fujimura H, Matsuki N, Ito M, Aruga C, Toriumi W, et al. Hepatic changes in the acute phase of streptozotocin (SZ)-induced diabetes in mice. Exp Toxicol Pathol. 2004;55(6):467-80.

428. Wold LE, Ren J. Streptozotocin directly impairs cardiac contractile function in isolated ventricular myocytes via a p38 map kinase-dependent oxidative stress mechanism. Biochem Biophys Res Commun. 2004;318(4):1066-71.
429. Sugimoto H, Grahovac G, Zeisberg M, Kalluri R. Renal fibrosis and glomerulosclerosis in a new mouse model of diabetic nephropathy and its regression by bone morphogenic protein-7 and advanced glycation end product inhibitors. Diabetes. 2007;56(7):1825-33.
430. Tian R, Abel ED. Responses of GLUT4-deficient hearts to ischemia underscore the importance of glycolysis. Circulation. 2001;103(24):2961-6.
431. Herlein JA, Fink BD, O'Malley Y, Sivitz WI. Superoxide and respiratory coupling in mitochondria of insulin-deficient diabetic rats. Endocrinology. 2009;150(1):46-55.
432. Ye G, Metreveli NS, Donthi RV, Xia S, Xu M, Carlson EC, et al. Catalase protects cardiomyocyte function in models of type 1 and type 2 diabetes. Diabetes. 2004;53(5):1336-43.
433. Jones DP, Go YM. Redox compartmentalization and cellular stress. Diabetes Obes Metab. 2010;12 Suppl 2:116-25.
434. Go YM, Jones DP. Redox compartmentalization in eukaryotic cells. Biochim Biophys Acta. 2008;1780(11):1273-90.
435. Murphy MP. How mitochondria produce reactive oxygen species. Biochem J. 2009;417(1):1-13.
436. Ballinger SW, Patterson C, Yan CN, Doan R, Burow DL, Young CG, et al. Hydrogen peroxide- and peroxynitrite-induced mitochondrial DNA damage and dysfunction in vascular endothelial and smooth muscle cells. Circ Res. 2000;86(9):960-6.
437. Richter C. Reactive oxygen and DNA damage in mitochondria. Mutat Res. 1992;275(3-6):249-55.
438. Yakes FM, Van Houten B. Mitochondrial DNA damage is more extensive and persists longer than nuclear DNA damage in human cells following oxidative stress. Proc Natl Acad Sci U S A. 1997;94(2):514-9.
439. Herlein JA, Fink BD, Sivitz WI. Superoxide production by mitochondria of insulin-sensitive tissues: mechanistic differences and effect of early diabetes. Metabolism. 2010;59(2):247-57.
440. Bers DM. Cardiac excitation-contraction coupling. Nature. 2002;415(6868):198-205.
441. Kammermeier H, Schmidt P, Jungling E. Free energy change of ATP-hydrolysis: a causal factor of early hypoxic failure of the myocardium? J Mol Cell Cardiol. 1982;14(5):267-77.
442. Wyss M, Smeitink J, Wevers RA, Wallimann T. Mitochondrial creatine kinase: a key enzyme of aerobic energy metabolism. Biochim Biophys Acta. 1992;1102(2):119-66.
443. Wallimann T, Wyss M, Brdiczka D, Nicolay K, Eppenberger HM. Intracellular compartmentation, structure and function of creatine kinase isoenzymes in tissues with high and fluctuating energy demands: the 'phosphocreatine circuit' for cellular energy homeostasis. Biochem J. 1992;281 (Pt 1):21-40.
444. Kupriyanov VV, Ya Steinschneider A, Ruuge EK, Kapel'ko VI, Yu Zueva M, Lakomkin VL, et al. Regulation of energy flux through the creatine kinase reaction in vitro and in perfused rat heart. 31P-NMR studies. Biochim Biophys Acta. 1984;805(4):319-31.
445. Hallsten K, Virtanen KA, Lonnqvist F, Janatuinen T, Turiceanu M, Ronnemaa T, et al. Enhancement of insulin-stimulated myocardial glucose uptake in patients with Type 2 diabetes treated with rosiglitazone. Diabet Med. 2004;21(12):1280-7.
446. Neely JR, Morgan HE. Relationship between carbohydrate and lipid metabolism and the energy balance of heart muscle. Annu Rev Physiol. 1974;36:413-59.
447. Lopaschuk GD, Belke DD, Gamble J, Itoi T, Schonekess BO. Regulation of fatty acid oxidation in the mammalian heart in health and disease. Biochim Biophys Acta. 1994;1213(3):263-76.
448. Peterson LR, Herrero P, McGill J, Schechtman KB, Kisrieva-Ware Z, Lesniak D, et al. Fatty acids and insulin modulate myocardial substrate metabolism in humans with type 1 diabetes. Diabetes. 2008;57(1):32-40.

449. Khalfallah Y, Fages S, Laville M, Langin D, Vidal H. Regulation of uncoupling protein-2 and uncoupling protein-3 mRNA expression during lipid infusion in human skeletal muscle and subcutaneous adipose tissue. Diabetes. 2000;49(1):25-31.
450. Wang CM, Almsherqi ZA, McLachlan CS, Matthews S, Ramachandran M, Tay S, et al. Acute starvation in C57BL/6J mice increases myocardial UCP2 and UCP3 protein expression levels and decreases mitochondrial bio-energetic function. Stress. 2011;14(1):66-72.
451. Jenkins RL, McDaniel HG, Digerness S, Parrish SW, Ong RL. Adenine nucleotide metabolism in hearts of diabetic rats. Comparison to diaphragm, liver, and kidney. Diabetes. 1988;37(5):629-36.
452. Allison TB, Bruttig SP, Crass MF, 3rd, Eliot RS, Shipp JC. Reduced high-energy phosphate levels in rat hearts. I. Effects of alloxan diabetes. Am J Physiol. 1976;230(6):1744-50.
453. Pieper GM, Murray WJ. In vivo and in vitro intervention with L-carnitine prevents abnormal energy metabolism in isolated diabetic rat heart: chemical and phosphorus-31 NMR evidence. Biochem Med Metab Biol. 1987;38(1):111-20.
454. Buchanan J, Mazumder PK, Hu P, Chakrabarti G, Roberts MW, Yun UJ, et al. Reduced cardiac efficiency and altered substrate metabolism precedes the onset of hyperglycemia and contractile dysfunction in two mouse models of insulin resistance and obesity. Endocrinology. 2005;146(12):5341-9.
455. Vidal-Puig AJ, Grujic D, Zhang CY, Hagen T, Boss O, Ido Y, et al. Energy metabolism in uncoupling protein 3 gene knockout mice. J Biol Chem. 2000;275(21):16258-66.
456. Himms-Hagen J, Harper ME. Physiological role of UCP3 may be export of fatty acids from mitochondria when fatty acid oxidation predominates: an hypothesis. Exp Biol Med (Maywood). 2001;226(2):78-84.
457. Rousset S, Alves-Guerra MC, Mozo J, Miroux B, Cassard-Doulcier AM, Bouillaud F, et al. The biology of mitochondrial uncoupling proteins. Diabetes. 2004;53 Suppl 1:S130-5.
458. Cadenas S, Buckingham JA, Samec S, Seydoux J, Din N, Dulloo AG, et al. UCP2 and UCP3 rise in starved rat skeletal muscle but mitochondrial proton conductance is unchanged. FEBS Lett. 1999;462(3):257-60.
459. Bezaire V, Hofmann W, Kramer JK, Kozak LP, Harper ME. Effects of fasting on muscle mitochondrial energetics and fatty acid metabolism in Ucp3(-/-) and wild-type mice. Am J Physiol Endocrinol Metab. 2001;281(5):E975-82.
460. Essop MF, Razeghi P, McLeod C, Young ME, Taegtmeyer H, Sack MN. Hypoxia-induced decrease of UCP3 gene expression in rat heart parallels metabolic gene switching but fails to affect mitochondrial respiratory coupling. Biochem Biophys Res Commun. 2004;314(2):561-4.
461. Ozcan C, Palmeri M, Horvath TL, Russell KS, Russell RR, 3rd. Role of uncoupling protein 3 in ischemia-reperfusion injury, arrhythmias, and preconditioning. Am J Physiol Heart Circ Physiol. 2013;304(9):H1192-200.
462. Echtay KS, Roussel D, St-Pierre J, Jekabsons MB, Cadenas S, Stuart JA, et al. Superoxide activates mitochondrial uncoupling proteins. Nature. 2002;415(6867):96-9.
463. Marciniak C, Marechal X, Montaigne D, Neviere R, Lancel S. Cardiac contractile function and mitochondrial respiration in diabetes-related mouse models. Cardiovasc Diabetol. 2014;13:118.
464. Boudina S, Sena S, Theobald H, Sheng X, Wright JJ, Hu XX, et al. Mitochondrial energetics in the heart in obesity-related diabetes: direct evidence for increased uncoupled respiration and activation of uncoupling proteins. Diabetes. 2007;56(10):2457-66.
465. Goglia F, Skulachev VP. A function for novel uncoupling proteins: antioxidant defense of mitochondrial matrix by translocating fatty acid peroxides from the inner to the outer membrane leaflet. FASEB J. 2003;17(12):1585-91.
466. Nishimura H, Pallardo FV, Seidner GA, Vannucci S, Simpson IA, Birnbaum MJ. Kinetics of GLUT1 and GLUT4 glucose transporters expressed in Xenopus oocytes. J Biol Chem. 1993;268(12):8514-20.

467. Rosenblatt-Velin N, Montessuit C, Papageorgiou I, Terrand J, Lerch R. Postinfarction heart failure in rats is associated with upregulation of GLUT-1 and downregulation of genes of fatty acid metabolism. Cardiovasc Res. 2001;52(3):407-16.
468. Tardy-Cantalupi I, Montessuit C, Papageorgiou I, Remondino-Muller A, Assimacopoulos-Jeannet F, Morel DR, et al. Effect of transient ischemia on the expression of glucose transporters GLUT-1 and GLUT-4 in rat myocardium. J Mol Cell Cardiol. 1999;31(5):1143-55.
469. Wheeler TJ, Fell RD, Hauck MA. Translocation of two glucose transporters in heart: effects of rotenone, uncouplers, workload, palmitate, insulin and anoxia. Biochim Biophys Acta. 1994;1196(2):191-200.
470. Kono T, Suzuki K, Dansey LE, Robinson FW, Blevins TL. Energy-dependent and protein synthesis-independent recycling of the insulin-sensitive glucose transport mechanism in fat cells. J Biol Chem. 1981;256(12):6400-7.
471. Holmes BF, Kurth-Kraczek EJ, Winder WW. Chronic activation of 5'-AMP-activated protein kinase increases GLUT-4, hexokinase, and glycogen in muscle. J Appl Physiol (1985). 1999;87(5):1990-5.
472. Kurth-Kraczek EJ, Hirshman MF, Goodyear LJ, Winder WW. 5' AMP-activated protein kinase activation causes GLUT4 translocation in skeletal muscle. Diabetes. 1999;48(8):1667-71.
473. Russell RR, 3rd, Bergeron R, Shulman GI, Young LH. Translocation of myocardial GLUT-4 and increased glucose uptake through activation of AMPK by AICAR. Am J Physiol. 1999;277(2 Pt 2):H643-9.
474. Wu N, Zheng B, Shaywitz A, Dagon Y, Tower C, Bellinger G, et al. AMPK-dependent degradation of TXNIP upon energy stress leads to enhanced glucose uptake via GLUT1. Mol Cell. 2013;49(6):1167-75.
475. Barnes K, Ingram JC, Porras OH, Barros LF, Hudson ER, Fryer LG, et al. Activation of GLUT1 by metabolic and osmotic stress: potential involvement of AMP-activated protein kinase (AMPK). J Cell Sci. 2002;115(Pt 11):2433-42.
476. Lee CT, Ussher JR, Mohammad A, Lam A, Lopaschuk GD. 5'-AMP-activated protein kinase increases glucose uptake independent of GLUT4 translocation in cardiac myocytes. Can J Physiol Pharmacol. 2014;92(4):307-14.
477. Ojelabi O. Acute Stimulation of GLUT1 Cell Surface Localization in Blood-Brain Barrier Endothelial Cells (Abstract). FASEB J. 2015;29(1).
478. Chen ZP, McConell GK, Michell BJ, Snow RJ, Canny BJ, Kemp BE. AMPK signaling in contracting human skeletal muscle: acetyl-CoA carboxylase and NO synthase phosphorylation. Am J Physiol Endocrinol Metab. 2000;279(5):E1202-6.
479. Chen ZP, Mitchelhill KI, Michell BJ, Stapleton D, Rodriguez-Crespo I, Witters LA, et al. AMP-activated protein kinase phosphorylation of endothelial NO synthase. FEBS Lett. 1999;443(3):285-9.
480. Morrow VA, Foufelle F, Connell JM, Petrie JR, Gould GW, Salt IP. Direct activation of AMP-activated protein kinase stimulates nitric-oxide synthesis in human aortic endothelial cells. J Biol Chem. 2003;278(34):31629-39.
481. Zhang J, Xie Z, Dong Y, Wang S, Liu C, Zou MH. Identification of nitric oxide as an endogenous activator of the AMP-activated protein kinase in vascular endothelial cells. J Biol Chem. 2008;283(41):27452-61.
482. Wang S, Xu J, Song P, Viollet B, Zou MH. In vivo activation of AMP-activated protein kinase attenuates diabetes-enhanced degradation of GTP cyclohydrolase I. Diabetes. 2009;58(8):1893-901.
483. Xu J, Wu Y, Song P, Zhang M, Wang S, Zou MH. Proteasome-dependent degradation of guanosine 5'-triphosphate cyclohydrolase I causes tetrahydrobiopterin deficiency in diabetes mellitus. Circulation. 2007;116(8):944-53.
484. Park SH, Gammon SR, Knippers JD, Paulsen SR, Rubink DS, Winder WW. Phosphorylation-activity relationships of AMPK and acetyl-CoA carboxylase in muscle. J Appl Physiol (1985). 2002;92(6):2475-82.

485. Zordoky BN, Nagendran J, Pulinilkunnil T, Kienesberger PC, Masson G, Waller TJ, et al. AMPK-dependent inhibitory phosphorylation of ACC is not essential for maintaining myocardial fatty acid oxidation. Circ Res. 2014;115(5):518-24.
486. Zaha VG, Young LH. AMP-activated protein kinase regulation and biological actions in the heart. Circ Res. 2012;111(6):800-14.
487. Zmijewski JW, Banerjee S, Bae H, Friggeri A, Lazarowski ER, Abraham E. Exposure to hydrogen peroxide induces oxidation and activation of AMP-activated protein kinase. J Biol Chem. 2010;285(43):33154-64.
488. Vesce S, Jekabsons MB, Johnson-Cadwell LI, Nicholls DG. Acute glutathione depletion restricts mitochondrial ATP export in cerebellar granule neurons. J Biol Chem. 2005;280(46):38720-8.
489. Queiroga CS, Almeida AS, Martel C, Brenner C, Alves PM, Vieira HL. Glutathionylation of adenine nucleotide translocase induced by carbon monoxide prevents mitochondrial membrane permeabilization and apoptosis. J Biol Chem. 2010;285(22):17077-88.
490. Mailloux RJ, Seifert EL, Bouillaud F, Aguer C, Collins S, Harper ME. Glutathionylation acts as a control switch for uncoupling proteins UCP2 and UCP3. J Biol Chem. 2011;286(24):21865-75.
491. Mollica JP, Dutka TL, Merry TL, Lamboley CR, McConell GK, McKenna MJ, et al. S-glutathionylation of troponin I (fast) increases contractile apparatus Ca2+ sensitivity in fast-twitch muscle fibres of rats and humans. J Physiol. 2012;590(Pt 6):1443-63.
492. Lovelock JD, Monasky MM, Jeong EM, Lardin HA, Liu H, Patel BG, et al. Ranolazine improves cardiac diastolic dysfunction through modulation of myofilament calcium sensitivity. Circ Res. 2012;110(6):841-50.
493. Tong CW, Stelzer JE, Greaser ML, Powers PA, Moss RL. Acceleration of crossbridge kinetics by protein kinase A phosphorylation of cardiac myosin binding protein C modulates cardiac function. Circ Res. 2008;103(9):974-82.
494. Clancy RM, Levartovsky D, Leszczynska-Piziak J, Yegudin J, Abramson SB. Nitric oxide reacts with intracellular glutathione and activates the hexose monophosphate shunt in human neutrophils: evidence for S-nitrosoglutathione as a bioactive intermediary. Proc Natl Acad Sci U S A. 1994;91(9):3680-4.
495. Tocchetti CG, Wang W, Froehlich JP, Huke S, Aon MA, Wilson GM, et al. Nitroxyl improves cellular heart function by directly enhancing cardiac sarcoplasmic reticulum Ca2+ cycling. Circ Res. 2007;100(1):96-104.
496. Froehlich JP, Mahaney JE, Keceli G, Pavlos CM, Goldstein R, Redwood AJ, et al. Phospholamban thiols play a central role in activation of the cardiac muscle sarcoplasmic reticulum calcium pump by nitroxyl. Biochemistry. 2008;47(50):13150-2.
497. Adachi T, Weisbrod RM, Pimentel DR, Ying J, Sharov VS, Schoneich C, et al. S-Glutathiolation by peroxynitrite activates SERCA during arterial relaxation by nitric oxide. Nat Med. 2004;10(11):1200-7.
498. Hughes MN. Relationships between nitric oxide, nitroxyl ion, nitrosonium cation and peroxynitrite. Biochim Biophys Acta. 1999;1411(2-3):263-72.
499. Townsend DM. S-glutathionylation: indicator of cell stress and regulator of the unfolded protein response. Mol Interv. 2007;7(6):313-24.
500. Kazumasa Yamamoto MN, Nobuo Nakanishi, Hiroyuki Hasegawa. A Comparison of Sepiapterin and Tetrahydrobiopterin Uptake by BRL2H3 Cells. Pteridines. 1996;7(4):154-6.
501. Sawabe K, Wakasugi KO, Hasegawa H. Tetrahydrobiopterin uptake in supplemental administration: elevation of tissue tetrahydrobiopterin in mice following uptake of the exogenously oxidized product 7,8-dihydrobiopterin and subsequent reduction by an anti-folate-sensitive process. J Pharmacol Sci. 2004;96(2):124-33.
502. Cunnington C, Van Assche T, Shirodaria C, Kylintireas I, Lindsay AC, Lee JM, et al. Systemic and vascular oxidation limits the efficacy of oral tetrahydrobiopterin treatment in patients with coronary artery disease. Circulation. 2012;125(11):1356-66.

503. Crider KS, Yang TP, Berry RJ, Bailey LB. Folate and DNA methylation: a review of molecular mechanisms and the evidence for folate's role. Adv Nutr. 2012;3(1):21-38.
504. Reimer KA, Hill ML, Jennings RB. Prolonged depletion of ATP because of delayed repletion of the adenine nucleotide pool following reversible myocardial ischemic injury in dogs. Adv Myocardiol. 1983;4:395-407.
505. Moens AL, Champion HC, Claeys MJ, Tavazzi B, Kaminski PM, Wolin MS, et al. High-dose folic acid pretreatment blunts cardiac dysfunction during ischemia coupled to maintenance of high-energy phosphates and reduces postreperfusion injury. Circulation. 2008;117(14):1810-9.
506. Panagia V, Okumura K, Makino N, Dhalla NS. Stimulation of Ca2+-pump in rat heart sarcolemma by phosphatidylethanolamine N-methylation. Biochim Biophys Acta. 1986;856(2):383-7.
507. Ganguly PK, Panagia V, Okumura K, Dhalla NS. Activation of Ca2+-stimulated ATPase by phospholipid N-methylation in cardiac sarcoplasmic reticulum. Biochem Biophys Res Commun. 1985;130(1):472-8.
508. Panagia V, Taira Y, Ganguly PK, Tung S, Dhalla NS. Alterations in phospholipid N-methylation of cardiac subcellular membranes due to experimentally induced diabetes in rats. J Clin Invest. 1990;86(3):777-84.
509. Stefan M, Zhang W, Concepcion E, Yi Z, Tomer Y. DNA methylation profiles in type 1 diabetes twins point to strong epigenetic effects on etiology. J Autoimmun. 2014;50:33-7.
510. Sharma P, Garg G, Kumar A, Mohammad F, Kumar SR, Tanwar VS, et al. Genome wide DNA methylation profiling for epigenetic alteration in coronary artery disease patients. Gene. 2014;541(1):31-40.
511. Newman PE. Can reduced folic acid and vitamin B12 levels cause deficient DNA methylation producing mutations which initiate atherosclerosis? Med Hypotheses. 1999;53(5):421-4.
512. Facchini FS, Stoohs RA, Reaven GM. Enhanced sympathetic nervous system activity. The linchpin between insulin resistance, hyperinsulinemia, and heart rate. Am J Hypertens. 1996;9(10 Pt 1):1013-7.
513. Fein FS, Strobeck JE, Malhotra A, Scheuer J, Sonnenblick EH. Reversibility of diabetic cardiomyopathy with insulin in rats. Circ Res. 1981;49(6):1251-61.
514. Kern W, Peters A, Born J, Fehm HL, Schultes B. Changes in blood pressure and plasma catecholamine levels during prolonged hyperinsulinemia. Metabolism. 2005;54(3):391-6.
515. Thackeray JT, Radziuk J, Harper ME, Suuronen EJ, Ascah KJ, Beanlands RS, et al. Sympathetic nervous dysregulation in the absence of systolic left ventricular dysfunction in a rat model of insulin resistance with hyperglycemia. Cardiovasc Diabetol. 2011;10:75.
516. Freccero C, Svensson H, Bornmyr S, Wollmer P, Sundkvist G. Sympathetic and parasympathetic neuropathy are frequent in both type 1 and type 2 diabetic patients. Diabetes Care. 2004;27(12):2936-41.
517. Ganguly PK, Beamish RE, Dhalla KS, Innes IR, Dhalla NS. Norepinephrine storage, distribution, and release in diabetic cardiomyopathy. Am J Physiol. 1987;252(6 Pt 1):E734-9.
518. Chatham JC, Forder JR. A 13C-NMR study of glucose oxidation in the intact functioning rat heart following diabetes-induced cardiomyopathy. J Mol Cell Cardiol. 1993;25(10):1203-13.
519. Chatham JC, Gao ZP, Forder JR. Impact of 1 wk of diabetes on the regulation of myocardial carbohydrate and fatty acid oxidation. Am J Physiol. 1999;277(2 Pt 1):E342-51.
520. Bollano E, Omerovic E, Svensson H, Waagstein F, Fu M. Cardiac remodeling rather than disturbed myocardial energy metabolism is associated with cardiac dysfunction in diabetic rats. Int J Cardiol. 2007;114(2):195-201.
521. Borbely A, van der Velden J, Papp Z, Bronzwaer JG, Edes I, Stienen GJ, et al. Cardiomyocyte stiffness in diastolic heart failure. Circulation. 2005;111(6):774-81.
522. Shah AM, Shin SH, Takeuchi M, Skali H, Desai AS, Kober L, et al. Left ventricular systolic and diastolic function, remodelling, and clinical outcomes among patients with diabetes following myocardial infarction and the influence of direct renin inhibition with aliskiren. Eur J Heart Fail. 2012;14(2):185-92.

523. Xu Z, Okamoto H, Akino M, Onozuka H, Matsui Y, Tsutsui H. Pravastatin attenuates left ventricular remodeling and diastolic dysfunction in angiotensin II-induced hypertensive mice. J Cardiovasc Pharmacol. 2008;51(1):62-70.
524. van Heerebeek L, Hamdani N, Handoko ML, Falcao-Pires I, Musters RJ, Kupreishvili K, et al. Diastolic stiffness of the failing diabetic heart: importance of fibrosis, advanced glycation end products, and myocyte resting tension. Circulation. 2008;117(1):43-51.
525. Falcao-Pires I, Hamdani N, Borbely A, Gavina C, Schalkwijk CG, van der Velden J, et al. Diabetes mellitus worsens diastolic left ventricular dysfunction in aortic stenosis through altered myocardial structure and cardiomyocyte stiffness. Circulation. 2011;124(10):1151-9.
526. Liu YH, Carretero OA, Cingolani OH, Liao TD, Sun Y, Xu J, et al. Role of inducible nitric oxide synthase in cardiac function and remodeling in mice with heart failure due to myocardial infarction. Am J Physiol Heart Circ Physiol. 2005;289(6):H2616-23.
527. Liang D, Zhong P, Hu J, Lin F, Qian Y, Xu Z, et al. EGFR inhibition protects cardiac damage and remodeling through attenuating oxidative stress in STZ-induced diabetic mouse model. J Mol Cell Cardiol. 2015;82:63-74.
528. Rajesh M, Mukhopadhyay P, Batkai S, Patel V, Saito K, Matsumoto S, et al. Cannabidiol attenuates cardiac dysfunction, oxidative stress, fibrosis, and inflammatory and cell death signaling pathways in diabetic cardiomyopathy. J Am Coll Cardiol. 2010;56(25):2115-25.
529. Aragno M, Mastrocola R, Alloatti G, Vercellinatto I, Bardini P, Geuna S, et al. Oxidative stress triggers cardiac fibrosis in the heart of diabetic rats. Endocrinology. 2008;149(1):380-8.
530. Brady AJ. Mechanical properties of isolated cardiac myocytes. Physiol Rev. 1991;71(2):413-28.
531. Granzier HL, Irving TC. Passive tension in cardiac muscle: contribution of collagen, titin, microtubules, and intermediate filaments. Biophys J. 1995;68(3):1027-44.
532. Kruger M, Kotter S, Grutzner A, Lang P, Andresen C, Redfield MM, et al. Protein kinase G modulates human myocardial passive stiffness by phosphorylation of the titin springs. Circ Res. 2009;104(1):87-94.
533. Neagoe C, Opitz CA, Makarenko I, Linke WA. Gigantic variety: expression patterns of titin isoforms in striated muscles and consequences for myofibrillar passive stiffness. J Muscle Res Cell Motil. 2003;24(2-3):175-89.
534. Nagueh SF, Shah G, Wu Y, Torre-Amione G, King NM, Lahmers S, et al. Altered titin expression, myocardial stiffness, and left ventricular function in patients with dilated cardiomyopathy. Circulation. 2004;110(2):155-62.
535. Fukuda N, Wu Y, Nair P, Granzier HL. Phosphorylation of titin modulates passive stiffness of cardiac muscle in a titin isoform-dependent manner. J Gen Physiol. 2005;125(3):257-71.
536. Kruger M, Linke WA. Protein kinase-A phosphorylates titin in human heart muscle and reduces myofibrillar passive tension. J Muscle Res Cell Motil. 2006;27(5-7):435-44.
537. Alegre-Cebollada J, Kosuri P, Giganti D, Eckels E, Rivas-Pardo JA, Hamdani N, et al. S-glutathionylation of cryptic cysteines enhances titin elasticity by blocking protein folding. Cell. 2014;156(6):1235-46.
538. Tibbetts AS, Appling DR. Compartmentalization of Mammalian folate-mediated one-carbon metabolism. Annu Rev Nutr. 2010;30:57-81.
539. Elsner M, Guldbakke B, Tiedge M, Munday R, Lenzen S. Relative importance of transport and alkylation for pancreatic beta-cell toxicity of streptozotocin. Diabetologia. 2000;43(12):1528-33.
540. Ledoux SP, Wilson GL. Effects of streptozotocin on a clonal isolate of rat insulinoma cells. Biochim Biophys Acta. 1984;804(4):387-92.
541. Palm F, Ortsater H, Hansell P, Liss P, Carlsson PO. Differentiating between effects of streptozotocin per se and subsequent hyperglycemia on renal function and metabolism in the streptozotocin-diabetic rat model. Diabetes Metab Res Rev. 2004;20(6):452-9.

542. Cai L, Wang J, Li Y, Sun X, Wang L, Zhou Z, et al. Inhibition of superoxide generation and associated nitrosative damage is involved in metallothionein prevention of diabetic cardiomyopathy. Diabetes. 2005;54(6):1829-37.
543. Matsubara H, Mori Y, Yamamoto J, Inada M. Diabetes-induced alterations in atrial natriuretic peptide gene expression in Wistar-Kyoto and spontaneously hypertensive rats. Circ Res. 1990;67(4):803-13.
544. Muruganandan S, Gupta S, Kataria M, Lal J, Gupta PK. Mangiferin protects the streptozotocin-induced oxidative damage to cardiac and renal tissues in rats. Toxicology. 2002;176(3):165-73.
545. Ramanadham S, Decker P, Tenner TE, Jr. Effect of insulin replacement on streptozotocin-induced effects in the rat heart. Life Sci. 1983;33(3):289-96.
546. Misra M, Aiman U. Alloxan: an unpredictable drug for diabetes induction? Indian J Pharmacol. 2012;44(4):538-9.
547. Szkudelski T, Kandulska K, Okulicz M. Alloxan in vivo does not only exert deleterious effects on pancreatic B cells. Physiol Res. 1998;47(5):343-6.
548. Lenzen S TM, Jorns A, Munday R. Alloxan derivatives as a tool for the elucidation of the mechanism of the diabetogenic action of alloxan. In: Shafrir E, editor Lessons from Animal Diabetes Boston: Birkhauser; 1996 pp 113–122. 1996.
549. King AJ. The use of animal models in diabetes research. Br J Pharmacol. 2012;166(3):877-94.
550. Costa KD, Takayama Y, McCulloch AD, Covell JW. Laminar fiber architecture and three-dimensional systolic mechanics in canine ventricular myocardium. Am J Physiol. 1999;276(2 Pt 2):H595-607.
551. Spotnitz HM, Spotnitz WD, Cottrell TS, Spiro D, Sonnenblick EH. Cellular basis for volume related wall thickness changes in the rat left ventricle. J Mol Cell Cardiol. 1974;6(4):317-31.
552. LeGrice IJ, Takayama Y, Covell JW. Transverse shear along myocardial cleavage planes provides a mechanism for normal systolic wall thickening. Circ Res. 1995;77(1):182-93.
553. Banting FG, Best CH, Collip JB, Campbell WR, Fletcher AA. Pancreatic Extracts in the Treatment of Diabetes Mellitus. Can Med Assoc J. 1922;12(3):141-6.
554. Braaten JT, Faloona GR, Unger RH. The effect of insulin on the alpha-cell response to hyperglycemia in long-standing alloxan diabetes. J Clin Invest. 1974;53(4):1017-21.
555. Le Marchand SJ, Piston DW. Glucose suppression of glucagon secretion: metabolic and calcium responses from alpha-cells in intact mouse pancreatic islets. J Biol Chem. 2010;285(19):14389-98.
556. Muller WA, Faloona GR, Unger RH. Hyperglucagonemia in diabetic ketoacidosis. Its prevalence and significance. Am J Med. 1973;54(1):52-7.
557. Lee Y, Wang MY, Du XQ, Charron MJ, Unger RH. Glucagon receptor knockout prevents insulin-deficient type 1 diabetes in mice. Diabetes. 2011;60(2):391-7.
558. Lee Y, Berglund ED, Wang MY, Fu X, Yu X, Charron MJ, et al. Metabolic manifestations of insulin deficiency do not occur without glucagon action. Proc Natl Acad Sci U S A. 2012;109(37):14972-6.